PRACTICAL TOOLS FOR RANKING AND SELECTION OF GROUND-MOTION PREDICTION EQUATIONS (GMPEs) FOR PROBABILISTIC SEISMIC HAZARD ASSESSMENT AND DEVELOPMENT OF A REGIONAL GMPE

ÖZKAN KALE

SEPTEMBER 2014

PRACTICAL TOOLS FOR RANKING AND SELECTION OF GROUND-MOTION PREDICTION EQUATIONS (GMPEs) FOR PROBABILISTIC SEISMIC HAZARD ASSESSMENT AND DEVELOPMENT OF A REGIONAL GMPE

A THESIS SUBMITTED TO
THE GRADUATE SCHOOL OF NATURAL AND APPLIED SCIENCES
OF
MIDDLE EAST TECHNICAL UNIVERSITY

BY

ÖZKAN KALE

IN PARTIAL FULFILLMENT OF THE REQUIREMENTS
FOR
THE DEGREE OF DOCTOR OF PHILOSOPHY
IN
CIVIL ENGINEERING

SEPTEMBER 2014

Approval of the thesis:

PRACTICAL TOOLS FOR RANKING AND SELECTION OF GROUND-MOTION PREDICTION EQUATIONS (GMPEs) FOR PROBABILISTIC SEISMIC HAZARD ASSESSMENT AND DEVELOPMENT OF A REGIONAL GMPE

submitted by **ÖZKAN KALE** in partial fulfillment of the requirements for the degree of **Doctor of Philosophy in Civil Engineering Department, Middle East Technical University** by,

Prof. Dr. Canan Özgen
Dean, Graduate School of **Natural and Applied Sciences** _____

Prof. Dr. Ahmet Cevdet Yalçıner
Head of Department, **Civil Engineering** _____

Prof. Dr. Sinan Akkar
Supervisor, **Civil Engineering Dept., METU** (retired) _____

Dr. Laurentiu Danciu
Co-Supervisor, **Swiss Seismological Service** _____

Examining Committee Members:

Prof. Dr. Ayşen Akkaya
Statistics Dept., METU _____

Prof. Dr. Sinan Akkar
Civil Engineering Dept., METU (retired) _____

Prof. Dr. Ahmet Yakut
Civil Engineering Dept., METU _____

Assoc. Prof. Dr. Zehra Çağnan Ertuğrul
Civil Engineering Dept., TED University _____

Asst. Prof. Dr. M. Tolga Yılmaz
Engineering Sciences Dept., METU _____

Date: 11/09/2014

I hereby declare that all information in this document has been obtained and presented in accordance with academic rules and ethical conduct. I also declare that, as required by these rules and conduct, I have fully cited and referenced all material and results that are not original to this work.

Name, Last Name: Özkan Kale

Signature:

ABSTRACT

PRACTICAL TOOLS FOR RANKING AND SELECTION OF GROUND-MOTION PREDICTION EQUATIONS (GMPEs) FOR PROBABILISTIC SEISMIC HAZARD ASSESSMENT AND DEVELOPMENT OF A REGIONAL GMPE

Kale, Özkan

Ph.D., Department of Civil Engineering

Supervisor: Prof. Dr. Sinan Akkar

Co-Supervisor: Dr. Laurentiu Danciu

September 2014, 301 pages

This study starts summarizing the progresses in ground-motion databases and ground-motion models in pan-European region and consequent seismic hazard comparisons conducted for individual local and global predictive models. Then, the study presents the compilation of the Middle East region and Turkish ground-motion databases with principle seismological features to be mainly used in predictive model selection process in these regions. In the following step, using a high standard subset of the Middle East ground-motion database, a ground-motion prediction equation (GMPE) is developed for Turkey and Iran to investigate the possible regional effects on ground-motion amplitudes in shallow active crustal earthquakes. Next part introduces a method for ranking and selection of GMPEs based on Euclidean distance concept. The proposed method is capable of determining the proper set of predictive models for regional or site-specific

probabilistic seismic hazard assessment (PSHA) under a given set of observed ground-motion data. To this end, an alternative method for establishing ground-motion logic-tree framework for PSHA is represented in the following part of the study. The proposed method evaluates the effects of the predictive models and corresponding branch weights selected for logic-tree framework to properly capture the epistemic uncertainty in seismic hazard analysis. As a final point, a ground-motion logic-tree framework combining the functionalities of data-driven GMPE testing methods and logic-tree based sensitivity approach are proposed for shallow active crustal regions in EMME (**E**arthquake **M**odel of the **M**iddle **E**ast Region) project.

Keywords: Probabilistic seismic hazard assessment, ground-motion database, ground-motion prediction equation, regional difference, ranking and selection method

ÖZ

OLASILIKSAL SİSMİK TEHLİKE ANALİZLERİ İÇİN YER HAREKETİ TAHMİN DENKLEMLERİNİN SIRALANMASINDA VE SEÇİLMESİNDE KULLANILACAK PRATİK ARAÇLAR VE BÖLGESEL BİR YER HAREKETİ TAHMİN DENKLEMİNİN GELİŞTİRİLMESİ

Kale, Özkan

Doktora, İnşaat Mühendisliği Bölümü

Tez Yöneticisi : Prof. Dr. Sinan Akkar

Ortak Tez Yöneticisi: Dr. Laurentiu Danciu

Bu çalışma, Avrupa ve civarındaki kuvvetli yer hareketi veri tabanları ve yer hareketi tahmin denklemlerindeki ilerlemeleri ve bunların sonucu olarak ortaya çıkan seçilmiş yerel ve global denklemlerin herbiri için yapılan sismik tehlike karşılaştırmalarını özetleyerek başlamaktadır. Sonrasında bu çalışma, Orta Doğu bölgesi ve Türkiye için derlenen ve esas olarak bu bölgelere uygun yer hareketi tahmin denklemlerinin seçilmesi işleminde kullanılması öngörülen kuvvetli yer hareketi veri tabanlarının derlenmesini ve bunların temel sismolojik özelliklerini göstermektedir. Bunu izleyen aşamada, Orta Doğu veri tabanının yüksek kalitedeki bir alt grubu kullanılarak sığ aktif kabuk depremlerinin yer hareketi genliklerinde oluşması muhtemel bölgesel farklılıkları göstermek amacıyla Türkiye ve İran için bir yer hareketi tahmin denklemi (YHTD) geliştirilmiştir. Sonraki bölüm YHTD seçilmesi ve sıralanmasında kullanılacak olan Öklid uzaklığına bağlı bir yöntemi

tanıtmaktadır. Önerilen yöntem gözlemsel (ölçülmüş) yer hareketi veri seti altında bölgesel veya sahaya özel yapılan olasılıksal sismik tehlike analizleri (OSTA) için uygun bir YHTD setinin belirlenmesi işine yaramaktadır. Bu yönteme ek olarak çalışmanın sonraki bölümünde OSTA için yer hareketi denklemi mantık ağacı uygulamasının oluşturulmasında kullanılabilecek alternatif bir yöntem önerilmiştir. Bu yöntem sismik tehlike analizlerindeki epistemik belirsizliği uygun bir şekilde modelleyebilmek için seçilen tahmin denklemlerinin ve bunlara atanan ağırlıkların etkilerini değerlendirmektedir. Son olarak veri bazlı YHTD test yöntemlerinin ve mantık ağacı hassaslık analizlerine dayalı yöntemin fonksiyonelliği birleştirilerek EMME (Earthquake Model of the Middle East Region) projesindeki sığ aktif kabuk depremler meydana gelen bölgeler için uygun mantık ağacı uygulaması önerilmiştir.

Anahtar Kelimeler: Olasılıksal sismik tehlike analizi, kuvvetli yer hareketi veri tabanı, yer hareketi tahmin denklemi, bölgesel farlılık, sıralama ve seçme yöntemi

To Gizoş and Ada

ACKNOWLEDGMENTS

I would like to express my deepest gratitude to my supervisor Prof. Dr. Sinan Akkar for his enthusiasm during this research and continuous guidance.

I would also like to thank to Prof. Dr. Ayşen Akkaya, Asst. Prof. Dr. M. Tolga Yılmaz, Dr. Laurentiu Danciu, Asst. Prof. Dr. Karin Şeşetyan, Dr. Mine Betül Demircioğlu and Mr. Orhan Özalp for their support during this research. I also thank Prof. Dr. Ahmet Yakut and Assoc. Prof. Dr. Zehra Çağnan Ertuğrul for participating the defense jury.

I would like to express my sincere thanks to my friends Koray Kadaş, Gökalp Ulucan, Emrah Yenier, Abdullah Sandıkkaya, Bekir Özer Ay, Salim Azak, Tuba Eroğlu Azak, Abdullah Dilsiz and Vesile Hatun Akansel for their friendship, support and motivation. I also thanks to Nazile Tekin for her special coffees.

I would like to express my deepest appreciation to my parents Melek and Ethem Kale and my brother Volkan for the support, understanding and motivation that they provided me throughout my life. I would like to express also my deepest appreciation to my second family Suzan Erakça, Gönül and Uğur Çolakoğlu, and Bengi.

Finally, I would like to thank my lovely wife Gizem and my princess Ada for their confidence in me, for their understanding, support, patience and love.

TABLE OF CONTENTS

LIST OF TABLES

LIST OF FIGURES

FIGURES

CHAPTER 1

INTRODUCTION

Adapted from Akkar S and Kale Ö (2014). Developments in ground motion predictive models and accelerometric data archiving in the broader European region. Second European Conference on Earthquake Engineering and Seismology, İstanbul, Turkey, EAEE Theme Lecture No. 35.

1.1. General

The development of ground-motion prediction equations (GMPEs) for shallow active crustal regions in Europe has initiated with the efforts of Ambraseys (1975), approximately a decade after the first ground-motion model proposed by Esteva and Rosenblueth (1964)[1]. In the past 40 years, well over 100 GMPEs were developed in Europe and neighboring countries for estimating the future ground-motion levels in terms of elastic spectral ordinates and peak ground acceleration, PGA (Douglas, 2011)[2]. Most of these GMPEs are tailored from datasets specific to a region or country but there are also ground-motion models developed by combining strong motions of many countries in the broader Europe[3]. As

---

[1] Predictive model by Esteva and Rosenblueth (1964) was proposed for the Western USA whereas the Ambraseys (1975) GMPE was developed for Europe.
[2] There are other ground-motion equations estimating peak ground velocity (e.g., Akkar and Bommer, 2007; Tromans and Bommer, 2002) and ground-motion intensity measures such as vertical-to-horizontal spectral ratios (e.g., Akkar et al., 2014d; Bommer et al., 2011) for Europe and surrounding regions. These predictive models are not considered in this thesis.
[3] Datasets compiled from different European and neighboring countries are generally referred to as pan-European datasets (Bommer et al., 2010). The GMPEs developed from these datasets are called as pan-European GMPEs.

everywhere else in the world, the quality and quantity of GMPEs in Europe are directly related to the availability of observational data. Their level of complexity to explain the physical process of earthquakes has also direct connection with the strong-motion data collection efforts under international or national programs.

As indicated above, there are three common practices in Europe for the development of GMPEs. The first approach focuses on the regional datasets to estimate ground motions (e.g., Massa et al., 2008; Bragato and Slejko, 2005). The second approach uses country-based datasets (e.g., Akkar and Çağnan, 2010; Bindi et al., 2011), whereas the third group of model developers combines data from different countries in and around Europe (e.g., Ambraseys et al., 2005). (In some cases supplementary strong-motion data from USA or Japan are also used by the third group modelers). Researchers from the first two groups aim to capture the region-specific source, path and site effects on the ground-motion amplitude estimates without contaminating the indigenous data from other regions. The GMPEs developed from regional and country-based datasets are generically called as local GMPEs. Researchers following the last approach accentuate that recordings from countries that are located in similar tectonic regimes are expected to exhibit similar features. This assumption generally yields larger ground-motion datasets with better distribution, for example in magnitude-distance space, with respect to regional or country-based datasets. Therefore, the regressed functional forms of the third group models are generally better constrained in terms of main estimator parameters. However, possible data contamination, for example due to regional attenuation differences, may provoke speculations on their efficient use in some hazard studies. As the third group ground-motion models are developed from datasets of multiple countries, they are called as global GMPEs. Their datasets are also referred to as global databases.

Different perspectives in the above approaches raise questions about the existence of regional dependence among the European GMPEs with emphasis on the epistemic and aleatory uncertainties. The aleatory uncertainty (assessed with the

standard deviation, sigma, of GMPE) that is generally referred to as intrinsic variability of ground motions may also reflect the uncertainties stemming from dataset quality and its composition (e.g., local vs. global databases), modeling of GMPE and regression technique used in fitting (Strasser et al., 2009). For example, GMPEs for PGA that are developed from local or pan-European datasets do not show a clear difference in sigma distribution as given in Figure 1.1. Thus, the better constrained pan-European GMPEs do not possess lesser aleatory variability with respect to their local counterparts. The converse of this argument is also defendable: local GMPEs do not show reduced aleatory variability to speculate lesser contamination in their data.
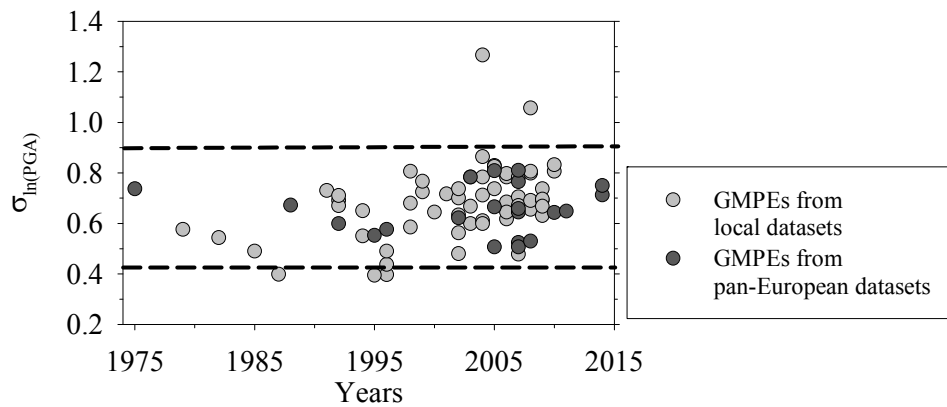
Figure 1.1 Comparisons between the standard deviations of local and pan-European predictive models that estimate PGA.

Figure 1.2 compares the period-dependent sigma trends between NGA-West1[4] (Power et al., 2008), NGA-West2[4] (Bozorgnia et al., 2014) and the most recent pan-European GMPEs (Akkar et al, 2014; Bindi et al., 2014; Akkar and Bommer, 2010; Ambraseys et al., 2005). NGA-West1 and NGA-West2 GMPEs use wide spread shallow active crustal ground motions mainly from California, Taiwan (NGA-West1) and additionally from Japan, China and New Zealand (NGA-West2). They are also referred to as global GMPEs. The comparisons in Figure 1.2

---

[4] NGA-West1 and NGA-West2 are two projects to develop shallow active crustal GMPEs for seismic hazard assessment in the Western US. NGA-West2 project is the successor of NGA-West1.

are done for M_w 5 and M_w 7 and the shaded areas in each panel represent the upper and lower sigma bounds of the chosen pan-European equations. The NGA-West1 and NGA-West2 GMPEs tend to yield lower sigma with respect to pan-European GMPEs. Note that the NGA-West2 predictive models were developed to bring improvements over NGA-West1 GMPEs in terms of additional data, explanatory variables and extended magnitude and distance ranges but their sigma values are larger with respect to their predecessors. The larger standard deviations in NGA-West2 GMPEs can be the manifestations of aggregated uncertainty due to new data and additional explanatory variables. Interestingly, the core accelerometric data sources of NGA-West1 and NGA-West2 GMPEs do not include large numbers of ground motions from Europe that can, speculatively, be a factor for the observed differences in the sigma variation between NGA and pan-European GMPEs.
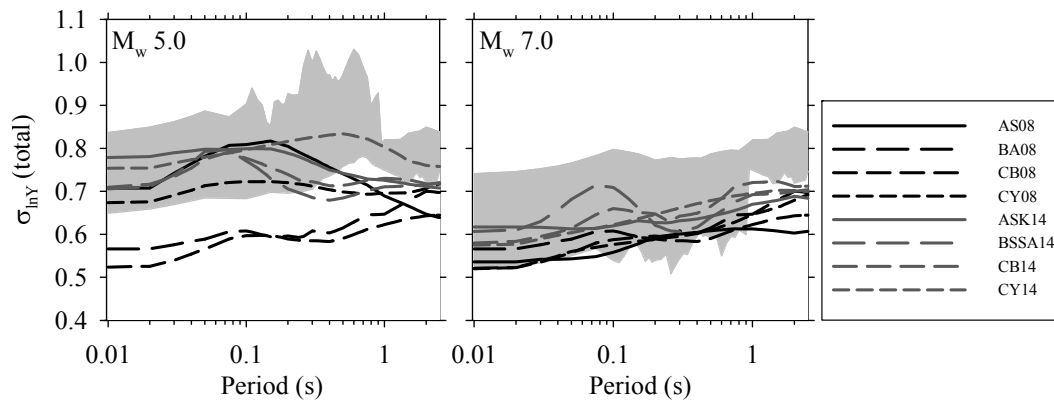
Figure 1.2 Comparisons of sigma between NGA-West1 (Abrahamson and Silva (2008) - AS08, Boore and Atkinson (2008) - BA08, Campbell and Bozorgnia (2008) - CB08, Chiou and Youngs (2008) - CY08), NGA-West2 (Abrahamson et al. (2014) - ASK14, Boore et al. (2014) - BSSA14, Campbell and Bozorgnia (2014) - CB14, Chiou and Youngs (2014) - CY14) and some representative pan-European GMPEs (Akkar et al., 2014; Bindi et al., 2014; Akkar and Bommer, 2010; Ambraseys et al., 2005). The gray shaded areas show the upper and lower sigma bounds of pan-European GMPEs. Comparisons are done for a rock site (V_{S30} = 760 m/s) located 10 km away from a 90-degree dipping strike-slip fault. The selected magnitudes for comparisons are M_w 5 (left panel) and M_w 7 (right panel).

The above observations suggest that further systematic studies are required to understand the sources of differences or similarities in the aleatory variability between local and pan-European GMPEs. Such studies should also be performed between European and other well constrained global ground-motion models that are developed outside of Europe. An extensive summary about the factors controlling sigma and worldwide studies aiming to reduce sigma can be found in Strasser et al. (2009).

Douglas (2004, 2007) indicated that there is no strong evidence confirming regional dependence for the GMPEs produced in the broader European region since the empirical observations are still limited. He also emphasized that the level of complexity in the current pan-European GMPEs is insufficient for a clear understanding about the contribution of epistemic uncertainty on the median ground-motion estimates (Douglas, 2010). However, complexity in ground-motion models does not necessarily imply a better identification of epistemic uncertainty as complex GMPEs contain superior numbers of estimator parameters that may lead to overfit to empirical observations (Kaklamanos and Baise, 2011). Bommer et al. (2010) showed that GMPEs developed from pan-European datasets and ground-motion models derived from NGA-West1 GMPEs would yield similar ground-motion estimates for moderate-to-large magnitude earthquakes. These authors indicated that the regional differences in ground-motion estimates would be prominent towards smaller magnitude earthquakes, which is a parallel observation with the studies conducted in the other parts of the world (Chiou et al., 2010; Atkinson and Morrison, 2009). On the other hand, Scassera et al. (2009) emphasized that the use of NGA-West1 GMPEs may over predict the hazard in Italy at large distances because Italian data attenuate faster than the trends depicted in NGA-West1 GMPEs. In a separate study, Akkar and Çağnan (2010) who developed a GMPE from an extended Turkish database showed that NGA-West1 GMPEs and ground-motion predictive models from pan-European datasets would yield conservative estimates with respect to their GMPE for different earthquake scenarios at different spectral ordinates. Recently, Kale et al. (2014) showed the

existence of distance and magnitude dependent differences between the Iranian and Turkish shallow active crustal ground-motion amplitudes. Yenier and Atkinson (2014) found evidence on the regional dependence of large magnitude earthquakes in New Zealand and western North America. Almost all NGA-West2 GMPEs consider regional differences in their ground-motion estimates (Gregor et al., 2014).

The observations on GMPEs developed since the 1960s indicate notable variations such as standard deviations, spectral ordinate estimates, etc. During the same period, the quality and size of strong ground-motion data archive within pan-European region has been increased intensely with the national and international research projects and the occurrence of numerous earthquakes in well-instrumented regions. It is believed that these advances enable the researchers to obtain more constrained predictive models because the understanding of strong ground-motion data has become more apparent. However, all efforts devoted to this realm of engineering seismology are capable of decreasing the modeling uncertainty. As long as there is randomness in the nature of earthquake process, obtaining a flawless ground-motion database with respect to, at least, magnitude and distance bins are impossible. Under these circumstances, it is inevitable that the researchers should find ways for dealing with the uncertainty by conducting more elaborate studies and developing more sophisticated methodologies. In this respect, this dissertation aims at addressing the different aspects of several topics related to database quality, predictive models, regional variations and characterization of the modeling uncertainty for seismic hazard in order to scrutinize the understanding of the driving factors behind the observations highlighted in the above paragraphs. The following sections summarize the history and current conditions of strong-motion databases and ground-motion relations in the broader European region as well as present the results of some probabilistic seismic hazard studies (PSHA) to evaluate the level of differences in the estimated hazard upon the use of most recent local and global pan-European and NGA GMPEs. The final section outlines the individual descriptions of each chapter.

1.2. Evolution of Major Strong-Motion Databases in the Broader Europe

Strong-motion data collection in Europe started in the beginning of 1970s in Imperial College under the leadership of Prof. Ambraseys (deceased in 2012). It is continued progressively through multi-national collaborations (Ambraseys, 1990; Ambraseys and Bommer, 1990; 1991) and a CD-ROM of 1068 tri-axial accelerometric data was released in 2000 as a solid product of this effort (Ambraseys et al., 2000). The data in the CD-ROM were expanded to a total of 2213 accelerograms from 856 earthquakes recorded at 691 strong-motion stations (Ambraseys et al., 2004a) and it is disseminated through the Internet Site for European Strong-Motion Data (ISESD) web page (http://www.isesd.hi.is). Figure 1.3.a shows the magnitude vs. distance scatter of ISESD strong-motion database. It spans accelerograms from broader Europe between 1976 and 2004. The earthquake metadata (e.g., geometry, style-of-faulting, magnitude estimations etc.) in ISESD was extracted either from specific earthquake studies (institutional reports and papers published in peer-reviewed journals) or ISC bulletin (International Seismological Center, www.isc.ac.uk). The earthquake location information was taken from local or national seismic networks whenever they were assessed as more reliable than the international networks. The strong-motion station information (site conditions, station coordinates, shelter type) was obtained from the network owners. The soil classification of strong-motion sites in ISESD relies on V_{S30} (average shear-wave velocity in the upper 30m soil profile). However, the V_{S30} data were mostly inferred from geological observations in ISESD as the measured shear-wave velocity profiles were typically unavailable by the time when it was assembled. The processed strong-motion records in ISESD were band-pass filtered using an elliptical filter with constant high-pass and low-pass filter cut-off frequencies (0.25Hz and 25Hz, respectively). After the release of ISESD, a small subset of this database was re-processed using the phaseless (acausal) Butterworth filter with filter cut-off frequencies adjusted individually for each accelerogram. The individual filter cut-off frequencies were determined from the signal-to-noise ratio of each accelerogram. This subset was published as another CD-ROM that is

referred to as European Strong-Motion Data (ESMD; Ambraseys et al., 2004b). The extent of ESMD in terms of magnitude and distance is given in Figure 1.3.b.
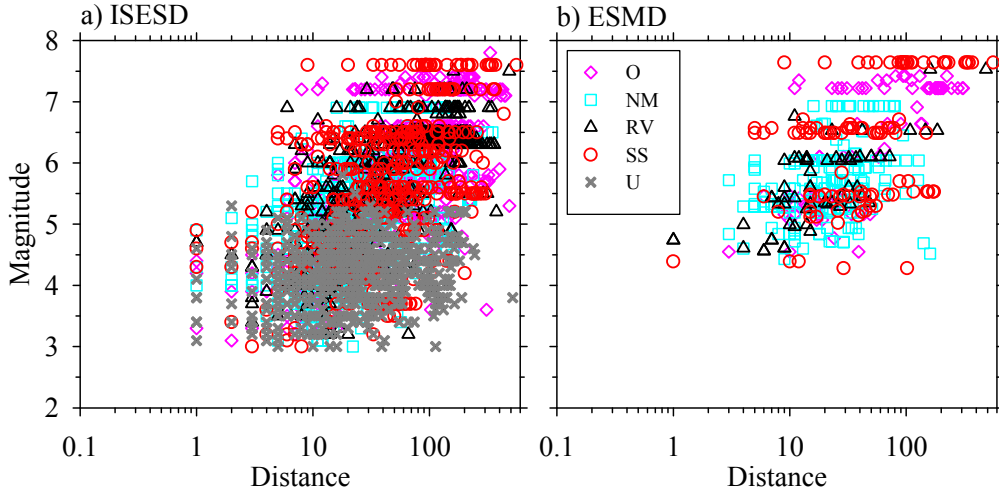
Figure 1.3 Magnitude vs. distance scatters of (a) ISESD, (b) ESMD. Different symbols with different color codes show the distribution of fault mechanisms in these databases (O: odd, NM: normal, RV: reverse, SS: strike-slip, U: Unknown). Almost 50% of the data in ISESD and ESMD are collected from Italy, Greece and Turkey. These countries are followed by Iran (11% of the whole data).

The dissemination of ISESD and ESMD strong-motion databases was followed by important national and international strong-motion and seismic hazard projects in Europe and surrounding regions. Among these projects, the **IT**alian **AC**celerometric **A**rchive[5] project (ITACA; http://itaca.mi.ingv.it; Luzi et al., 2008), the **T**urkish **N**ational **S**trong-**M**otion **P**roject (T-NSMP; http://kyh.deprem.gov.tr; Akkar et al., 2010) and the **HE**llenic **A**ccelerogram **D**atabase Project (HEAD; http://www.itsak.gr; Theodulidis et al., 2004) are national efforts to compile, process and archive local (national) accelerometric data using state-of-the-art techniques. Figures 1.4.a and 1.4.b show the magnitude vs. distance scatters of ITACA[5] and T-NSMP databases as of the day they were released. These national

---

[5] The ITACA database referenced in this article is now called as "ITACA v1" as a newer version is recently released on the same web site. The new release covers Italian strong-motion records from 1972 to the end of 2013.

projects improved the site characterization of strong-motion stations either by reassessing the existing shear-wave velocity profiles and soil column lithology information or by utilizing invasive or noninvasive site exploration techniques to compute the unknown V_{S30} and other relevant site parameters (e.g., see Sandıkkaya et al., 2010 for site characterization methods of Turkish accelerometric archive). They also uniformly processed the strong-motion records by implementing a reliable and consistent data processing scheme. None of these data processing algorithms implemented constant filter cut-off frequencies to remove the high-frequency and low-frequency noise from the raw accelerograms.
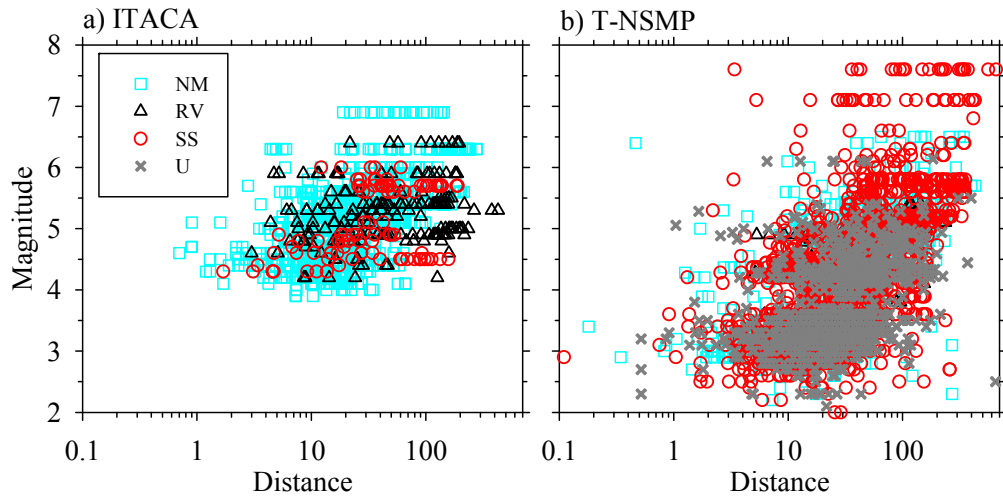
Figure 1.4 Magnitude vs. distance scatters of (a) ITACA and (b) T-NSMP databases. The ITACA[5] project compiled a total of 2182 accelerograms from 1004 events (Luzi et al., 2008) whereas T-NSMP studied 4607 strong-motion records from 2996 earthquakes recorded at 209 stations (Akkar et al., 2010). The symbols on the scatter plots show the distribution of fault mechanism in each database. (Refer to the caption of Figure 1.3 for abbreviations in the legends).

The NERIES (**NE**twork of **R**esearch **I**nfrastructures for **E**uropean **S**eismology; www.neries-eu.org) and SHARE (**S**eismic **H**azard H**AR**monization in **E**urope; www.share.eu.org) projects that are funded by European Council also contributed significantly to the integral efforts for collecting and compiling accelerometric data

in the broader Europe. The NERIES project created a new infrastructure to collect, process and distribute near-real time accelerometric data from across Europe (www.seismicportal.eu). The SHARE project compiled a comprehensive strong-motion database (Yenier et al., 2010) by collecting worldwide shallow active crustal accelerometric data that includes recordings from ISESD, ESMD, ITACA and T-NSMP. The SHARE strong-motion database (13500 records from 2268 events recoded at 3708 stations) was mainly used to test the candidate GMPEs for the seismic hazard calculations in the SHARE project. The developers of the SHARE database neither aimed for updating the metadata information nor developing a uniformly processed accelerometric data archive from the collected strong-motion recordings. The EMME (**E**arthquake **M**odel of the **M**iddle **E**ast Region; www.emme-gem.org) project that is funded by **G**lobal **E**arthquake **M**odel (GEM) organization with objectives parallel to the SHARE also established a strong-motion database for SACRs in the Middle East, Iran, Pakistan and Caucasus. The EMME strong-motion database that consists of 4920 accelerograms from 1803 events is mainly used to identify the most proper GMPEs for hazard computations in the SACRs covered by the project. One of the major differences between the EMME and SHARE strong-motion databases is the uniform data processing implemented to the accelerograms in EMME. Besides, the earthquake and strong-motion station metadata information of the EMME database was reassessed systematically by the project partners (Akkar et al., 2014a). Figures 1.5.a and 1.5.b compare the magnitude and distance distributions of these two databases. Note that the magnitude and distance coverage of EMME strong-motion database is not as uniform as in the case of SHARE database. This is because the latter strong-motion inventory includes shallow active crustal earthquake accelerograms from the entire world. The EMME strong-motion database is particularly rich in Iranian and Turkish recordings. When both databases are compared for accelerograms originating from the pan-European region, one may infer that the EMME and SHARE databases can reveal significant amount of information about the characteristics of strong-motion data from this region.

10

The efforts put forward in the development of the ISESD as well as other databases that are compiled from well-organized national and international projects had considerable impact on the improvement of accelerometric data quality in and around Europe. However, they suffer from certain drawbacks at different technical and operational levels. Although the ISESD is an integrated database representing the strong-motion data archive of broader Europe, the poor strong-motion site characterization and the use of constant filter cut-offs in data processing are the major shortcomings of this database. The use of fixed filter cut-offs has been proven to be inappropriate as it may result in wrong representation of actual ground-motion frequency content of the recorded events (e.g., Akkar and Bommer, 2006). The national strong-motion projects as well as the EMME project took their precautions against such drawbacks but they implemented their own methodologies while assembling the databases. Thus, there is a lack of uniformity among these projects for metadata compilation and record processing for their integration under a single strong-motion database. The SHARE project did no attempt to homogenize the data processing of accelerograms. Improvements in earthquake and station metadata were also out of scope of the SHARE. The recordings from the most recent pan-European earthquakes of engineering interest (e.g., 2009 L'Aquila Earthquake M_w 6.3; 2011 Van Earthquake M_w 7.1; 2011 Van-Edremit Earthquake M_w 5.6; 2011 Kütahya-Simav Earthquake M_w 5.9; 2010 Elazığ-Kovancılar Earthquake M_w 6.1) were either entirely or mostly discarded in the SHARE strong-motion database. The NERIES attempt was mostly limited to creating an infrastructure for integrated accelerometric data archive within Europe. However, the proposed infrastructure focuses on the near-real time accelerograms that are hosted by NERIES portal (www.seismicportal.eu). These recordings are from the last decade with limited engineering significance (i.e. mostly small magnitude events). Moreover, the proposed data archiving and dissemination structure by NERIES is not entirely devised for the engineering needs of accelerometric data use.
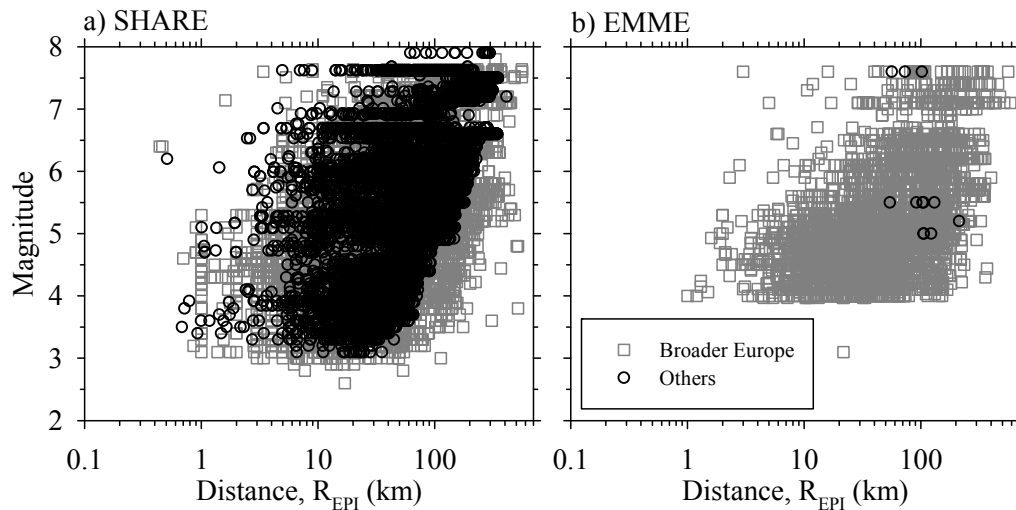
Figure 1.5 Magnitude and distance distributions of (a) SHARE and (b) EMME strong-motion databases. The SHARE accelerograms from the broader Europe are shown in cyan to give a more clear view on the fraction of recordings from this region in the SHARE database. Same color codes are used in the EMME scatter plot for comparing the strong-motion data distribution of broader Europe between these two databases.

Currently, the most up-to-date pan-European strong-motion database is RESORCE (Reference Database for Seismic Ground-Motion in Europe; http://resorce-portal.eu/) that is developed under the SIGMA (**Se**Ismic **G**round **M**otion **A**ssessment; http://projet-sigma.com/) project. The primary motivation of RESORCE (Traversa et al., 2014) is to update and extend the ISESD accelerometric archive by using the information gathered from recently carried out strong-motion database projects as well as other relevant earthquake-specific studies in the literature. To this end, RESORCE made use of the already compiled metadata and waveform information from ITACA, T-NSMP, HEAD, SHARE, ISESD and ESMD. The information gathered from these databases were extended by considering the French (French Accelerometric Network; RAP; www-rap.obs.ujf-grenoble.fr) and Swiss (Swiss Seismological Service; SED; seismo.ethz.ch) accelerometric data that are from moderate-to-small magnitude events. The RESORCE developer team also did an extensive literature survey from

12

peer-reviewed journals to improve the earthquake metadata information of earthquakes from the broader Europe. The uniform data processing of accelerograms following the discussions in Boore et al. (2012) as well as improved magnitude and source-to-site distance distributions constitute the other important achievements in RESORCE. The current data size of RESOCE is 5882 accelerograms recorded from 1814 events. The number of strong-motion stations included in RESORCE is 1540. The magnitude and distance range covered by RESORCE is $2.8 \leq M_w \leq 7.8$ and $R_{JB} \leq 370$ km. The strategy followed in the compilation of RESORCE as well as its main features are given in Akkar et al. (2014c) and Sandıkkaya and Akkar (2013). Figure 1.6 compares the magnitude vs. distance distribution of RESORCE and NGA-West2 database (Anchetta et al., 2014) that is used in the development of NGA-West2 GMPEs. The NGA-West2 database covers a small fraction of accelerograms from the broader European region. Thus, the information provided in RESORCE, when used systematically with NGA-West2 database, can be a good basis to understand the significance of regional differences in shallow active crustal earthquakes between Europe and the other parts of the world. Table 1.1 compares the essential features of major strong-motion databases compiled from the recordings of broader Europe. The information presented in Table 1.1 once again confirms that RESORCE contains the most up-to-date data for the broader European region. The main sources of accelerograms are Turkey, Italy and Greece. Yet to be considered in RESORCE, for example, is to extend it by including the strong-motion data of other seismic prone countries in the region (e.g., Iran). To this end, EMME strong-motion database can be a good source but, as indicated previously, differences in database compilation between RESORCE and EMME would create difficulties while integrating these strong-motion archives.
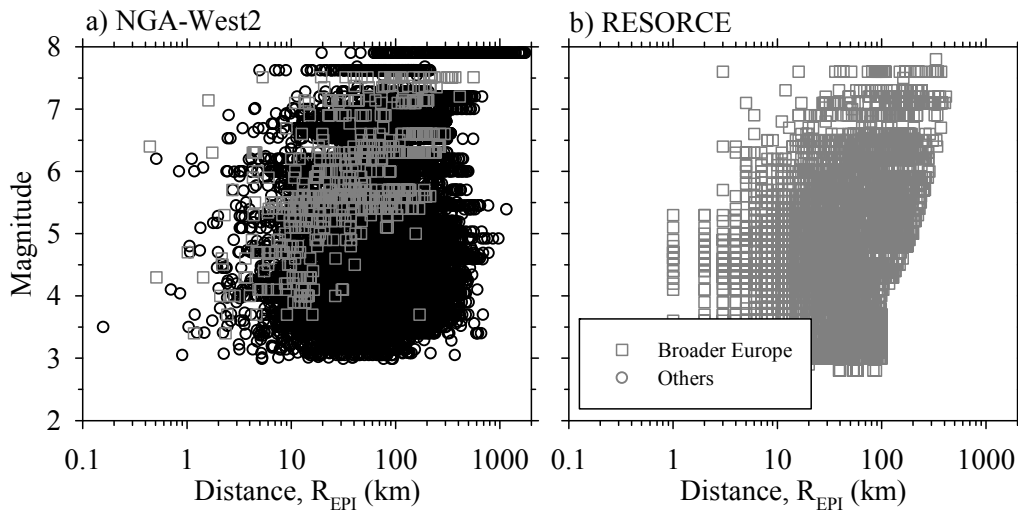
Figure 1.6 Comparison of (a) NGA-West2 and (b) RESORCE strong-motion databases in terms of magnitude and distance distribution. The NGA-West 2 database contains 21336 strong-motion recordings and only 2% of the data is from the pan-European region. The colored data given on the scatter plot of NGA-West2 show the pan-European accelerograms in this database.

Table 1.1 Important characteristics of strong-motion databases developed in broader Europe.

Database	Years covered	Region	No of Acc	No of Eqs	No of Sta	Data Process*	Main Count's[+]	M range	D range (km)
ISESD	1967 2004	Europe & Middle East	2213	856	691	Uni EBP	IT, TR & GR	3.0 - 7.8	0 – 558
ESMD	1973 2003	Europe & Middle East	462	110	261	Ind ABP	IT, TR & GR	4.3 - 7.6	0 – 558
T-NSMP	1976 2007	Turkey	4607	2996	209	Ind ABP	TR	1.6 - 7.6	0 – 655
ITACA	1972 2004	Italy	2182	1004	-	Ind ABP	IT	3.0 - 6.9	-
EMME	1973 2011	Middle East	4920	1803	1260	Ind & Uni ABP	TR & IR	3.1 - 7.6	0 – 586
RESORCE	1967 2012	Europe & Middle East	5882	1814	1540	Ind ABP	TR & IT	2.8 - 7.8	0 – 587

[*] Uni: Uniform; Ind: Individual; EBP: Elliptical bandpass filtering; ABP: Acausal bandpass filtering
[+] GR: Greece; IR: Iran; IT: Italy; TR: Turkey

14

The NERA (Network for European Research Infrastructures for Earthquake Risk Assessment and Mitigation; www.nera-eu.org) project builds a general framework on top of the above summarized efforts by proposing an integral infrastructure for a single, high-quality accelerometric database. The proposed system opts for the adoption of common data and metadata dissemination strategies and standards by forming a well-organized consortium among accelerometric data providers in and around Europe. The efforts to form this consortium have already started under Orfeus (Observatories and Research Facilities for European Seismology; www.orfeus-eu.org) with the contributions of NERA. The consortium will consist of the representatives of accelerometric data networks in the broader Europe for an integrated, sustainable and dynamically growing pan-European strong-motion database. In fact, the prototype of such accelerometric database has already been developed in NERA that is called as Engineering Strong Motion database (ESM_db). If the strong-motion consortium under Orfeus can be firmly established and if this consortium can maintain the so-called ESM_db with high standards, the pan-European endeavor to establish a long-term and reliable accelerometric data archive will make its most future promising progress for the last 40 years. The activities of NERA on accelerometric data networks as well as integrated pan-European accelerometric database are summarized in Akkar et al. (2014e).

1.3. Ground-Motion Prediction Equations (GMPEs) in the Broader European Region

Bommer et al. (2010) and Akkar et al. (2014b) give a detailed review on some of the selected pan-European (global) GMPEs. This section not only focuses on the evolution of global GMPEs in Europe and surroundings but also discusses the progress in the local European GMPEs by presenting overall statistics on some of the key aspects in these predictive models. It also makes comparisons among the local and global GMPEs in Europe and extends these comparisons to NGA-West1 and NGA-West2 GMPEs to emphasize the differences (or similarities) between these ground-motion models. The statistics in this section are primarily compiled

from Douglas (2011). The statistics of other reports and papers were used for GMPEs that are published after Douglas (2011).

Figure 1.7 gives the number of GMPEs developed in the broader Europe as a function of time. The trends given for every decade depict that the number of GMPEs increases significantly after 1990 when strong-motion database compilation and dissemination is accelerated in Europe. (See discussions in the previous section). After 2000, the modelers started to develop GMPEs on elastic spectral ordinates rather than deriving equations only for PGA. This observation may suggest the increased significance of spectral ordinates in engineering design in Europe after 2000. It may also indicate the improvements in strong-motion databases after mid 90s because computation of spectral ordinates requires implementation of strong-motion data processing on the raw accelerometric data.
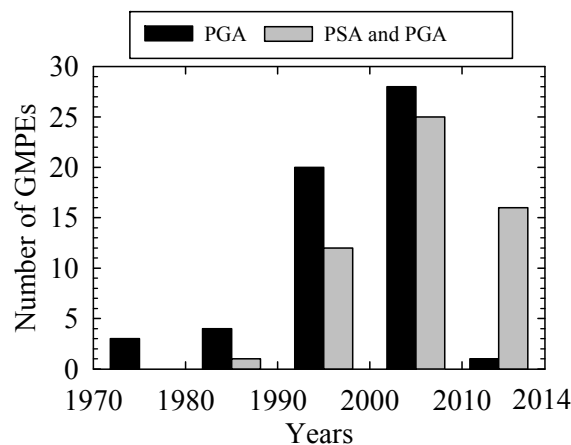
Figure 1.7 Number of GMPEs developed in the broader Europe between 1970 and present. The black vertical bars show the number of GMPEs estimating PGA only. The gray vertical bars display GMPEs estimating pseudo-acceleration spectral ordinates (PSA) and PGA.

Figure 1.8 presents the modeling complexity of GMPEs in the broader Europe. The histogram in this figure shows the change in the number of regression coefficients as a function of time. The majority of functional forms (~ 80%) in Europe are

relatively simple; consisting of regression coefficients up to 4 ($n_r \leq 4$) or between 5 and 6 ($4 < n_r \leq 6$). GMPEs from the first group ($n_r \leq 4$) are mainly developed before 2000 but their number is still significant in the decade following 2000. The second group GMPEs (i.e., $4 < n_r \leq 6$) has become frequent after 90s that coincides with the commencement of efforts for compiling higher quality databases in Europe. The functional forms with $4 < n_r \leq 6$ generally account for the site effects on ground-motion estimates that constitute the major difference with respect to the GMPEs of $n_r \leq 4$. More complicated GMPEs (i.e., equations having $n_r > 6$) became available after 2000 (more precisely in the last 10 years) because improvements in the database quality in and around Europe have come to a mature level following the dissemination of first pan-European strong-motion database CD-ROM by Ambraseys et al. (2004a). Currently, consideration of site effects and style-of-faulting has almost become standard in the local and global European GMPEs.
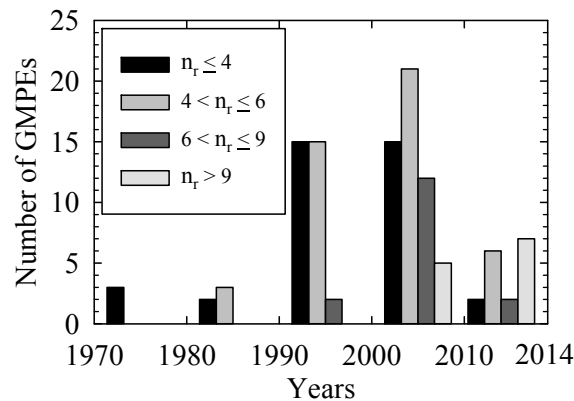
Figure 1.8 Number of regression coefficients in GMPEs developed in the broader Europe between 1970 and present.

Figure 1.9 shows another aspect of modeling complexity in the local and global European GMPEs by giving statistics on the specific features of estimator parameters. Figure 1.9.a presents the time-dependent variation of preferred magnitude scaling in the functional forms. Figure 1.9.b displays a similar statistics on the preferred distance measures whereas Figures 1.9.c and 1.9.d illustrate modeling of soil conditions and faulting type, respectively. The information given

in these histograms complements the discussions on Figure 1.8. The increased quality of strong-motion datasets leads to the utilization of more complicated estimator parameters for developing ground-motion models in the broader Europe. For example, the functional forms of GMPEs developed in the last 15 years generally use moment magnitude (Figure 1.9.a) and consider more rigorous schemes for site effects (Figure 1.9.c). In fact, some of the most recent local and global GMPEs in Europe describe the soil influence on ground motions by using continuous functions of V_{S30} (see Douglas et al., 2014). The use of point-source distance measures[6] (i.e., epicentral distance, R_{EPI} and hypocentral distance, R_{HYP}) that are always appealing among the GMPE developers in Europe reduced after 90s because strong-motion databases started to include extended-source distance measures (i.e., Joyner-Boore distance, R_{JB} and rupture distance, R_{RUP}). To this end, GMPEs utilizing only extended-source distance metrics or those that combine extended- and point-source distance metrics have become more frequent in the last 15 years as displayed in Figure 1.9.b. Local and global European GMPEs that use hybrid distance measures (i.e., R_{RUP} & R_{HYP} or R_{JB} & R_{EPI}) assume $R_{RUP} \approx R_{HYP}$ and $R_{JB} \approx R_{EPI}$ for small magnitude events (i.e., $M_w \leq 5.5$).

---

[6] The point-source distance measures do not consider the source geometry and approximates the ruptured fault segment as a point. The extended-source distance metrics account for the source geometry and can show the variation in ground-motion amplitudes more appropriately for large events at sites closer to the source.
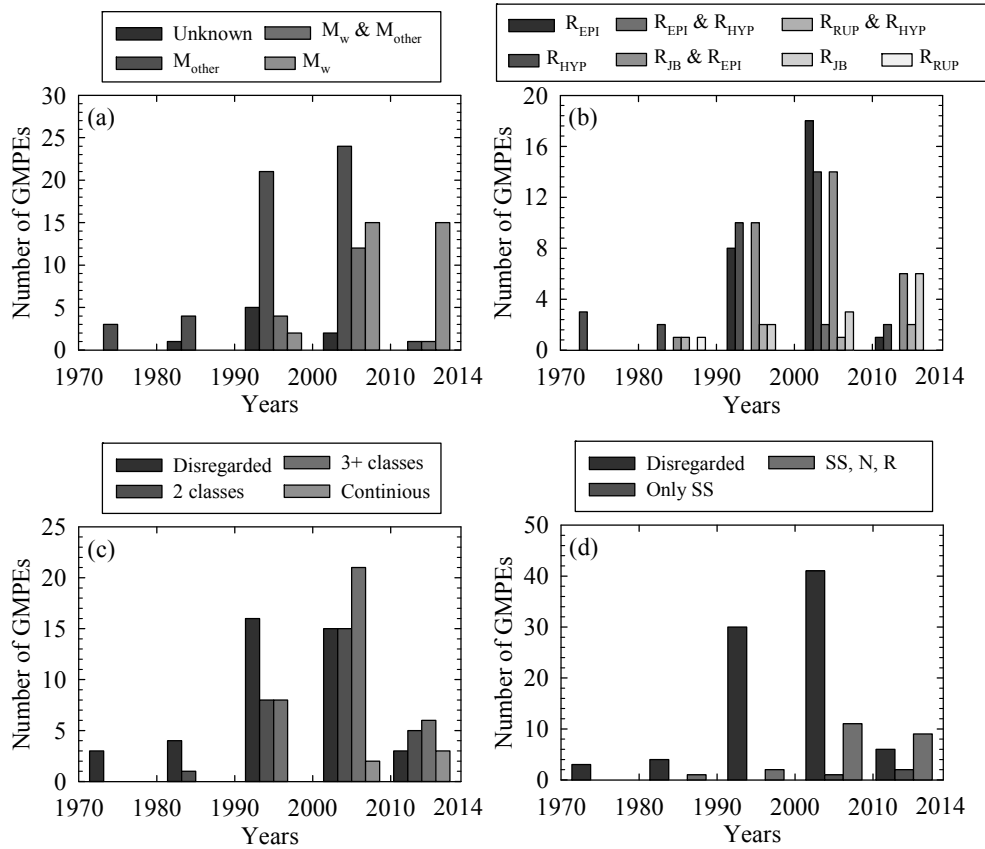
Figure 1.9 Statistics on (a) preferred magnitude scaling, (b) preferred distance measure, (c) consideration of site conditions and (d) consideration of faulting type in GMPEs developed in the broader Europe. (Explanation of abbreviations in the legends: "Unknown" refers to GMPEs that do not indicate the type of magnitude in their functional forms, "M_w & M_{other}" indicates GMPEs combining moment magnitude and other magnitude scales in their functional forms, "M_{other}" stands for GMPEs that use magnitude scales other than M_w. GMPEs that combine epicentral and hypocentral distances in their functional forms are abbreviated as "R_{EPI} & R_{HYP}." "R_{JB} & R_{EPI}" and "R_{RUP} & R_{HYP}" are used to indicate GMPEs using epicentral and Joyner-Boore distances and hypocentral and rupture distances, respectively. "Disregarded" stands for functional forms ignoring either site classification or style-of-faulting, "2 classes" and "3+ classes" indicate functional forms considering 2 and 3 or more site classes, respectively. "Only SS" describes GMPEs that treat strike-slip fault mechanism separately in their functional forms and "SS, N, R" is the abbreviation for functional forms that consider the effect of strike-slip, normal and reverse faults on ground-motions).

The discussions in the above paragraphs suggest that the efforts to improve strong-motion databases in the broader Europe result in enhanced local and global European GMPEs. Figure 1.10 shows the country-based distribution of predictive models for shallow active crustal earthquakes in the region of interest. Seismic prone countries that are active in database compilation are also active in developing GMPEs. As we have already emphasized, GMPEs developed from country-based (local) and global (multiple country) datasets are one of the topics of discussion among the research community in Europe. The limitations in local strong-motion datasets due to uneven distribution of major estimator parameters as well as poor quality metadata and waveforms are the major arguments augmenting the doubts about the reliability of GMPEs developed from such datasets. However, systematic attempts to improve the national strong-motion databases as well as international projects that make use of these well-studied national databases have brought another insight to such discussions. This point is demonstrated in Figures 1.11 and 1.12. Figure 1.11 shows the median PGA estimates of local and pan-European GMPEs as a function of distance. The median PGA estimates are computed for a 90-degree dipping strike-slip earthquake of M_w 6. The selected moment magnitude approximates the central magnitude value of the strong-motion databases used in the development of predictive models compared in this study. The site considered for the fictitious earthquake scenario is assumed to be rock with $V_{S30} = 760$ m/s. The hypocentral depth is taken as 9.7 km. The likely effects of epistemic uncertainty on the subject discussions were intended to be reduced by limiting the comparisons to median ground estimations and by using the central magnitude of the databases of compared GMPEs.

The local (country-based) GMPEs are selected from Turkey and Italy as they provide the largest amount of shallow active crustal earthquake recordings to pan-European databases. The ground-motion predictive models representing Turkey are Akkar and Çağnan (2010) - AC10 and Kale et al. (2014) - KAAH14 (Turkey version). These two recent GMPEs were developed from different versions of strong-motion datasets of Turkey. In a similar manner, Saffari et al. (2012) - Sfr12

and Kale et al. (2014) - KAAH14 (Iran version) GMPEs are selected for Iran as their datasets represent the progressive improvements of strong-motion data quality in Iran in recent years. The pan-European GMPEs used in the comparative plots [Ambraseys et al., 1996 (Amb96); Ambraseys et al., 2005 (Amb05); Akkar and Bommer, 2010 (AB10); Akkar et al., 2014 (ASB14) and Bindi et al., 2014 (Bnd14)] are among the best representatives of global European models at the time when they were developed. The horizontal component definition is geometric mean (GM) in the comparative plots. If any one of the above predictive models is originally developed for a different horizontal component definition, The Beyer and Bommer (2006) empirical relationships were used for its modification to GM. The geometry of fictitious fault were also used to utilize each GMPE with its original distance metric. However, the use of Joyner-Boore distance (R_{JB}) in the plots were preferred because the distance measure of most of the selected GMPEs for comparison is R_{JB}.
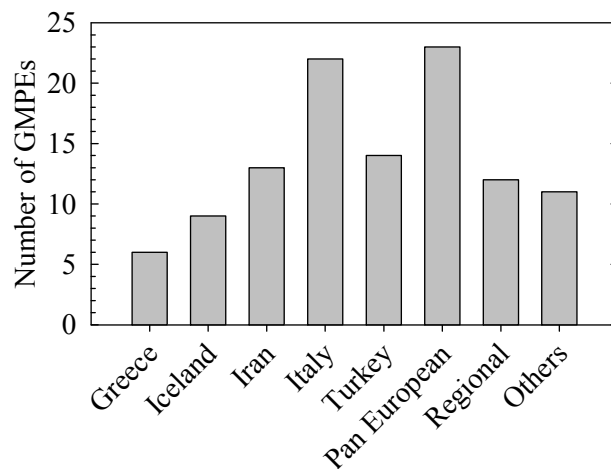
Figure 1.10 Country-based distribution of GMPEs that are developed in the broader Europe. "Regional" GMPEs are developed from databases of specific regions in and around Europe (e.g., northern Italy, western Balkans, etc.). The label "Others" indicate GMPEs of European countries that are not listed on the horizontal axis of the figure (e.g., France, Switzerland, etc.). The "Pan European" class refers to global GMPEs developed for Europe and surroundings by using strong-motion recordings of multiple countries in and around Europe.

The median PGA curves in Figure 1.11 depict that the Turkish GMPEs follow each other closely for M_w 6. Similar behaviors were observed within the Iranian and pan-European GMPEs. The distance-dependent PGA amplitudes of Turkish GMPEs are different than those computed from the Iranian and pan-European GMPEs. In a similar fashion, the PGA amplitudes of Iranian and pan-European GMPEs show discrepancies with respect to those obtained from the Turkish GMPEs. These observations can indicate the existence of regional differences that is verified by another set of comparisons in Figure 1.12.

The upper row panels in Figure 1.12 compare the median PGA estimates from Turkish (left panel) and Iranian (right panel) GMPEs with the upper and lower bound PGA estimates of pan-European GMPEs (represented as the gray shaded area in the panels). Note that the earthquake scenario and predictive models in Figure 1.12 are same as in Figure 1.11. The upper and lower bound PGA estimates of pan-European GMPEs are also compared with those predicted from the NGA-West1 and NGA-West2 GMPEs (bottom panel of Figure 1.12). The NGA-West1 GMPEs used in the comparative plots are Abrahamson and Silva (2008) - AS08, Boore and Atkinson (2008) - BA08, Campbell and Bozorgnia (2008) - CB08 and Chiou and Youngs (2008) - CY08. Abrahamson et al. (2014) - ASK14, Boore et al. (2014) - BSSA14, Campbell and Bozorgnia (2014) - CB14 and Chiou and Youngs (2014) - CY14 are the NGA-West2 GMPEs (successors of NGA-West1). The comparisons point differences in the median PGA estimates between local (pan-European) vs. global (pan-European) and global (pan-European) vs. global (NGA) GMPEs. The level of differences varies as a function of distance. The differences between the local and global GMPE estimates can be interpreted as the significance of regional effects that should be accounted for while developing consistent predictive models in broader Europe. The discrepancy between the global NGA and pan-European GMPEs advocate the implementation of a similar strategy while estimating the ground-motion amplitudes in the SACRs of broader Europe and the other parts the world. It is noted that the remarks highlighted from these comparisons should be augmented by further statistical tests to reach more

conclusive results about the indicatives of regional differences in micro and macro scale.
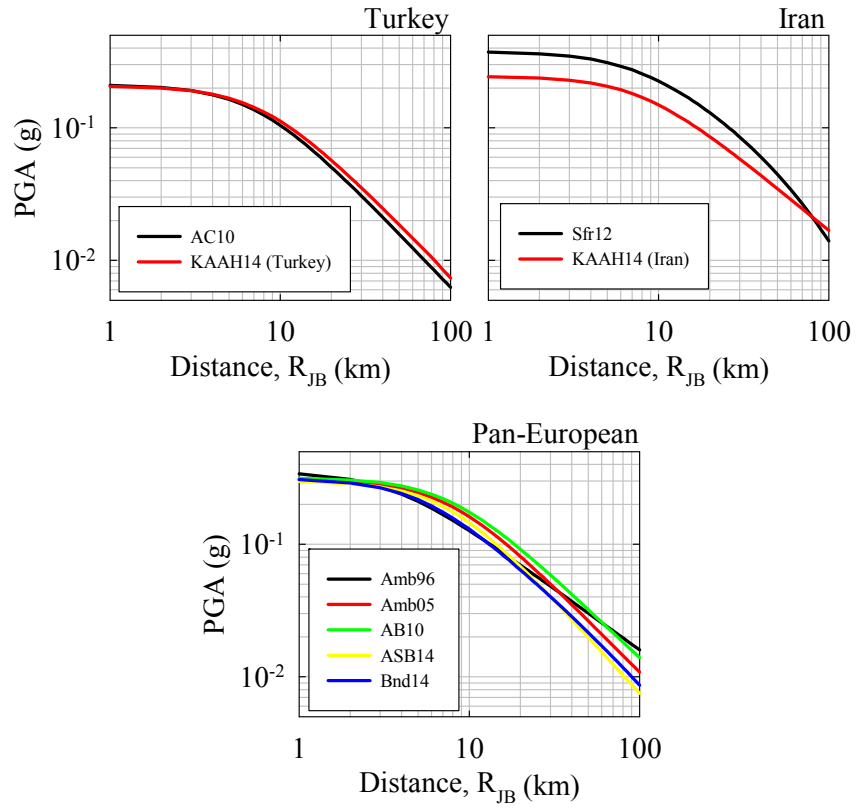
Figure 1.11 Median PGA trends of some selected Turkish, Italian and pan European GMPEs for M_w 6 and for a generic rock site.
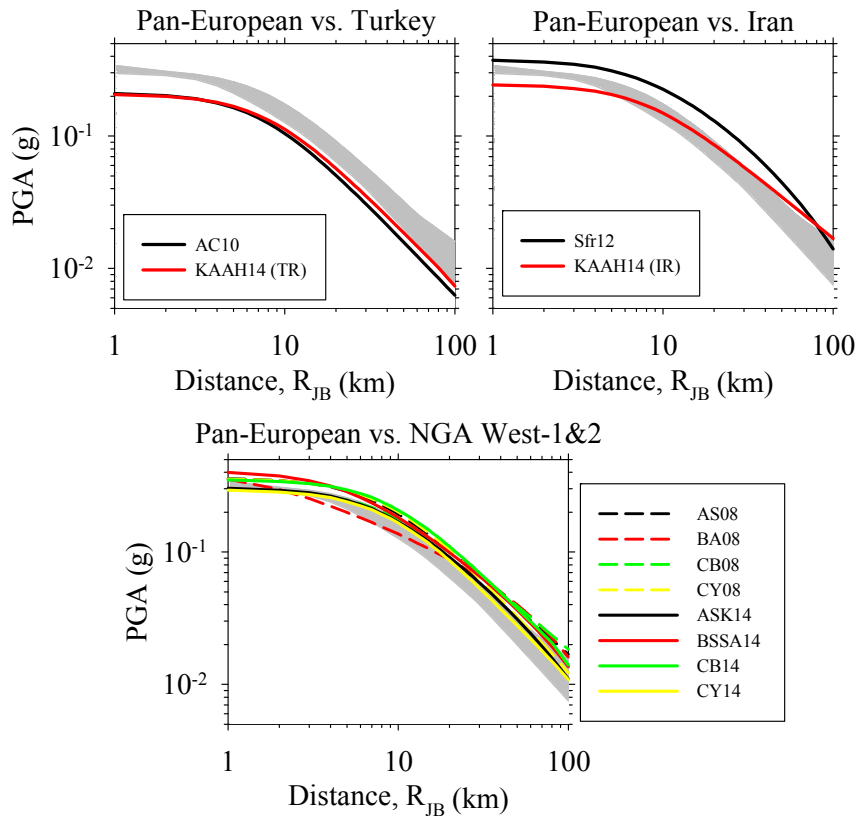
Figure 1.12 Comparisons of Turkish, Italian as well as NGA-West1 and NGA-West2 GMPEs with pan-European predictive models for the earthquake scenario given in Figure 1.11.

1.4. Implications of Using Local and Global GMPEs from Broader Europe in Seismic Hazard

The discussions in the previous section that show the differences between recent local and global GMPEs are deliberately based on a single earthquake scenario (M_w 6; central magnitude) and for median PGA. The selected earthquake scenario and comparisons on median ground-motion estimates would be a first-order approximation to give a clear idea on the level of discrepancies between the considered local and global GMPEs. However, they will fail to give an overall picture to understand how these differences would map onto probabilistic seismic hazard assessment of locations. Thus, using the same local and global pan-

European GMPEs of the previous case study, the PSHA results of two specific locations featuring different seismic patterns are presented. Such locations are common in the broader Europe. It is noted that running PSHA would show the influence of GMPE sigma and magnitude interval on the estimated ground motions for a given exceedance probability. Moreover, as the local and global European GMPEs discussed in the previous section are frequently used in Europe, the presented PSHA results would be the realistic indicators of how and when the local and pan-European GMPEs would differ from each other as a function of annual exceedance rate and for varying levels of seismicity. The PSHA results of NGA-West2 GMPEs were also included into the comparisons to augment the discussions for the ground-motion estimates between global European and non-European GMPEs. In essence, these case studies will convey a more complete but at the same time more complicated picture about the effects of using local and global European GMPEs on seismic hazard assessment in the broader Europe.

The PSHA case studies not only focus on PGA but also consider pseudo elastic spectral acceleration (PSA) at T = 0.2s, T = 1.0s and T = 2.0s for a broader view about the topic of discussion. PGA is currently the anchor spectral ordinate to describe design ground-motion demand in Eurocode 8 (CEN, 2004) whereas the US codes (ASCE, 2010) use spectral accelerations at T = 0.2s and T = 1.0s for design spectrum. PSA at T = 2.0s would show the estimated seismic hazard trends for local and global European GMPEs towards long-period spectral ordinates. Figure 1.13 shows the layouts of two locations used in the PSHA case studies. The location on the left panel is in the vicinity of active faults with significant seismicity. The seismic source pattern is complicated. The activity of seismic sources on the right panel is moderate and the configuration of seismic sources is simpler.

These sites (regions) were categorized as high seismicity (left panel) and moderate seismicity (right panel). Table 1.2 lists the seismic source parameters and their corresponding values used in PSHA modeling. The seismic source characterization

is compiled from different studies in the literature for the locations of interest and they are within the acceptable ranges to reflect the target seismicity level for each study region.
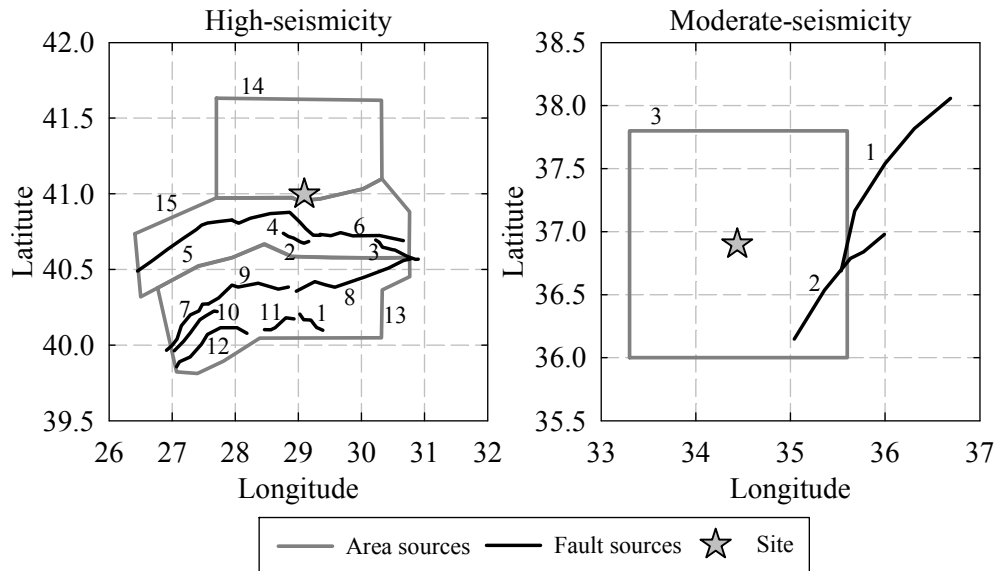
Figure 1.13 High-seismicity (left panel) and moderate-seismicity (right panel) sites and corresponding seismic source layouts used in the PSHA case studies.

Table 1.2 Seismic source parameters used in the PSHA modeling of high-seismicity and moderate-seismicity sites.

	Source ID	Type*- Dip Angle	B	$\dot{S}$ (mm/yr)*	$v_{M\min}$**	M_{min}	M_{max}
Moderate Seismicity	1	Strike slip-90°	0.	2.0	-	6.2	6.8
	2	Strike slip-90°	0.	6.0	-	7.0	7.5
	3	Area (Strike slip)	2.28	-	1.52	4.0	5.9
High Seismicity	1	Strike slip-90°	0.	3.0	-	6.5	7.0
	2	Normal-60°	0.	18.5	-	6.5	7.0
	3	Strike slip-90°	0.	24.0	-	6.5	7.2
	4	Strike slip-90°	0.	24.0	-	6.5	7.5
	5	Strike slip-90°	0.	24.0	-	6.5	7.5
	6	Strike slip-90°	0.	24.0	-	6.5	7.5
	7	Strike slip-90°	0.	3.0	-	6.5	7.2
	8	Strike slip-90°	0.	6.0	-	6.5	7.5
	9	Strike slip-90°	0.	4.5	-	6.5	7.5
	10	Strike slip-90°	0.	3.0	-	6.5	7.5
	11	Strike slip-90°	0.	3.0	-	6.5	7.0
	12	Strike slip-90°	0.	3.0	-	6.5	7.2
	13	Area (Strike slip)	2.03	-	2.08	4.0	6.4
	14	Area (Strike slip)	1.44	-	0.243	4.0	6.4
	15	Area (Strike slip)	1.86	-	2.34	4.0	6.4

* Used for estimation of $v_{M\min}$ for line sources.

** Estimated annual frequency of earthquake magnitudes greater than M_{min}.

Figure 1.14 displays the comparisons of moderate-seismicity hazard curves between Turkish vs. pan-European GMPEs (Figure 1.14.a) and Turkish vs. NGA-West2 GMPEs (Figure 1.14.b). Figure 1.15 displays the same comparisons for the high-seismicity region. The gray shaded areas in these figures display the upper and lower limits of hazard curves computed from the selected Turkish GMPEs (AC10 and KAAH14 - Turkey). The comparative plots for moderate seismicity (Figure 1.14) depict that both pan-European and NGA-West2 GMPEs tend to overestimate very short and short period spectral ordinates (i.e., PGA and PSA at T = 0.2s) with respect to Turkish GMPEs. The NGA-West2 GMPEs start to estimate

lesser ground motions towards longer periods whereas the pan-European and Turkish models yield similar spectral accelerations for longer periods (i.e., T = 1.0s and T = 2.0s). The pan-European GMPEs yield larger spectral values when compared to Turkish GMPEs for the high-seismicity site (Figure 1.15) for the whole spectral ordinates considered in this study. The hazard trends between the Turkish and NGA-West2 GMPEs in the high-seismicity region show similarities with those of Figure 1.14.b (i.e., moderate seismicity case). However, the hazard estimates of these two sets of predictive models (i.e., NGA-West2 and Turkish GMPEs) are closer to each other for the high-seismicity case. The discrepancy between the Turkish and global GMPEs (both European and non-European) increases with decreasing annual exceedance rates in most cases.
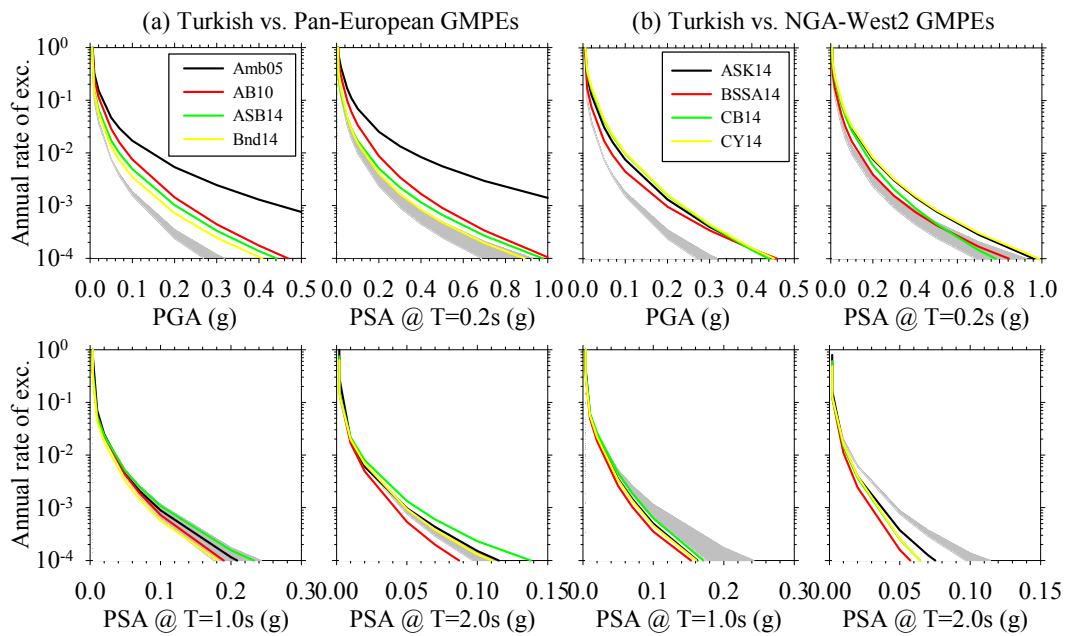
Figure 1.14 Comparisons of hazard curves for PGA, PSA at T = 0.2s, T = 1.0s and T = 2.0s between (a) Turkish vs. pan-European GMPEs and (b) Turkish vs. NGA-West2 GMPEs for the chosen moderate-seismicity region.

28
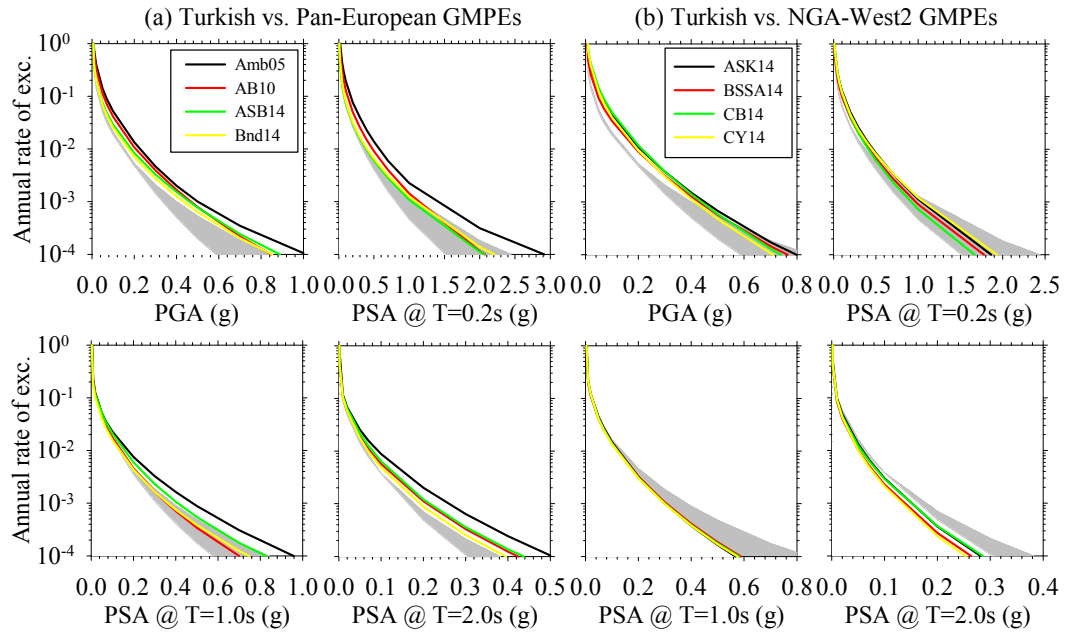
Figure 1.15 Comparisons of hazard curves for PGA, PSA at T = 0.2s, T = 1.0s and T = 2.0s between (a) Turkish vs. pan-European GMPEs and (b) Turkish vs. NGA-West2 GMPEs for the chosen high-seismicity region.

Figures 1.16 and 1.17 make similar comparisons as of Figures 1.14 and 1.15, respectively, for Iranian vs. pan-European and Iranian vs. NGA-West2 ground-motion equations. Sfr12 and KAAH14 (Iran) models are used as the Iranian GMPEs because they are developed from the latest versions of the Iranian ground-motion datasets. The comparisons in Figures 1.16.a and 1.16.b suggest that the pan-European GMPEs for entire period range and NGA-West2 models for PGA yield similar spectral accelerations with Iranian GMPEs. The only exception to this observation for PGA and T = 0.2s is the Amb05 pan-European model that yields significantly different acceleration values with respect to the rest of the GMPEs[7]. The NGA-West2 GMPEs tend to underestimate with respect to Iranian GMPEs towards short-to-longer period spectral acceleration values (i.e., T = 0.2s, T = 1.0s and T = 2.0s). The level of underestimation is more significant for spectral

---

[7] The magnitude-dependent standard deviation of Amb05 attains very large values at small magnitudes that govern the moderate-seismicity case. Although we did not explore the computed hazard results in great detail, it is believed that the large sigma of Amb05 at small magnitudes is the major reason behind the inflated short and very-short period PSA by this GMPE.

acceleration at T = 2.0s. It is noted that the general trends summarized in Figure 1.16 are fairly valid for Figure 1.17 as well.

The last comparative plots in this section show the differences between the hazard estimates of pan-European, NGA-West1 and NGA-West2 GMPEs. The format and order of the comparative plots follow the previous figures. Figure 1.18 compares the NGA-West1 (Figure 1.18.a) and NGA-West2 (Figure 1.18.b) predictive models with the pan-European GMPEs for moderate-seismicity case. Figure 1.19 does the same comparison for high-seismicity. The shaded areas in these plots represent the upper and lower limits of hazard curves computed from the pan-European GMPEs. The comparisons in these figures indicate that NGA models yield smaller spectral accelerations with respect to pan-European GMPEs. The underestimations are generally more pronounced for NGA-West2 GMPEs. The discrepancy between the European and non-European global GMPEs increases with decreasing annual exceedance rates. This observation is more notable towards longer period spectral accelerations. The underestimations between these two groups of predictive models are also more definite in the high-seismicity case (Figure 1.19).

The overall discussions in this section indicate that there are differences between the hazard estimates of local and global GMPEs developed from the ground-motion sets of broader Europe. The discrepancies depend on the level of seismicity and spectral period. They are generally significant with decreasing annual exceedance rates (i.e., less frequent but at the same time more critical earthquakes). Note that the local and global GMPEs employed in these case studies are recent and they are developed from reliable local and global databases of pan-European region. To this end, the highlighted observations from these case studies may partially point the consequential effect of regional differences on seismic hazard.
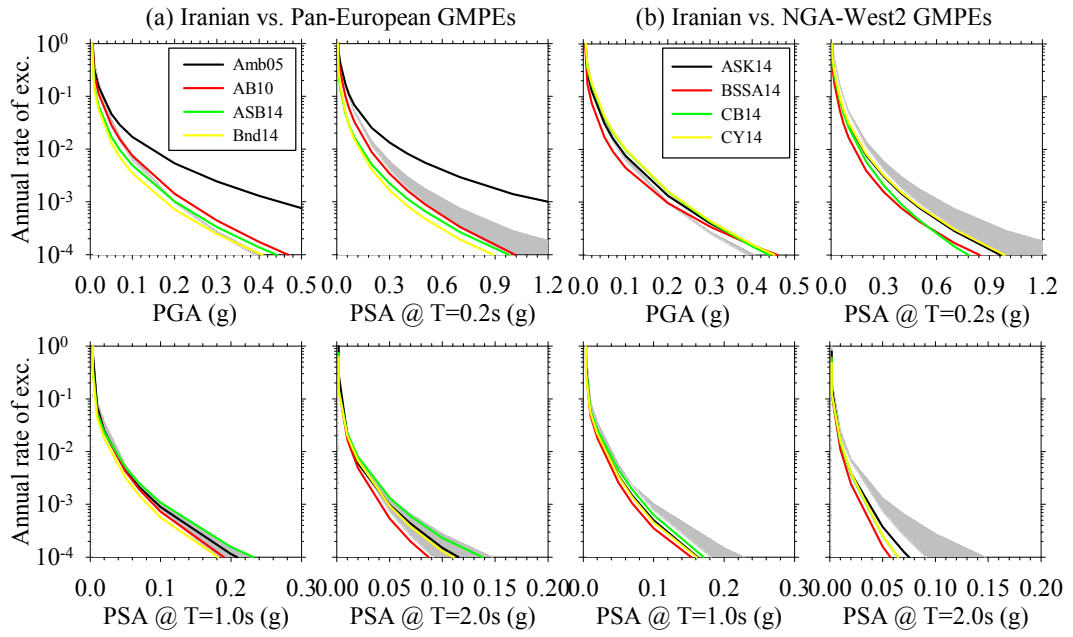
Figure 1.16 Same as Figure 1.14 but the comparisons are between (a) Italian vs. pan-European GMPEs and (b) Italian vs. NGA-West2 GMPEs for moderate seismicity.
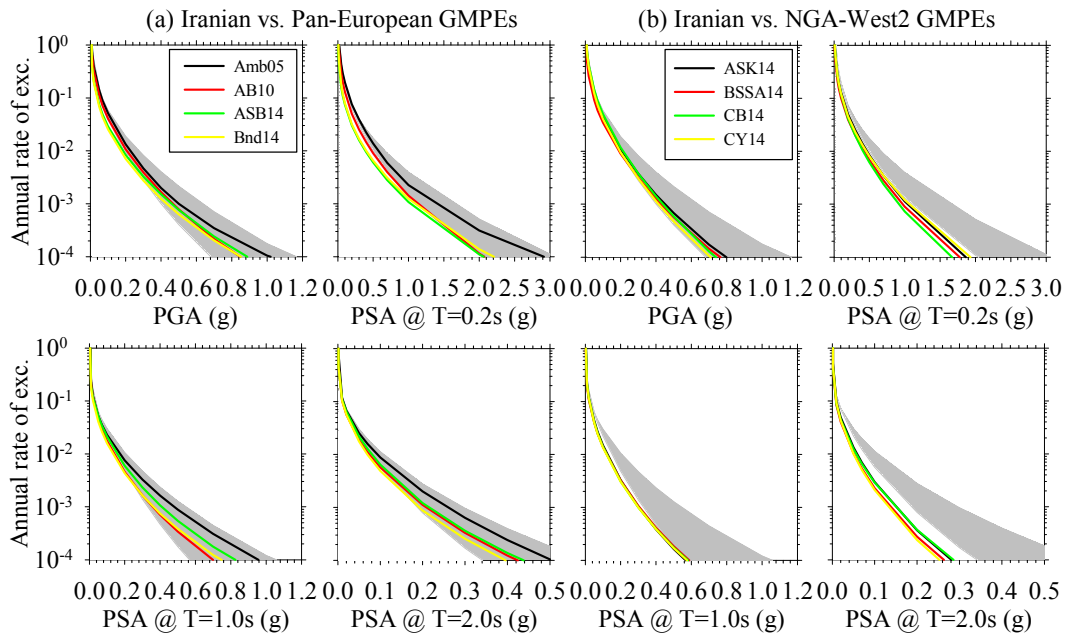
Figure 1.17 Same as Figure 1.15 but the comparisons are between (a) Italian vs. pan-European GMPEs and (b) Italian vs. NGA-West2 GMPEs for high-seismicity case.
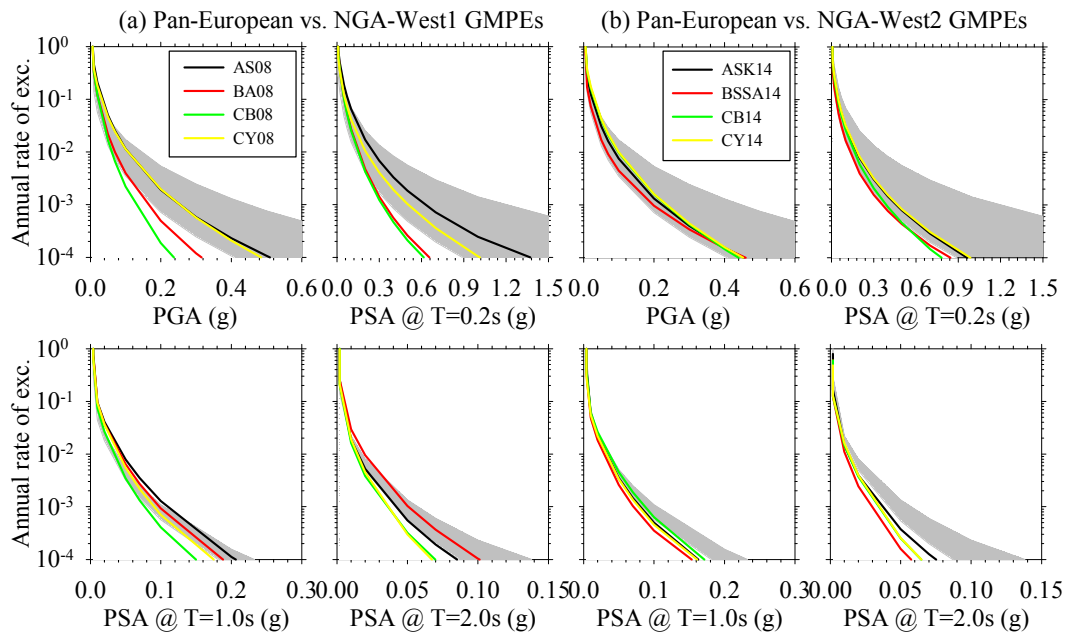
Figure 1.18 Same as Figures 1.14 and 1.16 but comparisons are between (a) NGA-West1 vs. pan-European GMPEs and (b) NGA-West2 vs. pan-European GMPEs for moderate-seismicity region.
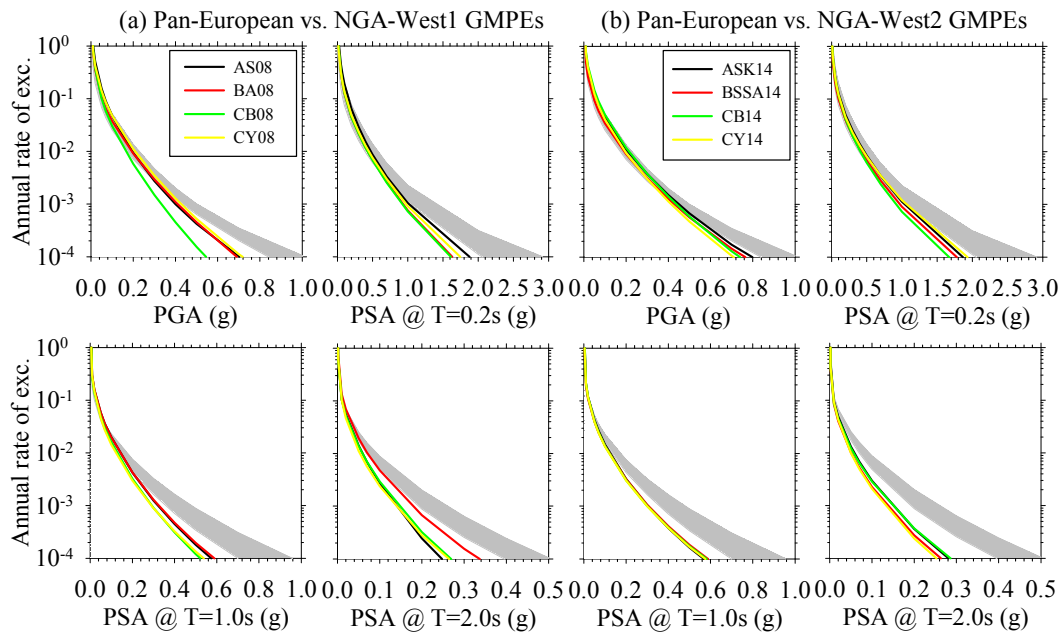
Figure 1.19 Same as Figures 1.15 and 1.17 but comparisons are between (a) NGA-West1 vs. pan-European GMPEs and (b) NGA-West2 vs. pan-European GMPEs for high-seismicity region.

1.5. General Comments

The evolution of accelerometric databases and GMPEs for SACRs in the broader Europe is summarized. The progress in these fields is quite significant in Europe in the last decade due to national and international research support. While presenting the major local and global GMPEs developed during this period, the differences in the estimated ground motions are emphasized although these predictive models are derived from the fairly reliable databases of shallow active crustal earthquakes occurred in and around Europe. The comparisons also indicate the existence of such differences between non-European (NGA) and European global as well as local GMPEs. Some part of the observed discrepancies between these ground-motion models can be the attributes of regional differences. This observation should be verified in a detailed manner because the observations are limited. Nevertheless, the hazard expert should be aware of the existence of such differences among the local and global GMPEs and should consider a proper set of GMPEs that are capable of representing model uncertainty and earthquake variability for the region (site) of interest. This can only be achieved by collecting and studying the reliable strong-motion recordings of the same region. This type of comprehensive study can be done via reliable pan-European strong-motion data archives. Currently, there are serious efforts among the European research community to establish a good infrastructure for such a long-term and integrated accelerometric data archive within the broader Europe. This endeavor is evolving under Orfeus (Observatories and Research Facilities for European Seismology; http://www.orfeus-eu.org/) in a systematic manner. Upon the success of this attempt, it is believed that more refined GMPEs will be developed for the broader Europe that properly accounts for the regional effects. Such predictive models would certainly increase the accuracy of seismic hazard assessment in Europe and surroundings.

1.6. Outline of the Thesis

This dissertation is organized into seven chapters. The first chapter summarizes the evolution of major strong-motion databases and ground-motion prediction equations (GMPEs) for shallow active crustal regions (SACRs) in Europe and surrounding regions. It also presents some case studies to show the sensitivity of hazard results at different seismicity levels for local (developed from country-specific databases) and global (based on databases of multiple countries) GMPEs of the same region. This chapter ends with describing the outline of the thesis.

Chapter 2 describes the recently developed Middle East and Turkish strong-motion databases serving for predictive model selection processes and their seismological features. The last section of this chapter compares the databases of recent Turkish ground-motion models with the latest version of Turkish strong-motion database.

Chapter 3 starts with an overview of the Turkish and Iranian GMPEs with emphasis on their limitations. Later, the new predictive relations for 5% damped horizontal component are introduced. These equations are applicable to extended-source distance metrics. This chapter ends by testing the limitations of the prediction equations and comparing them with the global, regional and local GMPEs.

Chapter 4 summarizes a new procedure for selection and ranking of GMPEs which can be useful for regional or site-specific probabilistic seismic hazard assessment (PSHA). The proposed method is called as Euclidean-Distance Based Ranking (EDR) because it modifies the Euclidean distance concept for ranking of GMPEs under a given set of observed data. The chapter ends with a case study indicated that separate consideration of ground-motion uncertainty (aleatory variability) and model bias or their combination can change the ranking of GMPEs.

Chapter 5 firstly discusses handling the epistemic uncertainty in probabilistic seismic hazard assessment. Later a new tool is proposed to suitably capture the epistemic uncertainty in seismic hazard studies by evaluating the performances of alternative logic-tree frameworks. It ends conducting a set of case studies to illustrate the application of the proposed logic-tree tool considering a region located along a part of the North Anatolian Fault zone

Chapter 6 presents the establishment of the final ground-motion logic-tree framework for the hazard computations of shallow active crustal regions in EMME region extending from Turkey to Pakistan. Within the context of the first part, the pre-selected candidate ground-motion models are tested under the EMME database considering data-driven testing methods. Then, the best performing GMPEs are evaluated thanks to trellis charts for representative earthquake scenarios. Finally, the EMME logic-tree framework is established by conducting the logic-tree based sensitivity analyses to the selected regions from Turkey.

The last Chapter terminates the dissertation by summarizing the main findings of the work presented herein and provides recommendations regarding future research on the related topics.

CHAPTER 2

STRONG-MOTION DATABASES

This chapter gives information about the compilation and improvements of strong-motion databases with emphasis on selection and testing of the ground-motion prediction equations (GMPEs) for the Middle East region and Turkey. In addition, the model-developing databases of some principal Turkish local GMPEs are evaluated by utilizing the latest version of the Turkish database to reflect the importance of strong-motion database related studies. The first part of this chapter identifies the compilation steps of EMME (**E**arthquake **M**odel of the **M**iddle **E**ast Region) strong-motion databank and describes its major features by illustrative plots. Armenia, Georgia, Iran, Jordan, Pakistan and Turkey are the main participants of the EMME project. In the second part, the primary characteristics of an extended strong ground-motion database which is compiled within the framework of the Updating the Seismic Hazard Map of Turkey (TSTHG) project is introduced. The database consists of the accelerograms gathered from the EMME (Turkish recordings), RESORCE (Reference Database for Seismic Ground-Motion in Europe; Akkar et al., 2014; Italian and Greek recordings) and NGA-West2 (Ancheta et al., 2014; Californian recordings) projects. This part is followed by the comparisons with respect to available catalog information such as magnitude, hypocentral depth, distance etc. between model-developing datasets of the most preferable Turkish GMPEs (Özbey et al., 2004; Kalkan and Gülkan, 2004; Akkar and Çağnan, 2010; Kale et al., 2014) and the updated version of the Turkish strong-motion database obtained in the previous step. This chapter of the dissertation finishes by the comments on the further improvement strategies of the current conditions of strong-motion databases.

2.1. EMME Strong-motion Database

An extended ground-motion database for the Middle East Region covering Caucasus (Georgia and Armenia), Iran, Jordan, Pakistan and Turkey is assembled to serve for predictive model selection, generating new GMPEs and using in further strong-motion related studies in EMME (**E**arthquake **M**odel of the **M**iddle **E**ast Region; http://emme-gem.org/index.php) project. The EMME strong-motion database is principally composed of the accelerograms of Turkey and Iran that are the two important accelerometric data providers in the region. Additional data with reliable seismological information (magnitude, distance, style-of-faulting, site class, etc.) from the other project Partners is also included as part of the strong-motion database.

2.1.1. Compilation of the Accelerometric Data Archive

The EMME accelerometric database is a collection of strong-motion accelerograms coming from Caucasus (Georgia and Armenia), Iran, Jordan, Pakistan and Turkey. The sources of the strong-motion accelerograms in the database are local seismological agencies, local projects and recently compiled global databanks.

The EMME database comprises of two stages which are raw and revised forms of the database. The raw form of the database includes all acceleration time series coming from each country in EMME project without consideration of any limitation. The raw form of the database comprises of 3713 multi-component accelerograms from the regions of Turkey (320 recordings), Iran (3117 recordings), Caucasus (142 recordings), Pakistan (106 recordings) and Jordan (28 recordings). Iran provides a significant amount of data in this form of the database. The accelerograms coming from RESORCE (Reference Database for Seismic Ground-Motion in Europe; 1426 for Turkey, 35 for Iran and 27 for Caucasus) are not included in the raw form of the database as RESORCE recordings are directly entered to the revised database since they already passed the main steps of

evaluation process in SIGMA (**SeI**smic **G**round **M**otion **A**ssessment; http://projet-sigma.com/index.html) project.

The revised form of the database is the refined version of the raw database and is going to serve for predictive model selection process. The refinement process has two main stages which are catalog- and record-based evaluations. In the catalog-based evaluation stage, the accelerograms are investigated in terms of a) availability of event, record and station information (i.e., epicentral coordinates, moment magnitude, hypocentral depth, style-of-faulting, fault rupture dimensions or fault-plane solutions, station coordinates and site class), b) pre-defined magnitude and distance limits ($M_w \geq 4.0$ and $0km \leq R_{JB} \leq 200km$). The strong-motion accelerograms that do not satisfy the above catalog information and prerequisites are not incorporated into the revised EMME strong-motion database. In the record-based evaluation stage, poor quality recordings, duplicated records between different accelerometric data sources and existence of both horizontal components are investigated. This form of the database includes only horizontal components of the recordings by considering the requirements of predictive model selection process. The poor quality recordings in the database are detected by considering the proposals of Douglas (2003). The recordings which classified as in poor quality or duplicated and do not have both horizontal components are excluded from the database.

Resultantly, the acceleration time series that satisfy and pass the above prerequisites and quality checks comprise the revised EMME strong-motion database (here-after referred to as EMME SMD). In essence, decomposition of the EMME SMD is illustrated in Figure 2.1 in terms of countries and sources of the strong-motion data. In Table 2.1, the sources mentioned with their acronyms in Figure 2.1 are described in terms of their full names and their reference information. The following sections describe the general aspects of catalog- and record-based evaluation stages.
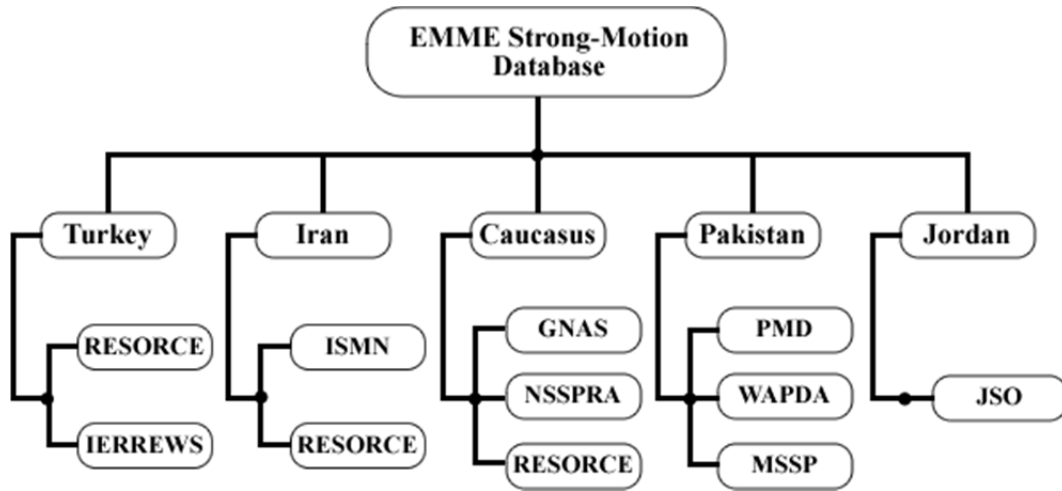
Figure 2.1 Node structure of the strong-motion accelerograms in EMME database.

Table 2.1 Descriptions of the accelerometric data providers given in Figure 2.1.

Acronyms of the Sources	Full Names of the Sources	Website References of the Sources	Paper References of the Sources
GNAS	Georgian National Academy of Sciences	http://www.science.org.ge/english.html	-
IERREWS	Istanbul Earthquake Rapid Response and Early Warning System	http://www.koeri.boun.edu.tr/sismo/default.htm	Erdik et al. (2003) Harmandar (2009)
ISMN	Iran Strong Motion Network	http://www.bhrc.ac.ir/portal/Default.aspx?tabid =635	-
JSO	Jordan Seismological Observatory	http://www.nra.gov.jo/index.php?option=com_ content&task=view&id=83&Itemid=122	-
MSSP	Micro Seismic Study Project under Pakistan Atomic Energy Commission	http://www.paec.gov.pk	-
NSSPRA	National Survey for Seismic Protection under the Government of the Republic of Armenia	http://www.adrc.asia/highlights/041/nsspra.htm	-
PMD	Pakistan Meteorological Department	http://www.pmd.gov.pk/	-
RESORCE	Reference database for seismic ground-motion in Europe	http://www.projet-sigma.com/index.html	Akkar et al. (2014)
WAPDA	Pakistan Water and Power Development Authority	http://www.wapda.gov.pk/htmls/auth-index.html	-

2.1.2. Catalog-Based Evaluation Stage of EMME SMD

The context of this part would be divided into three main groups as compilation of a) event information, b) station information and c) record information. The event information of the database consists of gathering the epicentral coordinates, moment magnitude, hypocentral depth, style-of-faulting, fault rupture dimensions and double-couple fault-plane solutions. The station information composes of locations of the stations in terms of latitude and longitude and site classes of the stations in terms of measured or estimated V_{S30} (average shear wave velocity in the upper 30m of the soil profile). Tables 2, 3 and 5 list the reference sources for event information, fault plane solutions and station information, respectively. In the light of the combined event and station information, the distance parameters of the strong-motion recordings (i.e., record information) are obtained.

RESORCE and WP-1 catalog of EMME project (Zare et al., 2014) are considered as the principal sources of the event information for the entire earthquakes in the database. RESORCE which regards the earthquake-specific literature studies are primary source for earthquake metadata. The other source, WP-1 catalog (Zare et al., 2014), collects metadata information considering all reliable references which are published in peer-reviewed journals and seismological agencies. That is, the information included in these catalogs is accepted by the seismological community. However, epicentral location and hypocentral depth information of some of the events (generally significant earthquakes) coming from those references are updated with respect to the EHB bulletin which is considered to provide most reliable event information. The event information which does not exist in RESORCE and WP-1 catalog is collected from the global and local seismic agencies listed in Table 2.2.

Table 2.2 Major reference sources considered in the compilation of event information.

Acronyms of the Sources	Full Names of the Sources	References of the Sources
RESORCE	Reference database for seismic ground-motion in Europe	Akkar et al. (2014)
WP-1 catalog	EMME Earthquake Catalog work package	Zare et al. (2014)
EHB	International Seismological Centre	http://www.isc.ac.uk/ehbbulletin/search/catalogue/
ISC	International Seismological Centre	http://www.isc.ac.uk/iscbulletin/search/catalogue/
NEIC	USGS National Earthquake Information Center	http://earthquake.usgs.gov/regional/neic/
GCMT	Global Centroid Moment Tensor Catalog Search	www.globalcmt.org
Local agencies	-	Table 2.1

In the current applications of the predictive models, the main estimator parameters are moment magnitude (M_w), extended-source distance metrics (R_{JB}: closest distance to the surface projection of the fault rupture; R_{RUP}: closest distance to the fault rupture), style-of-faulting and site classes based on V_{S30}. Accordingly, fault rupture dimensions which are broadly available for significant earthquakes and used to calculate the extended-source distance measures, and double-couple fault-plane solutions which are considered to calculate extended-source distance measures and determine the style-of-faulting of the considered earthquake are significantly improve the metadata quality of a strong-motion catalog. The primary source for these types of catalog parameters is the RESORCE. Furthermore, seismological agencies and projects listed in Table 2.3 and Ghasemi et al. (2009) which provides information for significant Iranian earthquakes also contribute an invaluable data to this part of the EMME strong-motion catalog. Double-couple fault-plane solutions include strike, dip and rake angles of both correct and auxiliary planes. The correct planes for most of the Turkish and Caucasian, and all of the Iranian and Jordanian events in the database are elicited by the local experts whereas the rest of the events (approximately 5%) have both the correct and auxiliary planes. In the light of the collected fault plane solutions, the style-of-

faulting classifications of the events are done with respect to the procedure proposed in Boore and Atkinson (2007) in which the T- and P-axes plunge angles calculated from the strike, dip and rake angles of the double-couple fault-plane solutions (Snoke, 2003) are used to obtain a homogenous catalog in terms of fault mechanisms. The style-of-faulting criteria proposed in Boore and Atkinson (2007) is tabulated in Table 2.4.

Table 2.3 Major reference sources considered in the compilation of fault rupture dimensions and double-couple fault plane solutions.

Acronyms of the Sources	Full Names of the Sources	References of the Sources
RESORCE	Reference database for seismic ground-motion in Europe	Akkar et al. (2014)
GCMT	Global Centroid Moment Tensor Catalog Search	www.globalcmt.org
Ghs09	Ghasemi et al. (2009)	Ghasemi et al. (2009)
NEMC	National Earthquake Monitoring Center	http://www.koeri.boun.edu.tr/sismo/default.htm
SED	The Swiss Seismological Service	http://www.seismo.ethz.ch/index
WSM	World Stress Map Project	http://dc-app3-14.gfz-potsdam.de/
JSO	Jordan Seismological Observatory	http://www.nra.gov.jo/index.php?option=com_content&task=view&id=83&Itemid=122

Table 2.4 Plunge angles based classification of style-of-faulting criteria.

Style-of-faulting	P-axis plunge angle	T-axis plunge angle
Normal	P-pl>40	T-pl<40
Reverse	P-pl<40	T-pl>40
Strike-slip	P-pl<40	T-pl<40

Table 2.5 summarizes the station information of the EMME SMD in terms of number of stations with unknown (NA), estimated (Est) and measured (Mea) V_{S30}-based site classes and sources of the station metadata. For the sites without V_{S30} but with geological estimations, V_{S30} values of 255m/s, 520m/s and 800m/s are assigned to soft, stiff and rock site condition stations, respectively. The locations of

the strong-motion stations are taken from the national seismological agencies, relevant projects and literature studies listed in Table 2.5. Turkey and Iran have a significant number of stations with measured V_{S30} values whereas the site characterizations of most of the stations in Caucasus and all of the stations in Pakistan and Jordan are based on estimated site classes from geological maps and field observations.

Table 2.5 Major reference sources considered in the compilation of station information with country-based distribution of stations with respect to existence and type of V_{S30}. The full names of the sources are given in Table 1.

Country or Region	Sources	Paper References of the Sources	NA V_{S30}	Est V_{S30}	Mea V_{S30}	Total Station
Turkey	RESORCE IERREWS	Akkar et al. (2014), Sandıkkaya et al. (2010), Erdik et al. (2003), Harmandar (2009)	0	27	286	313
Iran	ISMN	Sinaiean et al. (2008; 2010a; 2010b) Farzanegan et al. (2010a; 2010b) Alavijeh et al. (2010)	565	5	340	910
Caucasus	GNAS NSSPRA	-	1	12	9	22
Pakistan	MSSP PMD WAPDA	-	0	8	0	8
Jordan	JSO	-	0	7	0	7

To entirely complete the metadata of EMME strong-motion database, point-source (R_{EPI}: epicentral distance; R_{HYP}: hypocentral distance) and extended source (R_{JB} and R_{RUP}) distance metrics are computed from the combination of event and station metadata. The existing source-to-site distance measures of the recordings extracting from RESORCE are used directly in the EMME SMD. These accelerograms constitute approximately 30% of the database. For rest of the strong-motion recordings in the database, the point- and extended-source distance measures are computed considering the approach given in Kaklamanos et al. (2011). In this approach, the fault rupture dimensions (length and width) that are included in the metadata or estimated from Wells and Coppersmith (1994) are used

assuming the nucleation point of the rupture is located at the center of the rupture surface. R_{JB} and R_{RUP} source-to-site distance metrics are computed directly for the recordings which have correct fault plane solutions whereas these distances are calculated for both correct and auxiliary planes and average of these distance pairs reported as resultant distance value. In fact, using the average value as a resultant distance metric is an assumption; nevertheless, a substantial percentage of the recordings of EMME database suffering from this issue are far-source accelerograms and small-to-moderate magnitude events. Therefore, considering the observations in Akkar et al. (2014), the averaging procedure is applied to the recordings in this database.

2.1.3. Record-Based Evaluation Stage of EMME SMD

The accelerograms coming from RESORCE and Iran are directly included to the database since they are processed by acausal band-pass filtering. However, Turkish IERREWS, Caucasian, Pakistani and Jordanian recordings are band-pass filtered with respect to the procedure explained below.

Before conducting filtering, the records are subjected to a pre-selection process due to duplicated records, nonstandard errors, digitization problems etc. In essence, before conducting the band-pass filtering procedure, the strong-motion accelerograms in the database are categorized in terms of waveform qualities as specified in Douglas (2003). The categorization of waveform qualities are based on: i) nonstandard errors: spike, ii) insufficient digitizer resolution (IDR), iii) multiple shocks (MS), iv) S-wave triggered (S-WT), v) early termination during coda and clipping of recordings. The accelerograms out of this categorization are band-pass filtered. Some of the recordings suffering from non-standard problems (accelerograms with spike, multiple shock or IDR) are also band-pass filtered after applying a special treatment. The rest of the strong-motion recordings are excluded from the scope of processing. The strong-motion record processing procedure that is applied in EMME can be summarized as:

- An initial baseline adjustment is applied to the records. The mean of 90% of the pre-event time is removed from entire accelerogram for digital recordings. For analog accelerograms, the mean of the entire record is removed from whole acceleration time series.

- Low-cut filter frequencies are selected from Fourier amplitude spectrum (FAS) for removing the long-period noise from the accelerogram. This procedure is explained in Akkar and Bommer (2006). The decision of low-cut filter frequency is important since they directly influence the usable spectral period range.

- High-cut filter frequencies are selected for the records that have a flat portion at the end of the FAS. If a flat portion is not detected from the FAS of a record, high-cut filtering is not applied. The high-cut filter cut-off selection criterion is based on Douglas and Boore (2011) and detailed information about the influence of high-cut filtering on spectral ordinates is given in Akkar et al. (2011).

- Accelerograms are processed with the selected low- and high-cut filter cut-offs. The chosen filtering type is a 4th order acausal Butterworth filter that requires zero pads at the beginning and end of the records.

The similar individual data processing scheme is applied to the recordings in RESORCE databank whereas Iranian scheme is not based on individual processing of accelerograms. The Iranian analysts implement an automatic correction procedure while they determine the low- and high-cut filter frequencies. In their procedure, once all analog records are band-pass filtered with 0.2Hz (low-cut frequency) and 20Hz (high-cut frequency), signal + noise to signal ratio calculated from Fourier Spectrum analysis is used to determine the filter cut-off frequencies. The details of their method can be summarized as:

- The pre-event portion of the record is determined from the beginning of the record to the starting time of strong motion.

- If the length of the pre-event segment is more than 5sec, it is considered as the representative of noise and corresponding signal + noise to signal ratio (S+N/S) is calculated from Fourier Spectrum analysis.

- The cut-off frequencies are determined as the frequencies where S+N/S > 3.0. The upper and lower limiting frequencies are 0.2Hz and 15Hz for low- and high-cut filter frequencies, respectively. A lower limit of 0.05Hz is also applied as low-cut filter cut-off. In essence the low-cut filter frequency is between 0.05Hz and 0.2Hz.

- If the length of pre-event is less than 5.0sec, the default values of 0.1Hz and 30Hz are used as low- and high-cut filter frequencies, respectively.

2.1.4. General Seismological Features of EMME SMD

The compilation steps of EMME SMD except for considering pre-defined magnitude and distance limitations result in gathering 4920 accelerograms (at least two horizontal components) from 1803 ground-motion events and 1260 strong-motion stations. The country-based distribution of these data in terms of main seismological features is summarized in Table 2.6. Turkey and Iran provide a significant amount of strong-motion data to the database. When the total number of accelerograms with Mw, hypocentral depth, style-of-faulting, V_{S30} and extended-source distance metrics (R_{JB} and R_{RUP}) are regarded, it is obvious that such an extensive strong-motion archive is of its first kind in the Middle East region. To test a set of candidate ground-motion prediction equations (GMPEs) for seismic hazard assessments in EMME region, a sub-database with known values of the main seismological parameters (i.e., M_w, depth, V_{S30}, style-of-faulting, point- and extended source distance metrics) is extracted from this form of the database by considering the pre-define limits of $M_w \geq 4.0$ and $0km \leq R_{JB} \leq 200km$.

Table 2.6 Strong-motion data distribution of EMME SMD.

Number of component types	Turkey	Iran	Caucasus	Pakistan	Jordan	EMME
Records	1738	2988	164	12	18	4920
Events	507	1222	58	4	12	1803
Stations	313	910	22	8	7	1260
Records with M_w M_w range	1738 4.0 - 7.6	2539 3.1 - 7.4	164 4.0 - 6.9	12 5.0 - 7.6	18 4.0 - 7.1	4471 3.1 - 7.6
Records with depth depth range (km)	1738 0 - 98	2550 0 - 133	164 0 - 34	12 8 - 33	18 1 - 32	4482 0 - 133
Records with style-of-faulting	1691	1405	111	12	18	3237
Records with V_{S30} V_{S30} range (m/s)	1738 146 -1598	1556 155 -1961	160 255 -1100	12 255 - 800	18 255 - 800	3484 146 -1961
R_{EPI} R_{EPI} range (km)	1738 2 - 586	2988 1 - 476	164 3 - 190	12 54 - 212	18 18 - 439	4920 1 - 586
R_{HYP} R_{HYP} range (km)	1738 5 - 587	2550 4 - 476	164 4 - 191	12 57 - 213	18 21 - 439	4482 4 - 587
R_{JB} R_{JB} range (km)	1190 0 - 547	1404 0 - 456	111 2 - 185	12 41 - 210	18 16 - 410	2735 0 - 547
R_{RUP} R_{RUP} range (km)	1176 0 - 548	1404 1 - 456	111 7 - 186	12 41 - 211	18 19 - 411	2721 0 - 548

The sub-database database serving for predictive model selection to EMME ground-motion logic-tree applications includes 1869 strong-motion accelerograms recorded from 418 earthquakes and 611 strong-motion stations. The database comprises of recordings from shallow active crustal regions of Turkey (1078 accelerograms), Iran (660 accelerograms), Caucasus (107 accelerograms), Pakistan (11 accelerograms) and Jordan (13 accelerograms). Figure 2.2 shows M_w vs. point- and extended-source distance metrics scatter plots of strong-motion recordings in terms of countries. The numeric information for the number of data corresponding to each country is denoted next to each legend in this figure. Figure 2.3 shows M_w vs. R_{JB} scatter plots of strong-motion recordings in terms of style-of-faulting and site classification. The strike-slip, normal and reverse ground-motion records given in the top row of Figure 2.3 are abbreviated as SS, NM and RV, respectively. Half of the accelerograms in the database that are from strike-slip events dominate the database. The other half is almost equally distributed between normal (23%) and reverse (27%) events. The data scatter with respect to different site classes are

shown on the bottom row of Figure 2.3. The site classification of accelerograms is based on measured and inferred V_{S30} values. The site classes are in accordance with NEHRP (BSSC, 2009) which considers V_{S30} intervals such that NEHRP-A, B, C, D and E soil classes correspond to $V_{S30} > 1500\text{m/s}$, $760 < V_{S30} \leq 1500\text{m/s}$, $360 < V_{S30} \leq 760\text{m/s}$, $180 < V_{S30} \leq 360\text{m/s}$ and $V_{S30} \leq 180\text{m/s}$, respectively. The numeric information for the number of data corresponding to style-of-faulting and site classification is denoted next to each legend in the related figures. The database mainly consists of recordings from soft and stiff sites that correspond to a V_{S30} range of $180\text{m/s} < V_{S30} \leq 760\text{m/s}$. In the database, however, there are relatively a few strong-motion recordings (17% of entire data) satisfying rock conditions (i.e., NEHRP-A and B).
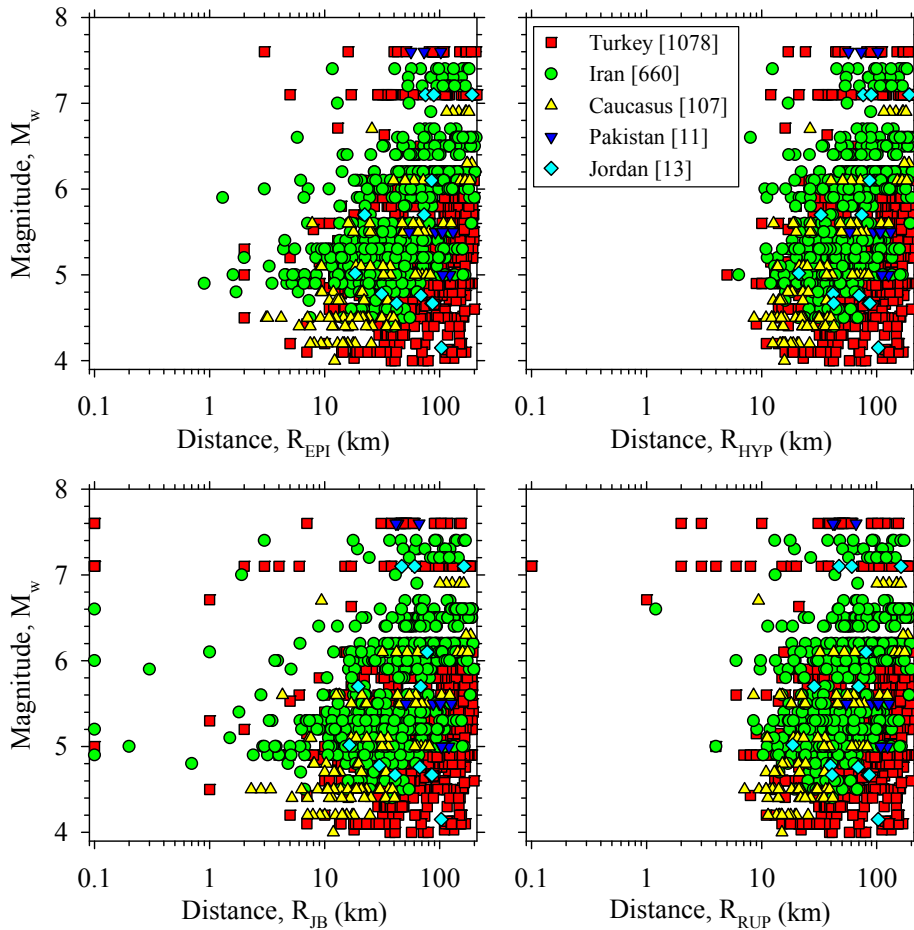
Figure 2.2 M_w vs. distance (R_{EPI}, R_{HYP}, R_{JB} and R_{RUP}) scatters of the strong-motion database in terms of countries.
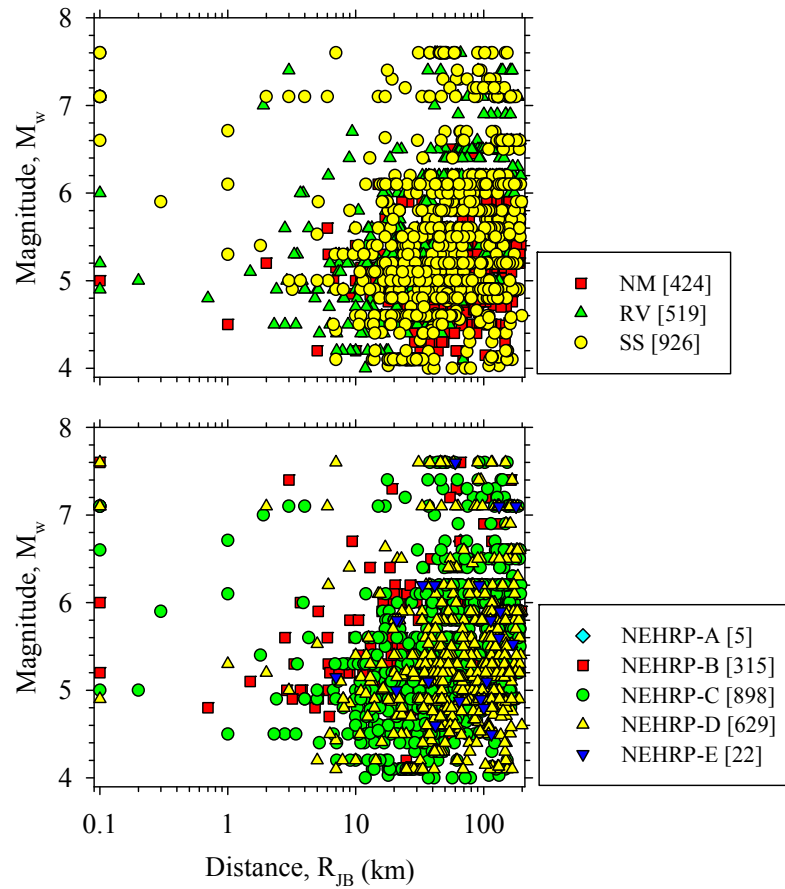
Figure 2.3 M_w vs. R_{JB} scatters of the EMME strong-motion data in terms of style-of-faulting (top row) and NEHRP site classes (bottom row).

Figure 2.4 displays the hypocentral depth vs. magnitude (M_w) distribution of the earthquakes in the database with respect to participants of the EMME project whereas the numbers of events and accelerograms within the pre-defined magnitude-depth bins as histograms are shown in Figure 2.5. These figures depict that nearly 95% of the events and accelerograms pertain to earthquakes with hypocentral depths less than 33km which is a representative value for shallow active crustal events. The rest of the events with depths of greater than 33km are situated in different parts of either Turkey or Iran. The database is not included any deep events from Makran region of Iran that generates subduction type earthquakes (Engdahl et al., 2006). To summarize the magnitude and depth distribution of the database, the map view of the recordings is given in Figure 2.6.
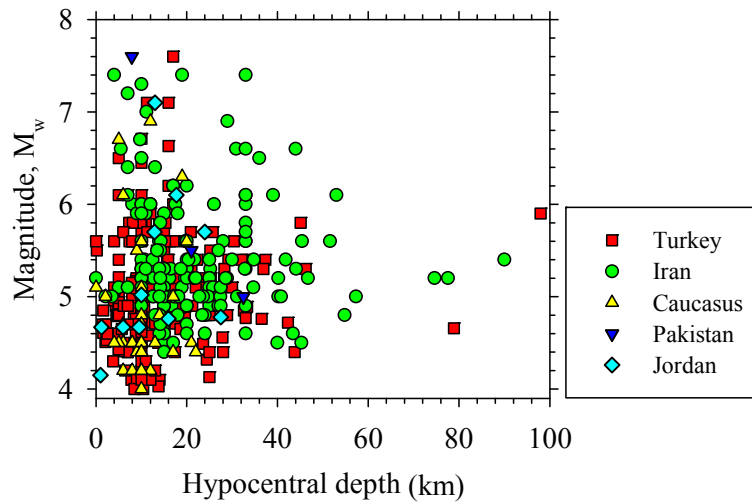
Figure 2.4 Country-based hypocentral depth vs. M_w scatters of the events in the EMME strong-motion database.
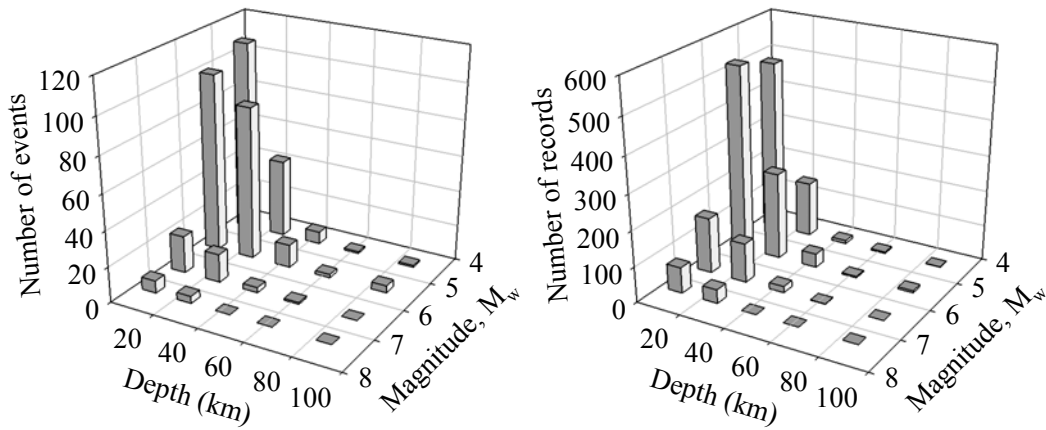
Figure 2.5 Hypocentral depth vs. M_w histograms of the events (left panel) and accelerograms (right panel) in the EMME strong-motion database. The depth intervals vary as 0-15km, 15-33km, 33-50km, 50-70km and 70-98km whereas magnitude bounds of the bins are 4.0-5.0, 5.0-6.0, 6.0-7.0 and 7.0-7.6.
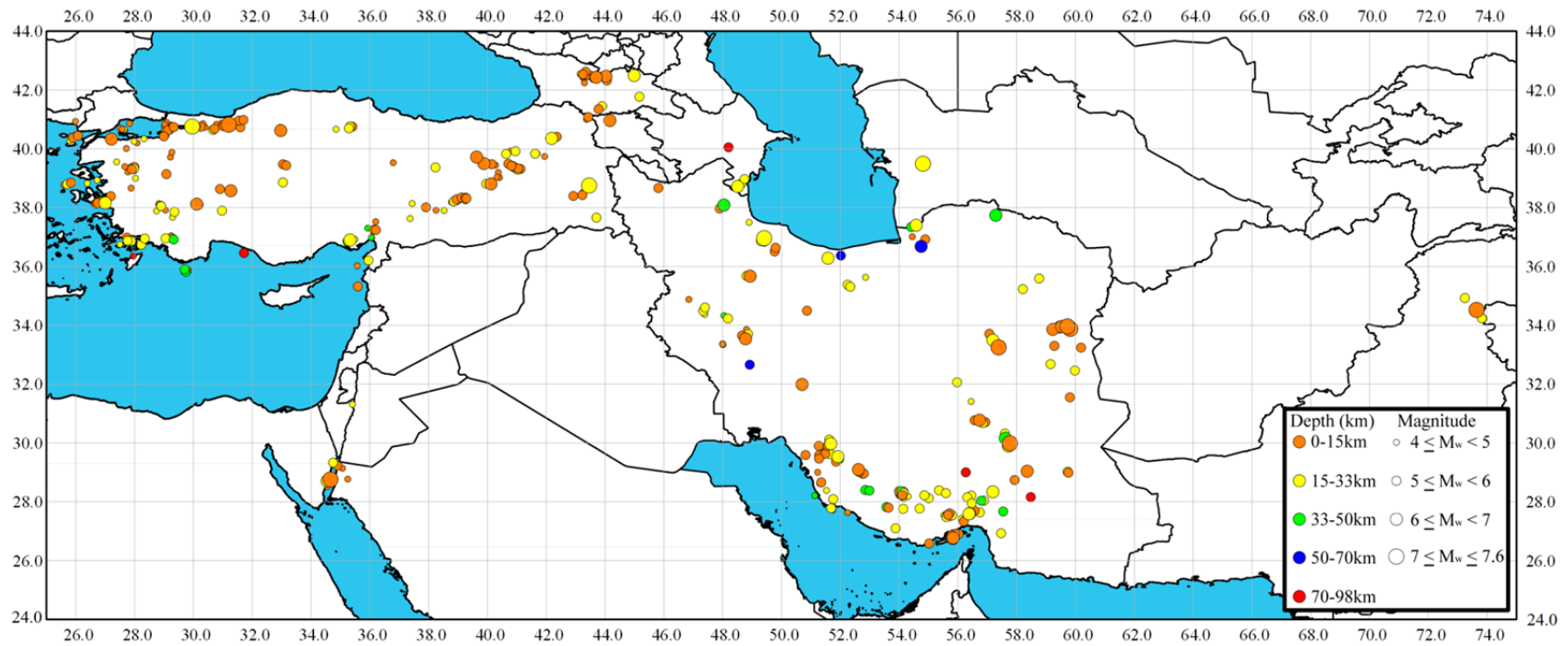
Figure 2.6 Map view of the events in the database in terms of hypocentral depth and M_w bins.

2.2. TSTHG Strong-motion Database

Under the Updating the Seismic Hazard Map of Turkey (TSTHG) project, TSTHG strong-motion database is assembled serving for GMPE selection process to establish the ground-motion logic-tree framework. Within the context of this dissertation, this database is used to evaluate the strong-motion databases of the Turkish GMPEs. The initial version of the TSTHG database is compiled from the Turkish strong-motion recordings which is included in EMME strong-motion dataset. The point- and extended-source distance measures of the recordings are recalculated by updating the metadata information (i.e., magnitude, hypocentral depth, epicenter locations) of the Turkish recordings in the EMME database with regard to the most recent Turkish catalog compiled by the WP-1 group members of this project (Kadirioğlu et al., 2014). However, M_w information for some of the small magnitude events whose magnitude information is extracted from magnitude conversion relations in the Kadirioğlu et al. (2014) catalog are not considered because EMME database contains calculated M_w values of those events extracted from RESORCE that compiles the information from SED (The Swiss Seismological Service, http://www.seismo.ethz.ch/index) and RCMT (The European and Mediterranean Regional Centroid Moment Tensor, http://www.bo.ingv.it/RCMT/).

Figure 2.7 shows the magnitude, hypocentral depth and distance metrics (R_{EPI}, R_{HYP}, R_{JB} and R_{RUP}) comparisons between Turkish sub-database of EMME and TSTHG dataset. Although the EMME database contains the most reliable metadata information for Turkish recordings, it shows some differences from TSTHG database. In Figure 2.7.a, the differences for small magnitude ($M_w < 5$) data are ignorable. For moderate magnitude events, the only significant difference between two databases is the M_w 5.22 Pülümür (15/03/1992) earthquake. The M_w value of this earthquake is considered as 5.9 in the TSTHG database since Kadirioğlu et al. (2014) catalog includes the more recent information for this event. The hypocentral depth comparison given in Figure 2.7.b indicates several points which are

considerably scattered away 1-to-1 line. The main reason for this dissimilar pattern is that while the EMME dataset updates the hypocentral depths of only significant events with respect to EHB catalog, the EHB information is considered for the all matching events in TSTHG database. Besides, the prioritization of the different seismological agencies between these databases results in scattered depth distribution for some of the events. A general comment on this issue would be that the reported depth outcomes considerably vary from agency to agency since significant uncertainties in depth computations. The inconsistencies for distance comparisons (Figures 2.7.c to 2.7.f) are prominent at short distance levels. The variations in magnitude, epicenter locations and hypocentral depth yield those disparities.

Consequently, the Turkish database includes 1066 pairs of horizontal accelerograms recorded from 183 events and 292 strong-motion stations since 1976, M_w and R_{JB} ranges of 4.0-7.6 and 0-200km, respectively, and hypocentral depths up to 30km. The site classification of almost 97% of the ground-motion recordings are based on measured V_{S30}. The rest of the recordings have estimated V_{S30} extracted from field observations and geological formations of the station sites. The ruptured fault information (i.e., fault length, fault width, strike, dip and rake angles) of the events in the database used for extended-source distance calculations are collected from the national and international seismological agencies listed in the previous section.

Once Figure 2.8.a displays the R_{JB} vs. M_w scatter plot of Turkish accelerograms, the top row of Figures 2.9 and 2.10 indicate the R_{JB} vs. M_w distribution of the recordings with respect to style-of-faulting (normal, reverse and strike-slip) and site classes (soft, stiff and rock soils). The title section of each sub-figure contains the number of recordings (N) in the relative plot. When the ground-motion data distribution in terms of fault mechanisms and site conditions of the Turkish database is evaluated, it is depicted that the accelerograms recorded from strike-slip and normal faulting, and soft and stiff soil sites events dominate the database.
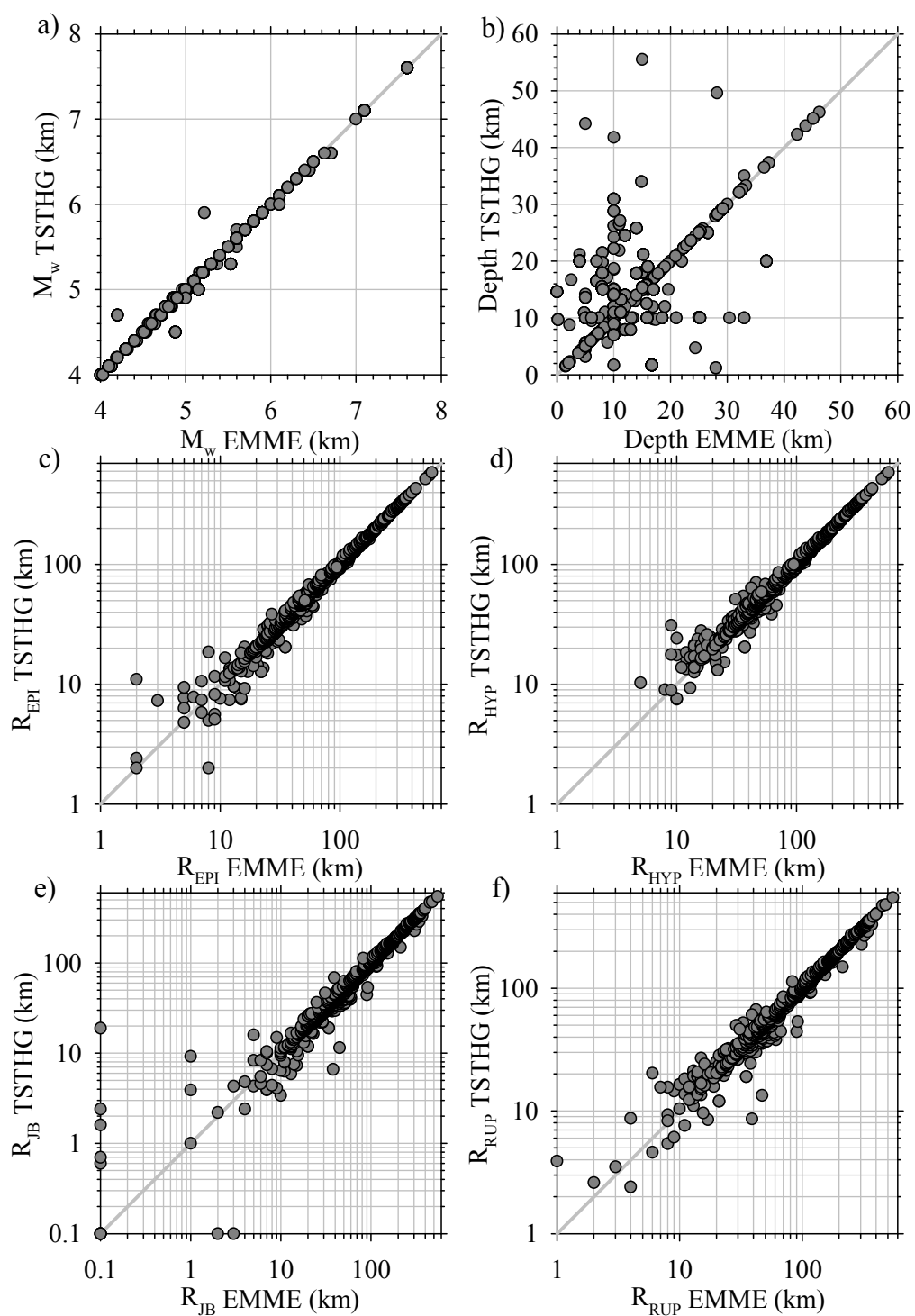
Figure 2.7 Magnitude, hypocentral depth and distance comparisons between EMME and TSTHG databases. The comparisons are conducted to 203 events for M_w and depth; 1190 records for R_{EPI}, R_{HYP}, R_{JB}; and 1176 records for R_{RUP}.
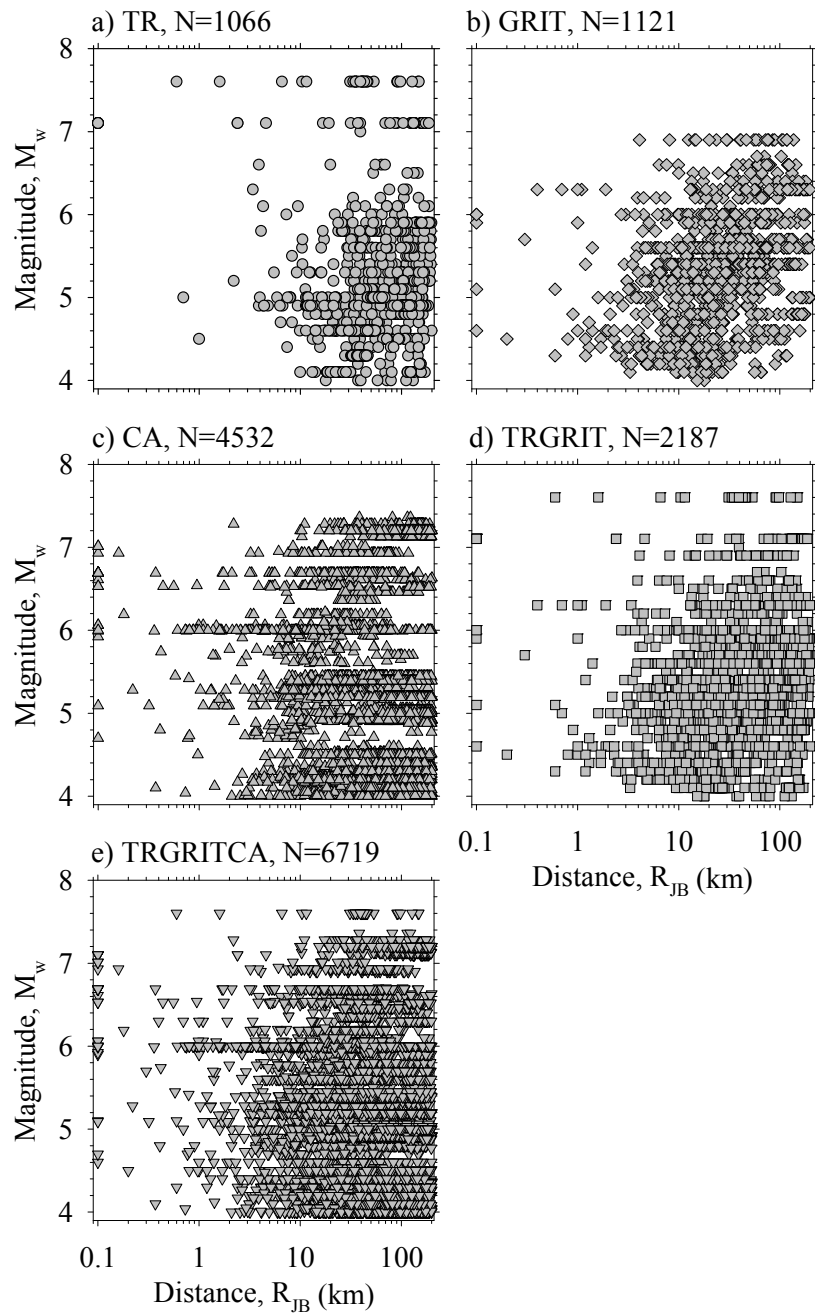
Figure 2.8 R_{JB} vs. M_w scatter plots of strong-motion data: a) Turkey (TR), b) Greece (GR) and Italy (IT), c) California (CA), d) Turkey, Greece and Italy (TRGRIT), e).Turkey, Greece, Italy and California (TRGRITCA).
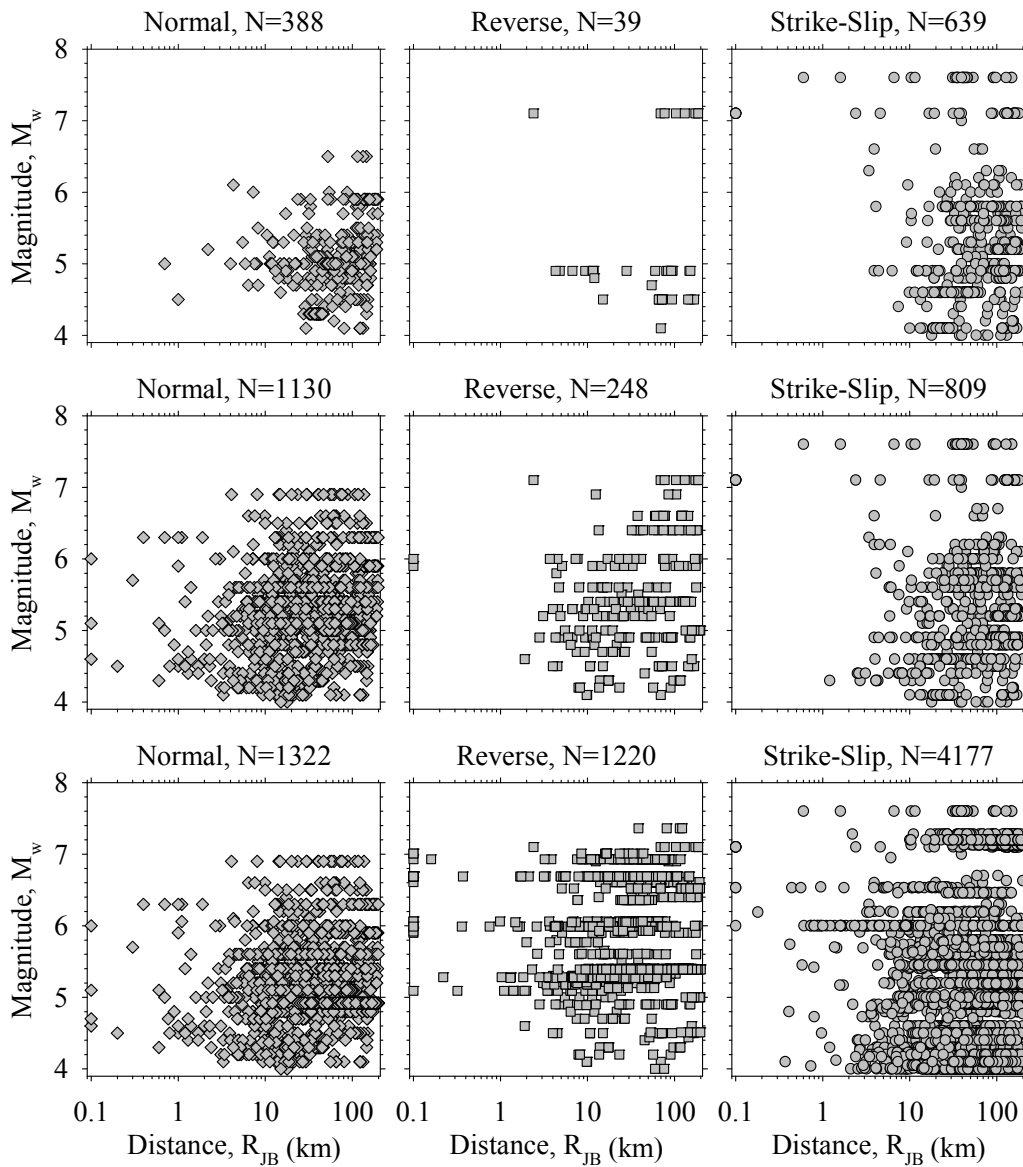
Figure 2.9 R_{JB} vs. M_w scatter plots of strong-motion data in terms of fault mechanisms: TR (top row), TRGRIT (middle row) and TRGRITCA (bottom row).
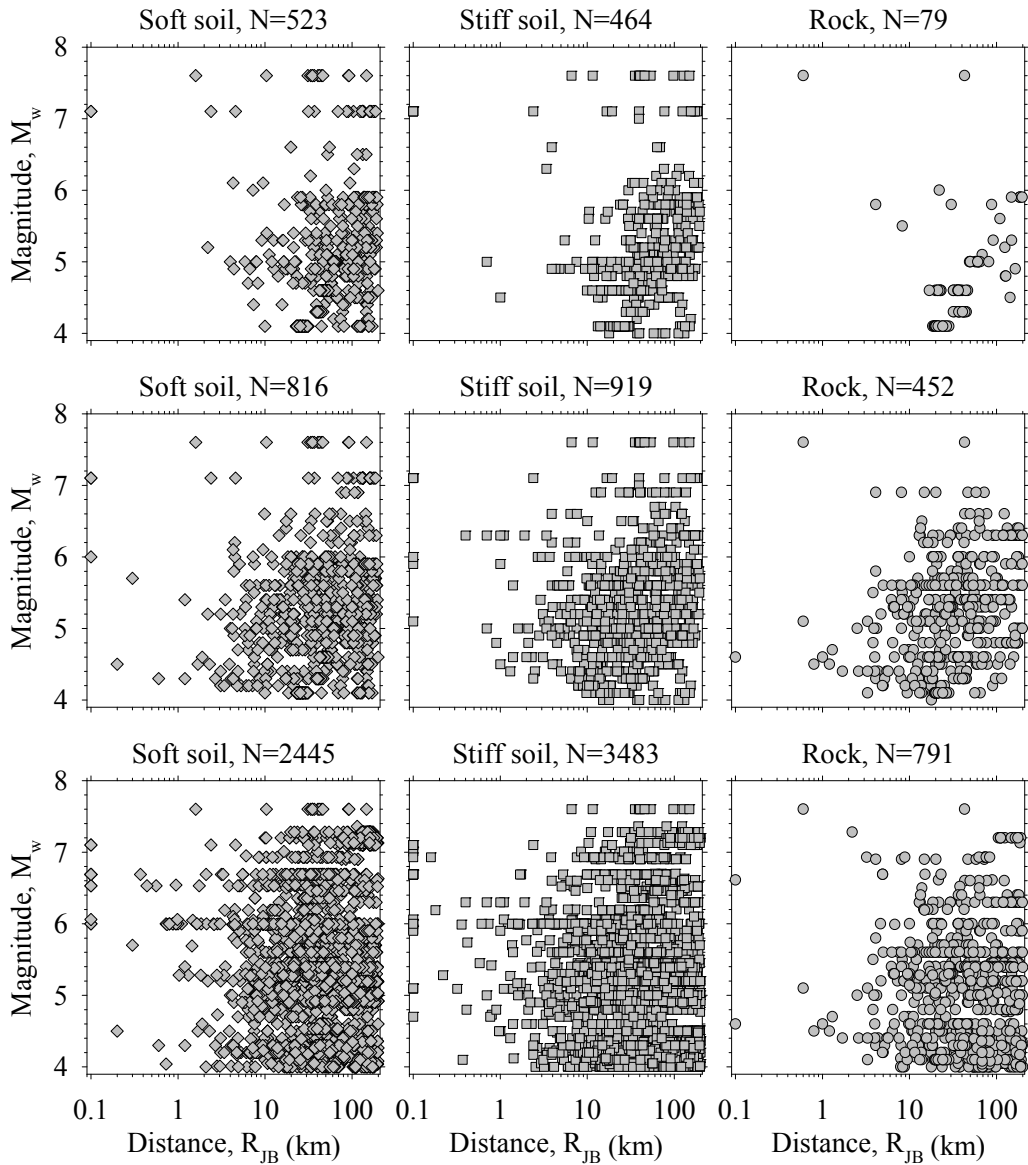
Figure 2.10 R_{JB} vs. M_w scatter plots of strong-motion data in terms of site conditions based on BSSC (2009): TR (top row), TRGRIT (middle row) and TRGRITCA (bottom row). Soft soil: NEHRP-E $V_{S30} < 180$m/s and NEHRP-D $180 \leq V_{S30} < 360$m/s; Stiff soil: NEHRP-C $360 \leq V_{S30} < 760$m/s; Rock NEHRP-B $760 \leq V_{S30} < 1500$m/s and $V_{S30} \geq 1500$m/s.

The ground-motion recordings in the databases should be uniformly distributed with respect to magnitude and distance at least, and magnitude and distance bins of the database contain sufficient data to obtain reliable results from data-driven

testing methods of predictive models. Accordingly, when the Turkish database (Figure 2.8.a) is analyzed, it is apparent that the number of records for M_w 6.0-7.0 and R_{JB} 0-20km are insufficient. In addition, the large magnitude ($M_w > 7.0$) strong-motion data is limited. In general, the ground excitations are more substantial up to 80km for seismic hazard assessments (Campbell and Bozorgnia, 2014). Besides, the contribution of the large magnitude earthquakes to the total hazard is significantly obvious. Subsequently, the candidate GMPEs should be scrutinized in order to reliably take into account the excitations related to fault segments having the potential to produce $M_w > 7.0$ earthquakes. In this respect, the ground-motion accelerograms from Greece, Italy and California that exhibits similar tectonic settings with Turkey are incorporated into the TSTHG database. Greek and Italian datasets are extracted from the RESORCE database whereas the NGA-West2 project (Ancheta et al., 2014) is the source of the Californian strong-motion data.

Although most of the Greek and Italian events in RESORCE database have double-couple fault plane solutions, there are several accelerograms without R_{RUP} distance measures. Therefore the distance calculations of those recordings that will be used in TSTHG database are replicated and the comparisons between original (RESORCE) and reassessed states (TSTHG) of the database with respect to R_{EPI}, R_{HYP}, R_{JB} and R_{RUP} are presented in Figure 2.11. Although the original M_w, hypocentral depth and epicenter coordinates are used in new distance calculations, the modified point-source distance comparisons (upper row of Figure 2.11) display noticeable variations for some of the recordings. The most important differences in extended-source distance metrics between original and modified versions of these data (lower row of Figure 2.11) are prominent at short distances. The major reasons for these observations are that the original ISESD distance measures are incorporated into the RESORCE databank without updating the distance metrics according to the modified epicenter and station coordinates (personal communication with S. Akkar and M.A. Sandıkkaya, 2014).

60
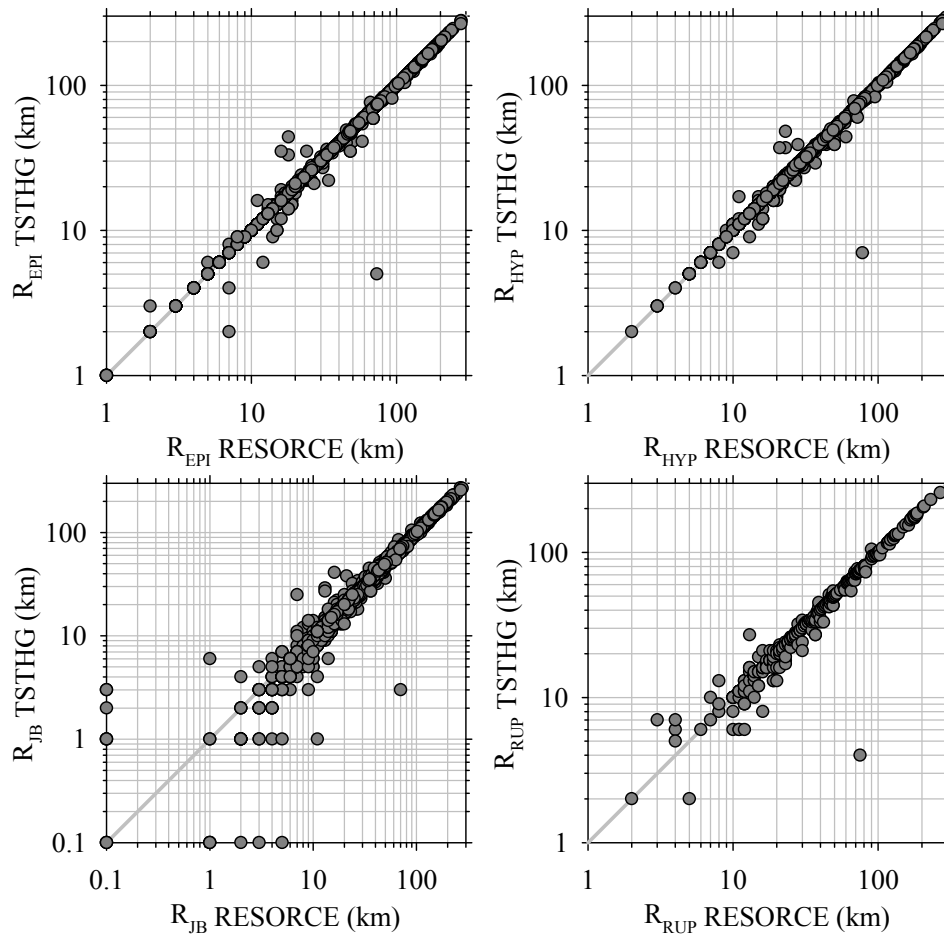
Figure 2.11 Point- and extended-source distance comparisons between RESORCE
and TSTHG databases. The comparisons are conducted to 1208 records for R_{EPI},
R_{HYP}, R_{JB}; and 337 records for R_{RUP}.

Distance-magnitude (R_{JB}-M_w) scatters for country-based datasets of Turkey (TR),
Greece+Italy (GRIT), California (CA), and regional datasets obtained from
combinations of these countries of Turkey+Greece+Italy (TRGRIT),
Turkey+Greece+Italy+California (TRGRITCA) are shown in Figures 2.8.a, b, c, d,
e, respectively. A total number of 1121 pairs of accelerograms from Italy (916
records) and Greece (205 records) are included in the final TSTHG database,
whereas the contribution of the Californian data is 4532 strong-motion records to
the final databank. The Californian data extracted from NGA-West2 database is
incorporated into the TSTHG database retaining their original metadata

information. If the importance of the recordings from short distances and large magnitude events are regarded, the contribution of the GRIT ground-motion data is minimal; however, the CA dataset plays a significant role in ameliorating the current condition of this issue.

The center and bottom rows of Figures 2.9 and 2.10 indicate R_{JB} versus M_w scatters of the TRGRIT and TRGRITCA ground-motion datasets with respect to style-of-faulting and NEHRP-based site classifications, respectively. When the strong-motion data distributions in the TRGRIT and TRGRITCA extended databases are compared with the TR database, it is obvious that more homogenized data distributions with respect to fault mechanisms and site conditions are obtained with the support of Italian, Greek and Californian data. Besides, IT, GR and CA ground-motion data provide a remarkable advance in the number of reverse fault mechanism and rock site condition recordings which are scarce in TR database.

2.3. Comparisons between TSTHG Database and Model-Developing Databases of Turkish GMPEs

The first ground-motion model studies in Turkey were conducted in 1996 (Aydan et al., 1996; İnan et al., 1996) and approximately 13 predictive models has been developed since 1996 (Douglas, 2011; Kale et al., 2014). However, when major features of GMPEs such as magnitude and distance type, applicable period ranges are considered to be used in current practice of engineering applications, four predictive models developed in the last decade come into prominence. These predictive models are Kalkan and Gülkan (2004) - KG04, Özbey et al. (2004) - Ozb04, Akkar and Çağnan (2010) - AC10, and Kale et al. (2014) - KAAH14. Their superiority on the rest of the Turkish predictive models is that they regard the moment magnitude and extended-source distance measures in ground-motion estimates which are available up to 2s at least.

In this part of the dissertation, the listed GMPEs above are evaluated by conducting catalog comparisons with the available ground-motion parameters between the most updated version of the Turkish strong-motion database (TSTHG) and model-developing databases of these ground-motion models. If the original magnitude and distance pairs of the records are accessible, the comparisons firstly classify the current situation of the recordings in the TSTHG database as problematic and common records. The accelerograms with estimated V_{S30}, or R_{JB}, low quality waveforms, etc. are categorized as problematic records. After that, the comparisons of the common recordings between TSTHG and considered model-developing dataset with respect to the existing ground-motion parameters (M_w, hypocentral depth, R_{JB}, V_{S30} and PGA) are presented. As a common format of the figures, the parameters related to GMPEs are indicated on the horizontal axis, whereas the vertical axis denotes the parameters of the TSTHG database. The R_{JB} values smaller than 0.1km is denoted as 0.1km in these figures since the use of logarithmic axis definition.

The ground-motion records in Ozb04 database cannot be sorted with respect to their current condition in the TSTHG database because the metadata information of Ozb04 database except for the magnitude and hypocentral depth could not be accessible. M_w and depth comparisons of the 17 earthquakes in Ozb04 model-developing dataset are given in Figure 2.12. This figure depicts considerable differences between two databases. Another interesting observation about Ozb04 dataset is that there is not any event in the magnitudes between 6 and 7 which introduces a significant bias to ground-motion estimates of this predictive model. The major factor of unevenly ground-motion data distribution is that this predictive model developed from a regional dataset (Northwestern Turkey).
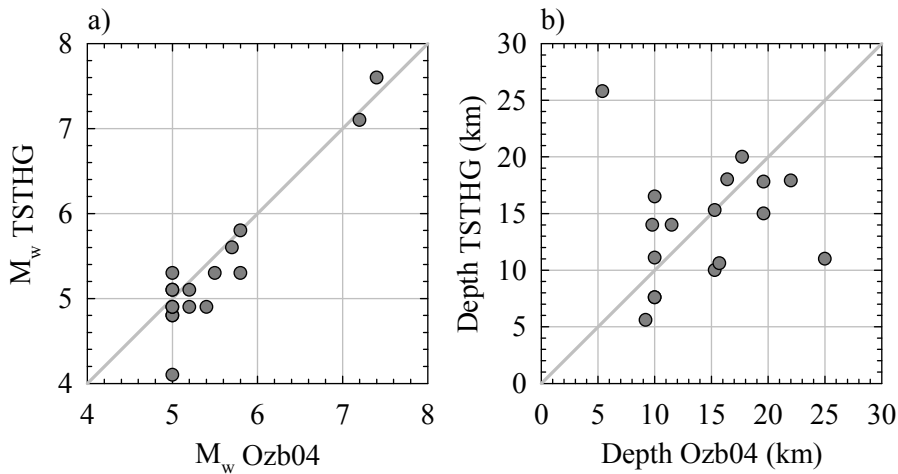
Figure 2.12 a) M_w, and b) hypocentral depth comparisons of the 17 common events between TSTHG and Ozb04 databases.

Kalkan and Gülkan (2004) paper reports the M_w, R_{JB}, estimated or measured V_{S30} and PGA of the strong-motion events and records in its model-developing dataset. Figure 2.13 indicates the original R_{JB} vs. M_w scatters of 112 records obtained from 57 earthquakes in KG04 database and their classification with respect to TSTHG database. The result of the classification depicts that 10 records suffering from estimated V_{S30} and R_{JB}, 22 records being low quality with respect to Douglas (2003) and 1 record having single horizontal component are excluded from TSTHG database. 79 accelerograms with two horizontal component recorded from 36 earthquakes are determined as common recordings between two databases.

The magnitude, distance, V_{S30}-based site condition and PGA differences of the common recordings between two databases are displayed in Figure 2.14. The magnitude comparison given in Figure 2.14.a displays noticeable variations for some small-to-moderate magnitude events ($M_w < 6$), whereas the updates of Turkish metadata information introduces slight differences to large magnitude earthquakes. The distance comparison plot is prepared for R_{JB} since KG04 uses this distance metric (Figure 2.14.b). Several conflicted distance couples are captured in this figure. Besides, for mismatching cases, KG04 distances generally yield larger R_{JB} values with respect to the version of TSTHG. The V_{S30} comparison given in

Figure 2.14.c indicates the most significant differences within the compared parameters of two databases. For the recordings in KG04 database with unknown V_{S30} values, the site conditions are estimated from geological features of the strong-motion stations. Accordingly, V_{S30} values of 700, 400 and 200m/s are assigned to the stations classified as rock, stiff soil and soft soil, respectively (Kalkan and Gülkan, 2004). Approximately 80% of the V_{S30} values in the KG04 database are based on estimated site conditions. This fact ideally explains such a scattered picture encountered in Figure 2.14.c. The last plot given in Figure 2.14.d evaluates the modifications in PGA values. The geometric mean of two horizontal components is used in this comparison. The trend obtained in this figure represents that the PGA values are not severely altered except for some recordings of which data processing (i.e., filtering) may most probably vary the PGA values.
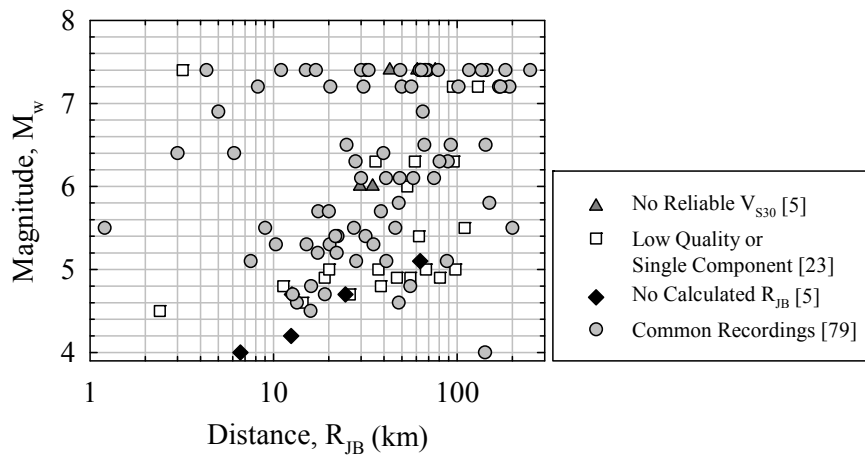
Figure 2.13 Original R_{JB} vs. M_w scatters of the recordings in KG04 database with representation of their current situations in up-to-date Turkish database.
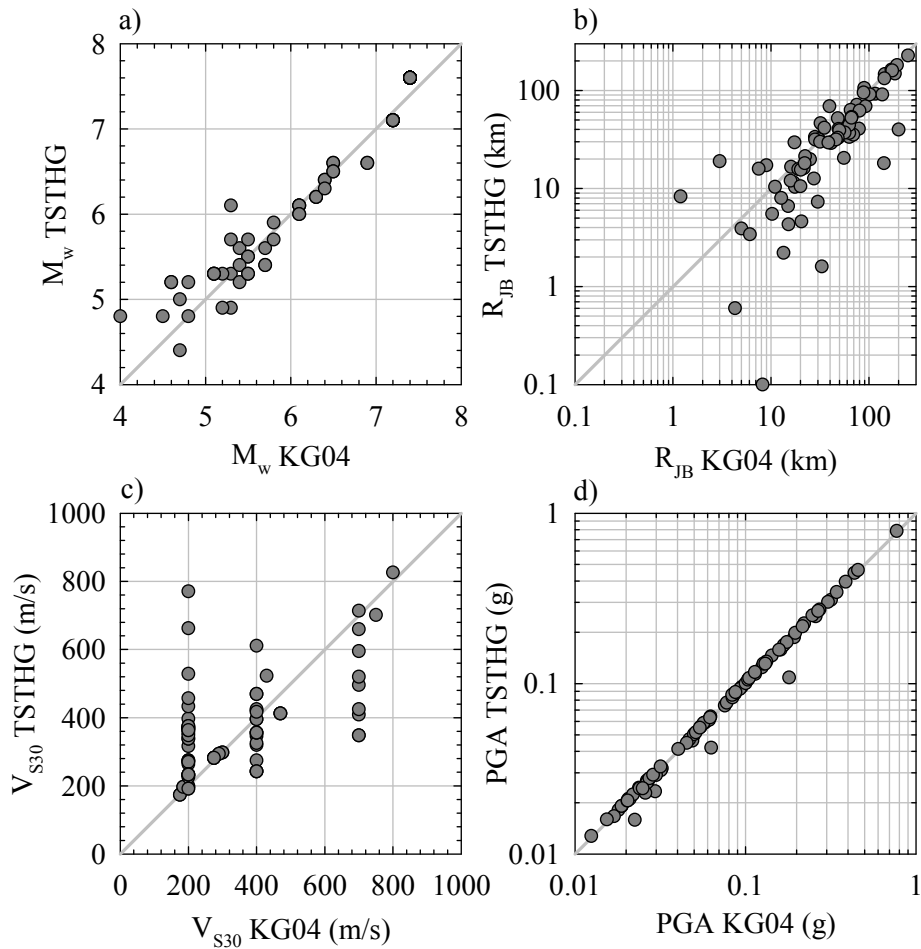
Figure 2.14 a) M_w, b) R_{JB}, c) V_{S30}, and d) PGA comparisons of the common data (79 recordings from 36 events) between TSTHG and KG04 databases.

AC10 predictive model was developed from a more up-to-date and comprehensive ground-motion database compiled in the project entitled "Compilation of Turkish Strong-Motion Network According to the International Standards" (Akkar et al., 2010) with respect to datasets of Ozb04 and KG04. The updated metadata information is supported by the measured V_{S30} values obtained from the site investigations (Sandıkkaya et al., 2010). The original R_{JB}-M_w distributions of 433 accelerograms recorded from 137 earthquakes included in AC10 database and their classification with respect to TSTHG database is presented in Figure 2.15. 364 problem-free accelerograms included commonly in both databases are detected, whereas the rest of the recordings in AC10 database are extracted from the updated

version of the Turkish database. The observed problems of the recordings are classified as low quality (24), no calculated R_{JB} (41) and Greek recordings (4).
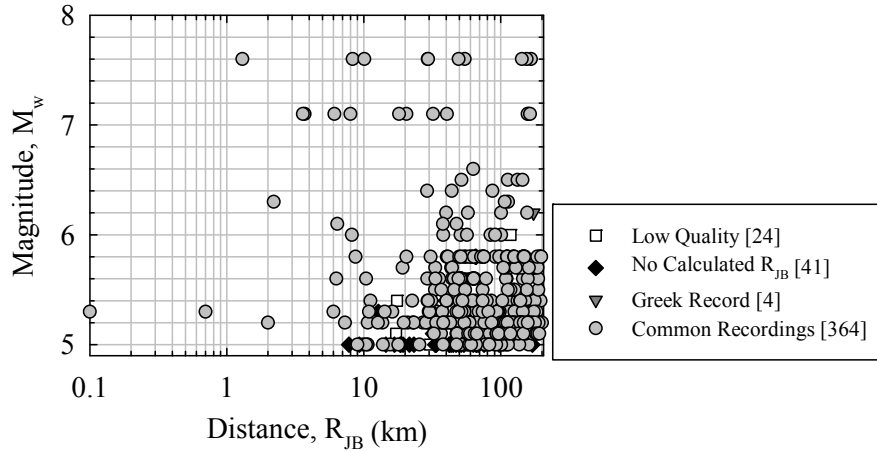
Figure 2.15 Original R_{JB} vs. M_w scatters of the recordings in AC10 database with representation of their current situations in up-to-date Turkish database.

The improvements in metadata information about Turkish recordings are examined by M_w, hypocentral depth, R_{JB}, V_{S30} and PGA comparisons indicated in Figure 2.16. The magnitude comparison given in Figure 2.16.a depicts some noticeable variations for only $M_w < 5.5$ earthquakes whose M_w values are mostly obtained from magnitude conversion relations. In Figure 2.16.b, the evaluation of hypocentral depth, one of the most uncertain earthquake parameters, represents that the depth values of larger amount of events have dissimilar pairs. The discrepancies between the considered seismological agencies and re-calculation process of some of the data providers to improve the certainty of the earthquake parameters cause to draw such a picture. Although R_{JB} distances of many of the recordings are not remarkably changed, some of the short distance accelerograms are subjected to considerable modifications (Figure 2.16.c). Almost all recordings in the databases have rather close V_{S30} and PGA values as shown in Figures 2.16.d and e, respectively.
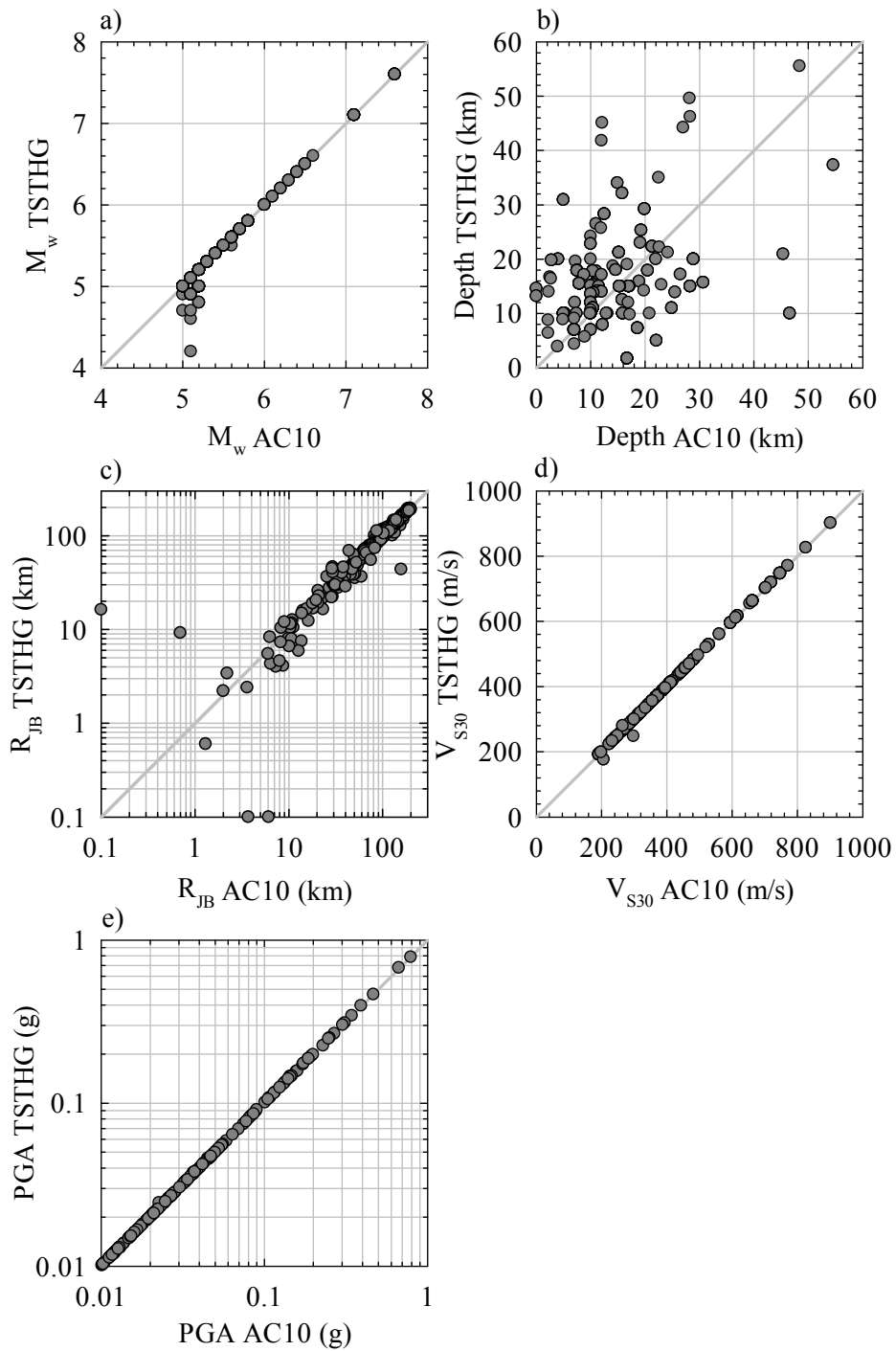
Figure 2.16 a) M_w, b) hypocentral depth, c) R_{JB}, d) V_{S30}, and e) PGA comparisons of the common data (364 recordings from 100 events) between TSTHG and AC10 databases.
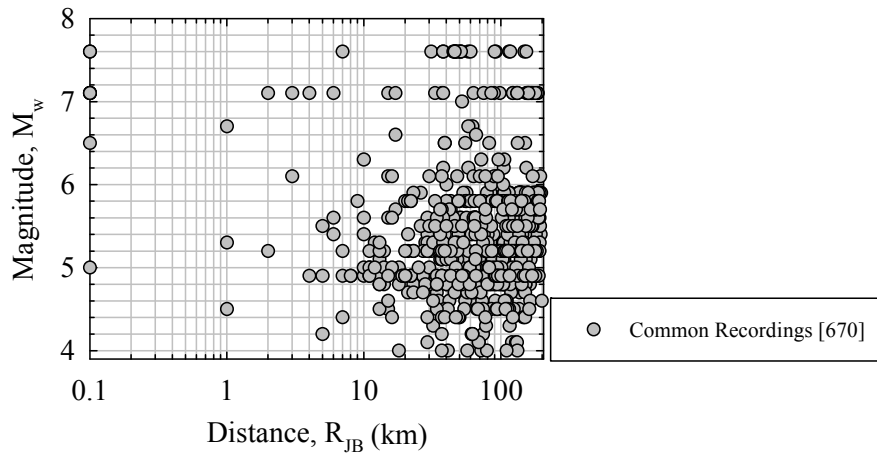
Figure 2.17 Original R_{JB} vs. M_w scatters of the recordings in KAAH14 database with representation of their current situation in up-to-date Turkish database.

While KAAH14 ground-motion model was developed, the Turkish strong-motion data selected from EMME database which is introduced in detail at the previous parts of this section is used in regression analysis. The TSTHG database covers the entire recordings (670 records from 175 strong-motion events) included in KAAH14 database of which Figure 2.17 presents the original R_{JB}-M_w distribution.

The comparisons made between EMME and TSTHG (see Figure 2.7) reflects the general perspective of KAAH14-TSTHG comparisons; however, magnitude, depth and R_{JB} distance comparisons in addition with V_{S30} and PGA scatters are displayed in Figure 2.18 since KAAH14 model-developing dataset is a sub-version of Turkish part of the EMME database. The scatter plot in Figure 2.18.a compares the moment magnitudes of these two databases that indicate almost exact matching of M_w trends. In Figure 2.18.b, the depth couples of considerable amount earthquakes represent almost identical trends, whereas the depths of a part of the data distribute in a scattered way because of considering different seismological agencies in these two databases. The observations on distance comparison given in Figure 2.18.c are parallel to the observations of AC10. V_{S30} and PGA trends of the compared databases indicate identical data pairs.
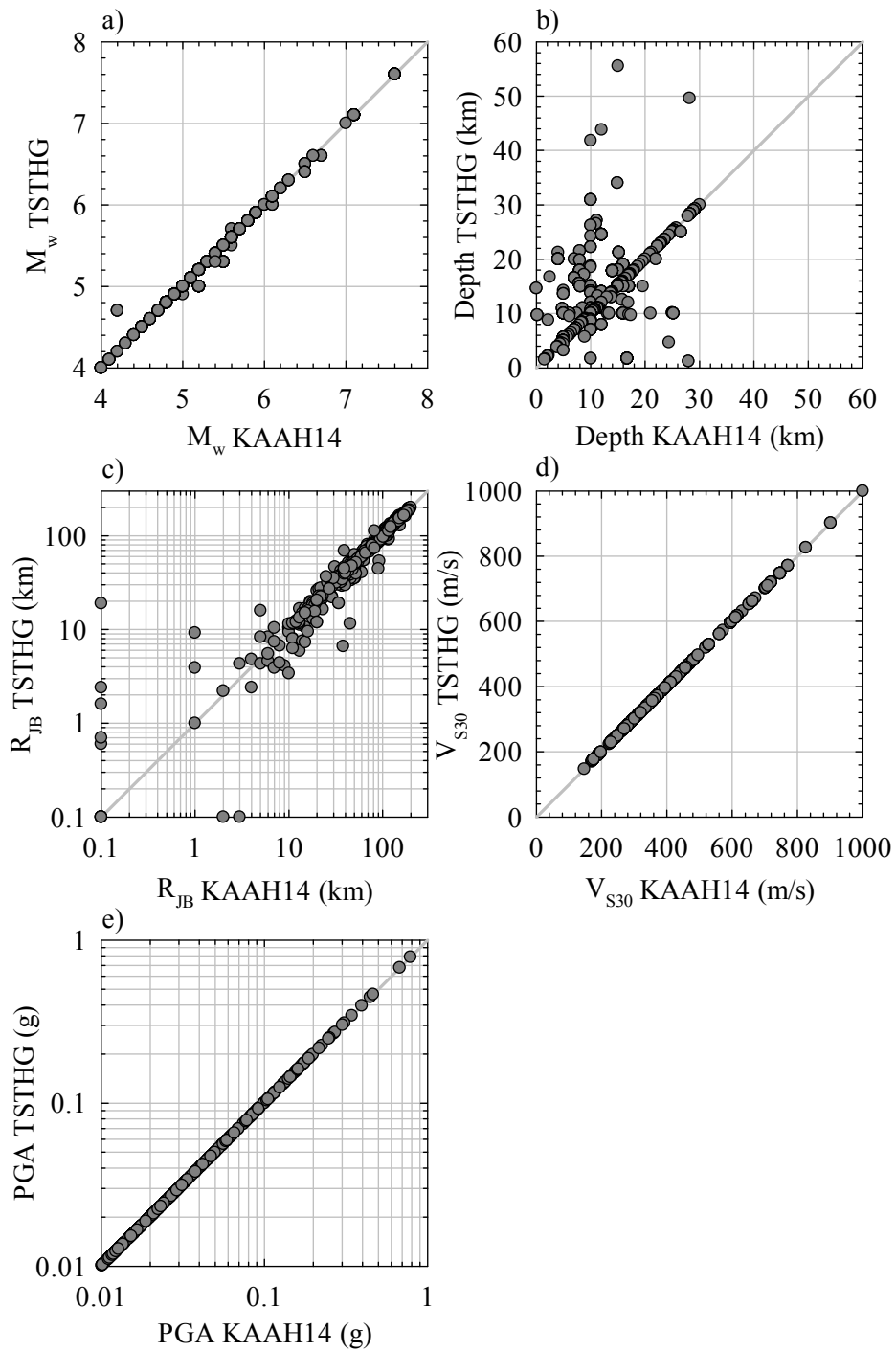
Figure 2.18 a) M_w, b) hypocentral depth, c) R_{JB}, d) V_{S30}, and e) PGA comparisons of the common data (670 recordings from 175 events) between TSTHG and KAAH14 databases.

2.4. General Comments on Further Improvements of the Databases

From the above observations on strong-motion catalogs (or metadata information) it can be seen that a fully agreement between different catalogs containing same regions still has not been reached in terms of magnitude, hypocentral depth, epicentral location, double-couple fault plane solutions or station coordinates. The followed strategies during the compilation of metadata information by the researchers introduce such kind of inconsistencies. In fact, all information included in the metadata of the databases is extracted from the reports of the reliable local and global seismological agencies or peer-reviewed publications. However, some of the stringent seismological agencies periodically update their outcomes for past earthquakes with the improvements in available ground-motion data and processing techniques (e.g., hypocenter determination algorithm). The most apparent example of such a case is the EHB catalog released by the International Seismological Center (ISC). The EHB is pronounced as the groomed version of the ISC catalog because it reassessed the most significant earthquakes between 1960 and 2008 around the world which was reported by the ISC bulletin in the past. In addition to this case, the ISC declare a new message that it will release such comprehensive ground-motion catalog including all ISC events at the beginning of 2015. As seen, the metadata information is always alive. The most important thing is to include these improvements to the regional or local strong-motion databases to estimate the future ground excitations more precisely.

In this chapter, the model developing dataset comparisons of local Turkish GMPEs clearly represent the alteration of Turkish strong-motion database. Accordingly, Figure 2.19 summarizes the significance of metadata information and data distribution while developing GMPEs. The prominent variations between the original ground-motion dataset of KG04 model and the latest version of the Turkish dataset result in displaying considerable differences as shown in Figure 2.19. This figure also depicts that Ozb04 regional predictive model cannot capture the near distance trends of other Turkish GMPEs. AC10 and KAAH14 ground-

motion relations that show little discrepancies with the latest version the Turkish database draw more compatible ground-motion estimates according to Figure 2.19.
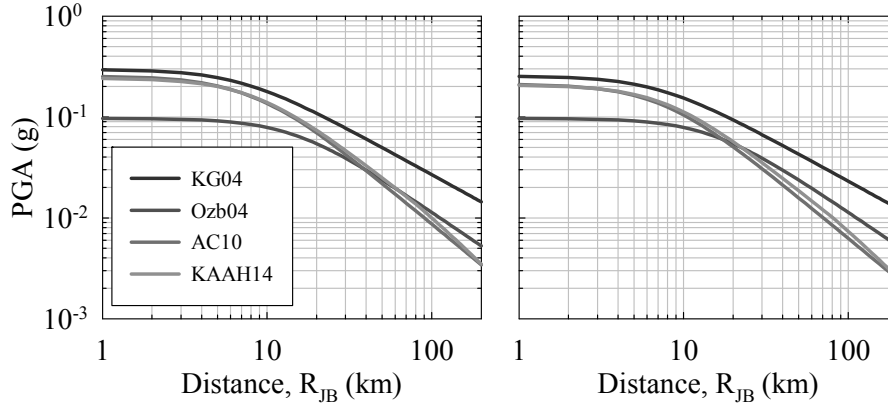
Figure 2.19 Comparison ground-motion estimates of Turkish GMPEs for a given earthquake scenario of M_w 6.0, strike-slip fault mechanism and V_{S30} 360m/s (left panel) and 760m/s (right panel).

In addition to above observations, there are some issues which can be considered for the future improvements in the EMME database. Firstly, it is important that the Iranian accelerograms could be processed with the individually selected filters cut-off frequencies for unification of the EMME database. The epicenter location and hypocentral depth information of all events in the database can be updated with respect to EHB catalog. The accelerograms recorded after 2011 could be integrated to the EMME accelerometric data archive to extend the size of the dataset.

Finally, as listed in the above paragraphs, there are many Iranian, Armenian, Georgian and Jordanian recordings which are included in the EMME database but not included in the RESORCE databank although these countries are within the considered boundaries of the RESORCE database. The combination of these two datasets would excessively improve the data coverage of RESORCE database in order to serve for the studies in the realm of earthquake engineering and engineering seismology.

CHAPTER 3

A GROUND-MOTION PREDICTIVE MODEL FOR IRAN AND TURKEY FOR HORIZONTAL PGA, PGV AND 5%-DAMPED RESPONSE SPECTRUM: INVESTIGATION OF POSSIBLE REGIONAL EFFECTS

This chapter presents a ground-motion prediction equation (GMPE) for Turkey and Iran to investigate the possible regional effects on ground-motion amplitudes in shallow active crustal earthquakes. The proposed GMPE is developed from a subset of recently compiled strong-motion database of the **E**arthquake **M**odel of the **M**iddle **E**ast Region (EMME; http://www.emme-gem.org/) project. A total of 670 Turkish and 528 Iranian accelerograms with depths up to 35 km are used to estimate 5%-damped elastic pseudo-acceleration spectral ordinates of $0.01s \leq T \leq 4s$. The GMPE also estimates PGA and PGV. The moment magnitude range of the model is $4 \leq M_w \leq 8$ whereas the maximum Joyner-Boore distance is $R_{JB} = 200$ km. The functional form considers 3 major fault mechanisms (strike-slip, normal and reverse). The nonlinear soil behavior is a function of V_{S30} (average shear-wave velocity in the upper 30 m of soil profile). The observations from empirical and estimated ground-motion trends advocate regional effects in the Iranian and Turkish ground-motion amplitudes that originate from the differences in Q-factors,

kappa and near-surface velocity profiles. These factors eventually affect the magnitude and distance dependent scaling of spectral amplitudes in Iran and Turkey. In essence, the ground-motion amplitudes of these two neighboring countries draw patterns different than the ground-motion estimates of GMPEs developed from the strong-motion databases of shallow active crustal earthquakes from multiple countries.

3.1. Introduction

Significant improvements have been observed in the size and quality of strong-motion databases in the past decade. Consequently, the number of ground-motion predictive models (GMPEs) has increased considerably in the same period. Most of these GMPEs are devised for estimating ground motions in shallow active crustal regions (SACRs). Their ground-motion datasets are composed of recordings either from a specific country or multiple countries that share similar tectonic features. Predictive models developed from databases compiled from multiple countries are generally defined as *global* GMPEs. The corresponding ground-motion datasets are also referred to as *global* databases. The terminology used for describing the ground-motion models originating from country-specific databases is called as *local* GMPEs. Global GMPEs are usually preferred in seismic hazard assessment as the distribution of their datasets is well-constrained in terms of essential estimator parameters such as magnitude, distance and faulting mechanisms. The metadata information and waveform quality of global GMPEs are generally well-studied and well-documented. Smaller sizes of local databases and their dubious metadata quality have been the repelling factors to disfavor the use of local GMPEs in hazard related studies (Cotton et al., 2006; Bommer et al., 2010). This view point has started to change because there are significant efforts in improving the quality of local strong-motion databases either through international or national projects (e.g., Theodulidis et al., 2004; Luzi et al., 2008; Akkar et al, 2010; **E**arthquake **M**odel of the **M**iddle **E**ast Region, EMME, www.emme-gem.org, **N**etwork of

European Research Infrastructures for Earthquake **R**isk **A**ssessment and Mitigation, NERA, www.nera-eu.org).

Model developers who use global strong-motion databases indicated that differences in observed ground-motion amplitudes compiled from different countries are insignificant as long as the seismotectonic regimes exhibit similar features. This assertion is verified through comparisons of global GMPEs developed from different datasets. For example, Bommer et al. (2009), Campbell and Bozorgnia (2006) and Stafford et al. (2008) indicated a good agreement between the global GMPEs of NGA-West1 project (Power et al., 2008) and pan-European GMPEs (models developed from the shallow active crustal earthquakes of broader Europe). The observed differences in the ground-motion estimates of these global GMPEs were interpreted as statistically tolerable by these studies. Parallel to these conclusive remarks and confined to the limitations in data, Douglas (2004; 2007) did not find firm evidence about regional differences within Europe for ground motions from small-to-moderate magnitude events. However, his comparisons of ground-motions from California, New Zealand and Europe suggested that ground motions from Californian earthquakes are higher in a statistical sense than those from European events. Studies by Ghasemi et al. (2009) and Scassera et al. (2009) yielded controversial results on the limitations of global GMPEs in capturing the regional effects. The former study suggested the use of NGA-West1 GMPEs for Iran whereas the latter paper noted differences in the distance scaling of NGA-West1 GMPEs and Italian strong-motion data. Contradictory to the findings of Ghasemi et al. (2009), Mousavi et al., (2012) favored local GMPEs for hazard estimates in Iran. Few researchers (e.g., Atkinson and Morrison, 2009; Chiou et al., 2010) emphasized the significance of regional differences for low magnitude events in SACRs. However, Yenier and Atkinson (2014) found evidence on the regional dependence of large magnitude earthquakes in New Zealand and western North America.

Note that GMPEs, no matter how complex they are, still have limitations to fully mimic the entire physical process behind the earthquakes. They can only map the overall seismotectonic features of the accelerograms covered by their ground-motion datasets that can be either local or global. Thus, a local GMPE developed from a reliable local dataset can reflect the likely regional characteristics that may not be fully addressed by a global model that lack representative strong motions of that region. Although the recent achievements in global strong-motion databases for SACRs are indisputable, they can still cover only a good portion of accelerograms with similar tectonic features. For example, the recent pan-European strong-motion database (Akkar et al., 2014c) is mainly composed of accelerograms from Italy and Turkey. The majority of NGA-West1 database (Chiou et al., 2008) consists of accelerometric data from the western North America and Taiwan. The NGA-West2 database (Ancheta et al., 2014) has extended the magnitude and distance limits of its predecessor by including moderate-to-large magnitude recordings of Japan and China. NGA-West2 database also integrated small magnitude events ($3 < M_w < 5$) from California to improve the ground-motion estimates of small earthquakes. However, shallow active crustal earthquakes from the Mediterranean region and other parts of the world are only partially represented in this database. These discussions can spot the sources of some of the contradictory results summarized in the previous paragraph that evaluate local and global GMPEs for regional effects.

The existence and significance of regional effects were investigated for SACRs in Iran and Turkey through a ground-motion model developed from the accelerograms of these two countries. The observations indicate that the ground-motion amplitudes of SACRs in Iran and Turkey differ in terms of distance, magnitude and style-of-faulting (SoF) scaling. The ground-motion amplitudes of these countries show differences with the ground-motion estimates of recent global GMPEs developed from the subsets of European and NGA-West2 databases. The model presented in this chapter is based on the recent updates of both Turkish and Iranian strong-motion data and can be of use for seismic hazard assessment in these

countries for moment magnitudes $4 \leq M_w \leq 8$, distances up to $R_{JB} = 200$ km (R_{JB} is Joyner-Boore distance; Joyner and Boore, 1981) and for major fault mechanisms (normal, strike-slip and reverse faults).

3.2. Review of GMPEs in Turkey and Iran

Table 3.1 lists the Turkish and Iranian GMPEs developed for SACRs during the last two decades. Most of this information is compiled from Douglas (2011). Aydan et al. (1996) and Inan et al. (1996) constitute the first ground-motion predictive models developed in Turkey for estimating PGA. These GMPEs were developed from poorly constrained datasets. They neither consider the site nor style-of-faulting (SoF) effects on PGA amplitudes. Inan et al. (1996) do not give any information about the major metadata features of the estimator parameters used in their functional form. The Schwarz et al. (2002) (Sch02) and Gülkan and Kalkan (2002) (GK02) GMPEs that are developed after the 1999 Kocaeli and Düzce earthquakes used comparatively larger local datasets with better metadata information. Both models were derived for estimating PGA and spectral accelerations (PSA) up to 2.0s. Sch02 focuses on the ground-motion estimates of northwestern Turkey whereas GK02 considers a ground-motion dataset from the entire country. Among these GMPEs, GK02 is the first model that used moment magnitude (M_w) and an extended-source distance measure (R_{JB}) to better account for source and radiation pattern effects for large magnitude events. The distance measure is inhomogeneous in GK02 as it uses both R_{EPI} and R_{JB}. GK02 model was superseded by Kalkan and Gülkan (2004) (KG04) with a larger dataset that extends the magnitude and distance ranges of the former study. Two additional Turkish GMPEs were published in 2004; Ulusay et al. (2004) (Uls04) and Özbey et al. (2004) (Ozb04). The former model is devised for estimating PGA whereas Ozb04 estimates PGA and PSA for northwestern Turkey as in the case of Sch02. The functional form of Ozb04 uses M_w and R_{JB} as of KG04. The functional forms of KG04 and Ozb04 also show significant similarities with a difference in their site function definitions. These predictive models are followed by Bindi et al. (2007)

77

(Bnd07), Aydan (2007) (A07), Akyol and Karagöz (2009) (AK09) as well as Ulutaş and Özer (2010) (UO10) GMPEs. Except for A07 (no clear information on the general features of this model), the rest of these GMPEs are modeled for estimating the ground-motion amplitudes in western Turkey with relatively large datasets when compared to the previously discussed Turkish equations. Akkar and Çağnan (2010) is currently the most recent ground-motion model developed for Turkey. The functional form of this equation is also the most complicated one (12 estimator parameters) among the Turkish GMPEs presented in this paragraph. It considers nonlinear soil behavior and includes the effects of three major faulting types (reverse, normal and strike-slip) on ground-motion amplitudes that are disregarded in the other local Turkish GMPEs discussed so far. Note that the Turkish model developers report sigma (standard deviation) associated with their equations except for Ayd96, In96 and A07.

The first empirical predictive model for Iran was developed by Ramazi and Schenk (1994) (RS94) to estimate PGA. This model was followed by Zare et al. (1999) (Zr99) to estimate PGA by extending the Iranian strong-motion database for M_w and SoF. The GMPE developed by Khademi (2002) (K02) estimates both PGA and PSA. The magnitude as well as distance parameters of these three GMPEs are heterogeneous. They consider multiple magnitude scales and use extended as well as point-source distance metrics. Iranian GMPEs of Nowroozi (2005) (N05), Mahdavian (2006) (M06), Zare and Sabzali (2006) (ZS06) and Ghodrati Amiri et al. (2007) (GAm07) are either tailored for a particular region in Iran or for the entire country. Their distance measures are R_{EPI} or R_{HYP} and disregard the extended fault geometry that becomes important to properly address the radiation pattern effects in large magnitude earthquakes. All of these models can estimate PGA. ZS06 also estimates PSA. Ghasemi et al. (2009) (Ghs09) proposed a GMPE to estimate PSA for Iran and West Eurasia from a large dataset. This study is followed by Sadeghi et al. (2010) (Sdg10), Ghodrati Amiri et al. (2010) (GAm10), Hamzehloo and Mohood (2012) (HM12) and Saffari et al. (2012) (Sfr12) who proposed ground-motion predictive models for the whole Iran (Sdg10 and Sfr12) or

for a specific zone in Iran (GAm10 and HM12). They are developed from larger ground-motion databases when compared to the datasets of previous Iranian GMPEs. They all estimate PSA. HM12 and Sfr12 can also estimate PGA. Sfr12, the most recent Iranian GMPE, accounts for different faulting mechanisms (a rare feature in the Iranian GMPEs). Its site functional form is in terms of V_{S30}. The Iranian GMPEs generally report sigma and only two of them (RS94 and K02) do not give any indication about the level of sigma in their equations.

The overall picture portrayed in Table 3.1 indicates that the database size in the Turkish and Iranian GMPEs tend to increase over the past years. However, the level of complexity in their functional forms does not follow the same trend except for a few models. Inhomogeneous nature of estimator parameters (use of several magnitude and distance measures in the same model), missing SoF and site effects, consideration of incomplete intensity measures (GMPEs either estimating PGA or PSA), and the use of estimator parameters (M_L, M_d, m_b, R_{EPI} and R_{HYP}) that may fail to explain the overall source and radiation path effects are the major deficiencies in these GMPEs. Needless to say these drawbacks provoke doubts about the database quality of most of these GMPEs that can jeopardize their efficient use in modern seismic hazard assessment. The referred shortcomings can also mask the existence of possible regional effects that may invoke differences in the ground motion trends of these two neighboring regions. These observations support the conclusive remarks of Douglas (2007) who emphasized the difficulties in assessing the regional dependency of ground motions due to limitations in the observed data and poorly constrained GMPEs.

Table 3.1 General features of empirical ground-motion predictive models from Iran and Turkey.

GMPE Acronym	Region	No of records & events	Magnitude scale	Magnitude interval	R type and R_{max} (km) [*]	Number of coefficients	Component [†]	Style-of-faulting [‡]	Site effect [**]	Sigma[¥]
Ayd96	Turkey	27, 19	M_S	3.5 – 7.6	R_{HYP}, 350	4	PGA in U	U	U	U
In96	Turkey	U	U	U	R_{EPI}, U	3	PGA in U	U	U	U
GK02	Turkey	93, 19	M_w	4.5 – 7.4	R_{JB} & R_{EPI}, 150	6	PGA, PSA in L	U	L	Yes
Sch02	Northwestern Turkey	683, U	M_L	0.9 – 7.2	R_{EPI}, 250	7	PGA, PSA in L	U	L	Yes
KG04	Turkey	112, 57	M_w	4.0 – 7.4	R_{JB}, 250	6	PGA, PSA in L	U	L	Yes
Ozb04	Northwestern Turkey	195, 17	M_w	5.0 – 7.4	R_{JB}, 300	7	PGA, PSA in GM	U	L	Yes
Uls04	Turkey	221, 122	M_w	4.1 – 7.5	R_{EPI}, 100	5	PGA in L	U	L	Yes
Bnd07	Northwestern Turkey	4047, 528	M_L	0.5 – 5.9	R_{HYP}, 200	5	PGA, PSA in L	U	L	Yes
A07	Turkey	U	U	U	R_{HYP}, U	4	PGA in U	U	L	U
AK09	Western Anatolia	168, 49	M_w, M_d, M_L	4.0 – 6.4	R_{HYP}, 200	4	PGA, PSA in L	U	L	Yes
UO10	Marmara Region	751, 78	M_w & M_d	4.0 - 7.4	R_{JB} & R_{EPI}, 197	3	PGA in L	S, N	U	Yes
AC10	Turkey	433, 137	M_w	5.0 - 7.6	R_{JB}, 200	12	PGA, PGV, PSA in GM	S, N, R	N	Yes

Table 3.1 Cont'd

GMPE Acronym	Region	No of records & events	Magnitude scale	Magnitude interval	R type and R_{max} (km) [*]	Number of coefficients	Component [†]	Style-of-faulting [‡]	Site effect [**]	Sigma[¥]
RS94	Iran	83, 20	M_S	5.1 - 7.7	R_{RUP} & R_{HYP}, 180	6	PGA in U	U	L	U
Zr99	Iran	468, 47	M_w & others	2.7 - 7.4	R_{RUP} & R_{HYP}, 224	7	PGA in B	S, R	L	Yes
K02	Iran	160, 28	M_w m_b & M_S	4.5 - 7.0	R_{JB} & R_{EPI}, 180	6	PGA, PSA in L	U	L	U
N05	Iran	279, 45	M_w & others	3.0 - 7.4	R_{EPI}, 245	5	PGA in V	U	L	Yes
M06	Central Iran	150, U	M_S & m_b	3.1 - 7.4	R_{HYP}, 98	4	PGA in U	U	L	Yes
ZS06	Iran	89, 55	M_w	2.7 - 7.4	R_{HYP}, 167	7	PGA, PSA in U	U	L	Yes
GAm07	Alborz & Central Iran	200, 50	M_S & m_b	4.5 - 7.3	R_{HYP}, 400	5	PGA in L	U	L	Yes
Ghs09	Iran & West Eurasia	893, 200	M_w	5.0 - 7.4	R_{RUP} & R_{HYP}, 100	7	PSA in GMRotI50	U	L	Yes
Sdg10	Iran	3894, 337	M_w	5.1 - 6.5	R_{EPI}, 340	6	PSA in U	U	L	Yes
GAm10	Alborz & Central Iran	416, 189	M_S & m_b	3.2 - 7.7	R_{HYP}, 400	3	PSA in L	U	L	Yes
HM12	East Central Iran	258, 109	M_w	5.0 - 7.4	R_{JB}, 100	5	PGA, PSA in L	U	U	Yes
Sfr12	Iran	351, 78	M_w	5.0 - 7.3	R_{RUP} & R_{HYP}, 135	8	PGA, PGV, PSA in GM	S, R	L	Yes

[*] R: distance, R_{max}: maximum distance, R_{EPI}: epicentral distance, R_{HYP}: hypocentral distance, R_{JB}: Joyner-Boore distance, R_{RUP}: closest distance
[†] B: both horizontal components, GM: geometric mean of horizontal components, GMRotI50: Boore et al. (2006), L: larger horizontal component, V: square root of sum of squares of the two components, U: Unknown
[‡] S: strike-slip faulting, N: normal faulting, R: reverse faulting, O: oblique faulting, U: unidentified
[**] U: Site effect is not considered, L: Linear site effects, N: Nonlinear site effects
[¥] U: Unknown

3.3. Iranian and Turkish Strong-Motion Databases and Some Preliminary Observations

The Turkish and Iranian strong-motion databases used in this study are subsets of the EMME strong-motion databank (Akkar et al., 2014a). This databank is compiled from the accelerograms of Turkey, Iran, Caucasus (Georgia and Armenia), Pakistan and Jordan and includes more than 4500 strong-motion records from 1721 earthquakes. 670 Turkish accelerograms and 528 Iranian accelerograms from were extracted the EMME strong-motion databank to develop the GMPEs. These data have the highest waveform quality and reliable metadata information in the entire databank. The total numbers of Turkish and Iranian earthquakes are 175 and 138, respectively. The accelerograms are recorded at 163 Turkish and 254 Iranian strong-motion stations.

All accelerograms are uniformly processed following Akkar and Bommer (2006). The maximum spectral period that can be used for each accelerogram is also determined from the empirical formulations given in Akkar and Bommer (2006). These expressions depend on the low-cut filter value and site conditions. The earthquakes included in the database have double-couple fault plane solutions reported by local and international agencies (Akkar et al., 2014a). This information is used to obtain the moment magnitudes, depths, fault mechanisms and distance measures of the data. The events whose moment magnitudes are estimated from magnitude-conversion equations were excluded. The strong-motion stations in the database have measured V_{S30} values. The Turkish site classification in terms of V_{S30} is given in Sandıkkaya et al. (2010) whereas the Iranian site measurements were obtained from local reports listed in Akkar et al. (2014a). The depth distributions of Turkish and Iranian earthquakes extend up to ~ 35 km. This depth gives a good range of shallow active crustal earthquakes in Iran and Turkey. The databases consist of singly recorded accelerograms to keep the good quality data as much as possible. Aftershock data were also not excluded from both datasets for the same reason. These features are the weak points of the database that may

introduce uncertainty in the regression coefficients and may inflate the sigma of the predictive model.

Figure 3.1.a shows the magnitude (M_w) vs. distance (R_{JB}) distribution of the database. Iranian and Turkish data are shown in different symbols and different color codes. The magnitude range of the database is $4.0 \leq M_w \leq 7.6$ and the maximum R_{JB} is 200 km. The magnitude distribution of Turkish data is more uniform than the Iranian data (Figure 3.1.b). The Iranian accelerograms are deficient in small magnitudes ($M_w \leq 5.0$). The distance distributions of Iranian and Turkish records draw similar patterns (Figure 3.1.c): they are better constrained at moderate to large distances (i.e., $R_{JB} \geq 30$ km). When magnitude and distance distributions are considered together, the Iranian data are scarce for $M_w < 5.0$ and $R_{JB} > 80$ km. Although the number of Turkish accelerograms decreases for $M_w < 5$, their distribution is better than the corresponding records in the Iranian database. As the regression coefficients of main estimator parameters were computed for distances up to 80 km, the low distance resolution of the Iranian accelerograms for $M_w < 5.0$ and $R_{JB} > 80$ km did not play a measure role in the analyses. The use of strong-motion data up to moderate distances (e.g., $R_{JB} \leq 80$ km) has been recently implemented in the NGA-West2 GMPEs (e.g., Abrahamson et al., 2014; Boore et al., 2014) as this distance range is of significance for most engineering applications as well as seismic hazard studies (Campbell and Bozorgnia, 2014). The details of regression analyses are discussed in the subsequent sections.

Figure 3.2 shows the distribution of Turkish and Iranian datasets in terms of soil conditions. The Iranian and Turkish datasets are plotted as magnitude vs. distance scatters. Different symbols and color codes on these plots define the distribution of accelerograms for different site classes. NEHRP (BSSC, 2009) site classification were used in the comparative plots because Turkish and Iranian design codes do not have similar site classification schemes. The Turkish database is dominated by NEHRP C ($360m/s \leq V_{S30} < 760m/s$) and D ($180m/s \leq V_{S30} < 360m/s$) sites (Figure

3.2.a). The vast majority of Iranian sites are NEHRP B (760m/s $\leq V_{S30} < 1500$m/s) and C (360m/s $\leq V_{S30} < 760$m/s) as given in Figure 3.2.b.
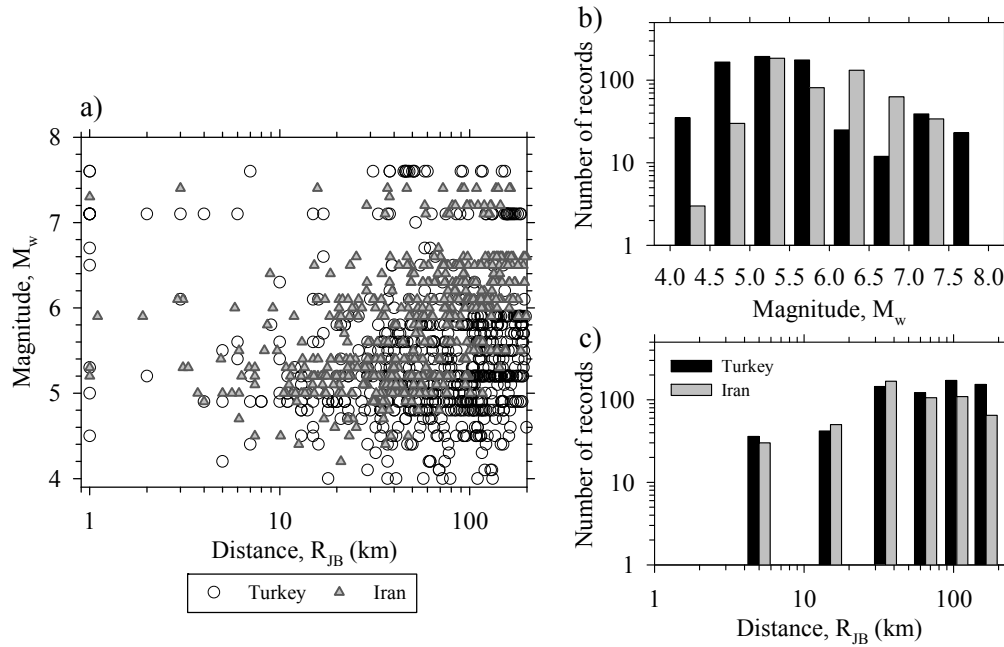
Figure 3.1 Strong-motion data distribution of Turkish and Iranian databases: a) R_{JB} vs. M_w scatters, b) Magnitude histogram, c) Distance histogram (Records having $R_{JB} < 1$ km are shown at $R_{JB} = 1$ km for illustrative purposes).
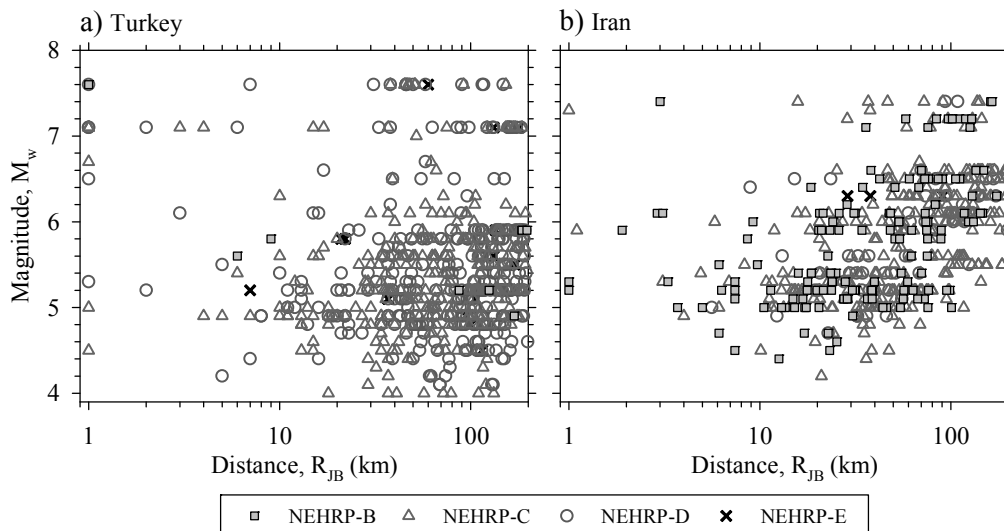
Figure 3.2 Distribution of the strong-motion data in terms site class: a) Turkish database, b) Iranian database.

Figure 3.3 compares both databases in terms of SoF. The scatter plots in Figure 3.3.a indicates uneven distribution of reverse (RV) faulting accelerograms in the Turkish database. Iranian database is poor in normal (NM) faulting events (Figure 3.3.b). Both datasets are better constrained for strike-slip (SS) earthquakes. Figure 3.4 compares the variation of observed PGA trends as a function of distance for different faulting mechanisms in the Turkish and Iranian databases. The first column shows the variations of SS vs. NM PGAs in the Turkish database. The second column does similar comparisons for SS vs. RV PGAs in the Iranian data. The selected SoF pairs from each dataset are those with better magnitude and distance distributions. Their comparisons would reveal reliable information about SoF effects specific to these databases. Strike-slip events constitute a good portion of data in both datasets. Thus, the last column plots in Figure 3.4 compare the observed PGA trends in the Iranian and Turkish data for SS accelerograms. The comparisons are done for $5 \leq M_w < 6$ and $6 \leq M_w < 7$ as the data number is more meaningful to compute first-order statistics within these magnitude intervals. All data were scaled to reference rock conditions ($V_{S30} = 750$ m/s) by using the Sandıkkaya et al. (2013) site model. The first column plots indicate that there are no systematic differences between SS and NM PGAs in the Turkish database. The diamond symbols that show the average NM and SS PGAs for different distance bins justify this observation. The second column plots depict either larger or similar SS PGAs with respect to their RV counterparts in the Iranian database. The larger SS PGAs in the Iranian data are noticeable towards shorter distances. The diamond symbols that describe the average SS and RV PGA trends for different distance bins in the Iranian data explain the above observation better. The comparative SS PGA plots from Iran and Turkey shows a systematic difference: Iranian PGA amplitudes seem to be larger than the corresponding PGA values of the Turkish dataset. The attenuation characteristics of the Turkish and Iranian PGAs also show differences. The Turkish data seem to decay faster than the Iranian data. These observations can be the indicatives of possible regional differences between the SACR accelerograms of the regions covered by the two countries.
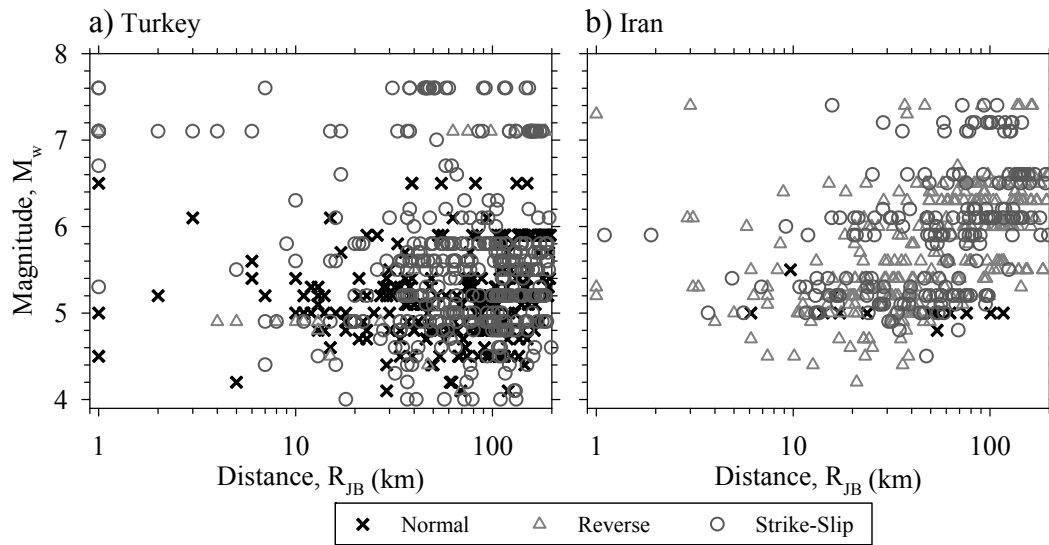
Figure 3.3 Distribution of strong-motion data in terms of magnitude, distance and style-of-faulting: a) Turkish database, b) Iranian database (NM, RV and SS are the abbreviations of normal, reverse and strike-slip fault mechanisms, respectively).
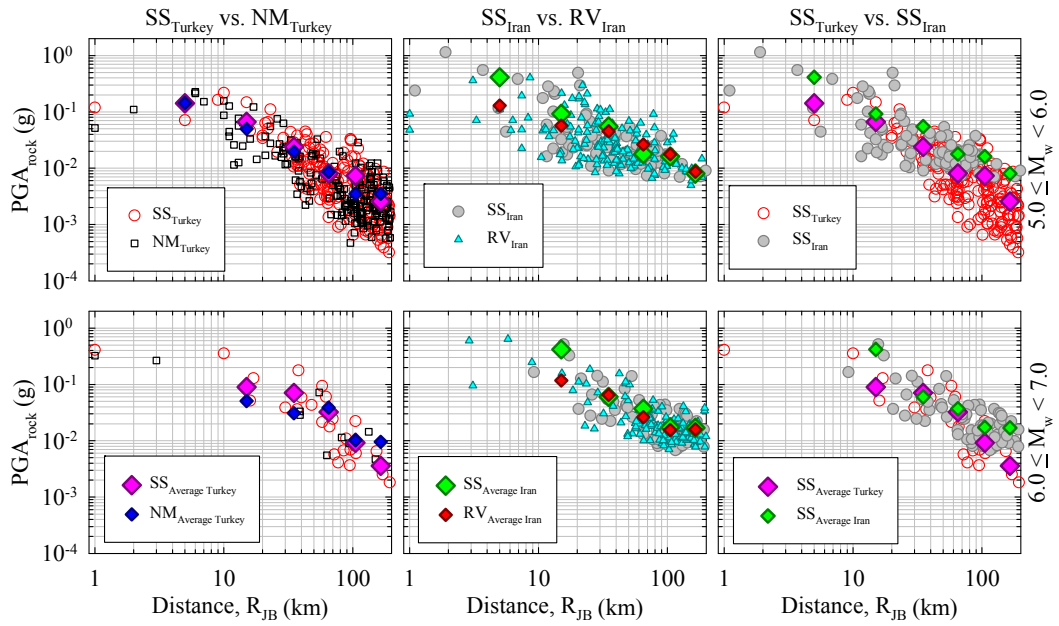
Figure 3.4 Comparisons of PGA trends in the Iranian and Turkish databases by considering style-of-faulting effects. All empirical data are modified for reference rock condition (V_{S30}=750m/s). First column plots compare SS vs. NM PGA trends within Turkish data whereas second column plots do similar type comparisons between SS vs. RV for the Iranian accelerograms. The last column compares the variation of Iranian and Turkish PGAs for SS events. First row comparisons are for $5 \leq M_w < 6$ and second row comparisons consider $6 \leq M_w < 7$ magnitude interval. The diamonds on each plot represent average PGA values for different R_{JB} bins. The selected R_{JB} bins are 0-10km, 10-20km, 20-50km, 50-80km, 80-130km and 130-200km where the data are meaningful for statistical computations.

Figure 3.5 shows the depth distribution of Iranian and Turkish events. The depth distributions are plotted for different faulting mechanisms and for different magnitude intervals. Note that SS and NM events show more uniform depth distribution between $4 \leq M_w \leq 6$ in the Turkish database (Figure 3.5.a). Moderate-to-large magnitude events ($M_w > 6$) in the Turkish database are mainly SS and they are accumulated between the depths of 10 km and 16 km. Iranian earthquakes seem to be deeper than the Turkish earthquakes (Figure 3.5.b) that is particularly more

noticeable for RV events. There are very few events in the first 5 km of depth in the Iranian data. SS as well as RV earthquakes follow similar distributions towards moderate-to-large magnitudes ($M_w > 6$), which is not observed in the Turkish dataset. The histograms in Figures 3.5.c to 3.5.e are shown for further discussions on the observed PGA trends in Figure 3.4. Figure 3.5.c indicates that the Turkish NM and SS earthquakes are mostly accumulated within the first 14 km depth and PGA amplitudes from these faulting mechanisms are not significantly different from each other (see Figure 3.4). The bulk of Iranian SS and RV events are within 7 km to 21 km (Figure 3.5.d) and PGA amplitudes of SS records are higher with respect to their RV counterparts towards shorter distances (see Figure 3.4). The Iranian and Turkish SS events are denser in the depth range of 7 km to 14 km and SS Iranian PGAs are generally higher than the corresponding Turkish ground motions in the entire distance interval of interest (see Figure 3.4). Thus, if the given data displays the general earthquake depth distributions of different faulting mechanisms in these countries, the depth dependence of ground-motion amplitudes change from one country to the other. The significance of depth on ground-motion amplitudes has been discussed in various publications. Akkar and Çağnan (2010) indicated smaller ground-motion amplitudes for deeper crustal earthquakes. McGarr (1984) explained the higher ground-motion amplitudes of some deeper crustal events by differences in stress conditions along the depth of the crust. Although the justification of the observations requires further investigation with the increase in data (see discussions in Douglas, 2007), they are mapped onto the regression model as explained in the following sections.
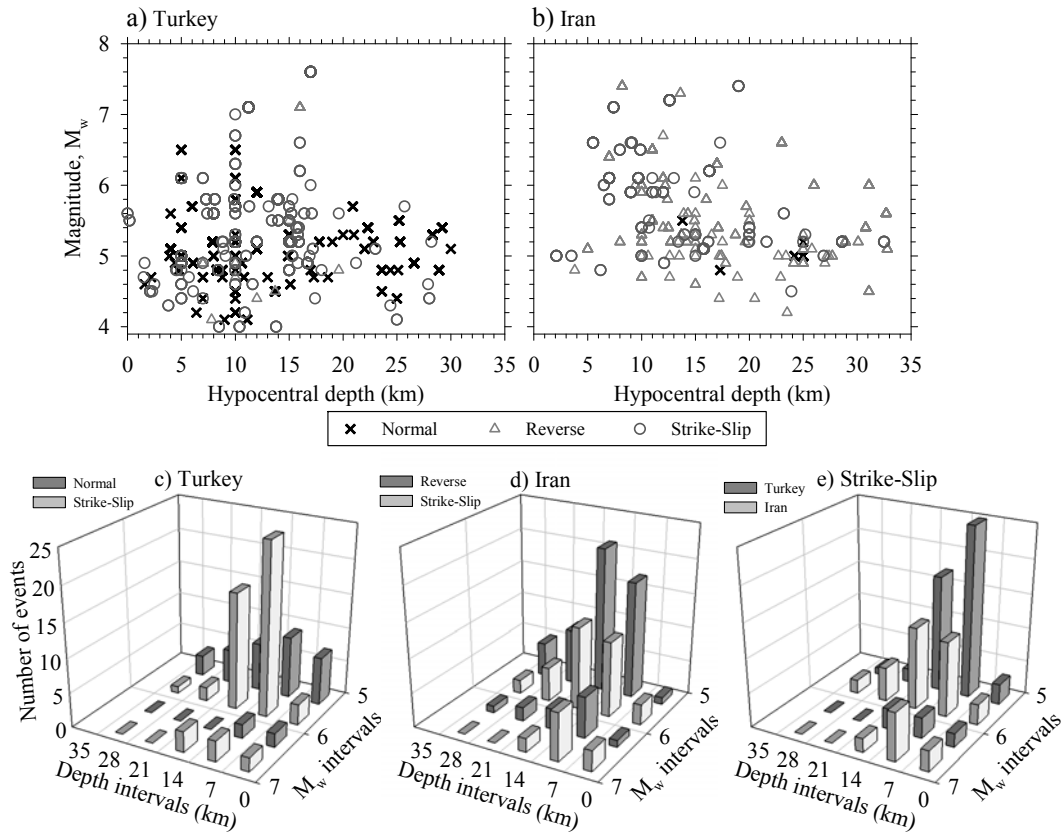
Figure 3.5 Distribution of strong-motion data in terms of magnitude (M_w), depth and style-of-faulting: a) Turkish database, b) Iranian database, c) M_w vs. depth histogram of Turkish NM and SS records for $5 \le M_w \le 7$, d) M_w vs. depth histogram of Iranian RV and SS records for $5 \le M_w \le 7$ and e) M_w vs. depth histogram of Turkish and Iranian SS records for $5 \le M_w \le 7$.

3.4. Functional Form of the GMPEs and Regression Analyses

The complexity of functional form is measured by the number of estimator parameters in a model. It should be optimized by considering the limitations of ground-motion dataset. Studies by Kaklamanos and Baise (2011) and Kale and Akkar (2013) concluded that complex functional forms do not necessarily perform better with respect to simpler ground-motion equations. Bearing on these results, the base function of Akkar and Çağnan (2010) in the GMPE were considered as the metadata information in the current database does not permit us to include very

89

complicated estimator parameters. As an improvement over the Akkar and Çağnan (2010) base function, the GMPE additionally accounts for anelastic attenuation and magnitude-dependent (heteroscedastic) standard deviation. Equation 3.1 shows the functional form for estimating the geometric means of horizontal PGA (g), PGV (cm/s) and PSA (g) that are designated as Y.

$$ln(Y) = \begin{cases} ln\,PGA; & PSA < PGA \quad and \quad T < 0.2s \\ f_{mag} + f_{dis} + f_{sof} + f_{aat} + f_{site} + \varepsilon\sigma; & otherwise \end{cases} \qquad (3.1)$$

The proposed model considers magnitude scaling (f_{mag}), geometric decay (f_{dis}), SoF (f_{sof}), site effects (f_{site}) and anelastic attenuation (f_{aat}) to estimate the logarithmic mean (median) of above intensity measures. σ (sigma) is the standard deviation and ε is the number of sigma above or below the median estimates of Y. The short-period PSA estimates are capped with PGA (Equation 3.1) as in some cases the estimated PSA for $T < 0.2s$ falls below the computed PGA at large distances. This phenomenon is also observed in the GMPEs developed by Chiou and Youngs (2014) and Campbell and Bozorgnia (2014). Both of these studies characterize this phenomenon as an artifact of numerical analysis that led us to implement such a constraint in the model. Equations 3.2 - 3.5 present f_{mag}, f_{dis}, f_{sof} and f_{aat}, respectively. The term c_1 in Equation 3.2 represents the hinging magnitude that accounts for magnitude saturation effects after $M_w > c_1$ (see discussions on Figure 3.11 for further information about c_1). F_{NM} and F_{RV} are dummy variables in f_{sof} and they are unity for normal and reverse faults, respectively. For strike-slip events, F_{NM} and F_{RV} are zero. Note that the regression coefficients of these functions have additional Δ terms that describe the difference between the Turkish and Iranian ground-motion amplitude estimates. When regression coefficients with additional Δ terms are used, the predictive model estimates ground-motion amplitudes for Iran.

90

$$f_{mag} = \begin{cases} M_w \leq (c_1 + \Delta c_1); \\ (b_1 + \Delta b_1) + (b_2 + \Delta b_2)(M_w - (c_1 + \Delta c_1)) + (b_3 + \Delta b_3)(8.5 - M_w)^2 \\ M_w > (c_1 + \Delta c_1); \\ (b_1 + \Delta b_1) + (b_7 + \Delta b_7)(M_w - (c_1 + \Delta c_1)) + (b_3 + \Delta b_3)(8.5 - M_w)^2 \end{cases} \quad (3.2)$$

$$f_{dis} = [(b_4 + \Delta b_4) + (b_5 + \Delta b_5)(M_w - (c_1 + \Delta c_1))]ln\sqrt{R_{JB}^2 + (b_6 + \Delta b_6)^2} \quad (3.3)$$

$$f_{sof} = (b_8 + \Delta b_8)F_{NM} + (b_9 + \Delta b_9)F_{RV} \quad (3.4)$$

$$f_{aat} = \begin{cases} 0; & R_{JB} \leq 80\,km \\ (b_{10} + \Delta b_{10})(R_{JB} - 80); & R_{JB} > 80\,km \end{cases} \quad (3.5)$$

The nonlinear site function proposed by Sandıkkaya et al. (2013) that is developed for the broader Europe is used to account for site effects (f_{site}). The site model proposed in Sandıkkaya et al. (2013) is given in Equation (3.6). The regression coefficients of Sandıkkaya et al. (2013) were smoothed in the GMPE as its unsmoothed coefficients introduce jagged spectral shapes for low V_{S30} values. The reference rock PGA (PGA$_{REF}$ for V_{REF} = 750m/s) used in Equation (3.6) is predicted from the base functional form. V_{CON} is 1000 m/s in the Sandıkkaya et al. (2013) site model that represents the V_{S30} value for the commencement of constant site amplification. The other constants in Equation (3.6) are c = 2.5 and n = 3.2. They represent the transition between higher and lower ground-motion amplitudes (c) and soil nonlinearity (n). The period dependent sb_1 and sb_2 coefficients of Equation (3.6) are listed in Table 3.2 for some selected periods in the GMPE. Note that the Sandıkkaya et al. (2013) site model is valid for 150 m/s ≤ V_{S30} ≤ 1200 m/s. Thus, the regression analysis did not consider the Iranian and Turkish accelerograms falling outside of this V_{S30} interval.

$$f_{site} = \begin{cases} sb_1 ln(\dfrac{V_{S30}}{V_{REF}}) + sb_2 ln\left[\dfrac{PGA_{REF} + c(V_{S30}/V_{REF})^n}{(PGA_{REF} + c)(V_{S30}/V_{REF})^n}\right]; & V_{S30} < V_{REF} \\ sb_1 ln\left[\dfrac{min(V_{S30}, V_{CON})}{V_{REF}}\right]; & V_{S30} \geq V_{REF} \end{cases} \quad (3.6)$$

Table 3.2 Period-dependent f_{site} coefficients (Sandıkkaya et al., 2013).

Period (s)	sb$_1$	sb$_2$
PGA	-0.41997	-0.28846
PGV	-0.72057	-0.19688
0.01	-0.41729	-0.28685
0.02	-0.39998	-0.28241
0.03	-0.34799	-0.26842
0.04	-0.27572	-0.24759
0.05	-0.21231	-0.22385
0.075	-0.13909	-0.17798
0.1	-0.26492	-0.28832
0.15	-0.48496	-0.39525
0.2	-0.64239	-0.44574
0.3	-0.82052	-0.45287
0.4	-0.90568	-0.41105
0.5	-0.95097	-0.37956
0.75	-1.00027	-0.32233
1	-1.01881	-0.28172
1.5	-0.96317	-0.22449
2	-0.91305	-0.18388
3	-0.84242	-0.12665
4	-0.79231	-0.08605

The total aleatory variability (σ) is given in Equation (3.7). The terms τ and ϕ describe inter-event (between-event) and intra-event (within-event) standard deviations, respectively.

$$\sigma = \sqrt{\tau^2 + \phi^2} \qquad (3.7)$$

ϕ and τ are calculated from Equations 3.8 and 3.9, respectively. sd_1 and sd_2 are the weighted standard deviations obtained from regression analyses whereas w designates magnitude-dependent weighting function. The weights are determined by examining the sigma trends of each ground-motion intensity parameter in different magnitude intervals. The weighting function, w, follows a trilinear backbone curve as in Boore et al. (2014). The magnitude bins were assembled with 0.5 magnitude units starting from M_w 4. Figure 3.6 illustrates the weights for PGA for the Iranian and Turkish data. The overall expression for w is given in Equation 3.10 where a_1 and a_2 are the weighting factors of the designated magnitude ranges.

The Δ terms indicate the difference between the Turkish and Iranian weighting factors. It is noted that the methodology to compute weighting functions is different than those implemented by Ambraseys et al. (2005) and Akkar and Bommer (2007). These studies did not cap the magnitude-dependent weights towards larger and smaller magnitudes that resulted in significant differences in sigma between small and large magnitude events.

$$\phi = w \cdot sd_1 \qquad (3.8)$$

$$\tau = w \cdot sd_2 \qquad (3.9)$$

$$w = \begin{cases} a_1 + \Delta a_1 & M_w < 6.0 \\ (a_1 + \Delta a_1) + ((a_2 + \Delta a_2) - (a_1 + \Delta a_1)) {}^{(M_w - 6.0)}\!/_{0.5} & 6.0 \le M_w < 6.5 \\ (a_2 + \Delta a_2) & M_w \ge 6.5 \end{cases} \qquad (3.10)$$
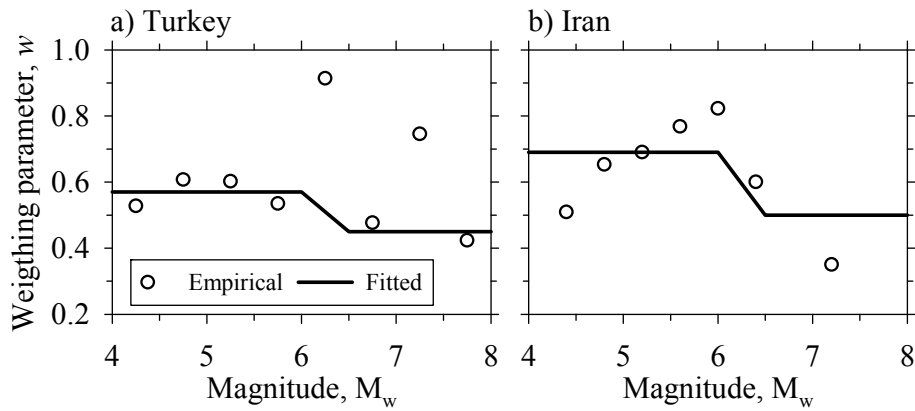
Figure 3.6 Illustration of weighting factors for the standard deviation of PGA: a) Turkey, b) Iran.

The mixed-effects regression algorithm (Abrahamson and Youngs, 1992) was used in the regressions. The spectral periods vary from 0.0s (PGA) to 4.0s that are represented by 63 discrete spectral periods. PGV is also estimated by this GMPE. Regressions were done for reference rock condition (V_{S30} = 750m/s) by scaling the

accelerograms to V_{S30} = 750m/s via Sandıkkaya et al. (2013). The coefficients of the GMPE were tailored in multiple steps. The first phase in the analyses was to compute weighting functions (*w*). The reason for computing weighting functions is two folded: (1) prevent excessive sigma due to higher uncertainty in small magnitude events, and (2) smooth out the uneven magnitude distribution in the Iranian and Turkish databases. The databases were divided into several magnitude bins of 0.5 magnitude units as indicated previously. Separate median curves were fit to the accelerograms falling into these bins for each spectral period. Given a period, the trends in the associated standard deviations were used to develop the magnitude-dependent weighting functions of sigma. An illustration to this step is already given in Figure 3.6 and regression coefficients for *w* are listed in Table 3.3. The rest of the regression coefficients were developed from weighted regression analyses.

Magnitude-dependent regression coefficients (b_2, b_3, b_5, b_6, b_7) as well as the regression coefficients to account for SoF effects (b_8 and b_9) were obtained from near-source records ($R_{JB} \leq 80$km) in the database. Distance scaling term (b_4) was computed using the entire database (accelerograms with $R_{JB} \leq 200$km). The anelastic attenuation coefficient (b_{10}) was obtained from the far-source accelerograms ($80 \leq R_{JB} \leq 200$km). The constant regression term (b_1) was also obtained by considering the entire database. This final step in the regression analyses also led to the computation of intra-event (sd_1) and inter-event (sd_2) sigma components. The coefficients were smoothed after each regression step to remove jagged variation of estimated response spectra. Tables 3.4 and 3.5 give the regression coefficients of the proposed model for some of the selected periods. As indicated previously, the Δ terms listed in parenthesis, should be considered as additive terms to account for the ground-motion estimates of Iran. The entire list of the regression coefficients of the ground-motion model are given in Appendix A of this thesis.

Table 3.3 Period-dependent sigma coefficients (Δ values in parenthesis designate the differences in the regression coefficients between Turkey and Iran).

Period (s)	a_1 (Δa_1)	a_2 (Δa_2)	sd_1 (Δsd_1)	sd_2 (Δsd_2)
PGA	0.570 (0.120)	0.450 (0.050)	1.0521 (-0.0808)	0.7203 (-0.3250)
PGV	0.560 (0.140)	0.460 (-0.020)	1.0449 (-0.0597)	0.6452 (-0.3013)
0.01	0.574 (0.116)	0.453 (0.047)	1.0444 (-0.0723)	0.7150 (-0.3231)
0.02	0.577 (0.113)	0.455 (0.045)	1.0424 (-0.0701)	0.7137 (-0.3180)
0.03	0.581 (0.109)	0.458 (0.042)	1.0459 (-0.0705)	0.7113 (-0.3143)
0.04	0.584 (0.106)	0.460 (0.040)	1.0557 (-0.0597)	0.7155 (-0.3064)
0.05	0.588 (0.122)	0.463 (0.037)	1.0609 (-0.0700)	0.7166 (-0.2770)
0.075	0.597 (0.143)	0.469 (0.031)	1.0692 (-0.0994)	0.7677 (-0.3045)
0.1	0.606 (0.154)	0.475 (0.025)	1.0429 (-0.0486)	0.7735 (-0.3358)
0.15	0.624 (0.136)	0.488 (-0.018)	1.0063 (0.0394)	0.7442 (-0.2839)
0.2	0.642 (0.118)	0.500 (-0.050)	0.9781 (0.1081)	0.7213 (-0.3050)
0.3	0.678 (0.082)	0.525 (-0.075)	0.9407 (0.0759)	0.6547 (-0.2651)
0.4	0.700 (0.060)	0.550 (-0.100)	0.9430 (0.0563)	0.6413 (-0.2308)
0.5	0.673 (0.087)	0.550 (-0.100)	0.9519 (0.0209)	0.6496 (-0.1724)
0.75	0.620 (0.140)	0.550 (-0.088)	1.0489 (-0.0161)	0.6582 (-0.2379)
1	0.620 (0.160)	0.550 (-0.025)	1.0534 (-0.0793)	0.6342 (-0.2569)
1.5	0.620 (0.160)	0.550 (0.050)	1.0988 (-0.1337)	0.6173 (-0.2358)
2	0.620 (0.160)	0.550 (0.050)	1.1594 (-0.2183)	0.5724 (-0.1482)
3	0.620 (0.160)	0.550 (0.050)	1.1596 (-0.2262)	0.6251 (-0.1356)
4	0.620 (0.160)	0.550 (0.050)	1.0373 (-0.2279)	0.5409 (-0.0862)

Table 3.4 Period-independent hinging magnitude and regression coefficients of the predictive model (Δ values in parenthesis designate the differences in the regression coefficients between Turkey and Iran).

c_1 (Δc_1)	b_2 (Δb_2)	b_5 (Δb_5)	b_6 (Δb_6)	b_7 (Δb_7)
6.75 (0.25)	0.193 (-0.146)	0.170 (-0.120)	8.00 (0.00)	-0.354 (0.396)

Table 3.5 Period-dependent regression coefficients of the ground-motion model (Δ values in parenthesis designate the differences in the regression coefficients between Turkey and Iran).

Period (s)	b_1 (Δb_1)	b_3 (Δb_3)	b_4 (Δb_4)	b_8 (Δb_8)	b_9 (Δb_9)	b_{10} (Δb_{10})
PGA	1.74221 (-0.21234)	-0.07049 (-0.03826)	-1.18164 (0.17210)	-0.01329 (-0.11697)	-0.09158 (0.00000)	-0.00156 (0.00156)
PGV	5.58266 (0.20834)	-0.13822 (-0.05505)	-0.94043 (0.04886)	-0.17037 (0.17037)	-0.08609 (0.00000)	-0.00052 (0.00052)
0.01	1.75746 (-0.22738)	-0.06981 (-0.03877)	-1.18362 (0.17408)	-0.01349 (-0.11677)	-0.09158 (0.00000)	-0.00156 (0.00156)
0.02	1.78825 (-0.24100)	-0.07058 (-0.03674)	-1.18653 (0.17587)	-0.01189 (-0.11837)	-0.09158 (0.00000)	-0.00160 (0.00160)
0.03	1.87916 (-0.25702)	-0.06976 (-0.0337)	-1.19699 (0.16911)	-0.00748 (-0.12278)	-0.09158 (0.00000)	-0.00170 (0.00170)
0.04	2.00393 (-0.25260)	-0.06732 (-0.02850)	-1.21315 (0.16032)	0.00788 (-0.13814)	-0.09158 (0.00000)	-0.00182 (0.00182)
0.05	2.16076 (-0.24029)	-0.06226 (-0.02834)	-1.24101 (0.16138)	0.03907 (-0.16933)	-0.09158 (0.00000)	-0.00197 (0.00197)
0.075	2.52625 (-0.13086)	-0.05082 (-0.03978)	-1.30390 (0.16548)	0.08131 (-0.21157)	-0.09158 (0.00000)	-0.00235 (0.00235)
0.1	2.72364 (-0.02321)	-0.05217 (-0.03843)	-1.32996 (0.15961)	0.10000 (-0.23026)	-0.09158 (0.00000)	-0.00267 (0.00267)
0.15	2.91835 (-0.23382)	-0.06397 (-0.03475)	-1.31888 (0.20607)	0.06727 (-0.19753)	-0.09158 (0.00000)	-0.00296 (0.00296)
0.2	2.85623 (-0.33645)	-0.07494 (-0.03634)	-1.27072 (0.22054)	0.01620 (-0.14646)	-0.09158 (0.00000)	-0.00275 (0.00275)
0.3	2.44252 (-0.30222)	-0.09387 (-0.03939)	-1.16008 (0.19687)	-0.03697 (0.03697)	-0.09158 (0.00185)	-0.00204 (0.00204)
0.4	1.97772 (-0.16785)	-0.10977 (-0.04263)	-1.05535 (0.14350)	-0.06582 (0.06582)	-0.09158 (0.09158)	-0.00161 (0.00161)
0.5	1.56410 (0.01469)	-0.12342 (-0.04586)	-0.97014 (0.08974)	-0.08511 (0.08511)	-0.01297 (0.01297)	-0.00127 (0.00127)
0.75	0.84856 (0.40612)	-0.15056 (-0.05345)	-0.83799 (-0.00312)	-0.11756 (0.11756)	0.00000 (0.00000)	-0.00066 (0.00066)
1	0.41833 (0.58724)	-0.17099 (-0.06008)	-0.77438 (-0.04979)	-0.14267 (0.14267)	0.00000 (0.00000)	-0.00022 (0.00022)
1.5	-0.10161 (0.75311)	-0.19999 (-0.07073)	-0.72272 (-0.08751)	-0.14621 (0.14621)	0.00000 (0.00000)	0.00000 (0.00000)
2	-0.45413 (0.83361)	-0.21978 (-0.07873)	-0.70389 (-0.10083)	-0.14621 (0.14621)	0.00000 (0.00000)	0.00000 (0.00000)
3	-0.95276 (0.90733)	-0.24530 (-0.08977)	-0.69065 (-0.10974)	-0.14621 (0.14621)	0.00000 (0.00000)	0.00000 (0.00000)
4	-1.29675 (0.82641)	-0.26119 (-0.09696)	-0.68620 (-0.11252)	-0.14621 (0.14621)	0.00000 (0.00000)	0.00000 (0.00000)

3.5. Evaluation of Proposed Ground-Motion Model: Effects of Regional Differences

The residual plots are shown in Figures 3.7 and 3.8 to explore the degree of agreement between the ground-motion estimates of the GMPE and the empirical observations from Turkish (Figure 3.7) and Iranian (Figure 3.8) datasets. The inter-event (η_i) and intra-event (ε_{ij}) residuals in these figures are plotted for PGV, PGA, PSA at T = 0.2s and T = 1.0s. The grey shaded regions in the residual plots indicate the mean ± standard deviation of residuals. The error bars indicate the standard errors on the estimates of the mean residuals. The inter-event residuals for M_w as well as intra-event residuals for R_{JB} and V_{S30} display random distributions for both datasets. The corresponding mean residuals also fluctuate about zero advocating that the estimates of the ground-motion model are unbiased with respect to these estimator parameters. The inter-event residual distribution of the Turkish data displays a more dispersive behavior when compared to the inter-event residual trends in the Iranian dataset. It is believed that the magnitude-dependent distribution of singly-recorded events in the Turkish and Iranian databases play a role in this observation. There are more singly-recorded events in the Turkish dataset (62 vs. 50) and ~65% of these events have M_w < 5.0. The corresponding fraction is ~20% in the Iranian data. The singly-recorded earthquakes tend to inflate inter-event sigma. It is believed that the skewed nature of singly-recorded event distribution towards smaller magnitudes in the Turkish dataset increases this adverse effect as observed in Figure 3.7.

The period-dependent variations of inter-event (τ) and intra-event (ϕ) standard deviations of the GMPE are shown in Figure 3.9 for M_w 5.0 and M_w 7.5. Both τ and ϕ decrease with increasing magnitude as the sigma model is heteroscedastic. The Turkish inter-event sigma (Figure 3.9.a) draws the upper bound with respect to its Iranian counterpart due to the skewed distribution of singly-recorded events towards lower magnitudes. The intra-event standard deviations (Figure 3.9.b) show fairly similar trends. The size of data for regression analysis reduces at longer

periods due to maximum usable period range of each accelerogram. This results in a decaying trend in ϕ towards longer periods as observed in Figure 3.9.b.
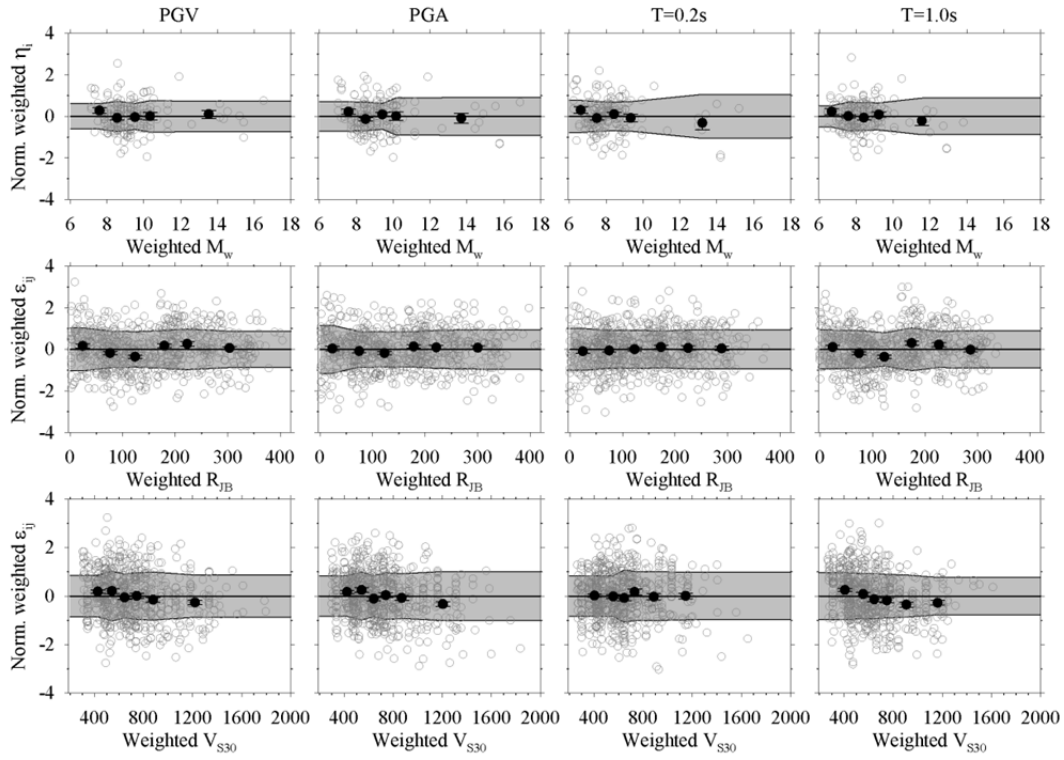
Figure 3.7 Inter-event (first row) and intra-event (second and third rows) residuals of the predictive model for Turkish data.
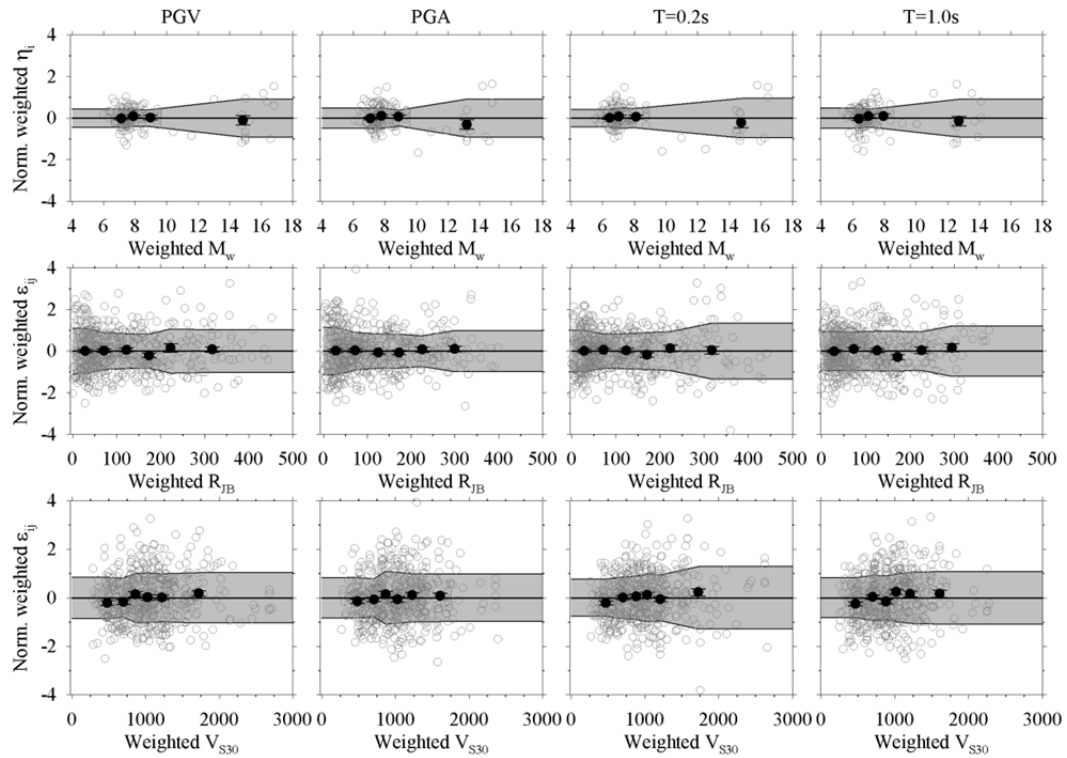
Figure 3.8 Inter-event (first row) and intra-event (second and third rows) residuals of the predictive model for Iranian data.
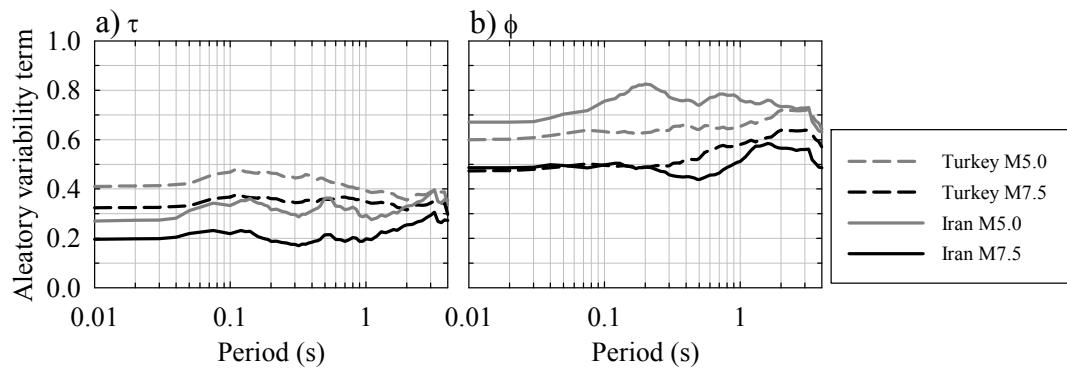
Figure 3.9 Comparisons of inter-event (left panel) and intra-event (right panel) sigmas for the entire period range for the Turkish and Iranian datasets. The comparisons are done for M_w 5.0 and M_w 7.5.

Figure 3.10 compares the distance scaling of the ground-motion model for Iran and Turkey. The comparisons are given for magnitudes ranging between M_w 4 and M_w 8. The chosen spectral ordinates are PGA and PSA at T = 0.2s, T = 1.0s and T =

3.0s. The median trends in Figure 3.10 are computed for reference rock ($V_{S30} = 750m/s$) conditions. The faulting mechanism is strike-slip. The estimated spectral ordinates are higher for Iran and the difference in the depth distribution of crustal earthquakes in Turkey and Iran can be one of the main reasons behind this observation (see discussions on Figures 3.4 and 3.5). The distance-dependent decay rates of Iranian and Turkish ground-motions also show differences, particularly, for moderate-to-small magnitudes: a more gradual decay is observed in the Iranian ground motions that can be the attributed to the higher Q factors in Iran. Studies by Akıncı and Eyidoğan (1996), Horasan et al. (1998) and Horasan and Boztepe-Güney (2004) indicate lower Q factors in Turkey with respect to those computed from different regions in Iran (e.g., Zafarani et al., 2012; Hassani et al., 2011; Zafarani and Soghrat, 2012).
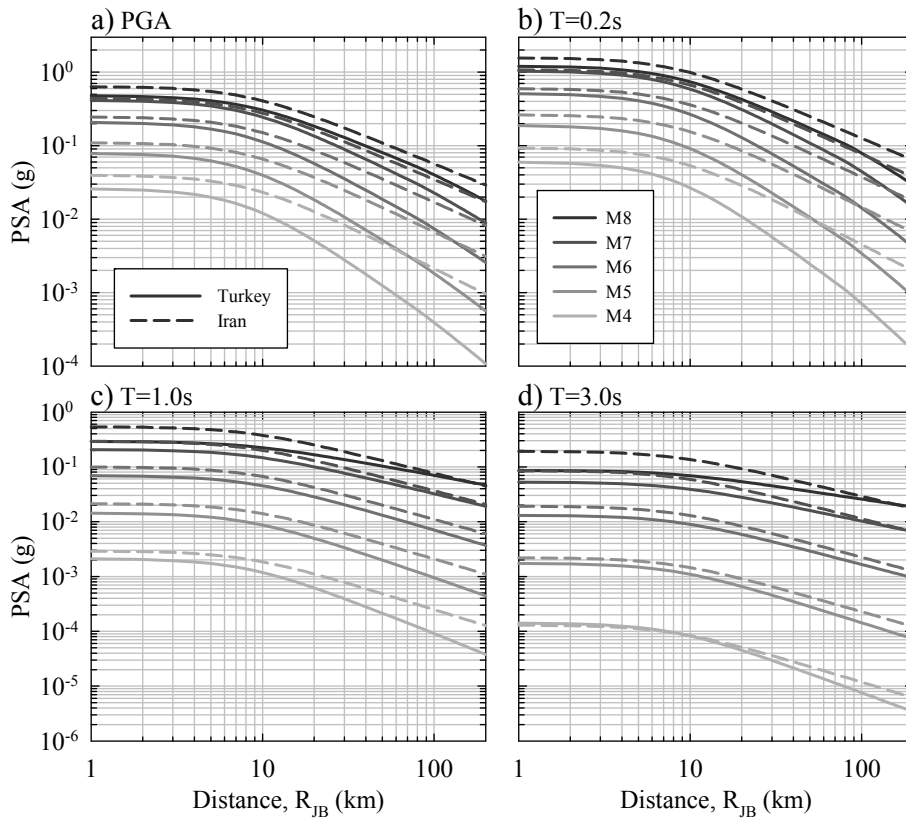
Figure 3.10 Distance scaling of the proposed GMPE for Iran and Turkey for reference rock ($V_{S30} =750m/s$) at different strike-slip spectral ordinates (PGA, PSA at T = 0.2s, 1.0s and 3.0s). The plots are given for a magnitude range of M_w 4 - 8.

The uneven distribution of small magnitude events ($M_w < 5$) in the Iranian and Turkish databases may affect the above observations. Thus, another set of regressions were run by limiting both datasets with earthquakes above M_w 5. Figure 3.11 compares the magnitude scaling of these new GMPEs with the one obtained from the original ground-motion model. The comparisons are done for PGA (Figure 3.11.a) and PSA at T = 1.0s (Figure 3.11.b) at a distance of R_{JB} = 10 km from a strike-slip fault. The site is once again chosen as reference rock site (V_{S30} = 750m/s). The plots also show the observed data scaled to mimic the above earthquake scenario. The scaling is done by using the new GMPEs developed for $M_w > 5$. No appreciable differences are observed from the median estimates of new ground-motion model and the original GMPE. Therefore, the discussions on the regional differences between SACRs in Iran and Turkey reflect the actual data trends. The magnitude scaling plots in Figure 3.11 also provide visual information about the hinging magnitude (c_1) differences between the two datasets. The magnitude saturation commences at slightly larger magnitudes ($\sim M_w$ 7) in the Iranian data (more noticeable in the observed PGA data) and the predictive model imposes Δc_1 = 0.25 to appreciate this difference while estimating the ground motions in Iran.
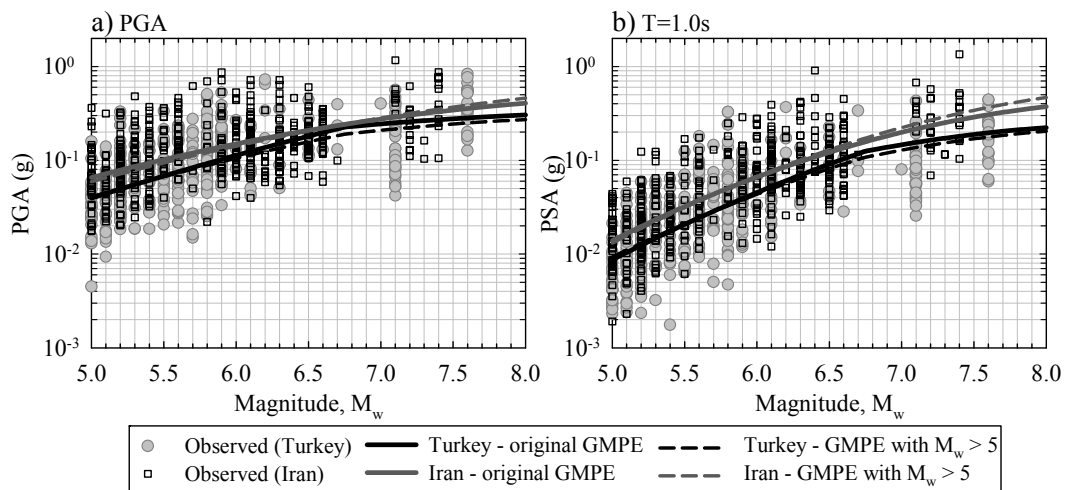
Figure 3.11 Magnitude-scaling comparison of the original GMPE with the new model developed from $M_w > 5$ empirical data. The comparisons are done for a rock site (V_{S30} = 750m/s) at a distance of R_{JB} = 10km from a strike-slip fault.

The strike-slip spectral acceleration estimates of Iran and Turkey for $0.0 \text{ s} \leq \text{T} \leq 4.0$ s are shown in Figure 3.12. The panels in the first row compare the median PSA values for M_w 6. The bottom row panels make similar comparisons for median + sigma spectral accelerations for M_w 8. The site conditions are represented by V_{S30} = 225 m/s in the scenario events. The spectral accelerations are plotted for $1 \text{ km} \leq R_{JB} \leq 30 \text{ km}$. It is noted that the M_w 8 case pushes the ground-motion model out of its limits as the maximum magnitude in the database is M_w 7.6. The larger spectral estimates from Iran are the immediate observation in this figure. This observation is highlighted in the other comparative figures in this section. The Iranian pseudo-acceleration spectra display a wider plateau in the acceleration sensitive spectral region. The faster decay of short-period spectral ordinates for Turkey reduces the width of acceleration plateau in the Turkish spectrum. This characteristic is more notable for the M_w 6 case. The Turkish spectral envelops also decay faster in the long-period range.

The differences in kappa behavior can contribute to the observed discrepancies in the spectral shapes, magnitude and distance scaling of Turkish and Iranian ground motions. The variation of kappa in the ground-motion database is given in Figure 3.13. Anderson and Hough (1984) were used in kappa computations by fitting a linear line to Fourier acceleration spectrum between 5 Hz and f_x that corresponds to a fraction of low-pass filter frequency to minimize the filtering effects on the Fourier acceleration components. The fraction that were used for f_x is based on the recommendations by Akkar et al. (2011). The choice of 5 Hz as the starting frequency of linear fits is parallel with the studies of Anderson and Hough (1984) and Douglas et al. (2010). The trends given in Figure 3.13 indicate that the Turkish data display higher kappa towards smaller magnitudes ($M_w \leq 6$), larger distances ($R_{JB} > 50 \text{ km}$) and softer sites ($V_{S30} \leq 400 \text{ m/s}$). These attributes would play a role in the faster decaying of short-period spectral ordinates in the Turkish data as given in Figures 3.10 and 3.12. The differences in the spectral shapes of Turkey and Iran can also stem from the regional discrepancies in the near-surface velocity profiles.
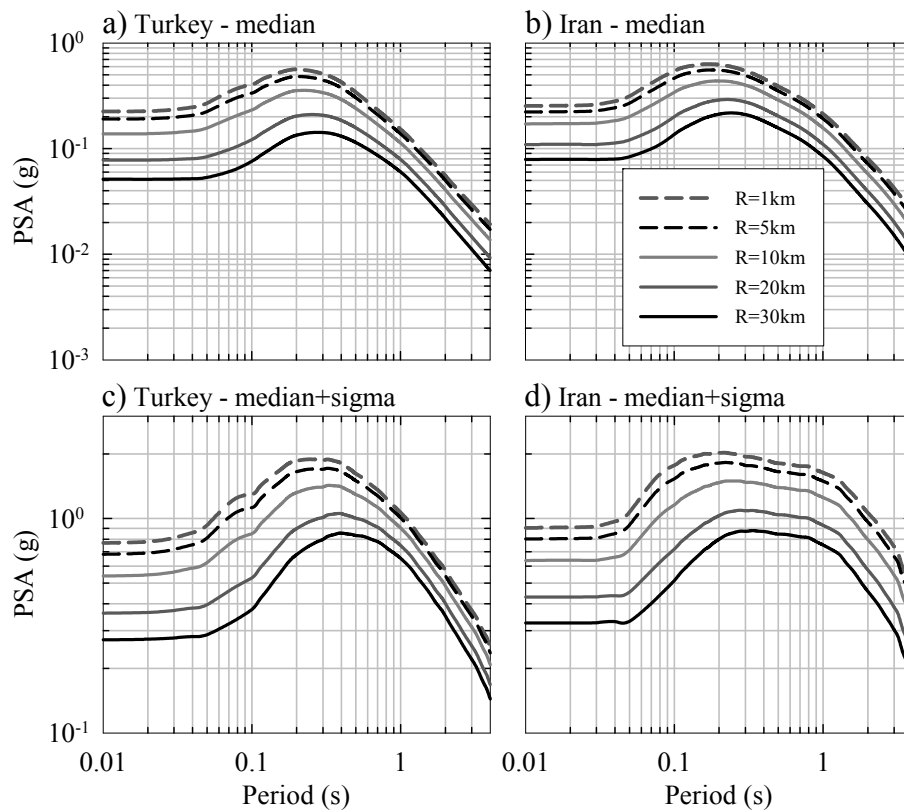
Figure 3.12 Comparison of spectral ordinates between Turkey (first column) and Iran (second column) for M_w 6 (top row) and M_w 8 (bottom row). The scenario earthquake is assumed to take place on a strike-slip fault at sites with distances ranging between 1 km $\leq R_{JB} \leq$ 30 km. The site condition is represented by V_{S30} = 225 m/s in the plots.
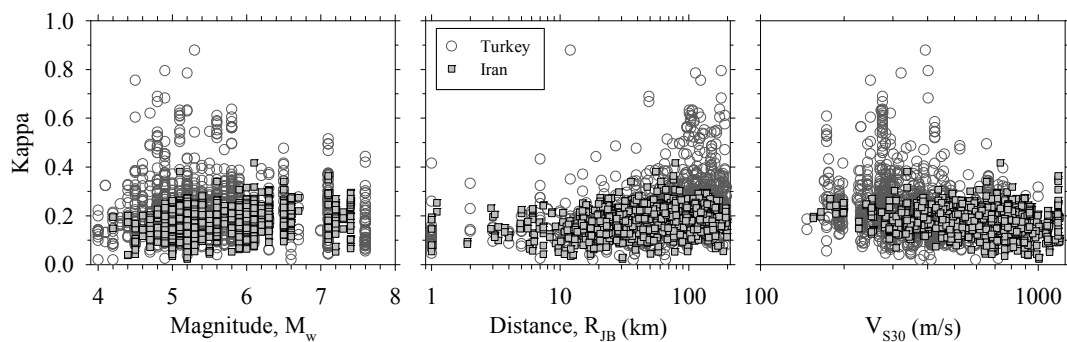
Figure 3.13 Variation of kappa in terms of magnitude, distance and V_{S30} for Turkish and Iranian data.

3.6. Comparison of Proposed Ground Motion Model with Other GMPEs

The ground-motion model was compared with the global GMPEs developed from Europe as well as NGA-West2 project (Bozorgnia et al., 2014). Figure 3.14 compares normal-to-strike slip (NM/SS, left panel) and reverse-to-strike slip (RV/SS, right panel) ratios of the predictive model with Akkar et al. (2014b) (ASB14), Bindi et al. (2014) (Bnd14), Abrahamson et al., 2014 (ASK14), Boore et al. (2014) (BSSA14), Campbell and Bozorgnia (2014) (CB14) and Chiou and Youngs (2014) (CY14) GMPEs. ASB14 and Bnd14 were developed from the subsets of the most recent pan-European database, RESORCE (Akkar et al., 2014c). The other global GMPEs (ASK14, BSSA14, CB14 and CY14) were developed from the different datasets of updated PEER-NGA database (Ancheta et al, 2014). A moment magnitude value of M_w 7.0 for ASK14, CB14 and CY14 is used as their style-of-faulting ratios are magnitude dependent. The style-of-faulting ratios given in Figure 3.14 draw a complicated picture even for global GMPEs that are developed from different subsets of the same strong-motion database. The NM/SS ratios also depict differences for the Iranian and Turkish data. This fact once again emphasizes the dependence of SoF function on the strong-motion database (Akkar et al., 2012) that may reflect some regional effects on ground-motion amplitudes as part of other factors. Although disparities in NM/SS are significant among the compared GMPEs, their general tendency is lower NM ground motions with respect to SS. The exception to this trend is the new GMPE for the Turkish data and Bnd14. They estimate higher NM ground-motions for certain intervals of spectral periods. Note that RR/SS ratios display a wider scatter among the compared GMPEs. The ground-motion model estimates lower RV ground-motion amplitudes with respect to SS at short periods. On average, the RV and SS ground-motion amplitudes attain the same values towards longer periods in the GMPE. The RR/SS ratios of the proposed model do not indicate significant differences for the Turkish and Iranian data. These trends carry some similarities with the RV/SS ratios of BSSA14 and ASK14 at short and long periods,

respectively. The rest of the GMPEs display different RV/SS patterns that could be considered as the indications of complexity in SoF ratios.
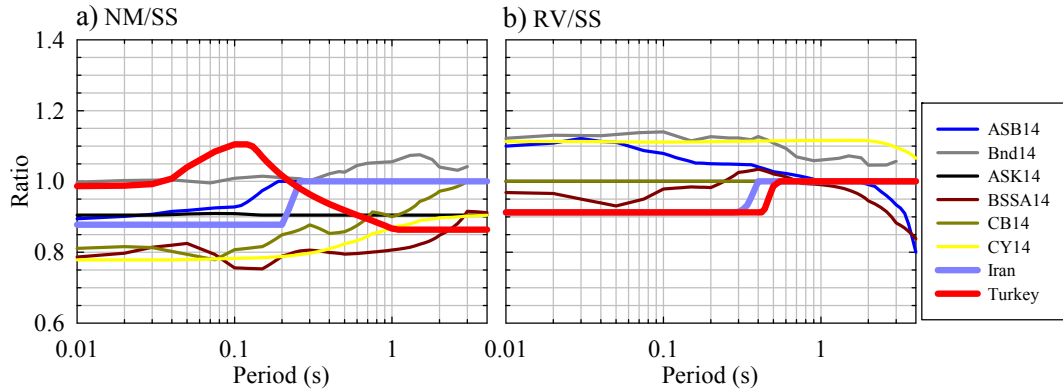
Figure 3.14 Period-dependent a) normal-to-strike-slip (NM/SS), b) reverse-to-strike-slip (RV/SS) ratios for selected local and global GMPEs. Style-of-faulting ratios of NGA-West2 GMPEs are calculated for M_w 7.0.

The comparisons of total sigma given in Figure 3.15 indicate that the GMPE yields similar standard deviations with those of NGA-West2 GMPEs both for small (M_w 4.5, left panel) and large (M_w 7.5, right panel) magnitudes. Note that standard deviations in the proposed ground-motion model and NGA-West2 GMPEs are heteroscedastic although the latter GMPEs describe the behavior of their standard deviations with more complicated models. The sigma model depends on M_w for each spectral period of interest whereas NGA-West2 GMPEs relate sigma with the variations in soil behavior, magnitude and distance. The sigma terms in Bnd14 and ASB14 only depend on spectral periods. They are comparable with the small-magnitude sigma of the proposed GMPE. The discrepancy between the sigma values of the proposed model and these two GMPEs are significant at large magnitudes (e.g., M_w 7.5) for the differences in sigma modelling. The magnitude-dependent sigma of the proposed model results in reductions in sigma levels at large magnitudes.
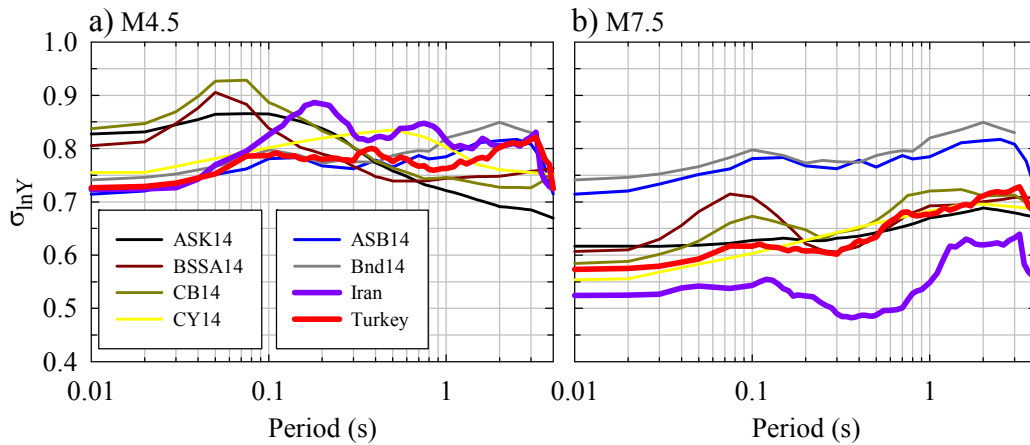
Figure 3.15 Total standard deviation comparisons of the proposed GMPE with global ground-motion models: a) M_w 4.5, b) M_w 7.5.

Figure 3.16 shows the comparisons between the proposed model and NGA-West2 GMPEs in terms of magnitude scaling. The NGA-West2 GMPEs are developed for $M_w > 3$ and most of the small magnitude events in their datasets were compiled from California. Their overall trends are similar to each other for the spectral ordinates (PGA, PSA at T = 0.2s, 1.0s, 3.0s) considered in the comparisons. The magnitude scaling of the GMPE shows a different pattern with respect to NGA-West2 GMPEs that is particularly notable at short (PSA at T = 0.2s) and very short (PGA) periods. The source of discrepancies between the magnitude-dependent decay rates of the model and NGA-West2 GMPEs can be two folded. The differences in the lower magnitude bounds of the GMPE and NGA-West2 GMPEs can be one of these sources. Bommer et al. (2007) concluded that lower magnitude limits (M_{low}) of datasets control the ground-motion estimates at small magnitudes. GMPEs developed from datasets with higher M_{low} would predict larger short-period spectral ordinates towards small magnitudes with respect to those developed from the ground-motion datasets of smaller M_{low}. The predictive model developed for $M_w \geq 5$ was used to verify the likely influence of this factor. The ground-motion estimates computed from the model developed from $M_w \geq 5$ dataset (dotted lines) do not show significant differences from the original model developed for $M_w \geq 4$. Therefore, the effect of M_{low} on the ground-motion estimates is insignificant at

least for $M_w \geq 4$. The other source of difference between the proposed model and NGA-West2 GMPEs could be the influence of regional differences that is discussed throughout this paper. The number of Turkish and Iranian accelerograms in the NGA-West2 database is insignificant and NGA-West2 GMPEs may not fully describe the variation of SACR earthquakes in the regions covered by Iran and Turkey. It is believed that the magnitude scaling of the proposed model and NGA-West2 GMPEs has similar levels of complexity. Thus, the differences addressed in this figure are unlikely to depend on the number of estimator parameters in the functional forms. The discrepancy between the magnitude-dependent variation of the ground-motion estimates and NGA-West2 GMPEs tends to disappear towards intermediate-to-large spectral periods (i.e., T = 1.0s and T = 3.0s, respectively).

The distance scaling of the GMPE is compared with the recent pan-European (first column; ASB14 and Bnd14) and NGA-West2 (second column; ASK14, BSSA14, CB14 and CY14) ground-motion models in Figure 3.17. As in many comparative scenarios of this article, the chosen site represents reference rock conditions (V_{S30} = 750m/s) and the causative fault is strike-slip. The comparisons are based on median PSA at T = 0.2s for M_w 6.0 (top row) and M_w 7.5 (bottom row). These magnitudes can represent moderate-to-large shallow active crustal events in Iran and Turkey. The discrepancies between ground-motion estimates of the proposed model and NGA-West2 GMPEs are pronounced for M_w 6.0 for the entire distance range. They tend to diminish in the large magnitude case (M_w 7.5) but one would still note the differences in distance scaling patterns after $R_{JB} > 20$ km. The pan-European GMPEs almost overlap with ground-motion estimates of the proposed model for Turkey as their datasets for strike-slip events are dominated by the Turkish accelerograms after M_w 6.0. However, the distance scaling of pan-European GMPEs draw a significantly different pattern with respect to the ground-motion estimates for Iran. The pan-European datasets of Bnd14 and ASB14 include few reverse, large-magnitude Iranian events that may partially explain this observed difference.

107
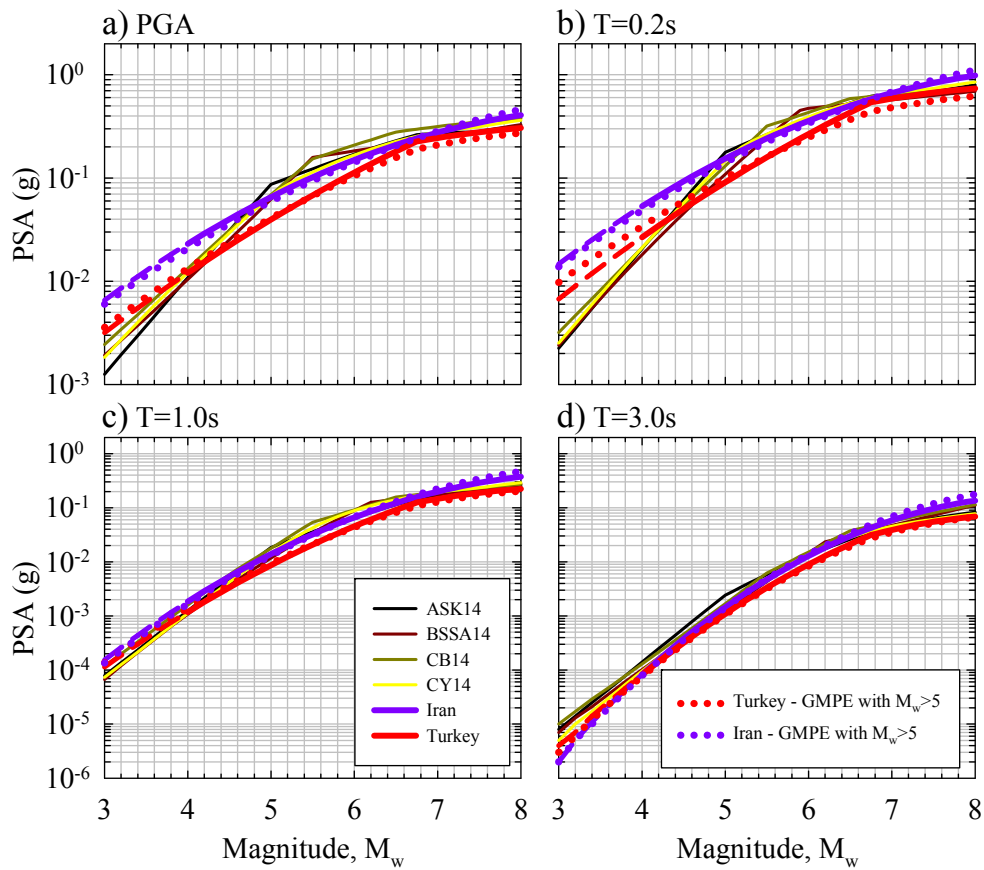
Figure 3.16 Magnitude scaling comparisons of the proposed GMPE with NGA-West2 ground-motion models for (a) PGA, (b) PSA at T = 0.2s, (c) PSA at T = 1.0s and (d) PSA at T = 3.0s. The plots are drawn for reference rock condition (V_{S30} = 750m/s) for a site located at R_{JB} = 10km from a vertical strike-slip fault. The dotted curves show the ground-motion estimates of a GMPE developed from accelerograms with $M_w \geq 5$ in the considered dataset.
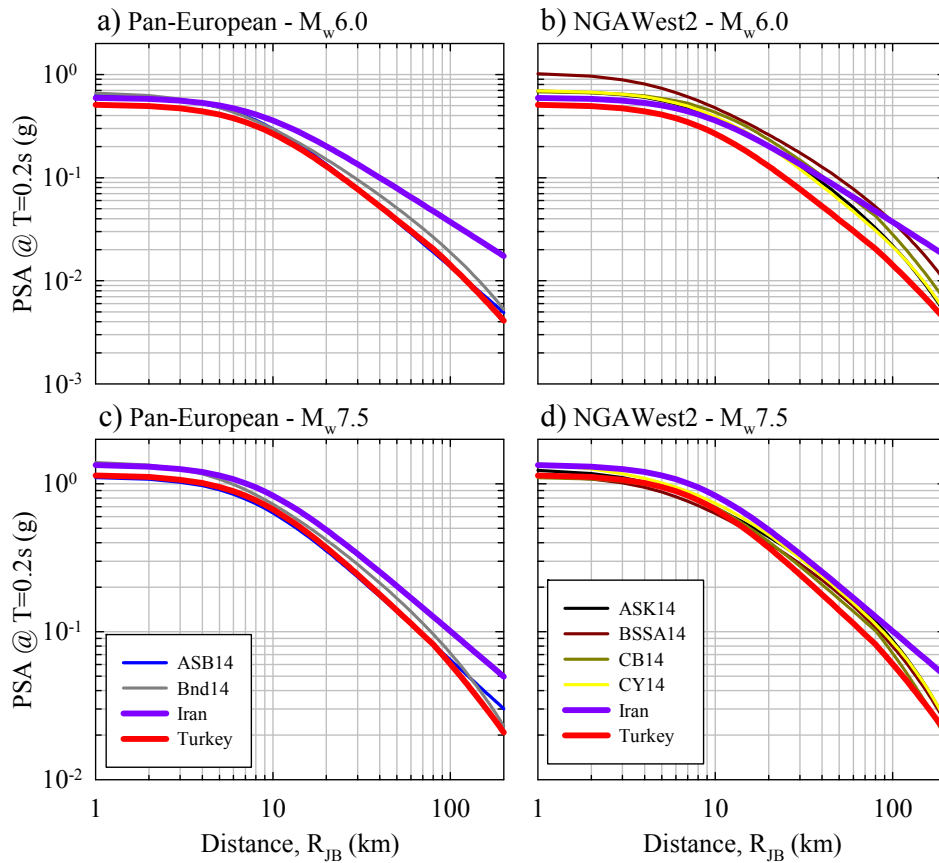
Figure 3.17 Distance scaling of the GMPE and its comparisons with the pan-European (ASB14 and Bnd14) GMPEs (1st column panels) as well as NGA-West2 GMPEs (2nd column panels) for M_w 6.0 (top row) and M_w 7.5 (bottom row). The comparisons are done for median PSA at T = 0.2s for a strike-slip fault. The site represents the reference rock conditions (V_{S30} = 750m/s).

3.7. Summary and Conclusions

A predictive model is proposed for 5%-damped horizontal spectral acceleration between 0 s (PGA) $\leq$ T $\leq$ 4 s and PGV for seismic hazard assessment of SACRs in Iran and Turkey. The proposed GMPE is developed from a recently compiled strong-motion database for the Earthquake Model of the Middle East Region (EMME) project. The applicability range of the predictions is bounded for distances (R_{JB}) up to 200 km, between 4 s $\leq M_w \leq$ 8 and 150 m/s $\leq V_{S30} \leq$ 1200

m/s. The amplitude differences due to major fault mechanisms are also considered in the estimated ground-motion intensities.

The emphasis of the proposed model is the consideration of regional differences in the variations of estimated ground motions in terms of magnitude and distance scaling as well as spectral shapes. The observations suggest that the depth distribution of shallow active crustal earthquakes in Iran and Turkey, the differences in near-surface velocity profiles, Q-factors, the variations in kappa as a function of magnitude, distance and V_{S30} result in different patterns in the estimated spectral intensities of Iran and Turkey. The ground motions in Iran are larger in spectral amplitude and their decay rates are slower at short- and long-period spectral ordinates for factors indicated above. Inherently, these factors lead to differences between predictions of the proposed model and those of global NGA-West2 and pan-European GMPEs. The differences between estimations of the proposed model and global GMPEs are not only observed in small magnitudes and distant sites but also for large magnitudes. Note that the discussions about regional effects on ground-motion estimates still constitute an important research topic and the observations in this paper would trigger more systematic studies to better address these effects in GMPEs.

CHAPTER 4

A NEW PROCEDURE FOR SELECTING AND RANKING GROUND-MOTION PREDICTION EQUATIONS (GMPES): THE EUCLIDEAN-DISTANCE BASED RANKING (EDR) METHOD

Adapted from Kale Ö and Akkar S (2013). A New Procedure for Selecting and Ranking Ground-Motion Prediction Equations (GMPEs): The Euclidean Distance-Based Ranking (EDR) Method. Bulletin of the Seismological Society of America, 103, no. 2A, 1069-1084.

This chapter introduces a procedure for selecting and ranking of ground-motion prediction equations (GMPEs) that can be useful for regional or site-specific probabilistic seismic hazard assessment (PSHA). The methodology is called as Euclidean-Distance Based Ranking (EDR) as it modifies the Euclidean distance concept for ranking of GMPEs under a given set of observed data. The Euclidean distance is similar to the residual analysis concept. Its modified form, as discussed in this paper, can efficiently serve for ranking the candidate GMPEs. The proposed procedure separately considers the ground-motion uncertainty (i.e., standard deviation of the ground-motion model) and the bias between the observed data and median estimations of candidate GMPEs (i.e., model bias). Indices computed from the consideration of aleatory variability and model bias or their combination can rank GMPEs to design GMPE logic-trees that can serve for site-specific or regional PSHA studies. These features are discussed through a case study and ranked a suite of GMPEs under a specific ground-motion database. The case study indicated that

111

separate consideration of ground-motion uncertainty (aleatory variability) and model bias or their combination can change the ranking of GMPEs. The ranking of GMPEs also showed that the ground-motion models having simpler functional forms generally rank at the top of the list. It is believed that the proposed method can be a useful auxiliary tool to improve the decision making stage while identifying the most proper GMPEs according to the specific objectives of PSHA.

4.1. Introduction

Ground-motion prediction equations (GMPEs) are the main tools in estimating ground-motion intensities that are used to assess seismic hazard in a seismic prone region. The increasing size and quality of the ground-motion databases in recent years has resulted in a significant number of new local and global predictive models. Consequently, engineering seismologists have started to propose a number of statistical and probabilistic procedures to rank and select GMPEs to properly address the seismotectonic features of the region considered for hazard assessment. One of the major objectives of these efforts is to reduce the uncertainty in ground-motion variability that, essentially, affects the computed hazard at long return periods.

There are many methods in the statistical literature to test the agreement between observed and predicted data (e.g., chi-square test, Kolmogorov-Smirnov test, variance reduction, Pearson's correlation coefficient and Nash-Sutcliffe efficiency coefficient). Recently, these methods have been evaluated by various studies to understand the suitability of a given predictive model under a set of collected ground motions (e.g., Scherbaum et al., 2004; Kaklamanos and Baise, 2011). That said, the most common methodology for assessing predictive model performance remains as classical residual analysis. This statistical method determines the existence of bias by means of mean residuals as well as the slopes of the straight lines fitted to the different residual components (i.e., between-event, within-event or total residuals) as functions of estimator parameters such as magnitude and

source-to-site distance. Studies like Bindi et al., (2006); Scassera et al., (2009); Shoja-Taheri et al., (2010) used residual analysis to evaluate GMPEs under different ground-motion databases. The recent likelihood-based testing and ranking techniques proposed in Scherbaum et al. (2004) (likelihood; LH method) and Scherbaum et al. (2009) (log-likelihood; LLH method) have also appealed the seismological and engineering community as they are easy to implement with well-tailored outcomes to envisage the best performing GMPEs for a given ground-motion dataset. The LH method calculates the normalized residuals for a set of observed and estimated ground-motion data. It assumes that the predictive model residuals are log-normally distributed and it calculates the exceedance probabilities of residuals as likelihood (LH) values. The suitability of candidate GMPEs is identified through the median LH value that is described as LH index, which takes values between 0 and 1. For an optimum case LH values are evenly distributed between 0 and 1, and the median of LH is about 0.5. The LLH method is an information-theoretic model selection procedure and it is based on the log-likelihood approach to measure the distance between two continuous probability density functions *f(x)* and *g(x)*. The distribution of *f(x)* that is supposed to exist for each individual data point in the observed ground-motion dataset is not known *a priori*. This method calculates the average log-likelihood of a predictive model whose distribution, *g(x)*, is known through its median and standard deviation (sigma). The method computes the occurrence probability of observed data point by using the probability distribution of candidate GMPE. This way it computes the LLH value as the model selection index.

Among the testing and ranking methods proposed by Scherbaum and his co-workers the LH method was initially applied to the border region of France, Germany and Switzerland for a small set of observed data (Scherbaum et al., 2004). Later Hintersberger et al. (2007) extended the dataset for the same region and implemented the same method using the same candidate GMPEs as of the former study. These two studies obtained similar ranking results for the same set of candidate GMPEs advocating the robustness of LH indices for selecting the proper

GMPEs in hazard analysis. Stafford et al. (2008) evaluated the applicability of Next Generation Attenuation (NGA; Power et al., 2008) GMPEs to Euro-Mediterranean region by using LH as well. This method was also considered in Kaklamanos and Baise (2011) as supplementary to the results of Nash-Sutcliffe model efficiency coefficient (Nash and Sutcliffe, 1970) to validate the NGA GMPEs by making use of a ground-motion dataset assembled from the recent earthquakes recorded in California. The information-theoretic LLH approach that supersedes the LH technique was used for the selection and ranking of GMPEs in various studies as well (e.g., Delavaud et al., 2009; Delavaud et al., 2012a; 2012b; Mousavi et al., 2012; Beauval et al., 2012a; 2012b). Of these studies the Delavaud et al. (2012b) paper uses LLH as an adjunct tool to determine the logic-tree weights of the GMPEs that are used in assessing the hazard in Europe and south Mediterranean regions under the framework of SHARE (**S**eismic **H**azard H**AR**monization in **E**urope) project.

This study presents an alternative testing and ranking approach for a pre-selected set of GMPEs. Although the working stage of this methodology is inspired by the LH and LLH methods, an approach different than those of LH and LLH methods is utilized while considering the model bias and aleatory variability in the estimated ground motions. The proposed method uses the Euclidean distance: the absolute difference between the observed and estimated data (analogous to the residual analysis concept) to account for the trend (model bias) between the observed and estimated ground-motion data. The method also employs Euclidean distance to account for the aleatory variability in ground motions (addressed by the standard deviation of GMPE) through an approach similar to that of PSHA. These two features: consideration of model bias and aleatory variability make the method appealing for PSHA projects that carry different types of objectives (e.g. regional vs. site-specific PSHA studies). The method presents ranking results that are normalized by the total number of data, which can be considered as an additional strength while selecting and ranking of GMPEs for regions of sparse data. The following sections first summarize some important observations on the most

114

frequently used testing and ranking methodologies and then describe the fundamental concepts of the proposed method. The paper ends with a case study to show the practical implementation as well as the specific features of the proposed methodology. It is believed that the proposed procedure can be used efficiently while identifying the proper suites of GMPEs for hazard studies of different objectives. However, it is also believed that the sole use of the procedure for testing and ranking of GMPEs would be insufficient as a rigorous selection methodology should be an integrative process that considers multiple statistical measures. The decision-making process could be improved significantly with the consideration of additional testing methods as well as the conventional residual analysis that is especially helpful as a visual tool.

4.2. Summary of Some Observations on the Current Testing and Ranking Methods:

Scherbaum et al. (2004) studied the simple statistical measures such as significance tests, variance reduction and Pearson's correlation coefficient while proposing the LH method. In their paper, the authors indicated that these methods do not produce consistent outcomes to properly rank the performance of candidate GMPEs for a given ground-motion dataset. The direct implementation of conventional residual analysis, despite of its visual efficiency in explaining the level of agreement between the median predictions and observed data (model bias), will also not provide flexible options for ranking candidate GMPEs. The model efficiency coefficient (Nash and Sutcliffe, 1970) is a major improvement over the goodness-of-fit statistics that are discussed above because it directly quantifies the amount of bias in a model (Pearson's correlation coefficient, for example, is not sensitive to additive and multiplicative biases). However, it does not quantify how well the aleatory variability (sigma) of the observations is predicted by the models.

Although the LH method was proven to be a robust approach for ranking the candidate GMPEs its dependence on the data size and subjectivity in choosing the

threshold LH-value led Scherbaum et al. (2009) to propose the LLH method that overcomes these weaknesses. The LLH method treats GMPEs as probability distributions by means of their medians and standard deviations. Provided the specific features of the ground-motion dataset used in testing, this method may favor GMPEs with larger standard deviations as they can predict the outlier observations with higher probabilities. Such a case can be observed, for example, during the testing of two GMPEs having fairly similar median estimations and different standard deviations. The LLH method can lead to better performance of the predictive model with larger sigma, in particular, if the observed data are accumulated away from the median estimations of the two GMPEs. Consistent with the underlying theory in LLH, the competing predictive model with larger sigma would yield larger probabilities of occurrence indicating that it can capture these outliers better than its alternative.

The above discussions about LLH are illustrated by a case study as presented in Figure 4.1. Figures 4.1.a and 4.1.b show the observed vs. estimated PGA data in natural logarithms for two candidate GMPEs (Akkar and Çağnan (2010) and Özbey et al. (2004) that are designated as models A and B, respectively). The observed dataset is extracted from a strong-motion databank that is compiled for the **E**arthquake **M**odel of the **M**iddle **E**ast project (EMME). Detailed information about this strong-motion databank is given in the latter parts of the paper. The scatter plot in the second row compares the median estimations of these two models for the same dataset indicating almost identical median trends. The almost exact matching of median estimations of the two GMPEs is also verified by calculating the model efficiency coefficient, E (Nash and Sutcliffe, 1970). The E values from models A and B are exactly the same (63%). The standard deviation of model A (σ_{modelA} = 0.832) is larger than the standard deviation of model B (σ_{modelB} = 0.599). The LLH testing results of these GMPEs are 1.91 (model A) and 2.21 (model B) for the given dataset pointing that LLH favors model A against the performance of B (Smaller LLH values can be interpreted as the accurate description of aleatory variability posed by the ground-motion dataset). Note that,

116

of the same GMPEs, the LLH method would have chosen the GMPE with smaller sigma if the observed data displays a closer distribution to the median estimations of the considered GMPEs.
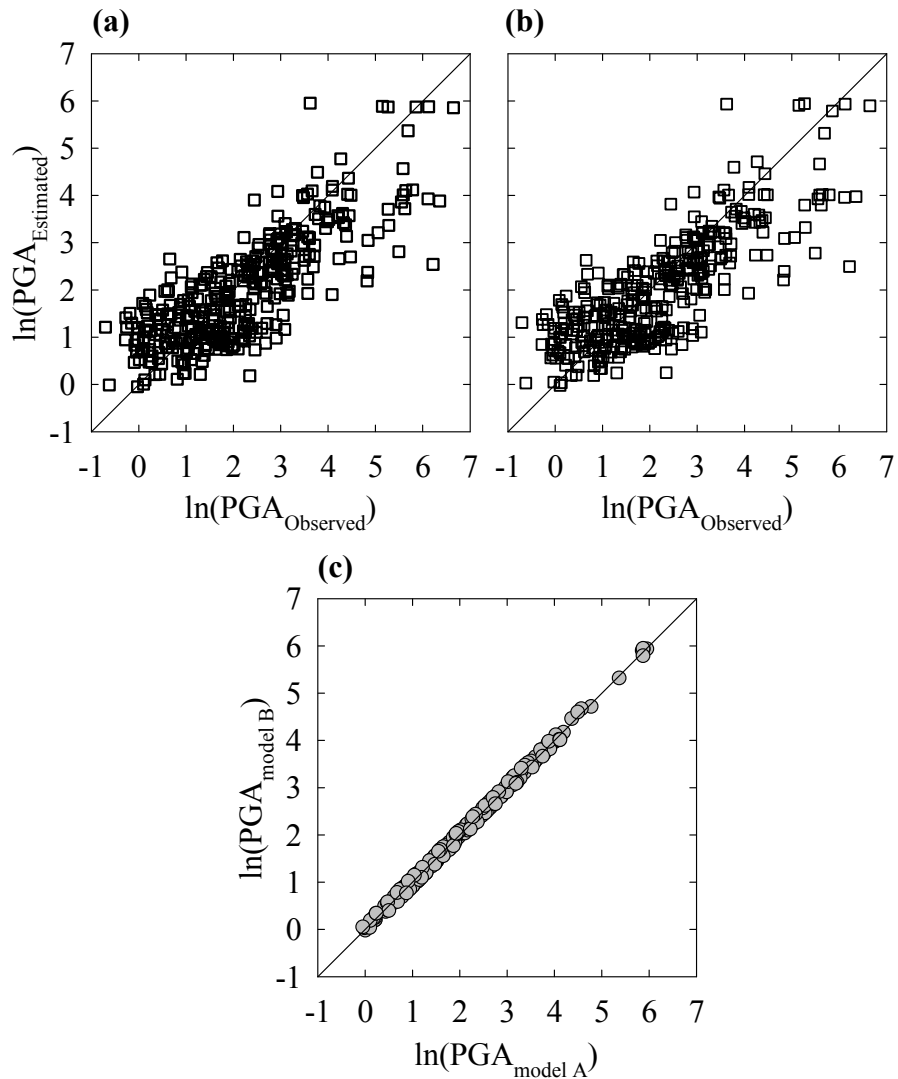
Figure 4.1 Natural logarithms of observed vs. estimated PGA data corresponding to (a) model A and (b) model B. Panel (c) shows the scatter plot comparisons of the ground-motion estimations of these 2 models for the observed data. The sigma values of models A and B are 0.832 and 0.599, respectively.

Discussions on the LLH method in the above paragraphs indicate that this method (as well as its predecessor, the LH method) focuses on selecting a suite of GMPEs

that can accurately represent the aleatory variability of the ground-motion dataset used in testing. As given in the above case study, this objective may favor GMPEs with large sigmas that may result in conservative probabilistic seismic hazard for long-return periods (Restrepo-Velez and Bommer, 2003). The proposed method provides an alternative approach to describe the aleatory uncertainty featured by the used ground-motion dataset. The dispersion of the ground-motion dataset and uncertainty of the estimations computed from the GMPE are considered together. This is achieved by computing the occurrence probabilities of differences between the observed data and a range of model estimations that are described for an interval of sigma values. Besides, the method accounts for model bias by using a factor computed from residual analysis. The method then combines these two separate effects as an index to rank the overall performance of GMPE. The effects of aleatory uncertainty and model bias can also be considered separately depending on the specific purposes of the PSHA study. The derivation of the proposed method as well as its specific properties is discussed in the subsequent sections of the paper.

4.3. Proposed Testing and Ranking Method:

The highlighted observations on the likelihood methods as well as other statistical measures revealed to present an alternative testing and ranking methodology that can lead to a practical and robust strategy for selecting the most appropriate set of GMPEs for a given size-independent ground-motion dataset. The interpretation from background studies advocate that a versatile ranking and selection procedure should account for the influence of sigma on the estimated ground motions and measure the bias between the observed data and median estimations. Accordingly these features are the central aspects for detecting a proper set of GMPEs to be used in probabilistic seismic hazard analysis (PSHA) that serve for different objectives such as site-specific or regional studies. Moreover, the competency of the method should not be limited to the data size because finding large numbers of ground-motion data might not be possible for some seismic prone regions.

118

The proposed methodology is called as the Euclidean-Distance Based Ranking (EDR) method as it is based on the Euclidean distance (*DE*) definition given in Equation 4.1. The Euclidean distance is a statistical index where square root of sum of squares of the differences between *N* data pairs (p_i, q_i) is calculated. The parameters p_i and q_i in Equation 4.1 designate the observed and estimated ground motion data in the methodology that will be explained in detail in the subsequent sections. In the proposed ranking method, *DE* definition is slightly modified considering some basic probability rules to account for the criteria mentioned in the previous paragraph. These modifications and the theory behind are discussed in the following subsections.

$$DE^2 = \Sigma_{i=1}^{N}(p_i - q_i)^2 \tag{4.1}$$

4.3.1. Consideration of Sigma: Uncertainty in Ground-Motion Estimations

While considering the influence of standard deviation (sigma), an analogy is made from the implementation of GMPEs in PSHA. The GMPEs are used for a range of sigma values in PSHA to address the randomness in ground motion estimations. In the proposed methodology, the estimated ground-motion intensity for a single data point (that consists of a certain magnitude, distance, style-of-faulting and site class) is assumed to take a set of values that are computed from a predetermined range of standard deviation of the considered GMPE. In other words, for a single observed data, the candidate GMPE can estimate a range of values due to the aleatory variability in ground motions. The differences between the observed point and the range of estimations for that single point result in a probability distribution. The procedure considers this distribution while assessing the performance of the candidate GMPE under the considered dataset. The following paragraphs describe the background theory of this approach.

The EDR method assumes that the natural logarithm of the predictive model as well as the Euclidean distances computed for each data point is normally

distributed. Let D in Equation 4.2 denotes the difference between the natural logarithms of an observed (a) and estimated (Y) data point. In this expression, a is scalar quantity (single observation) whereas Y, the estimator for a predictive model, is a Gaussian random variable with mean, μ_Y, and variance, σ^2_Y. From the basic principles of the summation of random variables, D can be proven to be a normally distributed variety (Devore, 2004) with parameters given in Equations 4.3.

$$D = a - Y \qquad (4.2)$$

$$\mu_D = a - \mu_Y \qquad (4.3.a)$$

$$\sigma^2_D = \sigma^2_Y \qquad (4.3.b)$$

For each single point, the square of D values contributing to DE are non-negative. If an analogy between D and DE is wanted to establish, the probability distribution of the absolute values of D [i.e., $Pr\,(|D|)$] must be considered. Equation 4.4 shows the probability of $|D|$ being less than a certain value d [i.e., $Pr\,(|D| < d)$], which is actually the difference between $Pr\,(D < d)$ and $Pr\,(D < -d)$ as shown in Figure 4.2. The parameter Φ denotes normal cumulative distribution function in Equation 4.4. This equation will be used to derive the probability distribution of $|D|$.

$$Pr\big(|D| < d\big) = Pr\big(D < d\big) - Pr\big(D < -d\big) = \Phi\left(\frac{d - \mu_D}{\sigma_D}\right) - \Phi\left(\frac{-d - \mu_D}{\sigma_D}\right) \qquad (4.4)$$
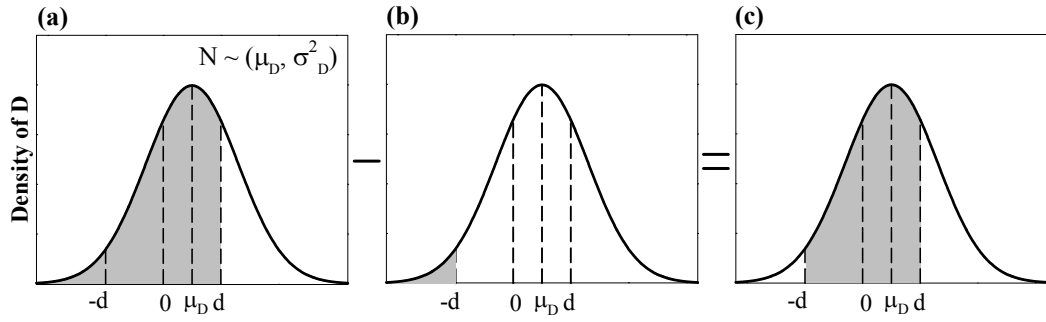
Figure 4.2 Probability distribution definitions given in Equation 4.4: (a) *Pr (D < d)*, (b) *Pr (D < -d)*, (c) *Pr (|D| < d)*.

For discrete values of D, which are denoted by d_j in this terminology, the occurrence probability of d_j [i.e., *Pr (d_j)*] is described within an infinitesimal bandwidth dd around d_j [i.e., *Pr (d_j-dd/2 < D < d_j+dd/2)*]. As the method considers the occurrence probabilities of d_j via analogy made between DE and D, this probability have to be modified as *Pr (|d_j-dd/2| < |D| < |d_j+dd/2|)*. Such a relationship can be derived by making use of Equation 4.4 and it is given in Equation 4.5. Figure 4.3 and its caption describe the meanings of each term in Equation 4.5.

$$Pr\left(\left|d_j - \frac{dd}{2}\right| < |D| < \left|d_j + \frac{dd}{2}\right|\right) = Pr\left(|D| < \left|d_j + \frac{dd}{2}\right|\right) - Pr\left(|D| < \left|d_j - \frac{dd}{2}\right|\right) \quad (4.5)$$
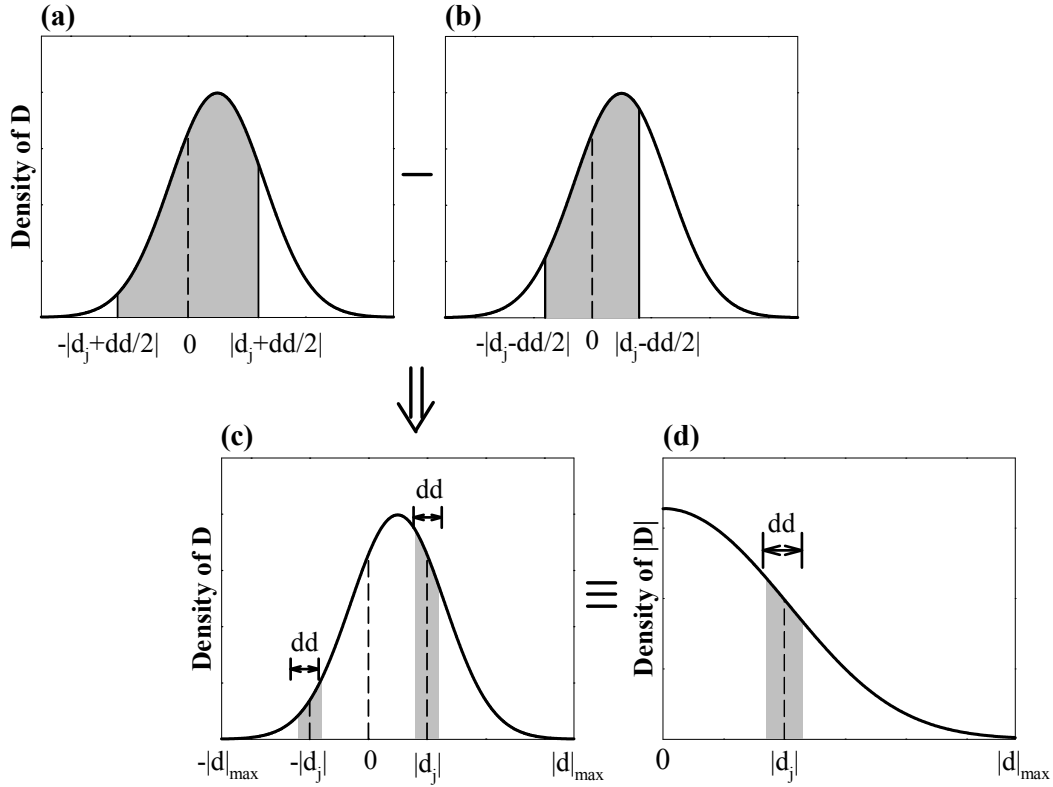
Figure 4.3 Probability distribution definitions given in Equation 4.5: (a) *Pr (-|dj+dd/2| < D < |dj+dd/2|)*, (b) *Pr (-|dj-dd/2| < D < |dj-dd/2|)*, (c) difference between the probabilities given in (a) and (b); total discrete probability, *Pr (|dj-dd/2| < |D| < |dj+dd/2|)*, (d) probability density function of |D|. The probabilities of (a) and (b) are equivalent to *Pr (|D| < |dj+dd/2|)* and *Pr (|D| < |dj-dd/2|)*, respectively. The gray shaded area in (d) represents the summation of the discrete probabilities in negative and positive sides of the probability density function in (c) [i.e., *Pr (|dj-dd/2| < |D| < |dj+dd/2|)*]. D is normally distributed random variable with μ_D and σ^2_D while |D| is a non- negative random variable.

The probability-based average for a set of $|d_j|$ values is called as Modified Euclidean distance (*MDE*) in this procedure. Equation 4.6 defines the discrete Modified Euclidean Distance (*MDE$_d$*) when |D| is described in discrete points. In this equation, *n* is the number of discrete points that depends on the bandwidth of *dd* (Figures 3c and 3d) and the maximum value of |d| (i.e., $|d|_{max}$). If |D| is assumed

to be continuous, the integral expression given in Equation 4.7 is used to calculate the continuous Modified Euclidean Distance (MDE_c).

$$MDE_d = \Sigma_{j=1}^n |d_j| Pr\left(\left|d_j - \frac{dd}{2}\right| < |D| < \left|d_j + \frac{dd}{2}\right|\right) \tag{4.6}$$

$$MDE_c = \int_0^{|d|_{max}} d \cdot \frac{1}{\sqrt{2\pi} \cdot \sigma_D} \cdot exp\left(\frac{-(d - \mu_D)^2}{2\sigma_D^2}\right) \cdot dd$$

$$+ \int_0^{|d|_{max}} d \cdot \frac{1}{\sqrt{2\pi} \cdot \sigma_D} \cdot exp\left(\frac{-(-d - \mu_D)^2}{2\sigma_D^2}\right) \cdot dd \tag{4.7}$$

MDE can be considered as a probability-based average that is used as an index to account for the effect of sigma while testing the performance of GMPEs under a given ground-motion dataset (Equations 4.6 and 4.7). The entire methodology is based on the Euclidean distance concept that is very similar to residual analysis. Euclidean distance is preferred instead of residual analysis, as it results in non-negative differences between observations and estimations that can be easily transformed into an index.

For practical applications of the proposed method it is suggested that $|d|_{max}$ value should be selected in accordance with the following relationship:

$$|d|_{max} = max(|\mu_D \pm x \cdot \sigma_D|) \tag{4.8}$$

In Equation 4.8, *x* denotes the multiplier of sigma and $|d|_{max}$ depends on the value of this parameter. If *x* is selected as 3, the procedure would approximately cover 99.7% of the differences between the observed and estimations of a candidate ground-motion model provided that the normality assumption holds for the considered variables in the methodology. Note that the distribution of *D* is unsymmetrical about zero unless there is a one-to-one match between the observed data point and the corresponding median estimation. On the other hand the $|d_j|$ pairs

123

(i.e., $|d_j|$ and $-|d_j|$) are always symmetric about zero. These remarks are illustrated in Figure 4.3.c.

Table 4.1 provides an insight about the variation of *MDE* for a set of *x* and *dd* values by considering an arbitrary ground-motion model and a sample dataset. The *MDE* values are computed by considering the probability distribution of *D* either as discrete (MDE_d) or continuous (MDE_c). The results given in Table 4.1 are derived for $\mu_D = 0.75$ and $\sigma_D = 0.5$. They suggest that when *x* is 3 and bandwidth of *dd* is 0.1, MDE_d and MDE_c almost overlap each other. Thus, taking *x* = 3 and *dd* = 0.1 can be considered as sufficient for reliable calculation of *MDE* while testing the performance of a candidate GMPE. Numerous other case studies were also conducted for various μ_D - σ_D pairs and they did not change the major observations presented in Table 4.1. Therefore, choosing *x* > 3 to cover a larger ground-motion estimation range or taking *dd* < 0.1 for a better approximation of continuous probability distribution of *D* will only increase the computational burden but will not result in improvements in the computed *MDE*.

Table 4.1 Comparison of MDE values for discrete and continuous probability distributions by considering the variations in bandwidths (*dd*) and number of sigma (*x*).

x	MDE_d [*]			MDE_c [†]
	dd=0.1	dd=0.05	dd=0.01	
3	0.7754	0.7762	0.7761	0.7761
4	0.7796	0.7793	0.7792	0.7792
6	0.7797	0.7794	0.7793	0.7793
9	0.7797	0.7794	0.7793	0.7793

[*] MDE_d: MDE values for discrete probability (calculated from Equation 6)
[†] MDE_c: MDE values for continuous probability (calculated from Equation 7)

Some sensitivity analyses were also conducted by generating synthetic ground-motion datasets to see the variations in *MDE* when the intricate relation between the distributions of ground-motion datasets and GMPE estimations are of concern.

These sensitivity analyses indicated that the median and standard deviation of model estimations play a significant role on *MDE* values. Based on the sensitivity analyses, it is found that the index varies between 0.5 and 3.2 depending on the consistency of above two parameters with the overall trend and scatter of observed ground-motion dataset. Details of discussions on the results of sensitivity analyses are given in the following paragraphs.

Assuming log-normal distribution, the synthetic datasets are generated for different numbers of data. The number of data varies between 30 and 210 with increments of 30. The synthetics mimic the observed ground-motion datasets in these analyses. Figure 4.4 shows the distributions (histograms) of a sample set of synthetic datasets generated for $\mu = 0.5$ and $\sigma = 0.5$ (median and standard deviation of the generated synthetic dataset, respectively). The synthetic data that represent the observed values are plotted in logarithmic scale in this figure.

Figure 4.5 shows the variations in *MDE* (i.e., $\sqrt{\frac{1}{N}\Sigma_{i=1}^{N}MDE_i^2}$) in terms of different sample sizes of synthetic data. The median, μ, is taken as 0.5 in all cases whereas σ is varied as 0.5, 0.7, 0.8 and 1.0 while generating the synthetic data for each set. The standard deviations of model estimations (σ_Y) are assumed to follow the standard deviations of the generated synthetic datasets (i.e., $\sigma_Y = \sigma$). The medians of model estimations (μ_Y) systematically take different values in each case. Four different μ_y levels are considered in the sensitivity analyses: $\mu_Y = \mu$, $\mu_Y = \mu + \sigma$, $\mu_Y = \mu + 2\sigma$ and $\mu_Y = \mu + 3\sigma$. The plots in Figure 4.5 summarize the changes in *MDE* for the entire sensitivity analyses by making use of above cases.
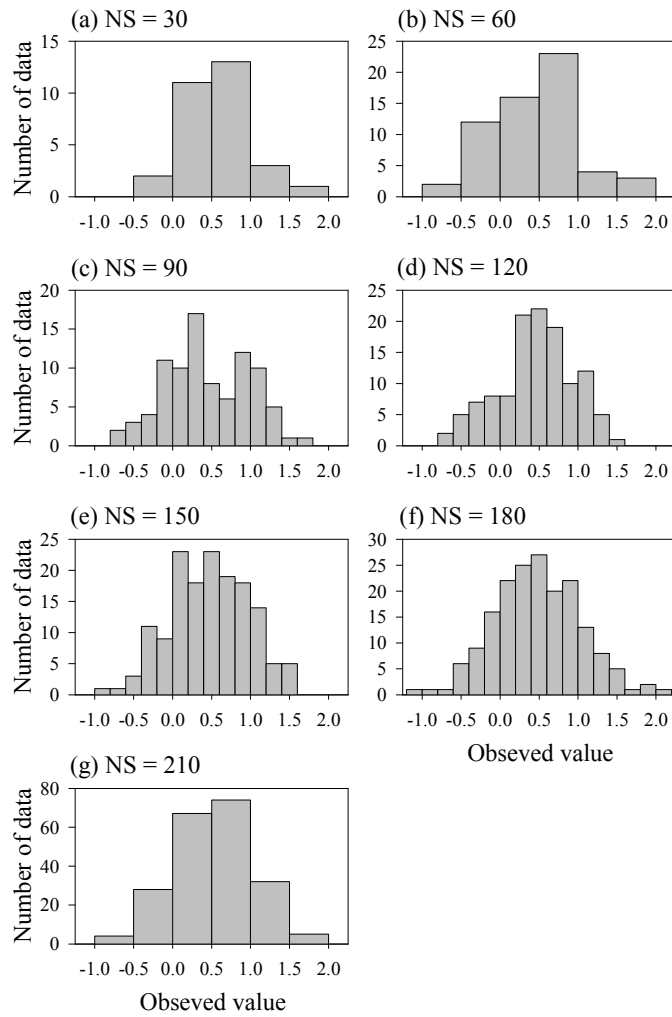
Figure 4.4 A sample set of synthetic datasets with different data sizes (NS).

One can infer that *MDE* is independent of data size from the plots in Figure 4.5. When median and standard deviations of model estimations are very similar to the average trend and scatter of observed data (i.e., $\mu_Y = \mu$ and $\sigma = \sigma_Y$), *MDE* attains values between 0.5 and 1.2 depending on the level of scatter in the observed data. In other words as the scatter in observed data increases *MDE* starts to increase even if the standard deviations of model estimations follow very similar trends to those of observed data. *MDE* varies between 1.5 and 3.2 when the model estimations significantly differ with respect to the observed data (i.e., $\mu_Y = \mu + 3\sigma$). The increase in *MDE* depends on the dispersion of observed ground-motion dataset as in the previous case.

126
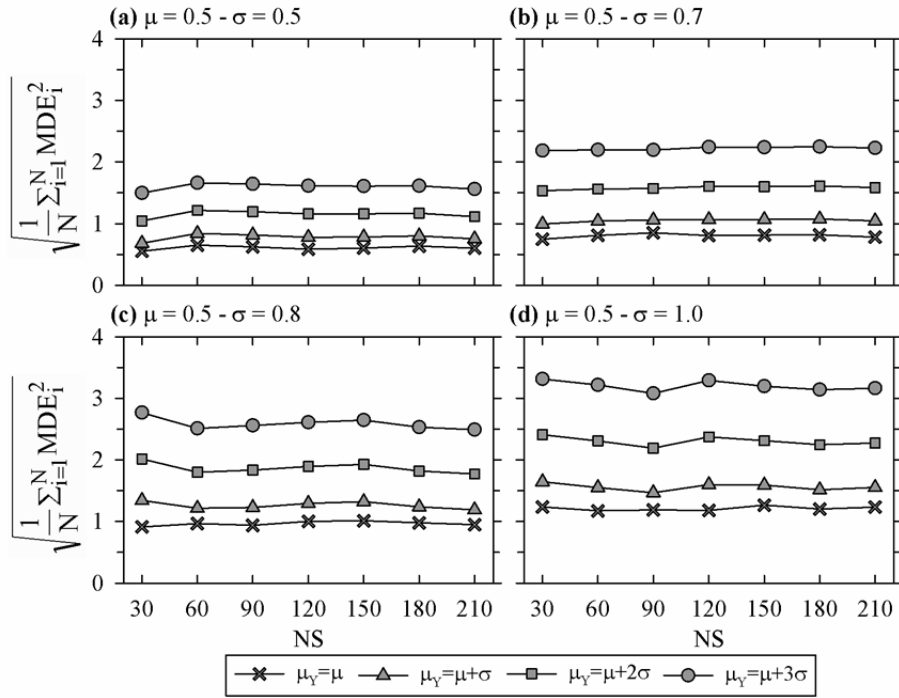
Figure 4.5 Variation of *MDE* (i.e., $\sqrt{\frac{1}{N}\Sigma_{i=1}^{N}MDE_i^2}$) for different scenarios in terms of ground-motion model estimations with different median (μ_Y) and standard deviations (σ_Y) that are adjusted by considering the median (μ) and standard deviations (σ) of generated synthetic datasets.

Given two GMPEs, the *MDE* index computed for the small-sigma predictive model will always be smaller with respect to the other one provided that the median estimations of these GMPEs follow similar patterns. The EDR method selects $|d|_{max}$ by considering the area under the normally distributed parameter D that gives the difference between the absolute value of natural logarithms of observed and estimated data points (Equation 4.2). The value of $|d|_{max}$ depends on the standard deviation of GMPE (Equation 4.8) and the probabilities of discrete d_j that are greater or less than $|d|_{max}$ are almost zero if the area to be considered under this probability distribution is chosen as 99.7%. Figure 4.6 shows the normally distributed D parameters of two models having the same median estimations but different standard deviations. The standard deviation of Model 2 is greater than the standard deviation of Model 1 that results in higher d_{max} in Model 2 (i.e., $|d|_{max,2} >$

$|d|_{max,1}$). As depicted in Figure 4.6, d_j values that are close to median of both models attain small values with high occurrence probabilities. The occurrence probabilities of d_j values become smaller as they start shifting away from the median. When d_j takes larger values between $-|d|_{max,2}$ and $-|d|_{max,1}$ or $|d|_{max,1}$ and $|d|_{max,2}$, their occurrence probability is almost zero for Model 1 but is still significant for Model 2. From these discussions and the expression used for computing *MDE* (Equation 4.6) one can infer that *MDE* value computed for Model 1 will always be smaller than that of Model 2. In addition to that, a detailed clarification of selecting small sigma predictive model is given in Appendix B.
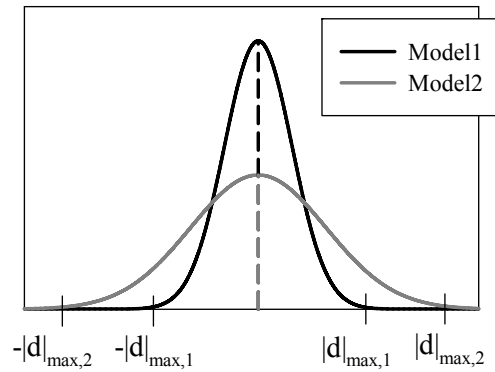
Figure 4.6 Comparisons between two GMPEs (predictive models) having the same medians and different standard deviations.

4.3.2. Consideration of Trend between Observed and Estimated Data: Model Bias

A significant trend between the observed data and corresponding median estimations can be interpreted as the biased representation of the ground-motion data by the candidate predictive model. In the proposed method the κ parameter (Equation 4.9.a) is introduced to measure the level of bias between the observed and estimated data. Unlike *MDE*, this parameter should be computed using the entire ground-motion database. This parameter is the ratio of original ($DE_{original}$) and corrected ($DE_{corrected}$) Euclidean distances that are given in Equations 4.9.b and

4.9.c. Note that the squared Euclidean distances in Equations 4.9.a and 4.9.b are equivalent to the sums of the squared residuals.

$$\kappa = \frac{DE_{original}}{DE_{corrected}} \tag{4.9.a}$$

$$DE_{original}^2 = \Sigma_{i=1}^N (a_i - Y_i)^2 \tag{4.9.b}$$

$$DE_{corrected}^2 = \Sigma_{i=1}^N (a_i - Y_{c,i})^2 \tag{4.9.c}$$

In the above equations a_i and Y_i are the natural logarithms of the ith observed and estimated data, respectively. N denotes the total data number in the assembled ground-motion database. The parameter $Y_{c,i}$ stands for the corrected estimation of the ith data after modifying Y_i with the straight line fitted on the logarithms of the estimated and observed data. Equation 4.10 shows the calculation of $Y_{c,i}$.

$$Y_{c,i} = Y_i - (Y_{fit,i} - a_i) \tag{4.10}$$

where $Y_{fit,i}$ is the predicted value from the regression of Y_i on a_i.

Note that the optimum value of κ is 1.0 and it occurs when estimations take very close values to the corresponding observations. Illustrations for the computation of κ for 2 representative predictive models (Model 1 and Model 2) are given in Figure 4.7. The κ values of the example cases in Figure 4.7 are 1.18 and 3.41 for Model 1 and Model 2, respectively. As inferred from the left-hand side panels on this figure, κ increases when the fitted straight line on a_i vs. Y_i becomes more noticeable, which indicates the dominant bias in the estimations of the considered GMPE (Model 2 for the cases given in Figure 4.7). In this ranking method, κ penalizes the predictive model by comparing the DE values obtained from original and corrected residual trends. The overall calculation of EDR index is described in the following section.
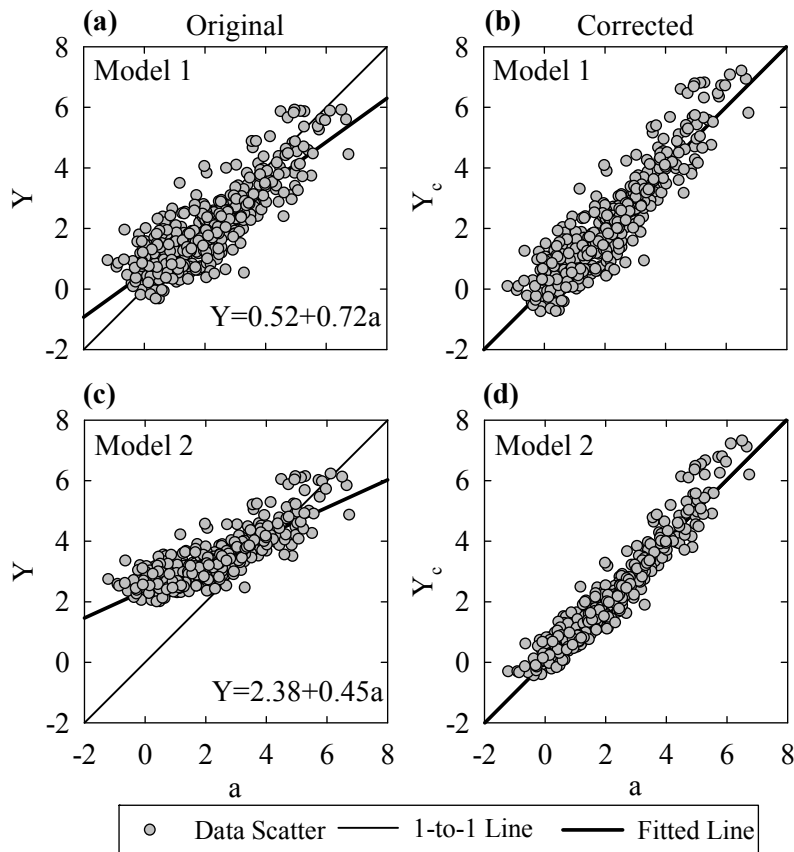
Figure 4.7 Original scatter plots of the natural logarithms of observed data, *a*, and corresponding median estimations, *Y*, obtained from Model 1 and 2 [Panels (a) and (c), respectively]. These scatter plots also show the thick straight lines fitted on the logarithms of observed and estimated data (given on the lower right corner of each plot). Panels (b) and (d) show the relationship between the corrected median estimations (*Y$_c$*) and observed data for Model 1 and 2, respectively. Corrected estimations of each model are calculated by using the corresponding straight-line fits given on the panels (a) and (c). The κ value for each model is the ratio of *DE* values computed from original and corrected median estimations.

4.3.3. Final Form of the EDR Index and Its Use in Ground-Motion Logic-Tree Applications

The calculations presented for a single data point while describing *MDE* should be repeated for the entire ground-motion database as *EDR* index must represent the

overall probability of the differences between the estimated and observed data. This probability should then be modified by κ to penalize the considered predictive model according to the level of bias detected between the median estimations and overall trend in empirical data. To eliminate the dependency of *EDR* results on data size the compound effect of κ and *MDE* should be normalized by the total data number, *N*, in the ground-motion dataset. Equation 4.11 shows the mathematical expression of *EDR*. It is noted that *EDR* index is the square root of the expression given in Equation 4.11. A smaller *EDR* value implies better representation of the ground-motion dataset by the predictive model.

$$EDR^2 = \kappa \cdot \frac{1}{N} \cdot \Sigma_{i=1}^{N} MDE_i^2 \tag{4.11}$$

4.4. Implementation of EDR: Influence of κ and MDE on the Ranking of GMPEs:

The main emphasis up to this point is the consideration of sigma (aleatory variability) and detection of model bias on the overall observed data for optimum ranking of candidate GMPEs. This section presents a case study to show how the proposed procedure accounts for these two components separately while ranking the predictive models. The case study uses an empirical ground-motion dataset[8] compiled for ground-motion model selection and ranking under the framework of the **E**arthquake **M**odel of the **M**iddle **E**ast (EMME) project. The database comprises of 1703 horizontal-component accelerograms from active shallow-crustal regions of Turkey (984 records), Iran (602 records), Caucasus (100 records), Jordan (6 records) and Pakistan (11 records). The moment magnitude (M_w) vs. Joyner-Boore distance (R_{JB}; closest distance to the surface projection of fault rupture) scatter plots of the used database in terms of country, style-of-

---

[8] This database is a preliminary version of the EMME strong-motion database given in Chapter 2. Although this version shows some differences with respect to number of data and metadata information from the final version of the EMME database, it reflects the main seismological features well.

faulting and site class distributions are given in Figure 4.8. The information revealed from the scatter diagrams in Figure 4.8 indicates that Turkey and Iran are the major data providers to the database. The dominant rupture mechanism is strike-slip (S) that is followed by reverse (R) and normal (N) fault events. The number of reverse and normal style-of-faulting accelerograms is close to each other but strike-slip recordings are approximately equal to the total number of normal and reverse faulting data. Accelerograms of B and C soil categories according to Eurocode 8 (CEN, 2004) site classification dominate the site conditions. Notwithstanding there are quite a few accelerograms (14% of total data) satisfying rock conditions (described as site class A in Eurocode 8) in the database. Almost 95% of the accelerograms pertain to events with hypocentral depths less than 30km as shown in Figure 4.9. Events with hypocentral depths greater than 30km (up to 60km) are located either in eastern Turkey or different parts of Iran. None of the deep events from Iran fall into the Makran region whose seismotectonic settings generate subduction type earthquakes (Engdahl et al., 2006). The event- and record-based information of the database was compiled from various local and international sources that are listed in Table 4.2. Style-of-faulting and important fault-rupture geometries of almost all events were determined from double-couple fault solutions that are mainly retrieved from global centroid moment tensor (GCMT) solutions of Harvard (see Data and Resources section). To this end it can be advocated that the computed extended-source distance metrics (i.e., R_{JB} and R_{RUP}: closest distance to the ruptured fault surface) are fairly reliable. This feature of this database is important because most of the recent GMPEs make use of extended-source distance measures while describing the variation of ground-motion amplitude as a function of source-to-site distance. A uniform data processing procedure that is based on 4th-order acausal Butterworth band-pass filtering is implemented. The high-pass and low-pass filter cut-off values were mainly identified by following the discussions in Akkar and Bommer (2006) and Akkar et al. (2011).

132

(a) Country   **(b)** Rupture Mechanism   **(c)** EC8 Site Class
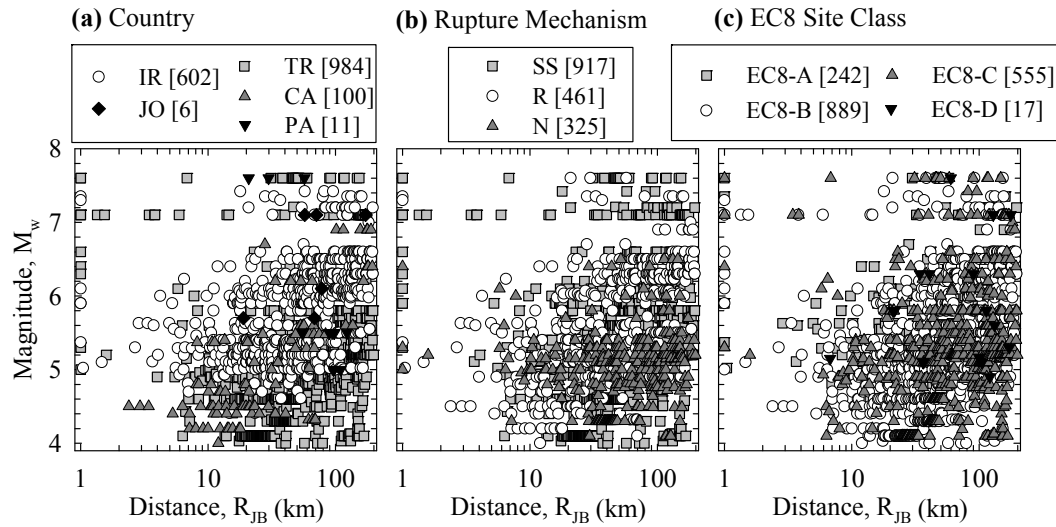
Figure 4.8 Magnitude (M_w) vs. Joyner-Boore distance (R_{JB}) scatter plots of the considered database in terms of (a) country, (b) rupture mechanism and (c) site class distributions. Eurocode 8, EC8, (CEN, 2004) site classification is adopted for soil definitions: Site classes A, B, C and D refer to V_{S30} (average shear velocity in the upper 30m of the soil profile) intervals of $V_{S30} \geq 800m/s$, $360m/s \leq V_{S30} < 800m/s$, $180m/s \leq V_{S30} < 360m/s$ and $V_{S30} < 180m/s$, respectively. Country or region abbreviations TR, IR, CA, JO and PA stand for Turkey, Iran, Caucasus, Jordan and Pakistan, respectively. The abbreviations S, R and N denote strike-slip, reverse and normal style-of-faulting on the middle panel. Numeric values next to each legend describe the number of data in that group.
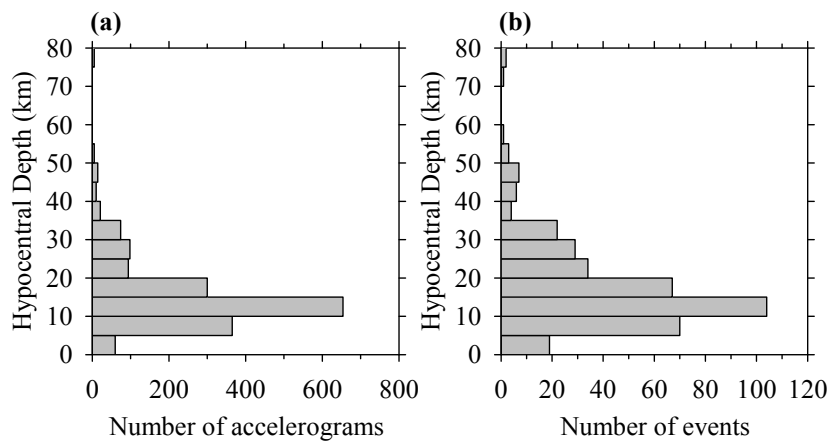
Figure 4.9 Hypocentral depth distributions in terms of (a) accelerograms and (b) earthquakes.

Table 4.2 Major information sources for each country-based strong-motion data.

Database Country	Sources of Strong-Motion Data [*]	Catalog References [†]	Sources of Fault Plane Solutions [‡]
Turkey	AFAD ESMD IERREWS	Akkar et al. (2010), Sandıkkaya et al. (2010), Erdik et al. (2003), Harmandar (2009)	Akkar et al. (2010), NEMC
Iran	ISMN ESMD	EMME and SHARE progress reports (2011)	Ghasemi et al. (2009), GCMT
Caucasus	GNAS NSSPRA ESMD	EMME and SHARE progress reports (2011)	WSM, GCMT
Pakistan	PMD WAPDA MSSP	EMME progress reports (2011)	GCMT
Jordan	JSO	EMME progress reports (2011)	GCMT

[*] AFAD: Disaster and Emergency Management Presidency, ESMD: European Strong-Motion Data, GNAS: Georgian National Academy of Sciences, IERREWS: Istanbul Earthquake Rapid Response and Early Warning System, ISMN: Iran Strong Motion Network, JSO: Jordan Seismological Observatory, MSSP: Micro Seismic Study Project under Pakistan Atomic Energy Commission, NSSPRA: National Survey for Seismic Protection under the Government of the Republic of Armenia, PMD: Pakistan Meteorological Department, WAPDA: Pakistan Water and Power Development Authority
[†] EMME: Earthquake Model of the Middle East Region Project, SHARE: Seismic Hazard Harmonization in Europe Project
[‡] GCMT: Global Centroid Moment Tensor, NEMC: National Earthquake Monitoring Centre, WSM: World Stress Map Project

The candidate GMPEs for testing are devised for shallow active crustal regions. They are compiled from ground-motion models that are developed either from local databases or from datasets that comprise of accelerograms from multiple countries or regions. The latter ground-motion models are denoted as global predictive models among the model developers. Figure 4.10 presents the country-based distributions of ground-motion datasets used in developing the candidate GMPEs considered in this chapter. As it can be inferred from these statistics the global models mainly contain data from one or two countries or regions. The selected GMPEs satisfy the Cotton et al. (2006) criteria that set *a priori* rules to preserve a certain level of quality control on the selected GMPEs. These criteria are further improved by Bommer et al. (2010) but these were not be used in order not to restrict the number of candidate GMPEs to a shorter list. It is noted that the GMPEs developed by Zhao et al. (2006) and Ambraseys et al. (2005) do not fully comply with the Cotton et al. (2006) criteria. Zhao et al. (2006) lack the complete

documentation of their model and ground-motion dataset. The model developed by Ambraseys et al. (2005) is recently superseded by the GMPE published in Akkar and Bommer (2010). These two GMPEs were not disregarded because they were evaluated in other regional hazard studies (e.g., Delavaud et al., 2012b). The important features of the 14 selected GMPEs are listed in Table 4.3. Most of these GMPEs use extended-source distance measures in their functional forms. Their moment magnitude range generally varies between 5 and 7.5. They are devised for estimating PGA and 5%-damped pseudo-spectral acceleration (PSA). The chosen ground-motion models generally account for major rupture mechanisms and their soil amplification terms are either continuous functions of V_{S30} or they make use of generic site definitions via dummy variables. The selected GMPEs use different horizontal component definitions; most of which are geometric mean (GM) or rotation independent average horizontal component (GMRotI50 defined in Boore et al., 2006). The original source-to-site distance, site class and horizontal component definition of each ground-motion model are used while testing their performance. This approach is overruled for GMPEs that use GMRotI50 and treated their ground-motion estimations as GM because, on average, the predicted ground motions from these 2 horizontal component definitions do not differ from each other (Beyer and Bommer, 2006). Note that while computing the ground-motion estimations of NGA GMPEs The software developed by Dr. D.M. Boore (one of the bi-products of Kaklamanos et al. (2010) report and Kaklamanos et al. (2011) paper) were used. While testing the selected GMPEs, the whole database were utilized without considering the magnitude and distance limitations imposed by each ground-motion model. The general practice in many PSHA studies requires extrapolation of GMPEs outside of their magnitude and distance ranges as few predictive models can satisfy all the magnitude and distance constraints imposed by each specific project. This fact is the major motivation behind the above decision and it is also implemented by other studies (e.g., Delavaud et al., 2012b; Arango et al., 2012).
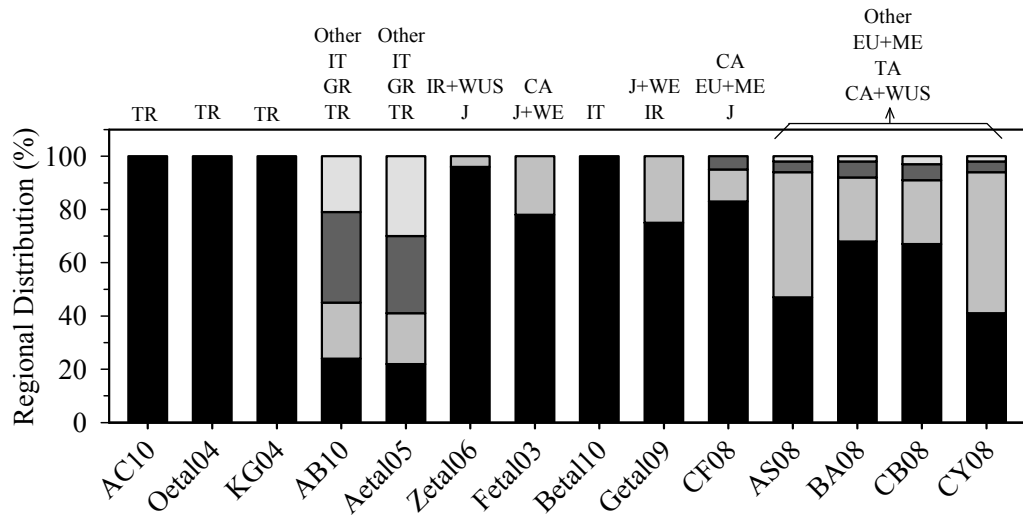
Figure 4.10 Countries or regions contributing to the databases used in the development of candidate GMPEs tested in this study. CA: California, EU: Europe, GR: Greece, IR: Iran, IT: Italy, J: Japan, ME: Middle East, TA: Taiwan, TR: Turkey, WE: West Eurasia, WUS: Western United States.

Table 4.3 General features of considered GMPEs.

GMPE	GMPE Acronym	Main Region(s)	No of records and events	No of estimators	M_w interval	R type and R_{max} (km) [*]	Component [†]	Style-of-faulting [‡]	Site effect
Akkar and Çağnan (2010)	AC10	Turkey	433, 137	4	5.0 - 7.6	R_{JB}, 200	PGA, PGV, PSA in GM	S, N, R	V_{S30}
Özbey et al. (2004)	Oetal04	Northwestern Turkey	195, 17	3	5.0 - 7.4	R_{JB}, 300	PGA, PSA in GM	U	Dummy variable
Kalkan and Gülkan (2004)	KG04	Turkey	112, 57	3	4.0 - 7.4	R_{JB}, 250	PGA, PSA in L	U	V_{S30}
Akkar and Bommer (2010)	AB10	Europe and the Middle East	532, 131	4	5.0 - 7.6	R_{JB}, 100	PGA, PGV, PSA in GM	S, N, R	Dummy variable
Ambraseys et al. (2005)	Aetal05	Europe and the Middle East	595, 135	4	5.0 - 7.6	R_{JB}, 99	PGA, PSA in L	S, N, T, O	Dummy variable
Zhao et al. (2006)	Zetal06	Japan	4726, 269	5	5.0 - 8.3	R_{RUP}, 300	PGA, PSA in GM	S, N, R	Dummy variable
Fukushima et al. (2003)	Fetal03	West Eurasia	740, 50	3	5.5 - 7.4	R_{RUP} and R_{HYP}, 235	PGA, PSA in B	U	Dummy variable
Bindi et al. (2010)	Betal10	Italy	561, 107	3	4.0 - 6.9	R_{JB} and R_{EPI}, 100	PGA, PGV, PSA in L PGA, PGV, PSA in V	U	Dummy variable
Ghasemi et al. (2009)	Getal09	Iran	716, 200	3	5.0 - 7.4	R_{RUP} and R_{HYP}, 100	PSA in GMRotI50	U	Dummy variable
Cauzzi and Faccioli (2008) and Faccioli et al. (2010)	CF08	Japan	1164, 60	4	5.0 - 7.2	R_{RUP}, 150	PGA, PSA in GM	S, N, R	Dummy variable

Table 4.3 Cont'd.

GMPE	GMPE Acronym	Main Region(s)	No of records and events	No of estimators	M_w interval	R type and R_{max} (km) [*]	Component [†]	Style-of-faulting [‡]	Site effect
Abrahamson and Silva (2008)	AS08	Western US and Taiwan	2754, 135	13	5.0 - 8.5	R_{RUP}, 200	PGA, PGV, PSA in GMRotI50	S, N, R	V_{S30}
Boore and Atkinson (2008)	BA08	Western US and Taiwan	1574, 58	5	5.0 - 8.0	R_{JB}, 200	PGA, PGV, PSA in GMRotI50	S, N, R	V_{S30}
Campbell and Bozorgnia (2008)	CB08	Western US and Taiwan	1561, 64	9	4.0 - 8.5	R_{RUP}, 200	PGA, PGV, PSA in GMRotI50	S, N, R	V_{S30}
Chiou and Youngs (2008)	CY08	Western US and Taiwan	1950, 125	12	4.0 - 8.5	R_{RUP}, 200	PGA, PGV, PSA in GMRotI50	S, N, R	V_{S30}

[*] R: distance, R_{max}: maximum distance, R_{EPI}: epicentral distance, R_{HYP}: hypocentral distance, R_{JB}: Joyner-Boore distance, R_{RUP}: closest distance
[†] GM: geometric mean of horizontal components, L: larger horizontal component, GMRotI50: rotation-independent average horizontal component (Boore et al., 2006), B: both horizontal components, V: vertical component
[‡] S: strike-slip faulting, N: normal faulting, R: reverse faulting, O: oblique faulting, U: unidentified

Figure 4.11 shows the testing results of candidate GMPEs for a spectral period band ranging from T = 0.0s (PGA) to T = 2.0s. 8 discrete period values are used (i.e., T = 0.0s, 0.1s, 0.2s, 0.5s, 0.75s, 1.0s, 1.5s, 2.0s) within this period band in order to fully understand the performance of each candidate model under the assembled ground-motion database. Figures 4.11.a and 4.11.b show the components of *EDR* index separately (i.e., $\sqrt{\frac{1}{N}\Sigma_{i=1}^{N}MDE_i^2}$ and $\sqrt{\kappa}$) to understand the significance of sigma (ground-motion uncertainty) and agreement between the median estimations and overall data trend (model bias) for the general performance of each candidate GMPE. The last panel on this figure, Figure 4.11.c, displays the product of these two components; the actual *EDR* index. Table 4.4 presents a similar type of information as Figure 4.11. This table lists the average values of *EDR* components as well as the average *EDR* value computed for each predictive model over the entire period range of interest. The immediate observation from Figure 4.11 and Table 4.4 is that given the ground-motion database the performance of GMPEs shows differences in terms of addressing the aleatory variability and model bias. For example AB10, Zetal06 as well as CF08 and CY08 perform better while addressing the aleatory uncertainty for the considered strong-motion database. The ground-motion models Betal10, AC10, AB10, and CF08 better represent the general trend of the observed data with respect to other candidate GMPEs. When the influence of these two factors is considered together the method favors the performances of AB10, Zetal06, AC10 and Betal10. It is believed that these observations are important since PSHA studies can follow different strategies depending on the specific objectives of each project. For example, site-specific hazard projects may prefer separate consideration of sigma influence and success of GMPEs in estimating reasonable median ground motions. To this end such projects may design two GMPE logic-trees having different sets of GMPEs that perform better in median ground-motion estimations and sigma. Separate consideration of *MDE* and κ indices may be useful for such type of objective-specific hazard studies. In particular, *MDE* would provide valuable information in site-specific hazard studies if the concern is very long return periods

139

(e.g., $T_R > 2500$ years). It might also be speculated that the overall *EDR* index can be more favorable to identify the most suitable set of GMPEs for regional hazard studies because fairly better performance of GMPEs in representing the overall data trend and aleatory variability may yield more realistic hazard results for return periods that are of interest by regional hazard programs (e.g., $T_R \leq 2500$ years). In passing, it is noted that a separate regional project (SHARE) designed the ground-motion logic-tree for PSHA by selecting AB10, Zetal06, CY08 and CF08 that are also listed among the top-ranked GMPEs in this chapter (see details in Delavaud et al., 2012b for SHARE GMPE logic-tree). The SHARE project proposed these GMPEs by a two-step approach that is composed of expert elicitation and model evaluation through LLH methodology. The ground-motion dataset used in SHARE is different than the one used in this chapter. This remark may suggest the proximity of LLH and EDR methods, even if they conceptually differ. The other important observation that is extracted from this remark is the effectiveness of statistical tools (such as EDR or LLH) in providing valuable supplementary information to hazard experts while deciding on the most suitable predictive models for the specific purposes of PSHA studies.

Table 4.4 Performances of tested GMPEs for each individual component of EDR as well as the EDR index.

GMPEs	$\sqrt{\dfrac{1}{N}\Sigma_{i=1}^{N}\mathrm{MDE}_i^2}$	$\sqrt{\kappa}$	EDR
AB10	**1.05**	**1.10**	**1.15**
AC10	1.14	**1.09**	**1.24**
Aetal05	1.22	1.19	1.45
AS08	1.22	1.26	1.54
BA08	1.14	1.25	1.42
Betal10	1.17	**1.06**	**1.25**
CB08	1.18	1.31	1.55
CF08	**1.12**	**1.13**	1.27
CY08	**1.12**	1.15	1.29
Fetal03	1.60	1.59	2.55
Getal09	1.16	1.21	1.41
KG04	1.40	1.59	2.24
Oetal04	1.27	1.16	1.46
Zetal06	**1.08**	1.14	**1.23**

The reported indexes are the averages over spectral ordinates of interested period range. Top 4 best performing models are shown in bold.
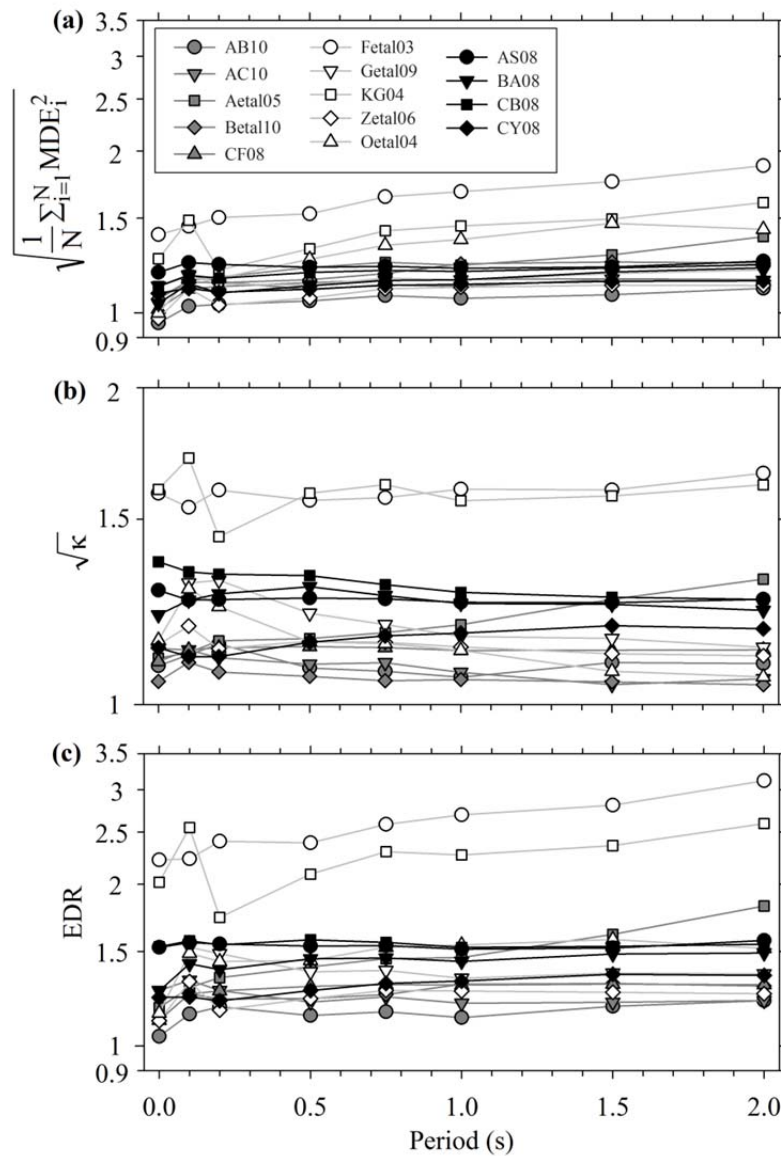
Figure 4.11 Separate EDR components: (a) $\sqrt{\dfrac{1}{N}\sum_{i=1}^{N} MDE_i^2}$, (b) $\sqrt{\kappa}$, (c) the actual

EDR index.

Another interesting observation from the testing results is the relatively better performance of GMPEs with simpler functional forms (i.e., predictive models containing the most basic estimator parameters to describe the source, path, site and rupture mechanism). Examples to such simple-format GMPEs are AB10, AC10, CF08 or Zetal06. It is believed that the metadata of the basic estimator

parameters used by these GMPEs was elaborated in a careful manner prior to their complete development. In other words, their strong-motion databases (either local or global) can be considered as reliable in that sense. The reliability of metadata information is important and if it is inconsistent (or rather old), then predictive models can yield lower performance even if their functional forms are simpler. Typical examples to this case are KG04 (derived from an older version of Turkish strong-motion database, which is recently updated as documented in Akkar et al., 2010) and Fetal03 (whose metadata information for the same events features inconsistencies with the database used in this study that is compiled from the most recent seismological information). Ground-motion models of complex functional forms (more complicated NGA models such as AS08, CB08 and CY08) require reasonable assumptions (such as those suggested in Kaklamanos et al., 2011) for most of their estimator parameters. This additional effort is necessary since the current strong-motion databases, even if they are assembled after significant efforts, would not contain all the required metadata information for the consistent execution of such GMPEs. Thus, the testing methods would not be able to acknowledge the merits of such complicated models unless the ground-motion and seismic-source information is determined in all details for the study area. Kaklamanos and Baise (2011) drew the same conclusion on the model-complexity vs. model-performance stating that the more complicated NGA models do not have a predictive improvement over the simpler NGA models. The experiences in strong-motion database and earthquake catalog compilation suggest that the state of seismological knowledge in many seismic prone regions is currently insufficient for the efficient use of complex GMPEs. However, this comment is not meant to discourage the use or development of such high-quality GMPEs. On the contrary the seismological community is fully supported to conduct long-term research to improve the metadata information for developing well-constrained GMPEs to better address the contribution of source, path and site effects in hazard estimations.

4.5. Summary and Conclusions:

In this chapter an alternative testing procedure for selecting and ranking of GMPEs that can be used for designing GMPE logic-trees in PSHA studies is proposed. The method is based on the Euclidean distance concept that carries similar features with the conventional residual analysis. It is believed that the method can be a good guide to build ground-motion logic-trees from properly ranked GMPEs, if it is used together with other well-designed testing methods as well as visual tools, such as residual analysis.

The proposed procedure accounts for aleatory variability in ground motion estimations (through standard deviations of GMPEs). It also considers the bias between median estimations and observed ground-motion data (model bias). The bias between the median ground-motion estimations and general variation of observed data is identified by the κ parameter that makes an analogy to the residual analysis concept. The uncertainty in ground-motion variability is addressed by finding the probability distribution of the differences between the observed data and corresponding estimations for a range of sigma values. This approach is different than the one in the LLH method (Scherbaum et al., 2009) because LLH computes the occurrence probability of the observed data point by using the corresponding estimation that is assumed to be log-normally distributed with median and sigma values of the candidate GMPE.

A case study is presented to illustrate the general features of the proposed procedure using a database that is compiled from the shallow active crustal recordings of the Middle East, Caucasus and Pakistan. 14 GMPEs for the presented case study that are suitable for estimating the ground-motion intensities of seismotectonic features mimicked by the strong-motion database are selected. The results of the case study suggest that the aleatory uncertainty (i.e., sigma) and the bias between median estimations and observed ground-motion data (model bias) play separate roles on the performance of GMPEs to properly represent the selected

ground-motion dataset. The proposed procedure is capable of providing this useful information to the seismic hazard analyst. Such information can be used in different ways to establish the GMPE logic-tree depending on the objective of the hazard project that can be either forecasting the regional or site-specific hazard. The case study also indicated that GMPEs having simpler functional forms rank better than those whose predictive equations contain complicated estimator parameters. If the metadata of the strong-motion database lacks information about these estimator parameters, they should be computed by making reasonable assumptions. However, no matter how reasonable these assumptions are they impose additional uncertainty to the estimations of such complicated GMPEs that in turn affects their performance.

CHAPTER 5

AN AUXILIARY TOOL TO BUILD GROUND-MOTION LOGIC-TREE FRAMEWORK FOR PROBABILISTIC SEISMIC HAZARD ASSESSMENT

In the context of this chapter, an alternative approach is proposed to build predictive model logic-tree applications for site-specific or regional probabilistic seismic hazard assessments. The use of logic-tree framework within probabilistic seismic hazard assessments is a standard practice to properly characterize the epistemic uncertainty in ground-motion estimates which causes of insufficient knowledge. The application of this method is based on seismic hazard sensitivity analyses conducting with respect to alternative logic-tree frameworks. It is suggested that the proposed method should be used in combination with the existing predictive model selection approaches. This practical tool needs a set of ground-motion prediction equations (GMPEs) that reflects the main characteristics of the site or region being examined. These GMPEs are then utilized for establishing alternative logic-trees with various predictive model groups and sub groups including different weighting schemes of the GMPEs in the main group. The spectral quantities of each alternative logic-tree for a specific return period obtained from seismic hazard analyses are normalized with respect to their median value. This process is repeated for each site under consideration. The method aims at selecting the logic-tree framework which yields normalized spectral values about the median value (i.e., unity). The application of the new tool is discussed through site-specific and regional case studies. The results of the case studies emphasize that although logic-tree set-ups are established from the selected GMPEs which are the best representatives among the candidates to the site or region of interest, some

combinations may result in excessive spectral amplitudes. The proposed method accomplishes capturing those unforeseeable trends in hazard outcomes.

5.1. Introduction

Empirical ground-motion prediction equations (GMPEs) are developed through some regression analyses by using recorded ground-motion accelerograms from the past earthquakes. However, their mission is to predict potential future earthquakes by assuming that they mimic the behavior of the past ones. At this point, size and data distribution in ground-motion datasets of predictive models would make a concession to them. Even though a substantial effort is devoted to develop dense and uniformly distributed local and global strong-motion datasets, no such an immaculate database can be obtained yet because of the randomness in earthquake process and coverage of accelerograph networks. That is, although there are no data in some magnitude-distance bins that constrain the predictive model, GMPE estimates of those earthquake scenarios are included in the hazard integral (Bommer, 2012).

The nature of ground-motion prediction introduces two types of uncertainties to probabilistic seismic hazard assessment (PSHA) that are classified as aleatory or epistemic. The former is considered as intrinsic variability and represented by the standard deviation of the predictive model residuals which follow a normal distribution in logarithmic space. Taking into account the aleatory variability in hazard integral instead of using only median estimates is firstly coming into consideration by Bender (1984). Within the following PSHA applications, neglecting the aleatory variability cannot be regarded as genuine seismic hazard practices (Scherbaum et al., 2005). The latter uncertainty emerges as a result of incomplete knowledge. An indispensable tool to handle the epistemic uncertainty is ground-motion logic-tree framework which is firstly introduced by Kulkarni et al. (1984) to the realm of PSHA. In the conciseness of the current situations of strong-motion databanks, it is obvious that predictive model estimates still have slight or

considerable epistemic uncertainties (Scherbaum et al., 2005; Bommer, 2012; Douglas, 2012). An inevitable consequence to surpass this fact is to use ground-motion logic-tree framework with two or more predictive models in hazard applications.

In ground-motion logic-trees, although epistemic uncertainty cannot be handled using only one of the available GMPEs (Bommer and Scherbaum, 2005), an opposite case, keeping lots of predictive models (more than five) to consider epistemic uncertainty, is also an unacceptable situation since introducing complexity to hazard calculations (Delavaud et al., 2012). There is a consensus on using three or four GMPEs in current practice of PSHA in order to capture the ground-motion variability. In recent years; however, the developments in engineering seismology increase the number of ground motion prediction equations (GMPEs) that results in the selection process of the predictive models being too complicated. Accordingly, testing the applicability of predictive models to study area becomes more important in site specific or regional seismic hazard analyses in order to reduce the selection alternatives.

General conception and practice details of seismic source and ground-motion logic-tree frameworks were discussed in several peer-reviewed papers (Bommer et al., 2005; Scherbaum et al., 2005; Bommer and Scherbaum, 2008; Scherbaum and Kuehn, 2011; Bommer, 2012). Under the common consideration of logic trees, combination of predictive models within a ground-motion logic-tree framework to properly handle the epistemic uncertainty and to suitably predict the future ground excitations is the vital step of a hazard analysis (Bommer et al., 2005). In this respect, careful selection of GMPEs and their logic-tree weights play a significant role on the hazard results. Sabetta et al. (2005), Scherbaum et al. (2005) and Bommer et al. (2005) claim that increasing number of predictive models in a logic-tree branch decreases the importance of their weights; however, the weights significantly change the hazard results until a certain number of GMPEs (generally four or more) are included in the ground-motion logic tree. That is to say, they

emphasize that the importance of careful selection of GMPEs for logic trees has more impact on hazard results than the logic-tree branch weights assigned to each predictive model. In this instance, we come back to the problem of determining the appropriate predictive models to location of interest.

Several methods on selection and ranking of predictive relations were published in the last decade. These methods would be evaluated separating them as non-data-driven (or pre-selection) and data-driven testing methods. Cotton et al. (2006) as well as its updated and extended version Bommer et al. (2010) constitute the former group, whereas Nash and Sutcliffe (1970), Scherbaum et al. (2004, 2009) and Kale and Akkar (2013) are in the latter group methods. Non-data-driven approaches are serving for predictive model selection by considering their general characteristics (strong-motion database, seismotectonic regime, etc.) and intrinsic formulation details (regression method, explanatory variables, types of coefficients, etc.). The second group approaches use recorded strong-motion data and rank predictive models with respect to calculated scores. Besides, their dependency on size and distribution of the ground-motion datasets should not be forgotten by considering the requirements of the site under consideration.

Despite the pros and cons of the selection methods, the use of them would significantly help to hazard analysts during the decision making process and then an appropriate number of candidate GMPEs would be retained for logic-tree branches. Now the challenge herein is how many and which predictive relations will be included in the logic-tree framework. This is also a formidable task as much as the process of testing and selecting appropriate GMPEs to logic tree. At this stage, various approaches would be regarded to construct the final form of the ground-motion logic-tree framework such as expert opinions, final ranks of the selected GMPEs based on data-driven testing methods, seismic hazard sensitivity analyses, studies in literature, giving equal weights to predictive models if there are not so many selected GMPEs as in Petersen et al. (2008), detecting the trends in

ground-motion estimates of the selected models as proposed by Stewart et al. (2014).

In this section, an alternative approach is proposed to properly handle the epistemic uncertainty in seismic hazard assessment. The use of the proposed tool is suitable after the pre-selection and data-driven testing methods are applied and a set of GMPEs that exhibit well the general characteristics of the region of interest are obtained. The method evaluates the effects of the predictive models selected for logic tree and the weights assigned to them on PSHA results. To evaluate the properness of the predictive relations and their weights in logic tree, the method proposes to construct various logic trees which include different GMPEs with different weighting schemes by considering the approaches listed in the previous paragraph. The proposed method can be considered as an auxiliary tool to the current approaches because hazard analyst can apply it in combination with them.

5.2. Popular Approaches to Establish Ground-Motion Logic Trees

Hazard analysts and researchers follow some alternative ways while selecting the most appropriate GMPEs and assigning branch weights to them in logic trees. The GMPEs mentioned here, as a reminder, are selected via pre-selection and data-driven testing methods and now regarded as suitable for the site or region of interest.

Recently, while characterizing the ground-motion logic-tree framework, combining the pre-selection and data-driven test results with expert opinion gain popularity in PSHA. As an up-to-date example, SHARE (**S**eismic **H**azard H**AR**monization in **E**urope, http://www.share-eu.org/) project followed this way while establishing the ground-motion logic tree for PSHA in Euro-Mediterranean region (Delavaud et al., 2012). Firstly, they selected the candidate GMPEs and then, expert judgment of a research group and data-driven test results of Scherbaum et al. (2009) method were combined and final set of GMPEs were determined. After that, ground-motion

149

logic tree were built according to seismic hazard sensitivity analyses by considering different set of predictive model weights.

The studies that focus on testing the applicability of GMPEs to seismic prone regions sometimes help the hazard analyst on building logic trees. During the ground-motion relations selection for GEM (**G**lobal **E**arthquake **M**odel, http://www.globalquakemodel.org/) project, several studies in literature were considered as a supplementary tool for establishing ground-motion logic trees (Stewart et al., 2014). In addition, Stewart et al. (2014) have some proposals that may help to construct the final form of the ground-motion logic tree. They recommend three main criteria to select the GMPEs: i) the predictive relations derived from global or internationally reviewed local datasets should be favored; ii) the predictive models which include recent improvements such as magnitude saturation, magnitude-dependent distance decay in their functional forms should have more emphasis; iii) provided that the candidate GMPEs are definitely appropriate for the region of interest but represent dissimilar spectral behaviors, the selection should be made to represent the overall trends of candidate models to properly capture the epistemic uncertainty. First two of them, in fact, mimic the criteria of non-data-driven approaches whereas the last one proposes a new perspective for constructing ground-motion logic trees.

As another fact, a different situation may also be encountered once constructing the ground-motion logic trees as in the case of 2008 national hazard map of western United States (Petersen et al., 2008). There were limited numbers of predictive models that are applicable to the region. Therefore, the ground-motion variability in this project was captured by three NGA GMPEs (Boore and Atkinson, 2008; Campbell and Bozorgnia, 2008; Chiou and Youngs, 2008) which are developed from a common database and whose estimates do not exhibit different trends for significant earthquake scenarios. Accordingly this case may result in potential underestimation of epistemic uncertainty in PSHA. To surpass this fact, additional branches which are aimed to compensate the uncertainties coming from magnitude-

distance bins with sparse data were added to the ground-motion logic trees. Once Petersen et al. (2008) uses the number of data in different magnitude-distance bins to scale the estimates of NGA GMPEs, more elaborated studies that considers variance of regression coefficients and within-model uncertainties are proposed by Arroyo and Ordaz (2011) and Al Atik and Youngs (2014), respectively.

5.3. Theoretical Framework of the Proposed Method

It is strongly recommended to end users that the proposed method should be applied considering all selection methods mentioned in previous sections and should be considered as an auxiliary tool for establishing ground-motion logic trees in all types of seismic hazard applications (i.e., classical PSHA and PSHA with additional uncertainty branches [Petersen et al., 2008]). Despite plenty of methods and approaches in the literature, the main reason of proposing a new method is to portray a new picture to hazard analysts during the predictive model selection for PSHA.

In this study, the third proposal of Stewart et al. (2014) is highly appreciated; however, the GMPEs that draw the epistemic uncertainty bounds may alter with respect to dominancy of earthquake scenarios for the considered sites. For site specific studies, capturing the behavior of the models is easy because dominant earthquake scenario (or scenarios) can be obtained from disaggregation but the capturing process is more complicated for regional seismic hazard analyses. At this point, the sensitivity analyses applied in SHARE project (Delavaud et al., 2012) in order to assign the weights of the GMPEs can be helpful. However, one could have a different opinion from SHARE project that the sensitivity analyses should also be used for selecting GMPEs to handle the effects of using different predictive models in logic tree and to prevent subjectivity in decision making.

In this article, a seismic hazard sensitivity-based method for building ground-motion logic trees is proposed. The method is based on basic statistical and

mathematical basis and reflects the effects of selected GMPEs and assigned weights to them on PSHA results in a numerical and pictorial form. This method enables hazard analyst to choose GMPEs and their weights that prevent a particular GMPE dominating the hazard. The need preventing the dominancy of a predictive model is relevant to the inherent form of the logic-tree framework. When a particular GMPE come into prominence in logic tree, handling the epistemic uncertainty process is committed by that predictive model which conflicts the belief of what logic tree works as mentioned in the previous sections.

In the proposed method, the selected GMPEs that exhibit the general seismotectonic settings of the study area are used to establish N major predictive model groups. Each major group is then divided into M different sub-groups by varying the weights of GMPEs in that group. In essence, NxM different GMPE logic-trees (from LT-1 to LT-NxM) are established for the sensitivity analyses. If N = 4 major group predictive models with M = 3 different weighting schemes are considered, 12 sets of logic tree are obtained and the node structure of this arrangement is displayed as in Figure 5.1.
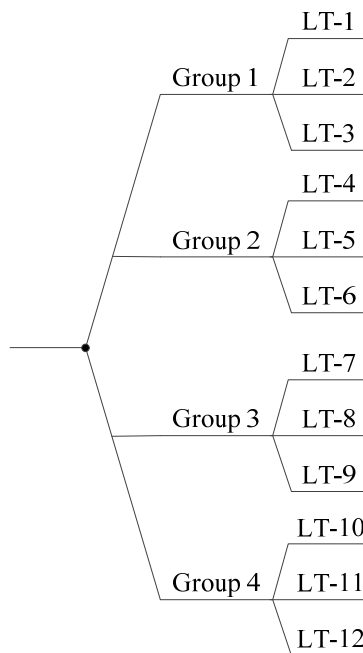
Figure 5.1 Node structure of sensitivity analyses.

Given a spectral period of interest, *N*x*M* hazard curves are computed similar to the above established logic-trees for a previously determined site or a set of sites in the region under consideration. Spectral accelerations (*SA*s) corresponding to alternative logic trees take different values for a specific return period. Given a site, spectral accelerations corresponding to the selected return period are normalized with their median (*SA*$_{med}$) to obtain *N*x*M* normalized *SA*s (*NSA*s). Finally, the normalized *SA*s of all sites for a particular return period and spectral period are binned according to the logic trees given in Figure 5.1. The trends in the binned normalized *SA*s are evaluated for obtaining the most proper set of GMPEs and corresponding weights for the hazard calculations. If the scatters of a logic-tree branch fluctuate about unity, it can be said that none of the individual GMPEs within the considered logic-tree branch dominate the hazard results. To numerically evaluate the results for a considered site, the absolute differences of *NSA*s to unity are calculated for each alternative logic tree by Equation 5.1 where *i* represent the logic-tree number and takes values from 1 to *N*x*M*. When the regional scale is of concern, the differences are calculated for each site similar to Equation 5.1 and then their square root of sum of squares are calculated and normalized by the number of site (Equation 5.2) to represent the overall trend in numerical form. In Equation 5.2, *i* is similar to that of Equation 5.1 whereas *j* denotes the number of sites (*N*$_{site}$) in the region of interest. At the end, the logic tree with minimum $D_{LT,i}$ indicates the most suitable logic-tree set up to handle the epistemic uncertainty.

$$D_{LT,i} = \left| 1 - NSA_{LT,i} \right| \tag{5.1}$$

$$D_{LT,i} = \sqrt{ \frac{1}{N_{site}} \sum_{j=1}^{N_{Site}} \left| 1 - NSA^{j}_{LT,i} \right|^{2} } \tag{5.2}$$

Among the rational logic-tree alternatives, this method proposes to favor the logic tree that gives the median hazard spectrum for a given return period instead of supporting mean, minimum or maximum trends. Therefore, it uses the normalized spectral values with respect to their median once evaluating the logic-trees. The

reason of selecting median spectral quantity is that the median is less sensitive to the most severe trends (i.e., upper and lower bounds) of the alternative logic-trees. The use of the normalized values with respect to mean spectral acceleration may push the hazard analyst to select a logic tree close to boundaries mostly at long return periods. A similar situation is emphasized for disadvantages of using mean hazard curve instead of median or other fractiles by Abrahamson and Bommer (2005). As another option, selecting the minimum- or maximum-trend logic-trees would produce underestimated or overestimated hazard results, respectively.

Figure 5.2 shows 9 hazard curves obtained from 3 major group GMPEs and corresponding 3 sub-groups by mimicking the node structure given in Figure 5.1 for two specific sites at different locations to seismic sources. In this figure, the focus is only on the obtained results for different levels of return periods. Thus, the details of setting up the major groups and sub-groups are not stated here but are going to be discussed in the following sections within the light of site specific and regional case studies. In this figure, the hazard curves corresponding to the logic trees yield different spectral accelerations in a bandwidth for a selected return period level. The disparity of hazard estimates is minimal for short return periods whereas the bandwidth is widened by increasing return period. The site in Figure 5.2.a displays more dispersive behavior than that of Figure 5.2.b. Although all predictive models considered in these cases are reliable models and identical node structures are used, the established logic trees yield dissimilar spectral behaviors. The importance of using mean-normalized or median-normalized spectral quantities is more pronounced in Figure 5.2.a at long return periods. When mean-normalized values are used to evaluate the logic trees, the most appropriate logic-tree application is obtained as shown with red dashed line (LT-5) whereas considering median-normalized estimates proposes to select the logic tree assembled with solid red line (LT-4). If it is accepted that the logic-tree applications produced by Group 3 models significantly overestimate the hazard, favoring LT-4 provides more rational hazard estimates.
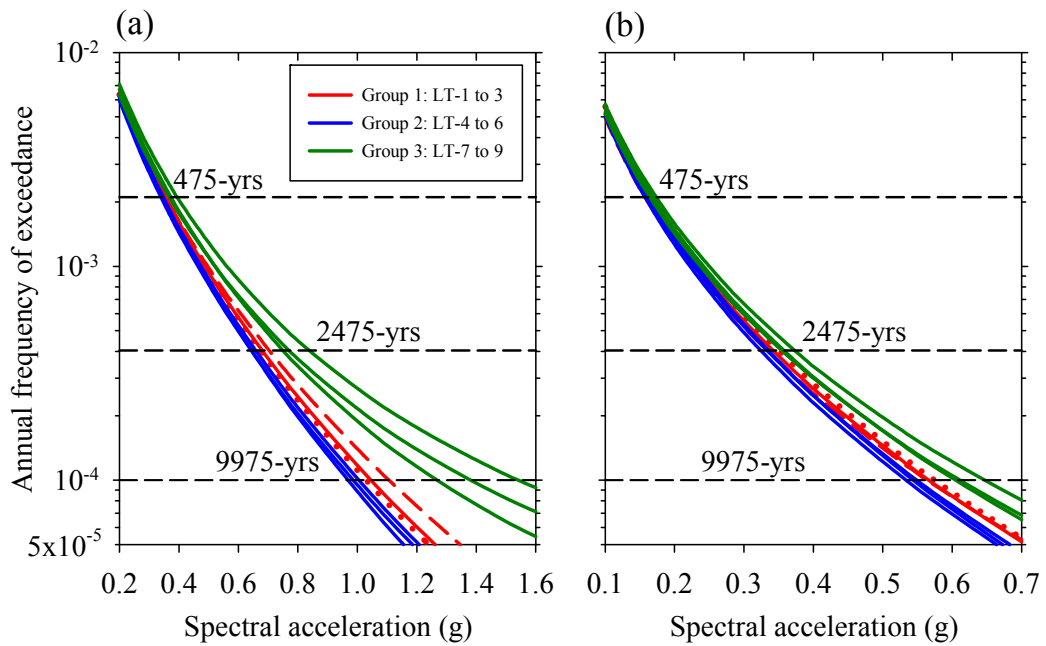
Figure 5.2 Hazard curves for two distinct seismic prone sites with respect to same sensitivity-based node structure.

5.4. Site-specific and Regional Case Studies

In this part, application of the proposed method is explicitly introduced by the help of site-specific and regional probabilistic seismic hazard case studies that are conducted to a region including the North Anatolian Fault (NAF) zone of Turkey. The studies in literature are considered to select the most reliable GMPEs for region being studied in order to establish the alternative logic trees. Thus, Akkar et al. (2014) - ASB14, Akkar and Çağnan (2010) - AC10, Cauzzi and Faccioli (2008) - CF08, Chiou and Youngs (2008) - CY08 and Zhao et al. (2006) - Zh06 predictive models are selected to be used for building ground-motion logic tree alternatives considering the proposals of Delavaud et al. (2012), Kale and Akkar (2012), Kale (2014) and Stewart et al. (2014). All of the cited references regard at least one of the selection approach mentioned in the previous sections of this study. The epistemic uncertainty can be well represented by the selected models because the constituted GMPE set includes local Turkish model (AC10), Pan-European model (ASB14), Japanese-data based models (CF08 and Zh06) and global model (CY08).

155

The trellis chart showing the median and median + 2 sigma trends of candidate predictive models for PGA and moment magnitudes (M) of 4.5, 6.0 and 7.5 is displayed in Figure 5.3. This chart assists to capturing epistemic uncertainty with respect to the approach given in Stewart et al. (2014). As a general perspective, it can be concluded from the ground-motion trends that AC10 draws the lower bound of epistemic uncertainty whereas the maximum bound is constituted by CF08 and Zh06. The median trend for epistemic uncertainty is denoted by ASB14 and CY08. Once establishing the major groups of logic trees, more emphasis is given to predictive models of AC10 and ASB14 as they contain Turkish strong-motion data in their model generating datasets. In addition, the GMPEs that shows median trend (ASB14 and CY08) are favored while assigning end branch weights.
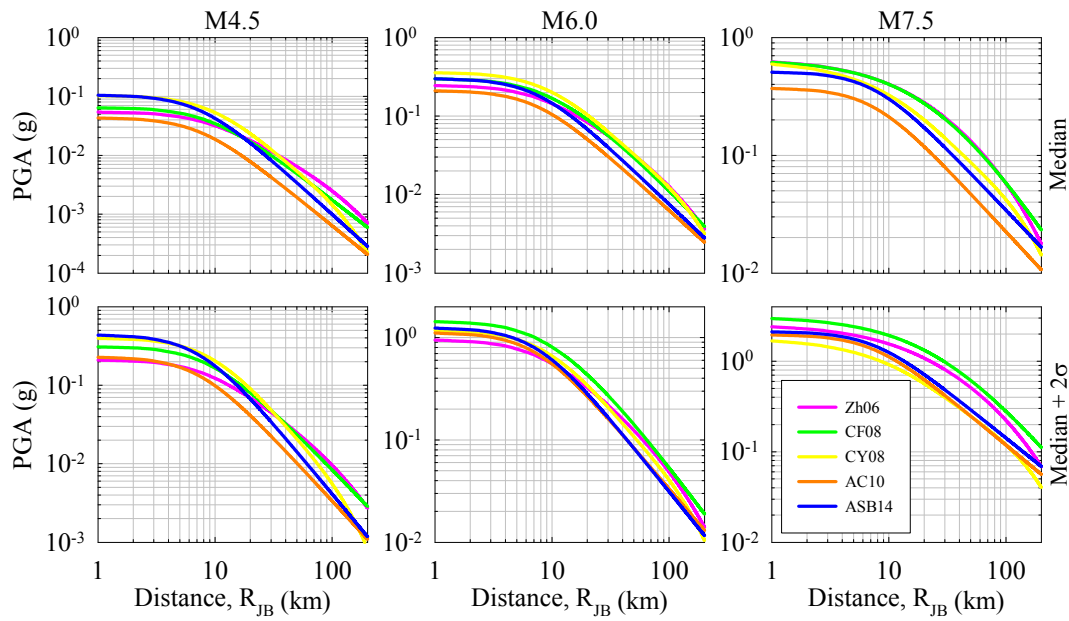
Figure 5.3 Trellis chart showing median (top row) and median + 2 sigma (bottom row) distance scaling of the selected GMPEs for magnitudes of 4.5 (first column), 6.0 (middle column) and 7.5 (last column), $V_{S30} = 760$m/s and strike-slip fault mechanism.

The node structure of the sensitivity analyses is similar to the illustration given in Figure 5.1. The selected 5 GMPEs are used to establish 4 major GMPE groups. The

first major group contains two best representative GMPEs (ASB14 and AC10) and global NGA model of CY08. The next two major groups include these GMPEs as well as an additional one from the other two upper bound predictive models (Zh06 and CF08). The last group represents the minimum, median and maximum trend predictive models (AC10, ASB14 and Zh06). Then, each major group is divided into 3 different sub-groups by assigning the various branch weights to GMPEs in that group. In essence, 12 different GMPE logic-trees (from LT-1 to LT-12) are established for the sensitivity analyses. The logic-tree structure of 4 major groups with their corresponding 3 weighting schemes is listed in Table 5.1.

Table 5.1 Weighting schemes applied to the predictive models.

GMPE	Group 1			Group 2			Group 3			Group 4		
	LT1	LT2	LT3	LT4	LT5	LT6	LT7	LT8	LT9	LT10	LT11	LT12
AC10	0.20	0.30	0.10	0.20	0.20	0.10	0.20	0.20	0.10	0.30	0.25	0.25
ASB14	0.40	0.35	0.45	0.35	0.30	0.40	0.35	0.30	0.40	0.40	0.50	0.60
CF08	-	-	-	-	-	-	0.10	0.20	0.10	-	-	-
CY08	0.40	0.35	0.45	0.35	0.30	0.40	0.35	0.30	0.40	-	-	-
Zh06	-	-	-	0.10	0.20	0.10	-	-	-	0.20	0.25	0.15

Figure 5.4 displays the location of selected sites as well as the area of interest in regional hazard case study and the area sources used for seismic hazard calculations. OpenQuake Engine (Pagani et al., 2014) was used to conduct hazard analyses. The area sources are taken from the EMME (Earthquake Model of the Middle East Region, http://emme-gem.org/) area source model.

Figure 5.4 Illustration of the selected sites and region of interest with considered area sources.

The first case study demonstrates the functionality of the logic-tree based sensitivity method for site-specific PSHA. Accordingly, two specific sites are selected from the region of interest to evaluate what is offered by the application of the proposed method to the hazard analyst. Figures 5.5.a and 5.5.b show the site-specific hazard curves obtained from different logic-tree applications given in Table 5.1 for Site-A and Site-B, respectively. It is immediately apparent that in both cases the behaviors of Group 3 logic trees are almost entirely different than those of others which are explained by the dominance of CF08 predictive model. The observed effect is more prominent for the close distance site (i.e., Site-B) to the North Anatolian Fault (NAF) zone. Another interesting observation can be made evaluating the hazard curves of Group 4 logic-tree applications. When short return period levels are considered for both cases, Group 4 hazard curves draw the lower bound; however, at long return periods, these hazard curves tend to climb across the Groups 1 and 2 curves. This observation is directly relevant to the different behaviors of the considered GMPEs in logic trees with respect to the exceedance levels. The point differentiating the Group 4 from the Groups 1 and 2 is that Group 4 does not include CY08 which has lower standard deviations with respect to other predictive models used in this case study. Thus, the effect of

158

standard deviation on hazard curves is observed for long return periods as depicted by Restrepo-Velez and Bommer (2003).
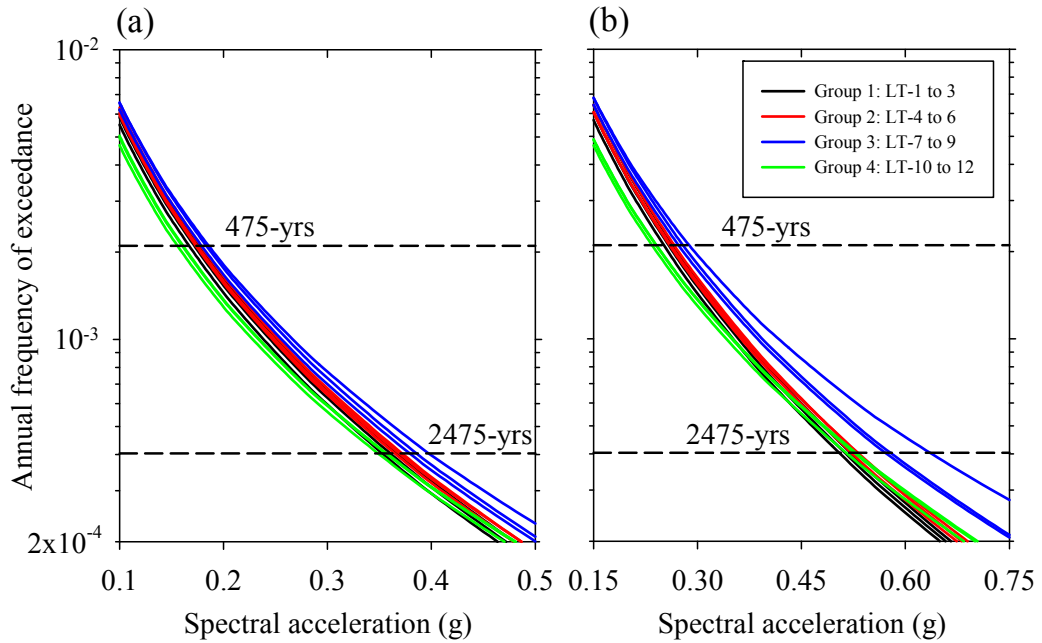
Figure 5.5 Hazard curves for the sites shown in Figure 4: a) Site-A, b) Site-B.

The general findings of this site-specific case study indicate that the selected GMPEs for logic-tree framework can significantly alter the seismic hazard results although they are ratified by the selection methods and experts. This case is identified clearly by the trends of Group 3 hazard curves in Figures 5.5.a and 5.5.b on which CF08 has greater impact. For the hazard outcomes, the effects of the predictive model selection are more influential than those of the ground-motion logic-tree branch weights in parallel to the findings of Sabetta et al. (2005), Scherbaum et al. (2005) and Bommer et al. (2005). Besides, assigning the relative weights to the branches results in diverse spectra for a specific return period even if none of the predictive models are biased for the case of interest (Figure 5.a). In addition to the findings, it can be inferred from the different trends between Figures 5.5.a and 5.5.b that the GMPEs would behave contrarily with respect to the location of the sites and considered return period. The imposed effect by CY08 to the assembled logic trees is an objective proof of the importance of considered

exceedance level. The importance of location of the site is again related to the logic trees including CF08 model in the considered case studies.

When regional or a large scale PSHA is of concern, the suggested method is applied to the pre-selected sites within the considered area (NAF). Accordingly, the region given in Figure 5.4 surrounded by red lines is selected in order to exemplify the regional application of the method. In this region, 880 discrete sites are assembled provided that they cover the entire area. The same process followed on the site-specific case study is repeated for the assembled sites. Resultantly, 12 hazard curves and corresponding *NSA*s with respect to return periods of 475 and 2475yrs are obtained for each pre-selected site in the NAF region. Figures 6 and 7 represent the *NSA*s of each logic-tree framework given in Table 5.1 for 475 and 2475yrs, respectively. The x-axes in these figures depict the site IDs numbered from 1 to 880. The illustrative plots in Figures 5.6 and 5.7 are for normalized PGA. In these figures, if the scatters of a logic-tree branch fluctuate about unity, the resulting hazard is close to the median hazard curve (i.e., none of the individual GMPEs within the considered logic-tree branch dominate the hazard results). When fluctuations of the scatters take place above or below the median level, considering the aim of the proposed method, it can be deduced that the related logic-tree framework overestimate or underestimate the hazard, respectively.
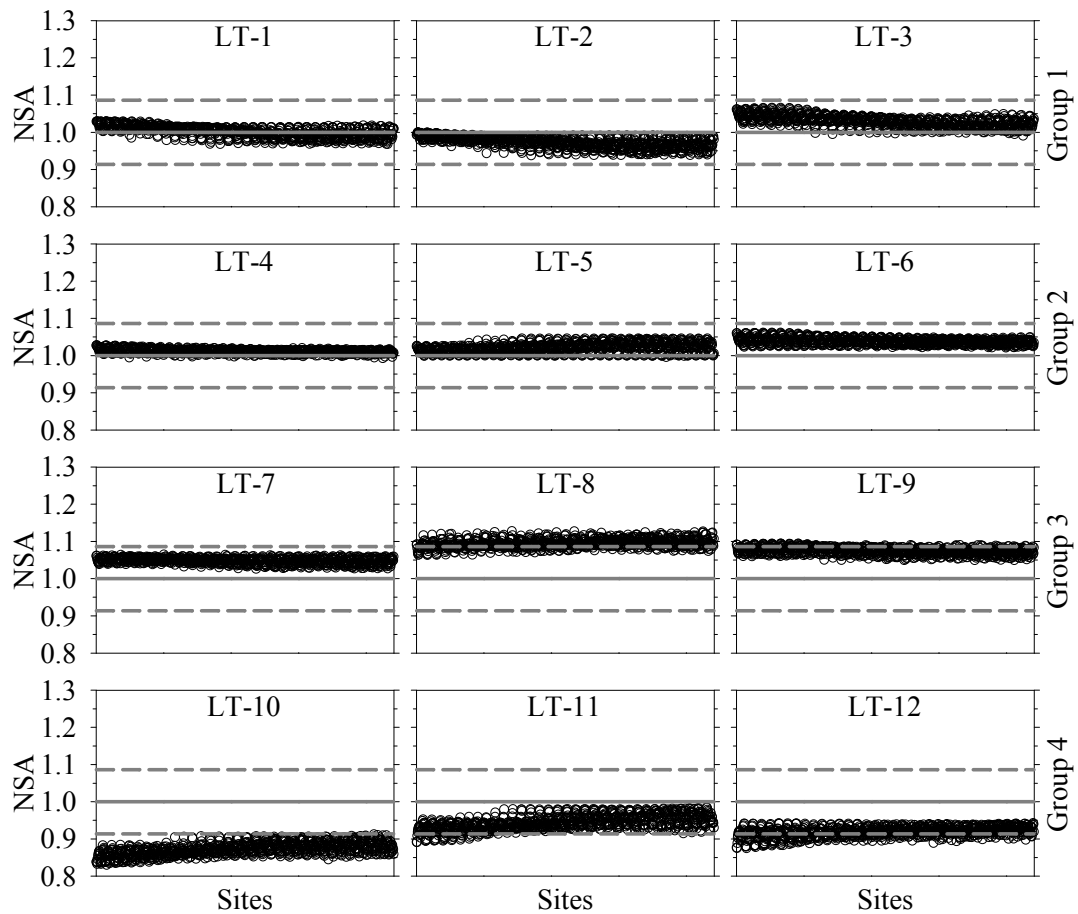
Figure 5.6 Results of logic-tree based sensitivity analysis of the selected region for PGA and return period of 475yrs. The solid gray line represents the median of NSAs whereas dashed gray lines show median ± standard deviation corresponding to the worst case among all alternatives.

The quick observation from Figures 5.6 and 5.7 is that given the binned *NSA*s the performance of alternative logic trees displays differences in terms of addressing the epistemic uncertainty. In parallel to the observations for site-specific cases, CF08 model significantly jump the hazard results above the median level. The NSAs of Group 4 logic trees are considerably below the median hazard level for 475yrs whereas the trends of the scatters get closer to the median level with increasing return period. The fluctuations of the scatters within the same logic-tree group display slight or considerable differences depending on the weighting

schemes of the predictive models. When both return periods are considered, LT-4 performs better while addressing the epistemic uncertainty for the considered region without any domination of a predictive model to the hazard results.
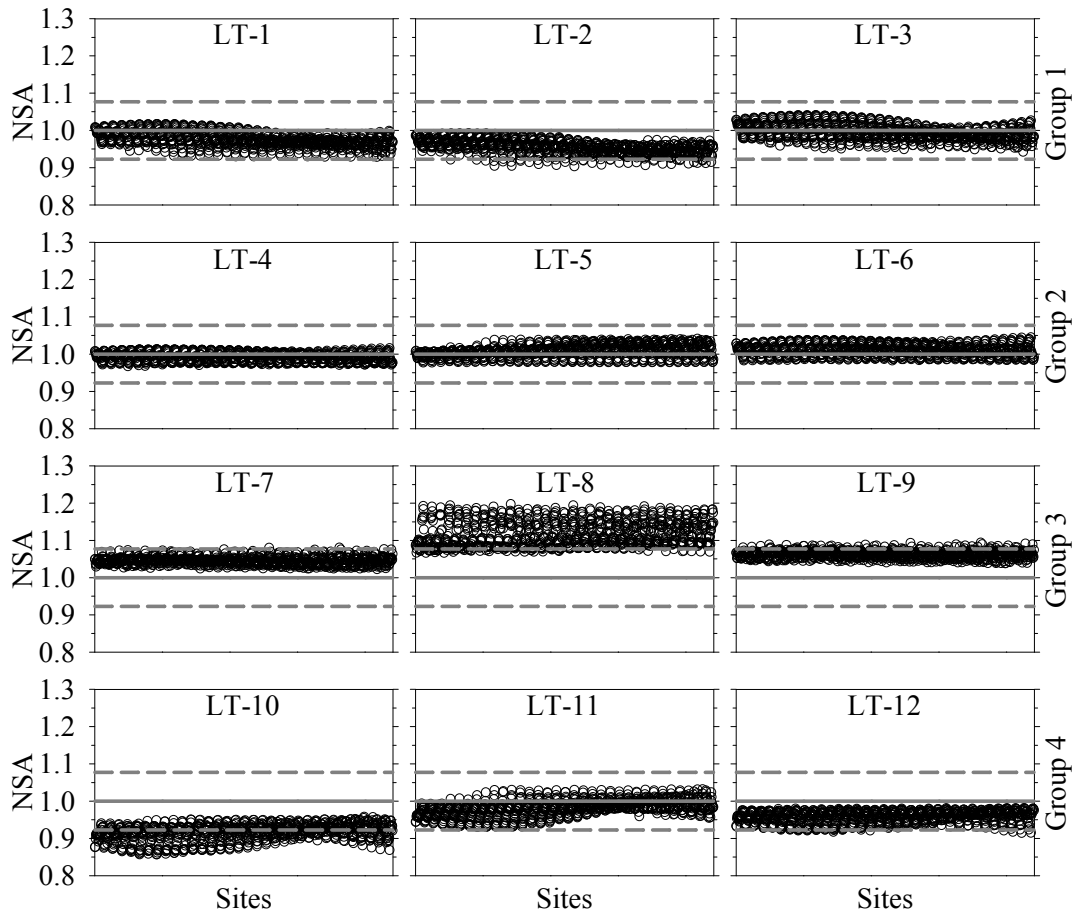
Figure 5.7 Results of logic-tree based sensitivity analysis of the selected region for PGA and return period of 2475yrs. The solid gray line represents the median of NSAs whereas dashed gray lines show median ± standard deviation corresponding to the worst case among all alternatives.

Table 5.2 presents the numerical information of case studies given in Figures 5.5, 5.6 and 5.7 instead of evaluating the alternatives by visual inspection. This table lists the logic-tree differences calculated from Equations 5.1 or 5.2 for each case study with respect to the return periods of 475 and 2475yrs. The immediate

observation from Table 5.2 is that the performances of logic-tree set-ups show differences with respect to the return period and region or site being considered. For example LT-1 performs better while considering both return periods for Site-A and the short return period for Site-B and region of interest, whereas when the long return period is of concern, the performances of LT-5 and LT-4 for Site-B and region, respectively, are more appreciated by the given method. To this end, the results of the case studies dictate that the logic-trees can be built having different sets of GMPEs and relative weights with regard to the sites and regions as they are objective-specific hazard components.

Table 5.2 Logic-tree distances (in terms of %) for the site-specific and regional hazard case studies for return periods (T_R) of 475 and 2475 yrs. The best performing logic-trees in each case are shown in bold.

$D_{LT,i}$	Site-A		Site-B		Region	
	T_R 475 yrs	T_R 2475 yrs	T_R 475 yrs	T_R 2475 yrs	T_R 475 yrs	T_R 2475 yrs
$D_{LT,1}$	**0.01**	**0.01**	**0.00**	0.15	**1.44**	3.07
$D_{LT,2}$	**0.04**	0.07	**0.03**	0.27	3.07	4.78
$D_{LT,3}$	0.14	**0.01**	0.08	0.07	3.28	2.19
$D_{LT,4}$	**0.04**	**0.00**	**0.01**	0.06	**1.24**	**1.42**
$D_{LT,5}$	0.07	**0.01**	**0.03**	**0.01**	2.45	**1.87**
$D_{LT,6}$	0.21	**0.03**	0.11	**0.02**	3.95	**1.94**
$D_{LT,7}$	0.24	0.11	0.28	0.34	4.85	4.62
$D_{LT,8}$	0.73	0.49	1.11	3.89	9.55	12.21
$D_{LT,9}$	0.55	0.22	0.53	0.57	7.50	6.29
$D_{LT,10}$	2.13	0.65	1.86	0.52	12.86	8.67
$D_{LT,11}$	0.38	0.04	0.38	**0.04**	5.93	2.85
$D_{LT,12}$	0.85	0.15	0.71	0.15	8.23	4.43

5.5. Summary and Conclusions

To handle the epistemic uncertainty in PSHA, there are several ways for establishing ground-motion logic trees in the open literature; however, the numbers of studies still cannot provide solid guidance on that issue. Rational contributions to that topic progressively enrich the relevant literature and would be appreciated by the seismological community. Correspondingly, in the present study, a new tool is offered to suitably capture the epistemic uncertainty in seismic hazard studies by

evaluating the performances of alternative logic-tree frameworks. The method is strongly recommended to be used in combination with such advances in the literature since the objective of proposing this approach is being conducive to build more reliable logic-tree applications.

Among the candidate predictive models, the proposed approach uses the selected GMPEs which are the best in representing the ground-motion trends for the site and region being studied. The alternative logic-tree frameworks are built considering the selected GMPEs and their relative weights in order to decrease the objectivity in decision making. The spectral ordinates for a predetermined exceedance rate and for a given logic-tree branch are normalized with respect to the median quantity. Then the trends in the obtained *NSA*s are evaluated for obtaining the most proper set of GMPEs and corresponding weights to properly handle the epistemic uncertainty for PSHA. The resultant set of predictive models and their weighting scheme are tailored such that none of the selected GMPEs dominate the hazard at a particular location.

A set of case studies are conducted to illustrate the application of the proposed logic-tree tool considering a region located along a part of the North Anatolian Fault zone. The considered case studies clearly demonstrate that although the selected GMPEs for establishing logic-tree applications are the best representative ones in the region, some of the alternative combinations yield extreme spectral quantities with respect to other alternatives. The case studies also depict that the importance of selected GMPEs and their weights in a logic-tree framework varies from site to site. The proposed auxiliary tool achieves to capture those issues in the considered case studies and would constitute an appreciable contribution to the field of PSHA. Nevertheless, it is believed that to improve the guidance on logic-tree topic, such contributions should be active as long as logic-tree framework is used for incorporating epistemic uncertainty into PSHA.

CHAPTER 6

GROUND-MOTION LOGIC TREE FRAMEWORK FOR PROBABILISTIC SEISMIC HAZARD ASSESSMENT IN EMME REGION

The major objective of WP-3 of the EMME (**E**arthquake **M**odel of the **M**iddle **E**ast Region) project is to describe the ground-motion model that is used in the hazard calculations of the EMME region (i.e., Caucasus, Middle East and western Asia). In this respect, a ground-motion logic-tree framework for shallow active crustal regions considering predictive model testing methods and logic-tree based sensitivity approach are proposed by the WP-3 of EMME project. The candidate ground-motion prediction equations (GMPEs) are selected considering the proposals of Cotton et al. (2006) and tested under a strong-motion database compiled in the framework of this project. The data-driven testing methods of NSE (Nash and Sutcliffe, 1970), LH (Scherbaum et al., 2004), LLH (Scherbaum et al., 2009) and EDR (Kale and Akkar, 2013) are used to test the ground-motion models. The evaluation of these methods leads to a set of GMPEs that can be applied confidently in seismic hazard studies for the EMME region extending from Turkey to Pakistan. At the final stage of establishing logic-tree application, the logic-tree based sensitivity method given in Chapter 5 is applied by using the final set of GMPEs. Then, the final ground-motion logic-tree framework for the hazard computations of shallow active crustal regions in the EMME is established. The selected predictive models and corresponding logic-tree weights are totally based on the procedures which are well accepted by the seismological community in order to prevent the subjective decision-making process. For subduction regions in the project area, the GMPEs selected in the SHARE project (acronym for the

Seismic **H**azard HA**R**monization in **E**urope; one of the regional projects of GEM) are used as there are no recorded subduction accelerograms in the EMME database for applying data-driven testing procedures.

6.1. Introduction

The Middle East region is placed in the junction of the African, Arabian and Eurasian active tectonic plates which produce periodically high seismic activities. This region has been suffered from several destructive earthquakes. In the consciousness of the effects of these disasters, a regional project called as **E**arthquake **M**odel of the **M**iddle **E**ast Region (EMME; http://emme-gem.org/) started in 2009 with a 4-year budget. The partner countries in the project are Armenia, Georgia, Iran, Jordan, Pakistan and Turkey. This project which was completed in late 2013 focused on the assessment of regional seismic hazard, the associated risk and the effects of relevant mitigation processes in the Middle East region in accordance with the **G**lobal **E**arthquake **M**odel (GEM; http://www.globalquakemodel.org/) project.

The ground-motion modeling part of the EMME regional seismic hazard assessment from which WP-3 is responsible, covers (a) identifying a set of ground-motion prediction equations (GMPEs) that characterize the overall neotectonic features of the EMME region of abundant strong-motion data, (b) adopting these GMPEs for the EMME region of sparse data via host-to-target relationships, and (c) modifying rock ground motions obtained from (a) and (b) for different soil conditions by a proxy site characterization method. However, this chapter only presents the details of the first target (i.e., establishing ground-motion logic-tree framework for seismic hazard analyses in this region).

The former regional projects such as GSHAP (**G**lobal **S**eismic **H**azard **A**ssessment **P**rogram; Giardini, 1999), SESAME (Seismotectonics and Seismic Hazard Assessment of the Mediterranean Basin; Jimenez et al., 2001) had a limited number

of predictive model options to be used in seismic hazard analyses. In general, the compatibility of model-developing datasets of the candidate GMPEs to region being studied are the primary factor for taking them into hazard analyses. After 2000, the number of predictive models significantly increases in parallel with the improvements in strong-motion catalogs and ground-motion data as illustrated in Figure 1.7. These seismological developments bring with them the necessity of selection and testing the appropriateness of candidate GMPEs to the region of interest. Recently, such efforts were conducted in some regional projects to properly handle the epistemic uncertainty in probabilistic seismic hazard assessment (PSHA). In the SHARE (**S**eismic **H**azard HA**R**monization in **E**urope) project, the GMPE selection for ground-motion logic-tree framework was based on the expert elicitation and the results of data-driven log-likelihood testing method (LLH; Scherbaum et al., 2009). Besides, the logic-tree branch weights of the predictive models are determined from some PSHA sensitivity analyses. The ground-motion logic-trees were proposed for PSHA in stable continental regions, subduction zones and shallow active crustal regions of Euro-Mediterranean region (Delavaud et al., 2012). The GEM (**G**lobal **E**arthquake **M**odel) project was also proposes global ground-motion logic-tree set-ups for the same tectonic regimes in the SHARE project. To construct the globally applicable logic-tree frameworks, they considered some pre-defined criteria, literature review and trellis plots of GMPEs with respect to response spectra, magnitude and distance scaling for different periods and earthquake scenarios (Stewart et al., 2014).

The ground-motion models for EMME regions of abundant data are going to be identified by testing a set of candidate GMPEs using a ground-motion dataset (see Chapter 2) compiled from the earthquake recordings of the EMME region. The compilation of EMME strong-motion databank has come to its final stage by collecting the accelerograms from Armenia, Georgia, Iran, Jordan, Pakistan and Turkey. More than 30 GMPEs are identified that can represent the general seismotectonic features of the region. Of these GMPEs, a set of 16 models are extracted by applying the pre-selection procedures (Cotton et al., 2006; Bommer et

al., 2010) and tested by the data-driven selection and testing methods (Nash and Sutcliffe, 1970; Scherbaum et al., 2004, 2009; Kale and Akkar, 2013) in the project period to select the most efficient group of GMPEs to be used in hazard estimations. The logic-tree based sensitivity analyses (explained in Chapter 5) proposes the final set of GMPEs and their corresponding weights that can be utilized in the logic-tree applications to address the epistemic uncertainty in ground-motion modeling.

This chapter, first, details the fundamental features of the mentioned selection and ranking methods. Then, for a pre-selected set of local and global GMPEs, the ranking results of these procedures are compared by using EMME ground-motion database that consists of 1869 recordings from 418 events recorded in EMME region. Within the following step of the study, the testing results are evaluated in conformity with the trellis charts of the predictive models to suggest a set of GMPEs that can be used in the logic-tree based sensitivity analysis. In the final part of this chapter, PSHA sensitivity analyses are conducted for a set of logic-tree framework established by the selected GMPEs and the final version of the logic-tree set-up is proposed to be confidently used in seismic hazard applications for EMME region.

6.2. Pre-Selection and Data-Driven Testing Methods of GMPEs

The testing procedures are capable of selecting and ranking the candidate GMPEs by assessing their intrinsic functionalities such as features of the database, regression type, functional form etc. or quantifying their performance from a ground-motion dataset compiled from the recorded accelerograms in the region of interest. The regional ground-motion dataset compiled for this purpose is given in Chapter 2 that consists of accelerograms recorded within the EMME region, which is considered to delineate the conspicuous seismic sources for the subject PSHA studies. The following paragraphs briefly describe each testing methodology except for EDR method (Kale and Akkar, 2013) as it is explained elaborately in Chapter 4.

6.2.1. Cotton et al. (2006) Pre-selection Method

Pre-selection of the local and global GMPEs is done by following the criteria described in Cotton et al. (2006) study. This method suggests that the GMPEs should be eliminated if 1) the model is from irrelevant tectonic regime, 2) the predictive model is not PEER-reviewed, 3) the documentation and dataset is insufficient, 4) the model has been superseded, 5) the period range is not appropriate, 6) the functional form is inappropriate, 7) the regression method or coefficients are inappropriate.

Although a more stringent set of GMPEs selection criteria is recently proposed in Bommer et al. (2010), they are not implemented at this stage since their application may significantly reduce the number of candidate GMPEs for testing.

6.2.2. LH (Likelihood) Method

LH method, which is proposed by Scherbaum et al. (2004), calculates the normalized residuals for a set of observed and estimated ground-motion data by considering that GMPEs are normally distributed in natural logarithm unit. The exceedance probabilities corresponding to calculated residuals are determined as LH values (Figure 5.1.a). By following Scherbaum et al. (2004), this likelihood parameter can be expressed by Equation 5.1:

$$LH(|z_0|) = Erf\left(\frac{|z_0|}{\sqrt{2}}, \infty\right) = \frac{2}{\sqrt{2\pi}} \int_{|z_0|}^{\infty} exp\left(\frac{-z^2}{2}\right) dz \qquad (6.1)$$

where z_0 represents the normalized residuals and Erf(z) is the error function while integrating the standard normal distribution. To describe the suitability of candidate GMPEs, the median LH values are reported as the resultant LH index that takes values between 0 and 1. For an optimum case, LH values are evenly distributed between 0 and 1, and the median of LH is about 0.5.
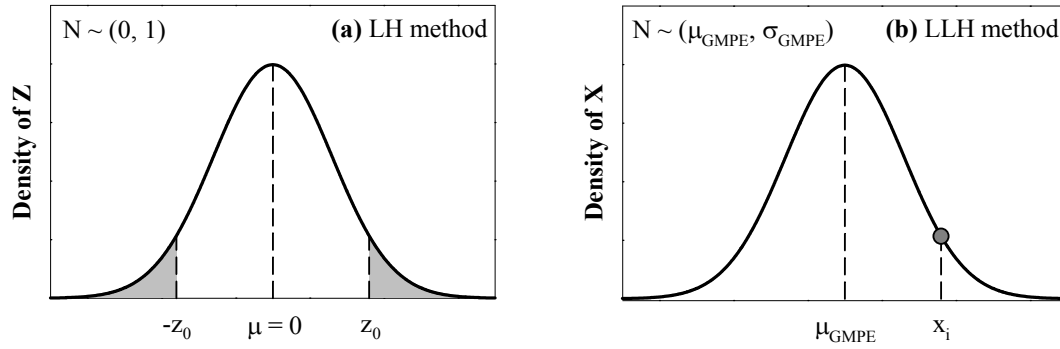
Figure 6.1 Illustrations of the probability calculations of (a) LH and (b) LLH methods. The summation of the shaded areas under the probability density function of Z is reported as LH index. Computation of LLH index is based on the occurrence probability of x_i by using median and sigma values of GMPE (μ_{GMPE} and σ_{GMPE}, respectively).

6.2.3. LLH (Log-Likelihood) Method

LLH method, which is an information-theoretic model selection method developed by Scherbaum et al. (2009) is based on log-likelihood approach to measure the distance between two continuous probability density functions f(x) and g(x). The function f(x) represents the distribution of an observed data point in the ground-motion dataset. The distribution of the estimated data point is described by g(x) and it is assumed as log-normal with the median and standard deviation of the considered GMPE. The distribution of f(x) is not known *a priori* and it is assumed to be log-normal with the same features of g(x). To obtain a model selection index, this approach calculates the average log-likelihood of the considered predictive model (Equation 5.2) using the observed dataset. An illustration of the probability consideration of LLH method is represented in Figure 5.1.b.

$$LLH(g,x) = -\frac{1}{N}\Sigma_{i=1}^{N}log_2(g(x_i)) \qquad (6.2)$$

170

In Equation 5.2, x_i represents the observed data for $i = 1,\ldots, N$. The parameter N is the total number of data. A small value of LLH ranking index indicates a better relationship between the observed and estimated ground-motion data.

6.2.4. NSE (Nash and Sutcliffe Efficiency Coefficient) Method

The model efficiency coefficient, NSE, (Nash and Sutcliffe, 1970) is a major improvement over the goodness-of-fit statistics because it directly quantifies the amount of bias in a model. However, it does not quantify how well the aleatory variability (sigma) of the observations is predicted by the models. The coefficient of efficiency is calculated from Equation (5.3) in logarithmic space.

$$NSE = 1 - \frac{\sum_{i=1}^{N}(ln\,Y_i - ln\,\hat{Y}_i)^2}{\sum_{i=1}^{N}(ln\,Y_i - \overline{ln\,Y})^2} \tag{6.3}$$

where N is the total number of ground-motion data, Y_i values are the observed data, $\hat{Y}_i$ values are the estimated median values of predictive models and $\overline{ln\,Y}$ is the mean value of the logarithms of the observed data. The NSE coefficient may take values between $-\infty$ and 1. The higher values of NSE coefficient indicate better agreement between observed and estimated data (Kaklamanos and Baise, 2011).

6.3. Selection and Testing of Candidate GMPEs for EMME Region

The EMME database is a collection of shallow active crustal accelerograms from Turkey, Iran, Caucasus (Georgia and Armenia), Pakistan and Jordan. The sources of the strong-motion accelerograms in the database are national seismological agencies and projects as well as recently compiled global strong-motion databanks. The EMME database includes 1869 strong-motion accelerograms recorded from 418 events and 611 strong-motion stations. The moment magnitude (M_w) and source-to-site distance (R_{JB}) ranges of the recordings are $4.0 \leq M_w \leq 7.6$ and $R_{JB} \leq$

200km, respectively. The site classification of accelerograms is based on measured and inferred V_{S30} values. The database mainly consists of recordings from soft and stiff sites that correspond to a V_{S30} range of 180m/s < $V_{S30} \leq$ 800m/s. Half of the accelerograms in the database that are from strike-slip events dominate the database. The other half is almost equally distributed between normal (23%) and reverse (27%) events. The acausal band-pass filtering procedure is applied in data processing. The filter cut-offs are determined from the frequency content of raw data.

The candidate GMPEs for shallow active crustal regions (SACRs) are collected from conference proceedings and peer-reviewed journals. Afterwards they are subjected to a further elimination based on the criteria proposed in Cotton et al. (2006) that results in 16 candidate GMPEs which are used in the data-driven testing of predictive models for seismic hazard analysis. These pre-selected candidate ground-motion models that fairly represent the primary seismotectonic settings of the region are listed in Table 6.1 with their acronyms and general features. Note that, among the candidate GMPEs, the criteria of Cotton et al. (2006) are not entirely complied by the predictive models proposed by Zhao et al. (2006), Ambraseys et al. (2005), Akkar and Bommer (2010) and Kale and Akkar (2013). Zhao et al. (2006) is suffered from incomplete documentation of their model-developing dataset. Akkar et al. (2014) predictive model supersedes the ground-motion relations developed by Ambraseys et al. (2005) and Akkar and Bommer (2010). These three GMPEs are not disregarded because they are evaluated in other regional hazard studies (e.g., Delavaud et al., 2012; Stewart et al., 2014). In addition, although Kale and Akkar (2013)[9] model is not PEER-reviewed, this predictive model is developed within the context of EMME WP-3 studies and tested in this part to evaluate its performance on EMME strong-motion database. The data-driven test results of these predictive models are given in the appendix of this chapter.

---

[9] The predictive model proposed by Kale and Akkar (2013) was published in a Turkish national conference and mostly different from the GMPE given in Chapter 3.

Table 6.1 General features of the candidate GMPEs.

GMPE	GMPE Acronym	Main Region(s)	Number of records and events	Number of estimators	M_w interval	R type and R_{max} (km) [*]	Component [†]	Period interval	Style-of-faulting [‡]	Site effect
Akkar and Çağnan (2010)	AC10	Turkey	433, 137	4	5.0 - 7.6	R_{JB}, 200	PGA, PGV, PSA in GM	0 - 2s	S, N, R	V_{S30}
Özbey et al. (2004)	Oetal04	Northwestern Turkey	195, 17	3	5.0 - 7.4	R_{JB}, 300	PGA, PSA in GM	0 - 4s	U	Dummy variable
Kalkan and Gülkan (2004)	KG04	Turkey	112, 57	3	4.0 - 7.4	R_{JB}, 250	PGA, PSA in L	0 - 2s	U	V_{S30}
Akkar and Bommer (2010) and Bommer et al. (2012)	AB10	Europe and the Middle East	532, 131	4	5.0 - 7.6	R_{JB}, 100	PGA, PGV, PSA in GM	0 - 2s	S, N, R	Dummy variable
Ambraseys et al. (2005)	Aetal05	Europe and the Middle East	595, 135	4	5.0 - 7.6	R_{JB}, 99	PGA, PSA in L	0 - 2.5s	S, N, T, O	Dummy variable
Zhao et al. (2006)	Zetal06	Japan	4726, 269	5	5.0 - 8.3	R_{RUP}, 300	PGA, PSA in GM	0 - 5s	S, N, R	Dummy variable
Fukushima et al. (2003)	Fetal03	West Eurasia	740, 50	3	5.5 - 7.4	R_{RUP} and R_{HYP}, 235	PGA, PSA in B	0 - 2s	U	Dummy variable
Bindi et al. (2010)	Betal10	Italy	561, 107	3	4.0 - 6.9	R_{JB} and R_{EPI}, 100	PGA, PGV, PSA in L PGA, PGV, PSA in V	0 - 2s	U	Dummy variable
Ghasemi et al. (2009)	Getal09	Iran	716, 200	3	5.0 - 7.4	R_{RUP} and R_{HYP}, 100	PSA in GMRotI50	0.05 - 3s	U	Dummy variable
Cauzzi and Faccioli (2008) and Faccioli et al. (2010)	CF08	Japan	1164, 60	4	5.0 - 7.2	R_{RUP}, 150	PGA, PSA in GM	0 - 20s	S, N, R	Dummy variable

Table 6.1 Cont'd.

GMPE	GMPE Acronym	Main Region(s)	Number of records and events	Number of estimators	M_w interval	R type and R_{max} (km) [*]	Component [†]	Period interval	Style-of-faulting [‡]	Site effect
Abrahamson and Silva (2008)	AS08	Western US and Taiwan	2754, 135	13	5.0 - 8.5	R_{RUP}, 200	PGA, PGV, PSA in GMRotI50	0 - 10s	S, N, R	V_{S30}
Boore and Atkinson (2008)	BA08	Western US and Taiwan	1574, 58	5	5.0 - 8.0	R_{JB}, 200	PGA, PGV, PSA in GMRotI50	0 - 10s	S, N, R	V_{S30}
Campbell and Bozorgnia (2008)	CB08	Western US and Taiwan	1561, 64	9	4.0 - 8.5	R_{RUP}, 200	PGA, PGV, PSA in GMRotI50	0 - 10s	S, N, R	V_{S30}
Chiou and Youngs (2008)	CY08	Western US and Taiwan	1950, 125	12	4.0 - 8.5	R_{RUP}, 200	PGA, PGV, PSA in GMRotI50	0 - 10s	S, N, R	V_{S30}
Akkar et al. (2014)	ASB14	Europe and the Middle East	1041, 221	4	4.0 - 7.6	R_{JB}, 200	PGA, PGV, PSA in GM	0 - 4s	S, N, R	V_{S30}
Kale and Akkar (2013)	KA13	Turkey	692, 178	4	4.0 - 7.6	R_{JB}, 200	PGA, PGV, PSA in GM	0 - 4s	S, N, R	V_{S30}

[*] R: distance, R_{max}: maximum distance, R_{EPI}: epicentral distance, R_{HYP}: hypocentral distance, R_{JB}: Joyner-Boore distance, R_{RUP}: closest distance
[†] GM: geometric mean of horizontal components, L: larger horizontal component, GMRotI50: rotation-independent average horizontal component (Boore et al., 2006),
 B: both horizontal components, V: vertical component
[‡] S: strike-slip faulting, N: normal faulting, R: reverse faulting, O: oblique faulting, U: unidentified

In this part of the study, the selected 16 local and global candidate GMPEs are tested under the ground-motion dataset for the spectral period band of interest ($0.0s \leq T \leq 4.0s$). After this point, the candidate GMPEs is cited with their acronyms which are given in the second column of Table 6.1. While the data-driven testing methods are applied, the implementation of the GMPEs such as considering magnitude and distance limitations, horizontal component definitions etc. are done by following the same process given in the Chapter 4. Different approaches are implemented during the testing of GMPEs. These approaches are categorized as consideration of entire EMME database, country- or region-based datasets (Turkey, Iran, and Caucasus), and fault mechanism-based datasets (normal, reverse, and strike-slip). The average testing results of all GMPEs for each of the testing approaches with respect to EDR components ($\sqrt{\frac{1}{N}\Sigma_{i=1}^{N}MDE_i^2}$ which is shown as MDE in the rest of the document and $\sqrt{\kappa}$), actual EDR index, NSE coefficient, LH and LLH indexes and are tabulated in Appendix C (Tables C.1 to C.7). The average results given in these tables represent the overall performances of the GMPEs for a spectral period band that comprises of T=0.0s (PGA), 0.1s, 0.2s, 0.5s, 0.75s, 1.0s, 1.5s and 2.0s. The upper limit of the period is selected as 2.0s for obtaining average values as all predictive models in the list yield spectral values until this period level. After 2.0s some of the GMPEs do not estimate the spectral ordinates. The performances of the predictive models after 2.0s are visually inspected from the figures given in the Appendix C. The general performances of the predictive models at each selected period and T=3.0s and 4.0s for each of the approaches are shown in the figures (Figures C.1 to C.7) given in Appendix C.

The tables and figures given in Appendix C depict that given the different combinations of the databases Zetal06, AB10 and KA13 models perform well with respect to regarded testing results, whereas the performance of Aetal05 is lower than the performances of the other GMPEs. ASB14 model which supersedes Aetal05 and AB10 is mostly positioned at the top of the ranking lists. Therefore, in the final evaluation of the predictive models, both Aetal05 and AB10 GMPEs were

extracted from the list of the candidate predictive models. KA13 and Oetal04 models were also not included in the final list because KA13 model was not as comprehensive as being practiced in a regional hazard analysis, and Oetal04 model was derived from a limited data (only Northwestern Turkey) and showed weak performance on the considered database. To this end, the model performances of the 12 candidate GMPEs are evaluated for the period band of interest. Figure 6.2 presents the period-based scatters of the testing indexes for entire EMME database. In fact, this figure contains same information with the Figure C.1 given in the appendix but the performances of the extracted models (Oetal04, Aetal05, AB10 and KA13) are not included in this version. Table 6.2 displays the top ranked models (first five GMPEs) with respect to the average test results of GMPEs in terms of EDR components and actual EDR index, NSE coefficient, LH and LLH ranking indexes. In this list, the five predictive models that perform better with respect to the overall rankings are shown in bold fonts. Tables 6.3 to 6.8 presents the same information with Table 6.2 for different database approaches (i.e., country- or region-based and style-of-faulting-based sub-datasets) implemented during the testing of GMPEs.

The summaries of data-driven test results given in Tables 6.2 to 6.8 show that EDR, NSE, LH and LLH methods generally yield similar rankings. One particular advantage of EDR method is that it not only provides an idea on the overall performance of the tested predictive models but also informs the analyst about the individual contributions of model sigma (i.e., the level of aleatory variability) and bias in median estimations to overall performance of GMPEs. For example, when testing results of entire database is of concern, BA08 performs better in terms of aleatory variability (MDE component in EDR). However, AC10 supersedes BA08 when the overall EDR index is considered. Accordingly, EDR offers different levels of information to the analyst for considering the aleatory uncertainty, degree of bias between observed and median estimations and combination of these two components.
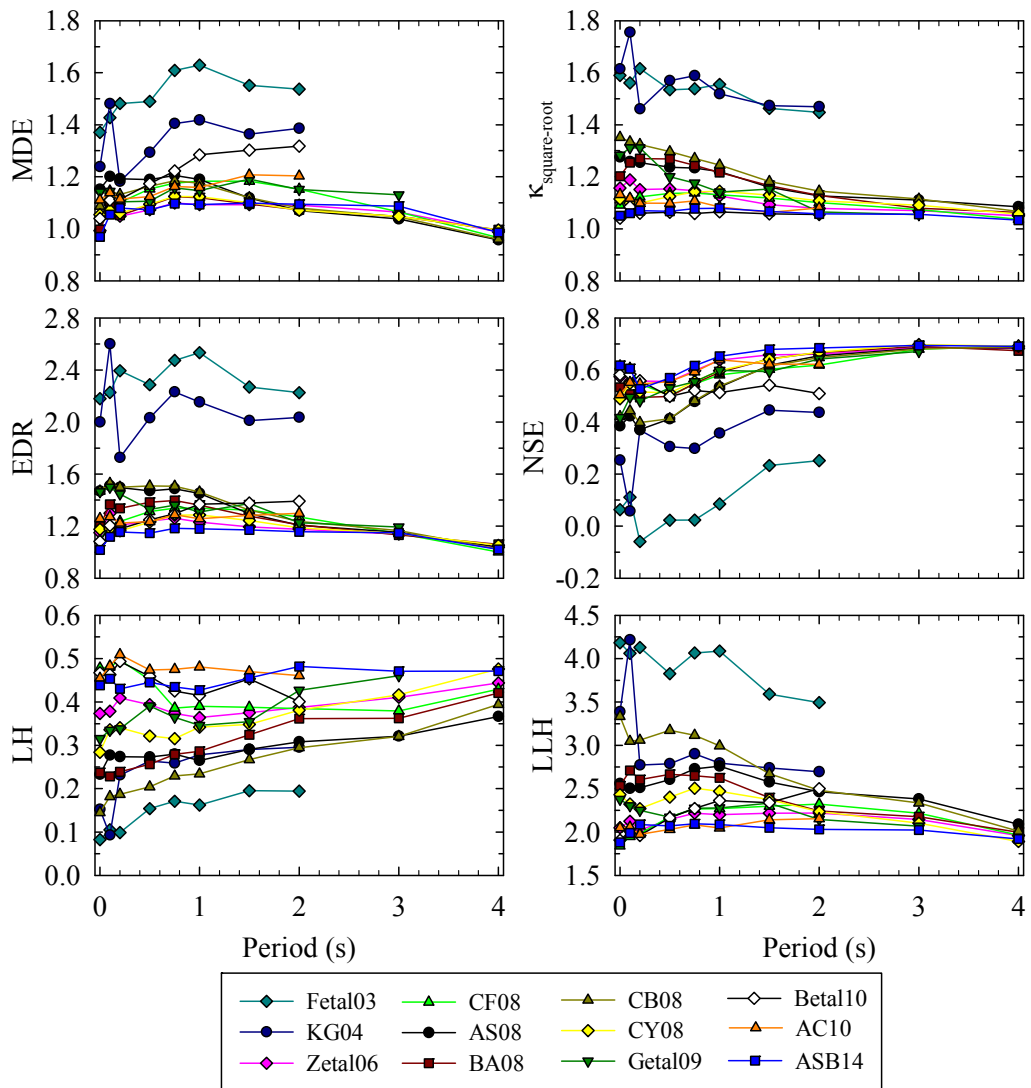
Figure 6.2 Performances of candidate GMPEs at the selected period levels when the entire EMME database is used for testing of GMPEs. Top row shows the components of EDR index ($\sqrt{\frac{1}{N}\Sigma_{i=1}^{N}MDE_i^2}$ and $\sqrt{\kappa}$), middle row shows the actual EDR and NSE, and bottom row shows the LH and LLH indexes.

Table 6.2 Rankings of the top 5 GMPEs for the entire EMME database. The first 5 predictive models that perform better in this case are shown in bold.

GMPE	MDE	κ	EDR	NSE	LH	LLH
Fetal03						
KG04						
Zetal06	2		3	2	5	4
CF08	5	4	4	4	4	3
AS08						
BA08	3					
CB08						
CY08	4	5	2	5		
Getal09						
Betal10		1			2	5
AC10		3	5	3	1	2
ASB14	1	2	1	1	3	1

Table 6.3 Rankings of the top 5 GMPEs for the Turkish sub-database. The first 5 predictive models that perform better in this case are shown in bold.

GMPE	MDE	κ	EDR	NSE	LH	LLH
Fetal03						
KG04						
Zetal06	3		5	4	5	4
CF08	2	4	2	3	3	3
AS08						
BA08						
CB08						
CY08	5	5	4	5		
Getal09						
Betal10		2			4	5
AC10	4	3	3	2	1	2
ASB14	1	1	1	1	2	1

Table 6.4 Rankings of the top 5 GMPEs for the Iranian sub-database. The first 5 predictive models that perform better in this case are shown in bold.

GMPE	MDE	κ	EDR	NSE	LH	LLH
Fetal03						
KG04				5	4	2
Zetal06	5				3	4
CF08						
AS08	3	4	3	4	5	3
BA08	2	5	1	3		5
CB08	1		2	1		
CY08		3	5			
Getal09	4		4	2	1	1
Betal10		1			2	
AC10						
ASB14		2				

Table 6.5 Rankings of the top 5 GMPEs for the Caucasian sub-database. The first 5 predictive models that perform better in this case are shown in bold.

GMPE	MDE	κ	EDR	NSE	LH	LLH
Fetal03						
KG04						
Zetal06	5			5	5	
CF08	1	4	2	2	2	2
AS08						
BA08						
CB08						
CY08		5	5			
Getal09						5
Betal10	4	2	3	3	3	3
AC10	2	1	1	1	1	1
ASB14	3	3	4	4	4	4

Table 6.6 Rankings of the top 5 GMPEs for the normal faulting sub-database. The first 5 predictive models that perform better in this case are shown in bold.

GMPE	MDE	κ	EDR	NSE	LH	LLH
Fetal03						
KG04						
Zetal06	3			4	5	5
CF08	2	5	3	2	3	3
AS08						
BA08	4					
CB08						
CY08		4	5			
Getal09						
Betal10		1	4	5	4	4
AC10	5	3	2	3	2	2
ASB14	1	2	1	1	1	1

Table 6.7 Rankings of the top 5 GMPEs for the reverse faulting sub-database. The first 5 predictive models that perform better in this case are shown in bold.

GMPE	MDE	κ	EDR	NSE	LH	LLH
Fetal03						
KG04						
Zetal06	3	2	5	3		4
CF08			4		5	
AS08						
BA08	1	3		2		
CB08	4					
CY08	5			4		
Getal09	2	4		1	3	1
Betal10		5	1	5	2	2
AC10			3		1	3
ASB14		1	2		4	5

Table 6.8 Rankings of the top 5 GMPEs for the strike-slip faulting sub-database.
The first 5 predictive models that perform better in this case are shown in bold.

GMPE	MDE	κ	EDR	NSE	LH	LLH
Fetal03						
KG04						
Zetal06	3		3	2	5	3
CF08	5	3	4	4	4	4
AS08						
BA08	4					
CB08						
CY08	1	5	2	3		5
Getal09						
Betal10		2			2	
AC10		4	5	5	1	2
ASB14	2	1	1	1	3	1

When the entire EMME database (Table 6.2) or Turkish sub-dataset (Table 6.3) are considered, Zetal06, CF08, CY08, AC10, and ASB14 perform better according to EDR and NSE procedures. LH and LLH methods reports Betal10 model instead of CY08 among the five best performing GMPEs while rest of the models are same with the rankings of EDR and NSE procedures. As another example, the results obtained for the reverse-faulting dataset indicate that the test methods yield different rankings. Therefore, to objectively combine the ranking results and decide on the most populated GMPEs for all ground-motion datasets, the five predictive models which are mostly preferred by each test method are identified for each dataset case. These GMPEs are indicated in bold fonts in the associated tables. At the end, when all ranking results are considered among these seven cases, the better performing GMPEs are chosen as Zetal06, CF08, BA08, CY08, AC10 and ASB14. Although the model performance of Betal10 is promoted in some cases, this model is not incorporated into the better performing models as it does not consider style-of-faulting effects on its ground-motion estimates and its upper magnitude limit (M_w 6.9) is biased for application to the EMME region in which there are numerous seismic sources with a maximum magnitude of about 8.0.

The above six GMPEs can be reduced further, if ground-motion variability is accepted to be addressed by 3 or 4 predictive models in GMPE logic-tree

applications. The strong-motion database is divided into different M_w and R_{JB} bins. The bins range from small to large magnitude earthquakes with various R_{JB} intervals spanning near- to far-distance accelerograms. Figure 6.3 shows the generated bins as well as the number of accelerograms in each bin. The M_w-R_{JB} bins are called with the numbers given in the horizontal axis of this figure. The individual performances of the six GMPEs are re-evaluated using these M_w-R_{JB} bins. The bin-dependent performances of the GMPEs are also important as the PSHA disaggregation results would identify different magnitude and distance values depending on the level of activity and proximity of seismic sources.
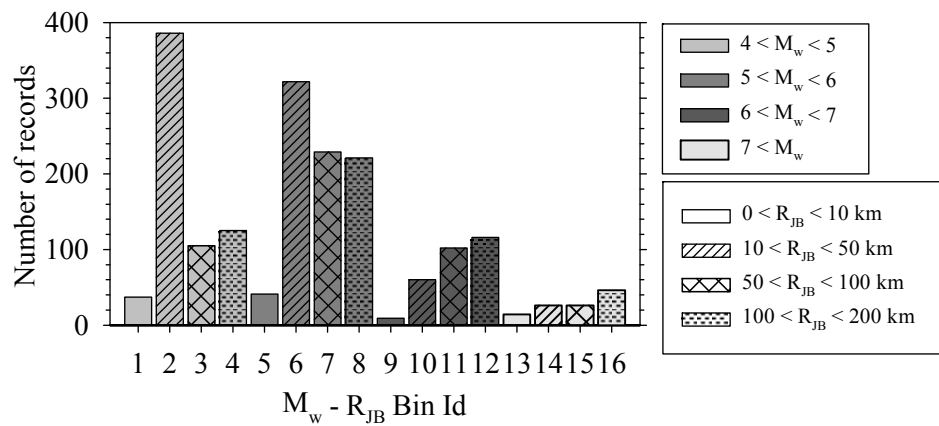
Figure 6.3 Data histograms of the generated M_w-R_{JB} bins. Intervals of M_w and R_{JB} are given next to each legend. Different magnitude intervals are represented by different colors while different patterns identify the distance intervals. For example, the 7th bin (i.e., M_w-R_{JB} bin Id=7) represents the data for $6 < M_w < 7$ and $50 < R_{JB} < 100$ km.

The GMPEs that show fairly stable ranking results for bin-based data as considered here can be used in the GMPEs logic-tree applications for the considered region. Figures 6.4 and 6.5 show the testing results of six GMPEs for the selected levels to assess their bin-based performances. Figure 6.4 represent the performances of the GMPEs in terms of MDE component of EDR approach. The similar comparisons for LLH method is shown in Figure 6.5. An immediate observation depicted from

MDE and LLH figures that almost all GMPEs show jagged behaviors in moderate and large magnitude - near distance bins (i.e., No.9 and No.13). The qualification of the GMPEs with respect to their performances in these bins is not a fair judgment since the scarce number of accelerograms that prevent reliably evaluating the models. Among the considered GMPEs, the LLH ranking indexes of BA08 do not display stable behavior especially for the small-magnitude bins. AC10 model shows slightly poor performance for bins of small magnitude and far-distance recordings (i.e., No.4). Another interesting observation from the presented results is the unstable performance of CF08 for close- and far-distances and moderate-magnitude recordings (i.e., No.5, No.8 and No.12). However, these models display fairly good performance for the rest of the bins. ASB14, CY08 and Zetal06 predictive models perform relatively better for all the bins. Under the light of these observations, GMPE logic-tree based sensitivity analysis to construct the final logic-tree application in EMME region can consider all GMPEs (i.e., Zetal06, BA08, CF08, CY08, AC10, and ASB14) for consistent hazard results. In the further step, these GMPEs are investigated using trellis charts to study their earthquake scenario based behaviors.
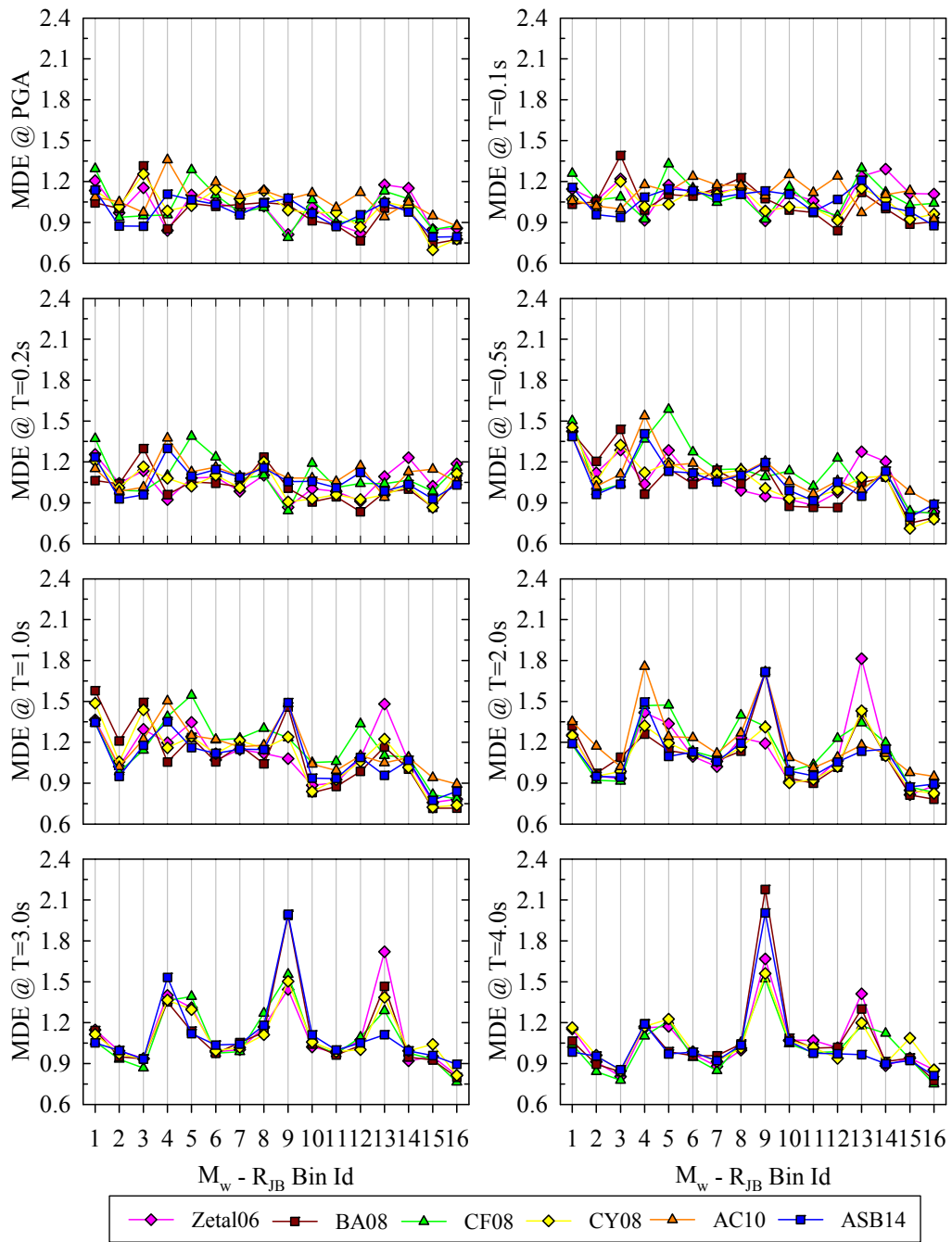
Figure 6.4 M_w-R_{JB} bin performances of the GMPEs at selected periods in terms of MDE index.
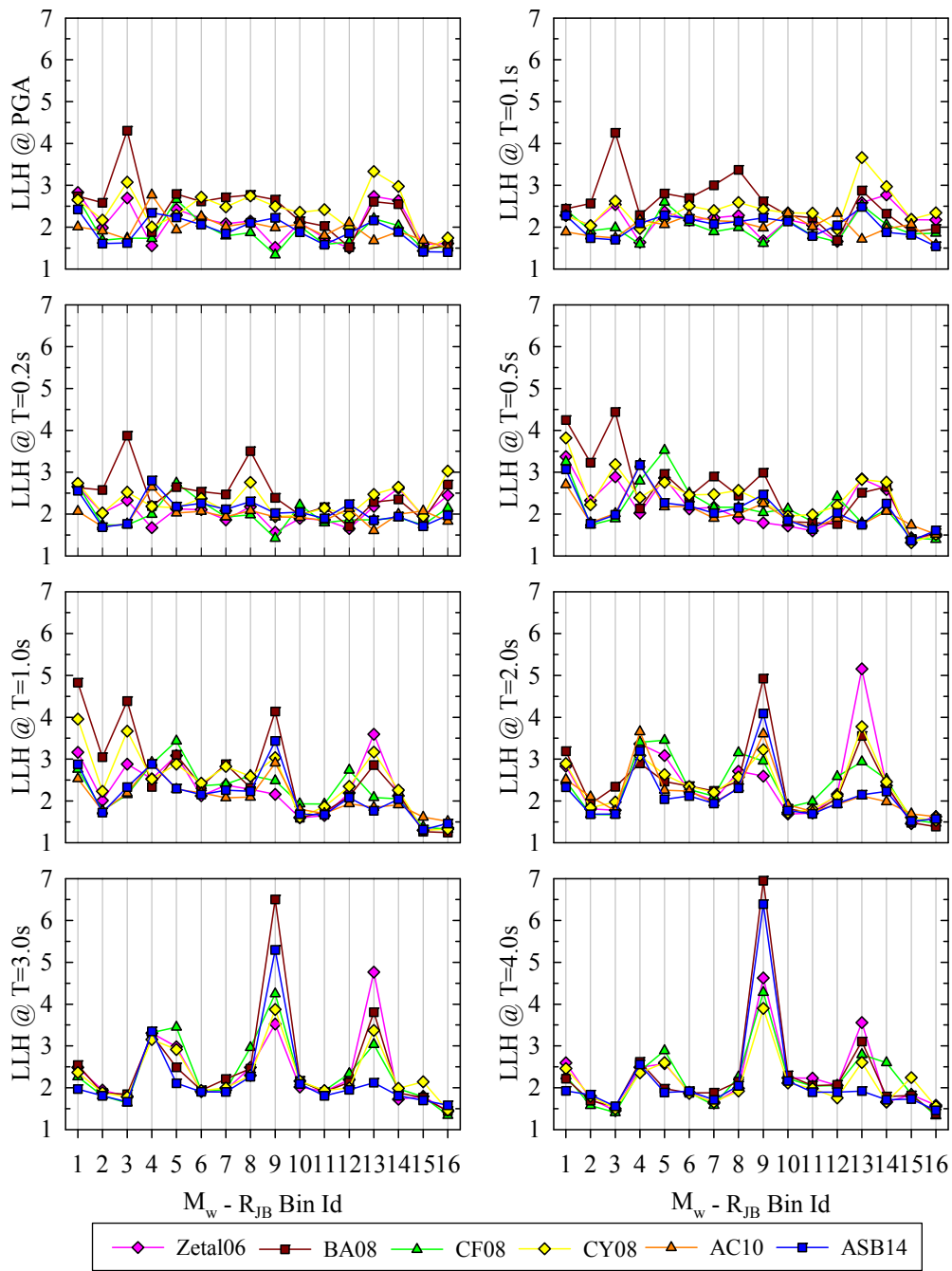
Figure 6.5 M_w-R_{JB} bin performances of the GMPEs at selected periods in terms of LLH index.

6.4. Trellis Charts of the Selected GMPEs

In addition to prior observations on testing of predictive models, the selected six GMPEs that represents relatively better performances among the candidate predictive models should examined with respect to trellis charts for different earthquake scenarios. Trellis charts are prepared to capture the general behaviors of the ground-motion estimates in multi-dimensional space (magnitude, distance, spectral period). Accordingly, they provide a captivating insight into the candidate predictive models while evaluating them. These charts help to hazard analyst for identifying the different trends (i.e., lower, median and upper bound behaviors) of candidate predictive models.

Within the context of this study, such kind of appraisals is important to obtain a proper set of GMPE logic-tree alternatives for conducting logic-tree based sensitivity approach. In this context, the spectral ordinate estimates of these particular GMPEs are plotted for different earthquake scenarios in Figures 6.6 and 6.7 for strike-slip, and Figures C.8 to C.11 for normal and reverse fault mechanisms. Each figure contains twenty panels and each panel shows the spectral ordinate estimates of the selected six GMPEs for a particular M_w-R_{JB} pairs. The selected moment magnitude values are M_w 5, M_w 6, M_w 7 and M_w 8 whereas the distance measures are R_{JB} 2.5km, R_{JB} 10km, R_{JB} 25km, R_{JB} 100km and R_{JB} 200km. The site condition is represented with a V_{S30} value of 760m/s (i.e., generic rock) in the earthquake scenarios. Among the considered predictive relations, the distance metric used by Zetal06, CF08 and CY08 are R_{RUP} whereas the other three GMPEs are based on the R_{JB} distance measure. To compute the ground-motion estimates of Zetal06, CF08 and CY08, the R_{RUP} distances corresponding to the R_{JB} values are calculated by the help of fault rupture parameters (i.e., depth-to-top of rupture, dip angle, hypocentral depth and rupture dimensions). First three of these parameters are estimated from the relationships proposed in Kaklamanos et al. (2010; 2011) whereas Wells and Coppersmith (1994) is used to estimate the rupture dimensions. The spectral amplitude estimations are for median (50 percentile) and

median+2sigma (96 percentile) in Figures 6.6, C.8, C.10 and Figures 6.7, C.9, C.11, respectively.

In general, for median ground-motion estimates, CY08, BA08, Zetal06 and CF08 constitute the upper bounds in various M_w-R_{JB} based earthquake scenarios. AC10 predictive model seems to draw lower bound spectral estimates whereas median trend is represented by ASB14. When 96 percentile (median+2sigma) trellis charts are of concern, the aleatory variability component of the ground-motion models is more prominent. In these cases, CF08 and Zetal06 seem to be the upper bound predictive models for most of the earthquake scenarios. Although BA08 model can be included in the upper bound predictive model list for small-to-moderate magnitude and far distance cases (M_w 5-6, R_{JB} 100km-200km), the general trend of this model is considered to draw lower bound together with AC10 predictive model. The GMPEs of CY08 and ASB14 are regarded to represent median behavior of the spectral estimates. The gradually increased spectral amplitudes of BA08 and CY08 models with respect to the other GMPEs can be explained with their lower standard deviations especially for the large magnitude earthquake scenarios.

The overall observations from the earthquake scenario plots suggest that the predictive model estimates of CF08 and Zetal06 are relatively larger than the other GMPEs. The ground-motion relations of CY08 and ASB14 seem to draw a median spectral amplitude band along the overall period range of interest, whereas lower bound can be assembled by AC10 and BA08 models. These classifications of the predictive models (i.e., upper, median and lower bound) guide the selection of models to capture the modeling (epistemic) uncertainty in ground-motion estimates fairly well. Thus, in the next step, these explorations are regarded to tailor the final set of GMPEs to be used in PSHA studies for the EMME region.
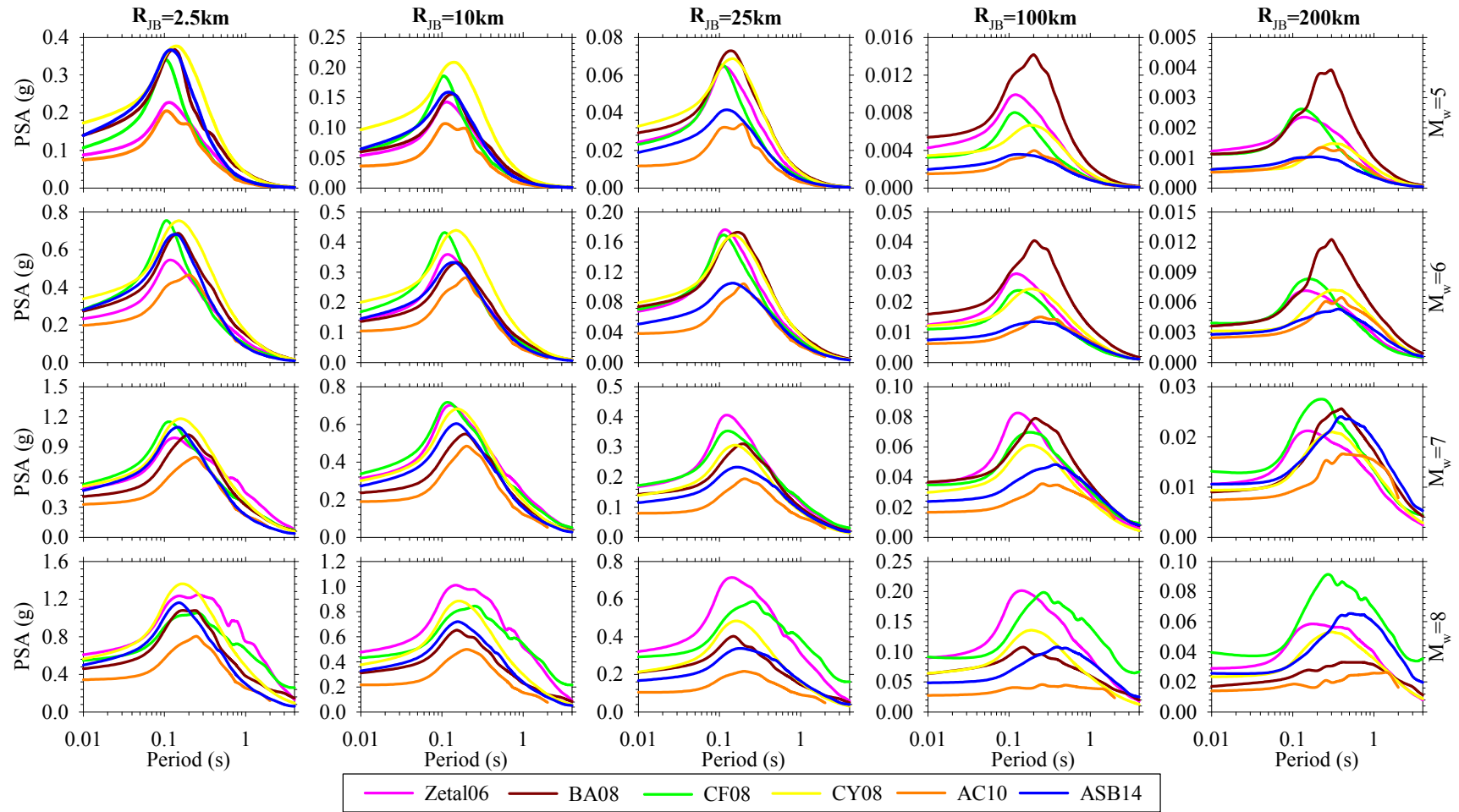
Figure 6.6 Trellis chart for PSA response spectra of the GMPEs (strike-slip events, median estimates and V_{S30}=760m/s).
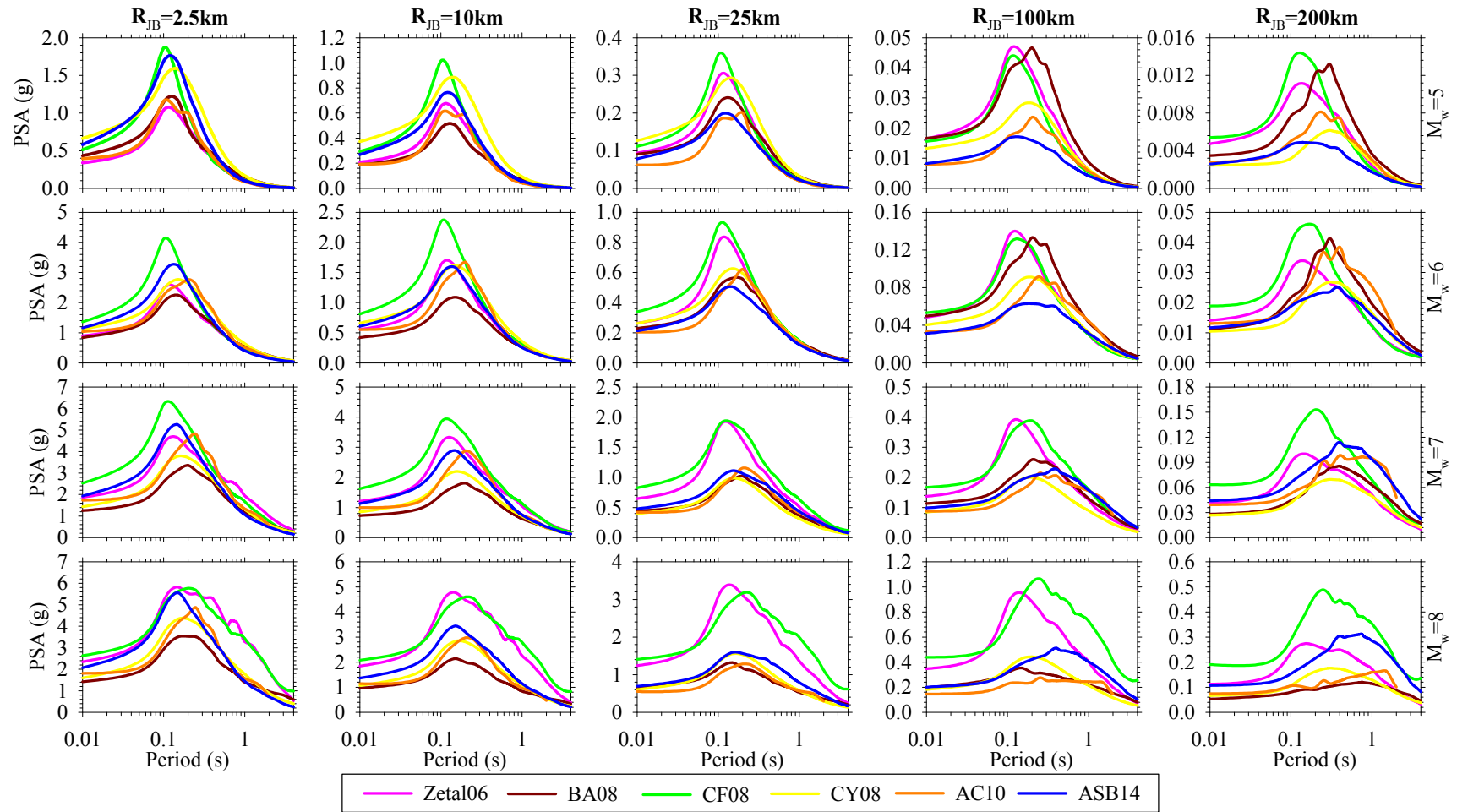
Figure 6.7 Trellis chart for PSA response spectra of the GMPEs (strike-slip events, median+2sigma estimates and V_{S30}=760m/s).

6.5. Logic-tree Based Sensitivity Analysis

The GMPEs and their branch weights that are used in the final EMME ground-motion model logic-tree application are decided according to the seismic hazard sensitivity tests. Figure 6.8 displays the background areal sources and selected regions from Turkey for conducting PSHA. The considered area source model shows some minor differences from the final version of the EMME source model as this issue was still alive while conducting the logic-tree based sensitivity analyses. The selected regions reflect low-to-moderate seismicity (Mersin region) and high seismicity (Aegean and North Anatolian Fault - NAF regions) levels. The OpenQuake platform (Pagani et al., 2014) was used as hazard engine in probabilistic seismic hazard calculations. While conducting the seismic hazard analyses, the areal seismic sources are treated as line sources instead of modeling them as point sources in the seismic hazard engine.
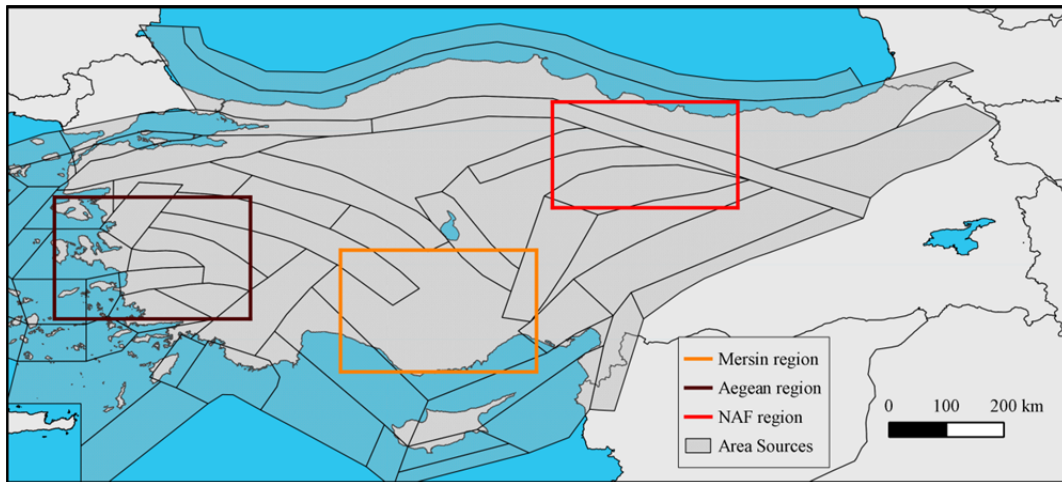
Figure 6.8 Illustration of the selected regions and background area sources considered in the PSHA.

The node structure of the sensitivity analyses is illustrated in Figure 6.9. The selected six GMPEs are used to establish four major GMPE groups. The first major group contains three best representative GMPEs (ASB14, CY08 and AC10) from all data-driven testing studies and trellis charts. The other major groups include

these GMPEs as well as an additional one from the other 3 predictive models (Zetal06, BA08 and CF08). Each major group is then divided into 3 different sub-groups by varying the logic-tree branch weights of the GMPEs in that group. In essence, 12 different GMPE logic-trees (from LT#1 to LT#12) are established for the sensitivity analyses and listed in Table 6.9. Among these logic-tree alternatives, Groups 1 and 3 are comprised from the GMPEs exhibiting median and lower bound behaviors, whereas Groups 2 and 4 combinations are capable of displaying overall trends (i.e., lower, median and upper bounds).
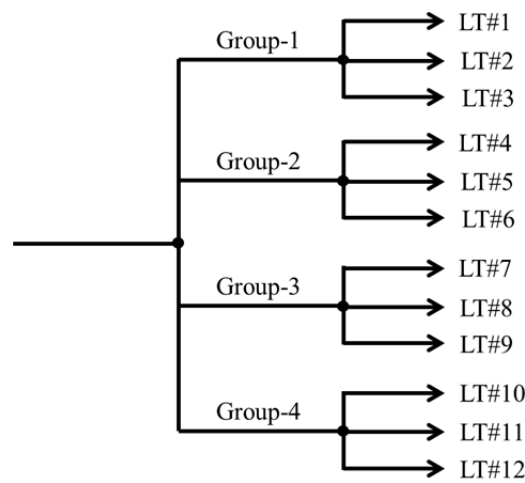
Figure 6.9 Node structure of the logic-tree based sensitivity analyses.

Table 6.9 Details of the logic trees established for the sensitivity analyses.

GMPE	Group-1			Group-2			Group-3			Group-4		
	LT1	LT2	LT3	LT4	LT5	LT6	LT7	LT8	LT9	LT10	LT11	LT12
Zetal06	-	-	-	0.10	0.20	0.10	-	-	-	-	-	-
BA08	-	-	-	-	-	-	0.10	0.20	0.10	-	-	-
CF08	-	-	-	-	-	-	-	-	-	0.10	0.20	0.10
CY08	0.40	0.35	0.45	0.35	0.30	0.40	0.35	0.30	0.40	0.35	0.30	0.40
AC10	0.20	0.30	0.10	0.20	0.20	0.10	0.20	0.20	0.10	0.20	0.20	0.10
ASB14	0.40	0.35	0.45	0.35	0.30	0.40	0.35	0.30	0.40	0.35	0.30	0.40

One might be criticized that ASB14, CY08 and AC10 predictive models are included in all alternative logic-tree applications. In this respect, there are quite reasonable explanations for these speculative selections. Firstly, these three

GMPEs are promoted by most of the data-driven testing methods for several test scenarios in this thesis. The observations getting from trellis charts are another justification for this selection. Finally, the model-developing datasets of these models are capable of reflecting the seismotectonic features of the region being studied. AC10 model developed using accelerograms from Turkey which covers large area in the entire EMME region. ASB14 pan-European predictive model uses a large amount of data from the region of interest. Among the candidate models, CY08 is the best representative of global ground-motion models for shallow active crustal regions. Thus, these three models are decided on considering in all logic trees with different weighting schemes.

Given a spectral period of interest, 12 hazard curves are computed from the above established logic trees for a set of previously determined sites in the selected regions. The total number of sites in Aegean, NAF and Mersin regions are 941, 881 and 953, respectively. The considered spectral periods are PGA, T=0.2s, 1.0s and 2.0s to compute seismic hazard in the regions. For each site and spectral period of interest, spectral accelerations (SAs) corresponding to a specific return period yield discrete spectral values as shown in Figure 6.10. Given a site, the spectral accelerations corresponding to the selected return period are normalized with their median (SA_{median}) to obtain 12 normalized SAs. Finally, the normalized SAs of all sites for a particular return period and spectral period are binned according to the logic trees given in Figure 6.9 and Table 6.9. The trends in the binned normalized SAs are evaluated for obtaining the most proper set of predictive models and corresponding branch weights for the regional hazard calculations in the EMME project.

Figure 6.11 represents the normalized SAs of each alternative logic tree given in Figure 6.9 and Table 6.9 for the pre-selected sites in the Aegean region. The illustrative plots in Figure 6.11 are for normalized spectral accelerations of T=0.2s and T=1.0s to reflect the short and intermediate period trends. In these sub-figures each row displays the pre-defined GMPE major groups whereas each column

presents the weighting schemes of these groups. The return period is selected as 2475yrs as any significant difference is not observed between 475yrs and 2475yrs plots. Figures 6.12 and 6.13 represent the same information with Figure 6.11 for NAF and Mersin regions, respectively. The rest of the figures for pre-selected periods (PGA, T=0.2s, 1.0s and 2.0s), return periods of 475yrs and 2475yrs and considered regions are illustrated in Appendix D (Figures D.1 to D.9). In these evaluation plots, if the normalized data scatters of a logic-tree branch fluctuate about median line (i.e., unity), the resulting hazard is close to the median hazard curve. In other words, the seismic hazard results are not controlled by any of the particular GMPEs within the considered logic-tree set-up. The numerical information for these figures are given in Tables 6.10 and 6.11 in terms of absolute differences ($D_{LT,i}$) of logic-tree based sensitivity analysis results (see Chapter 5 for details of $D_{LT,i}$ calculations) for return periods of 475yrs and 2475yrs.
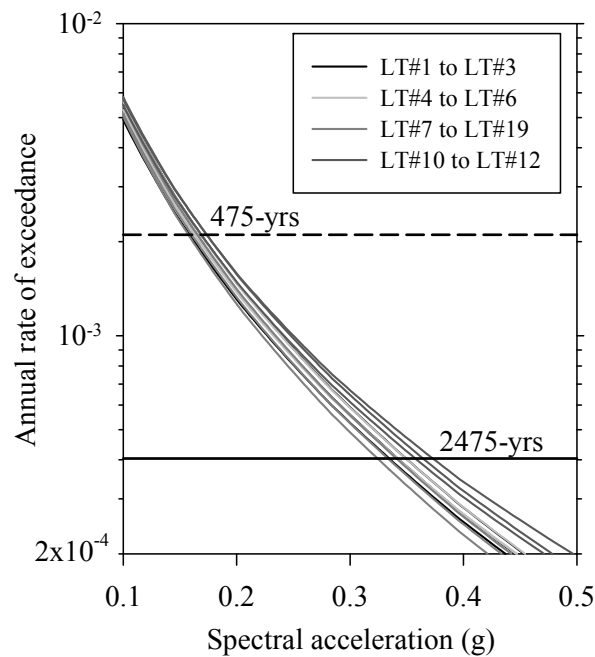
Figure 6.10 Site-specific hazard curves obtained from different logic-trees.

The examinations of individual normalized spectral acceleration scatters for each selected logic-tree framework alternatives given in Figures 6.11 to 6.13 and the D_{LT}

192

values of the logic-tree applications given in Tables 6.10 and 6.11 suggest that the considerations of BA08 and CF08 substantially alter the hazard results. While CF08 increase the hazard results, BA08 results in yielding lower hazard estimations for the sites of interest. Those effects are more prominent for LT#8 and LT#11 because, as shown in Table 6.9, the branch weights of these GMPEs in these cases are higher than the other cases (i.e., LT#7, LT#9, LT#10 and LT#12). To conclude, it can be mentioned that CF08 and BA08 predictive models dominate the hazard. The logic-tree applications belonging to Groups-1 and -2 seem to draw a reasonable scatter trend along the all sites being considered and they can be regarded as reliable candidates to represent the modeling (epistemic) uncertainty in ground-motion estimations fairly well. Among the best performing logic trees, the rankings indicated in Tables 6.10 and 6.11 depict that the logic-tree frameworks of LT#1 (Group-1), and LT#4 and LT#6 (Group-2) are the best alternatives for probabilistic seismic hazard applications in the EMME project.
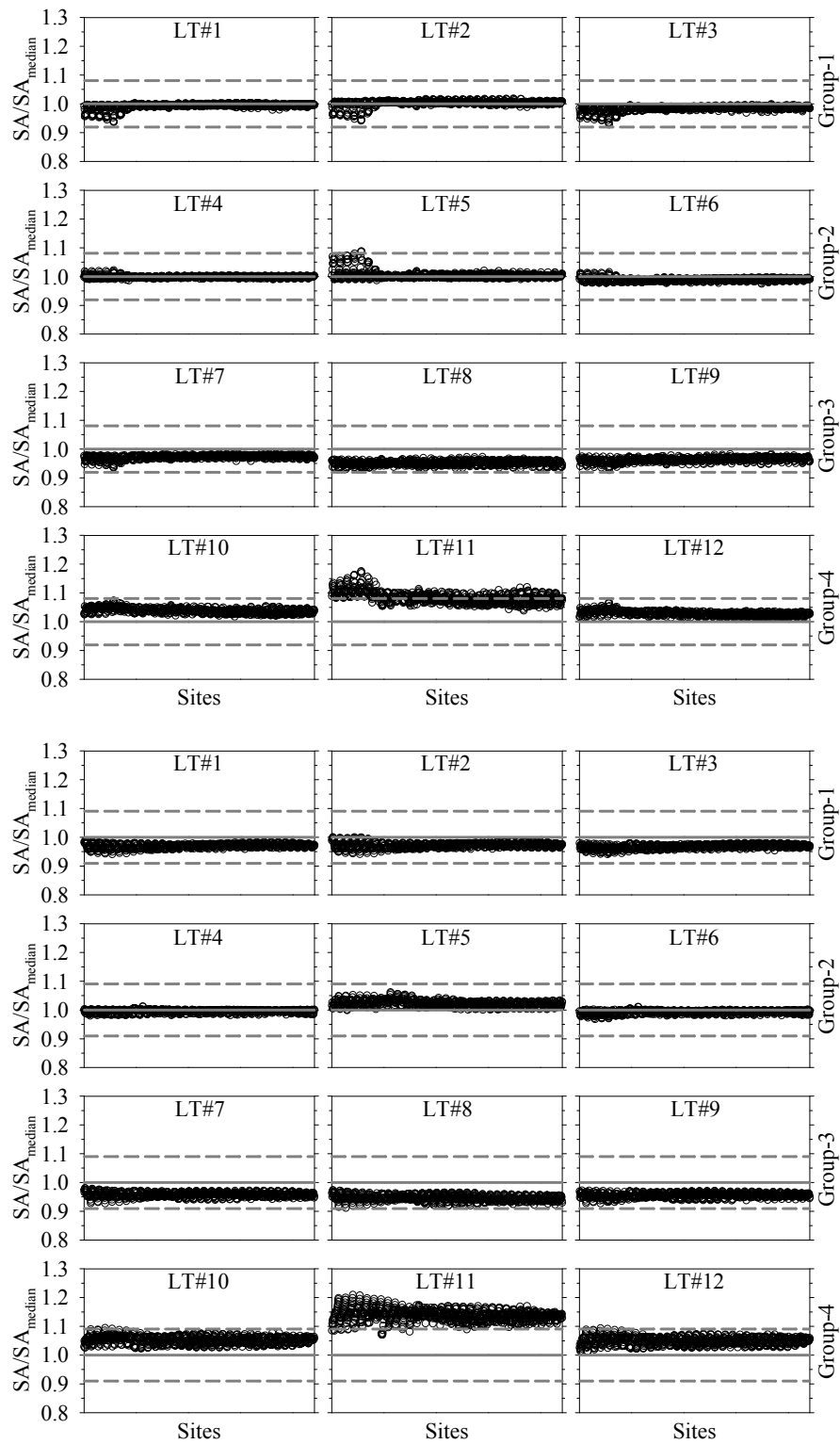
Figure 6.11 Results of logic-tree based sensitivity analysis of Aegean region for return period of 2475yrs and T=0.2s (top group), T=1.0s (bottom group). Solid line displays the median trend whereas dashed lines show median ± sigma bounds.
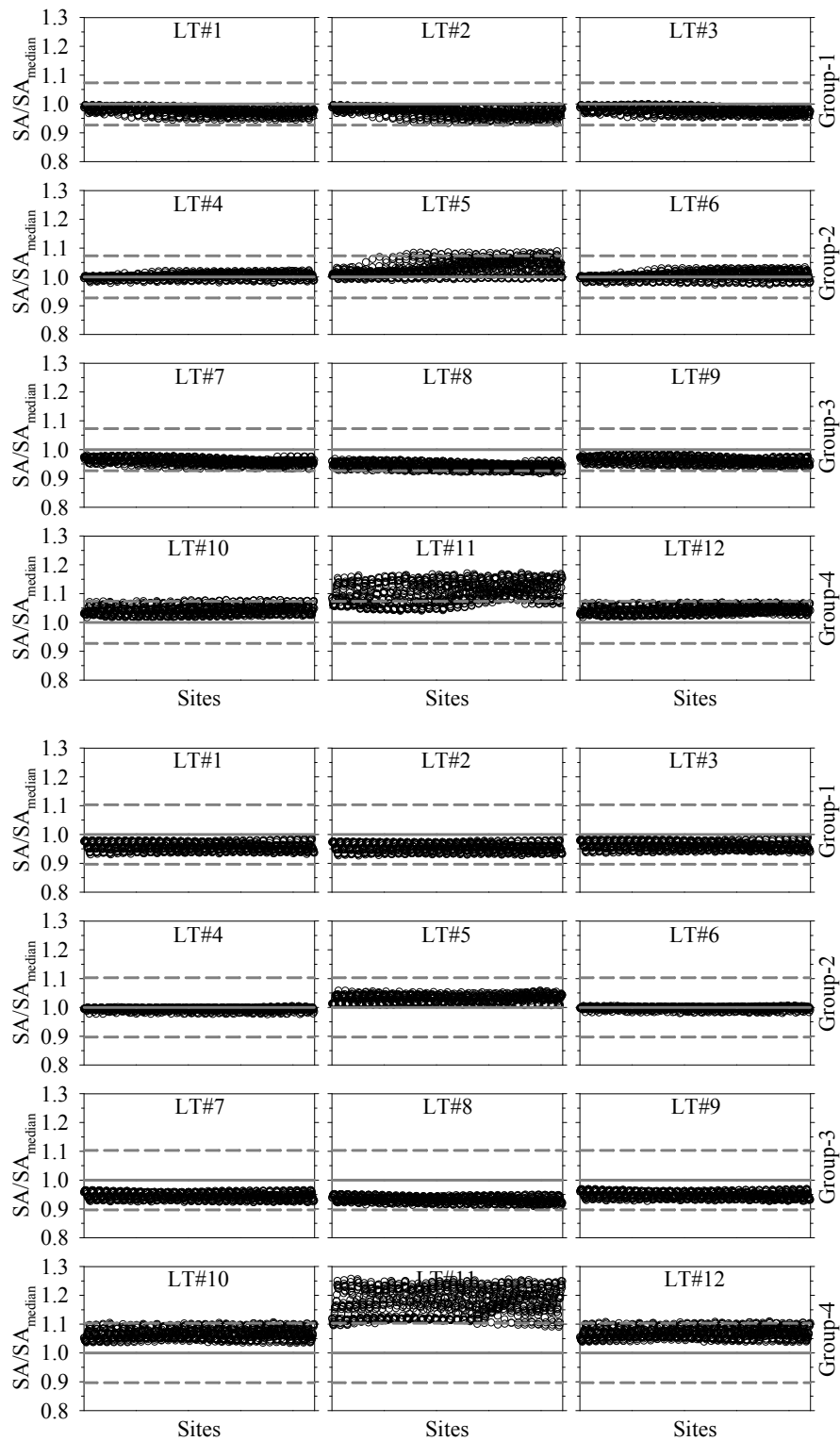
Figure 6.12 Results of logic-tree based sensitivity analysis of NAF region for return period of 2475yrs and T=0.2s (top group), T=1.0s (bottom group). Solid line displays the median trend whereas dashed lines show median ± sigma bounds.
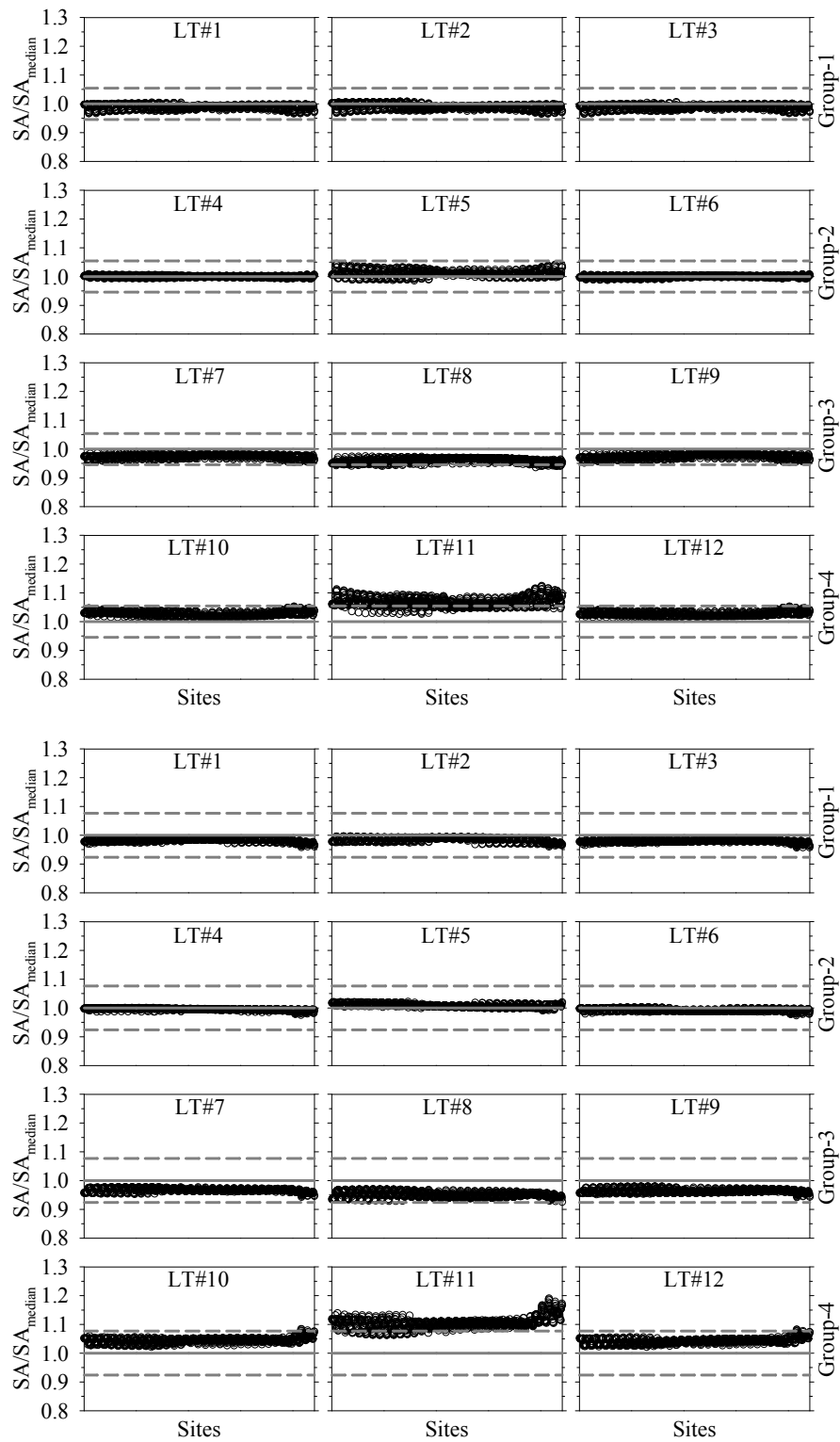
Figure 6.13 Results of logic-tree based sensitivity analysis of Mersin region for return period of 2475yrs and T=0.2s (top group), T=1.0s (bottom group). Solid line displays the median trend whereas dashed lines show median ± sigma bounds.

Table 6.10 Absolute differences ($D_{LT,i}$) of logic-tree based sensitivity analysis results for 475yrs return period. The top 3 logic-tree frameworks that perform better are shown in bold.

Region	Period	D_{LT01}	D_{LT02}	D_{LT03}	D_{LT04}	D_{LT05}	D_{LT06}	D_{LT07}	D_{LT08}	D_{LT09}	D_{LT10}	D_{LT11}	D_{LT12}
Aegean Region	PGA	**0.008**	0.026	0.014	**0.010**	0.017	**0.009**	0.029	0.053	0.011	0.027	0.060	0.044
	T=0.2s	**0.010**	0.011	0.010	**0.003**	0.013	**0.003**	0.024	0.042	0.024	0.025	0.056	0.024
	T=1.0s	0.017	0.016	0.019	**0.005**	**0.009**	**0.008**	0.027	0.037	0.029	0.034	0.085	0.032
	T=2.0s	0.012	0.019	**0.006**	**0.005**	0.006	**0.004**	0.021	0.032	0.015	0.021	0.056	0.028
NAF Region	PGA	**0.012**	0.049	0.023	**0.011**	0.015	0.017	0.033	0.046	**0.007**	0.026	0.073	0.052
	T=0.2s	**0.018**	0.038	0.028	**0.004**	0.030	**0.012**	0.029	0.034	0.019	0.024	0.073	0.033
	T=1.0s	0.020	0.023	0.021	**0.007**	**0.010**	**0.007**	0.026	0.032	0.026	0.033	0.092	0.035
	T=2.0s	0.013	0.032	0.022	**0.012**	**0.012**	**0.003**	0.026	0.031	0.016	0.032	0.087	0.042
Mersin Region	PGA	0.015	0.041	0.015	**0.010**	**0.012**	0.018	0.028	0.042	**0.004**	0.018	0.051	0.045
	T=0.2s	0.021	0.029	0.014	**0.002**	0.021	**0.008**	0.021	0.024	**0.013**	0.017	0.051	0.024
	T=1.0s	**0.008**	0.008	0.014	**0.006**	**0.004**	0.012	0.017	0.027	0.023	0.028	0.064	0.022
	T=2.0s	**0.005**	0.010	**0.005**	0.008	0.015	**0.004**	0.013	0.024	0.008	0.017	0.038	0.023

Table 6.11 Absolute differences ($D_{LT,i}$) of logic-tree based sensitivity analysis results for 2475yrs return period. The top 3 logic-tree frameworks that perform better are shown in bold.

Region	Period	D_{LT01}	D_{LT02}	D_{LT03}	D_{LT04}	D_{LT05}	D_{LT06}	D_{LT07}	D_{LT08}	D_{LT09}	D_{LT10}	D_{LT11}	D_{LT12}
Aegean Region	**PGA**	0.013	0.023	**0.007**	**0.010**	0.011	**0.005**	0.034	0.059	0.024	0.040	0.095	0.048
	T=0.2s	**0.011**	**0.010**	0.018	**0.004**	0.013	0.012	0.028	0.049	0.037	0.039	0.084	0.029
	T=1.0s	0.031	0.029	0.033	**0.007**	**0.025**	**0.009**	0.043	0.055	0.045	0.054	0.139	0.051
	T=2.0s	0.025	0.033	**0.018**	**0.005**	0.022	**0.008**	0.037	0.050	0.029	0.036	0.101	0.043
NAF Region	**PGA**	**0.014**	0.048	0.028	**0.012**	0.019	**0.014**	0.045	0.063	0.026	0.046	0.123	0.062
	T=0.2s	**0.025**	0.031	0.027	**0.009**	0.037	**0.014**	0.041	0.057	0.039	0.044	0.111	0.044
	T=1.0s	0.041	0.047	0.044	**0.009**	**0.032**	**0.006**	0.055	0.068	0.052	0.068	0.181	0.071
	T=2.0s	0.035	0.056	0.045	**0.016**	**0.022**	**0.007**	0.054	0.064	0.043	0.067	0.188	0.079
Mersin Region	**PGA**	0.012	0.031	**0.008**	**0.010**	0.011	**0.009**	0.031	0.051	0.013	0.030	0.071	0.047
	T=0.2s	**0.013**	0.014	0.013	**0.003**	0.014	**0.004**	0.026	0.041	0.027	0.028	0.070	0.028
	T=1.0s	0.020	0.019	0.022	**0.006**	**0.011**	**0.009**	0.035	0.052	0.038	0.047	0.110	0.045
	T=2.0s	0.015	0.025	**0.008**	**0.009**	0.012	**0.005**	0.033	0.053	0.023	0.036	0.086	0.046

6.6. Final EMME Logic-tree Frameworks

The procedure described in the previous section is repeated for spectral periods of PGA, T=0.2s, T=1.0s and T=2.0s for 475yrs and 2475yrs return periods. The results of the sensitivity analyses indicate the better performances of LT#1, LT#4 and LT#6 logic trees. The resultant PGA, T=0.2s, T=1.0s / 2475yrs hazard maps of these GMPE logic trees are given in Figures 6.14, 6.15 and 6.16 for the Aegean, NAF and Mersin regions, respectively. These figures also include the hazard maps of the SHARE project for comparative purposes. The SHARE logic-tree includes AB10, CF08, CY08 and Zetal06 GMPEs with branch weights of 0.35, 0.35, 0.20 and 0.10, respectively. The rest of the comparisons for pre-selected spectral periods, and 475yrs and 2475yrs return periods for the considered regions are displayed in Appendix D (Figures D.10 to D.18). The comparisons indicate minor differences between the hazard maps of LT#1, LT#4 and LT#6. Besides, the SHARE hazard results are slightly more conservative with respect to those computed from LT#1, LT#4 and LT#6.

The comparisons similar to those given in Figures 6.14, 6.15 and 6.16 for different return period (i.e., 475yrs) and for different spectral periods led the selection of LT#4 as the final ground-motion logic-tree framework in the hazard computations of shallow active crustal seismic regions in the EMME project. Table 6.12.a lists the LT#4 GMPEs and corresponding logic-tree weights. AC10 model included in this logic-tree framework estimates spectral ordinates for periods smaller than 2.0s whereas the others yield estimates up to T=4.0s. The spectral period differences between AC10 and the rest of the predictive models may cause a discontinuity in the uniform hazard spectrum. Therefore, the spectral ordinate estimations of AC10 are extended after 2.0s. The details of this extension are described in Appendix E.

As indicated previously, the SHARE project GMPE logic-tree application is used for the hazard analysis of subduction regions in the EMME. Table 6.12.b lists the corresponding subduction GMPEs and their weights for completeness.
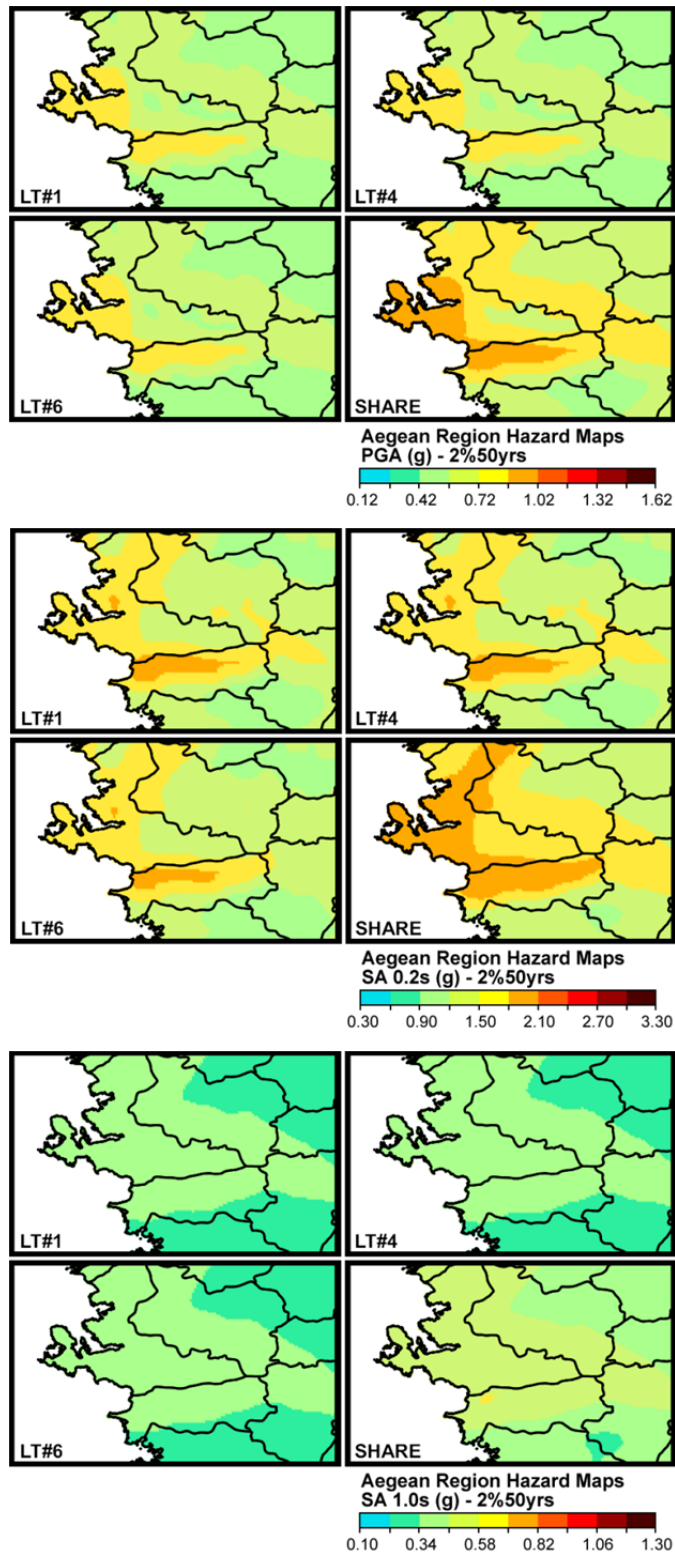
Figure 6.14 Comparison of PGA (top), T=0.2s (middle) and T=1.0s (bottom)
Aegean region hazard maps computed from LT#1, LT#4 and LT#6 for 2475yrs
return period. The lower right panels in each group give the SHARE hazard map.

200
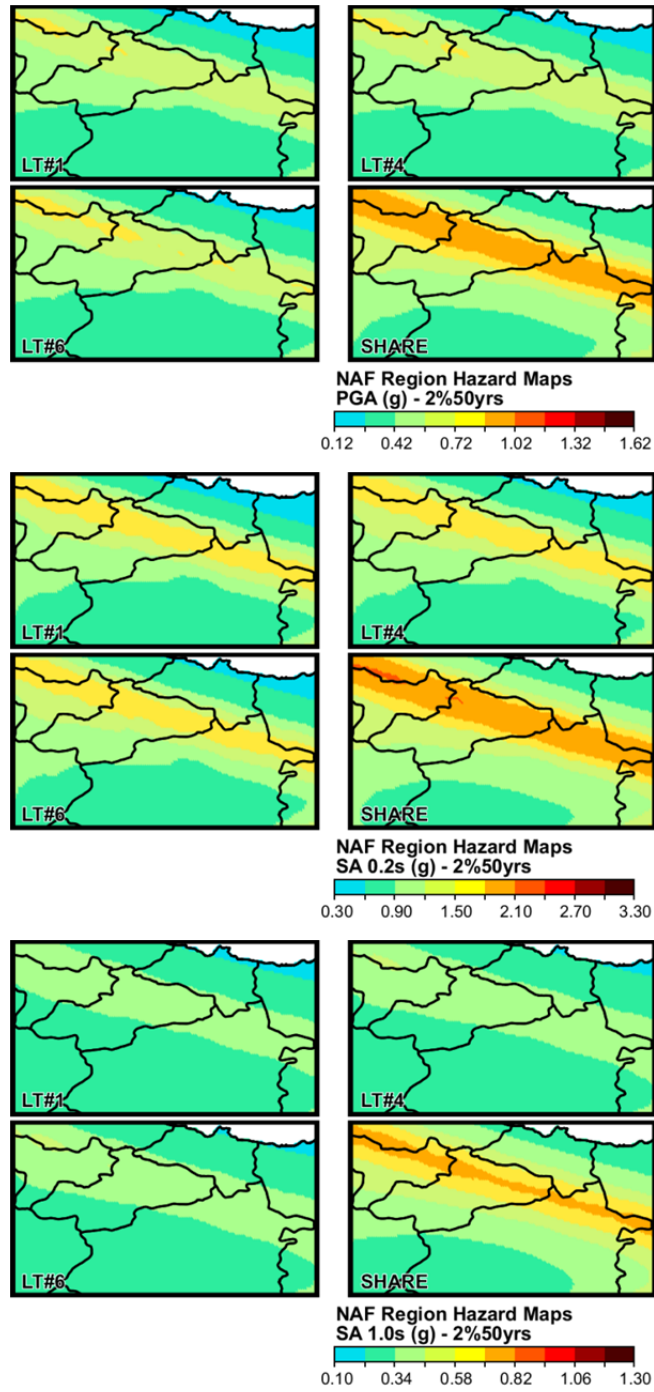
Figure 6.15 Comparison of PGA (top), T=0.2s (middle) and T=1.0s (bottom) NAF region hazard maps computed from LT#1, LT#4 and LT#6 for 2475yrs return period. The lower right panels in each group give the SHARE hazard map.
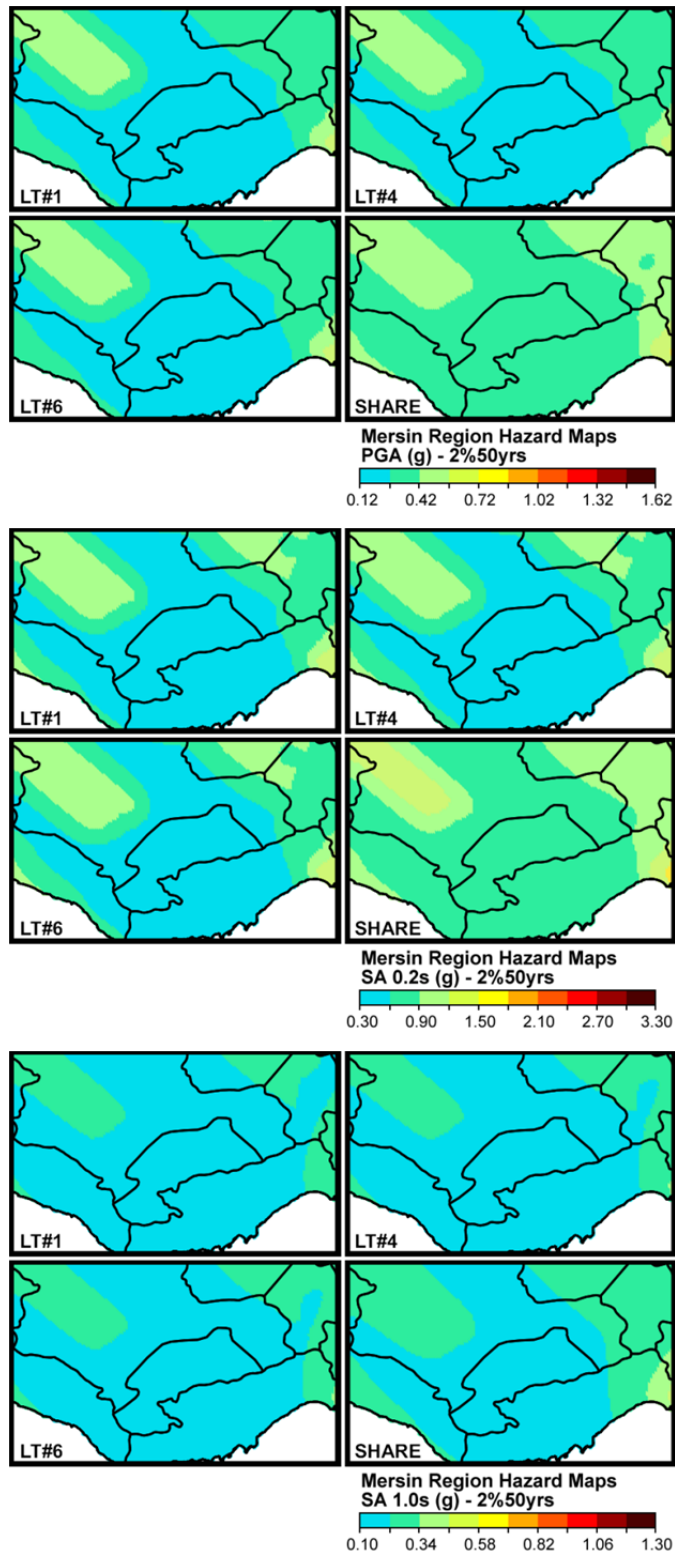
Figure 6.16 Comparison of PGA (top), T=0.2s (middle) and T=1.0s (bottom) NAF region hazard maps computed from LT#1, LT#4 and LT#6 for 2475yrs return period. The lower right panels in each group give the SHARE hazard map.

Table 6.12 Final EMME logic-tree for T ≤ 4.0s: a) shallow active crustal regions,
b) subduction regions.

a) Shallow Active Crustal Regions		b) Subduction Regions*	
GMPE	Weight	GMPE	Weight
ASB14	0.35	Zetal06	0.40
CY08	0.35	AB03	0.20
AC10	0.20	Yetal97	0.20
Zetal06	0.10	LL08	0.20

* Zetal06: Zhao et al. (2006) for subduction regions, AB03: Atkinson and Boore
(2003), Yetal97: Youngs et al. (1997), LL08: Lin and Lee (2008)

6.7. Summary and Conclusions

In this chapter, the establishment of the EMME ground-motion logic tree framework is presented by the help of selection and ranking methods of GMPEs and logic-tree based sensitivity analyses. A total of 16 candidate GMPEs from shallow active crustal regions were tested with a dataset that comprises of 1869 accelerograms from EMME region. The various testing methods (i.e., NSE, LH, LLH and EDR) describing also their essential features were used for selection and ranking of ground-motion models. Later, the best performing GMPEs were evaluated by trellis charts in a transparent way to capture the spectral trends of them. Finally, logic-tree based sensitivity analyses were conducted to the selected regions from Turkey which represents low-to-high seismicity levels by using the EMME background area source model.

The selection and weighting of GMPEs were based on analytical methods as no expert elicitation was formulated during the course of the EMME project. The proposed schemes were believed to be objective. Among the candidates, the selected GMPEs were the best in representing the ground-motion trends. The weighting scheme was tailored such that none of the selected GMPEs control the hazard at a particular location. The preliminary comparisons indicated that the seismic hazard results of the SHARE and EMME in the neighboring locations were comparable; however, SHARE hazard results are slightly more conservative.

CHAPTER 7

CONCLUSIONS

7.1. Conclusions

This dissertation addresses a number of practical issues related to ground-motion modeling in shallow active crustal regions. They would be separated into three main themes: a) compilation of strong-motion databases for shallow active crustal regions in Middle East and Turkey, b) development of regional ground-motion prediction equation (GMPE) and investigation of regional differences, c) development of practical tools for ranking and selection of GMPEs to properly handle the epistemic uncertainty in probabilistic seismic hazard assessment (PSHA) and their practical application to Middle East region. The main outcomes of the entire research are laid out in the following subsections.

7.1.1. Strong-Motion Database

- The EMME (**E**arthquake **M**odel of the **M**iddle **E**ast Region) strong-motion data archive covering Caucasus, Iran, Jordan, Pakistan and Turkey is of its first kind in the Middle East region.
- Event (e.g., magnitude, depth, epicenter location, double-couple fault plane solution) and station information (e.g., station coordinates, estimated or V_{S30} based site condition) of the database are compiled from reliable national and international seismological agencies, reports and peer-reviewed journal papers except for the accelerograms gathered from RESORCE (mainly for Turkey).

- The point- and extended-source distances are calculated using the moment tensor solutions reported by the local and global seismic agencies. The computations of finite-fault distance metrics (i.e., R_{JB} and R_{RUP}) mostly from actual fault-plane solutions increase the reliability of the database.

- The acausal band-pass filtering procedure is applied to the recordings in the database by following the procedures explained in Akkar and Bommer (2006) and Akkar et al. (2011). The filter-cutoff frequency selections are done automatically with respect to signal-to-noise ratio for Iranian recordings, whereas the rest of the accelerograms are filtered by individually selected filter frequencies.

- A more elaborate version of the Turkish strong-motion database, extracted from the EMME databank is obtained thanks to the updates according to the most recent metadata information provided by Kadirioğlu et al. (2014) catalog compilation study.

- The supplementary data from Italy and Greece (RESORCE) and California (NGA-West2) significantly improve the data distribution in the database utilized for GMPE selection.

- The comparisons made between model-developing datasets of the recent Turkish GMPEs and the latest version the Turkish database apparently emphasize that the Turkish metadata information is subject to significant modifications in the last decade through national and international research projects and studies.

- The consequential strong-motion databases principally serve for conducting all kind of ground-motion characterization topics (e.g., developing new GMPEs, data-driven testing and selection of GMPEs, time history analysis).

7.1.2. Ground-Motion Prediction Equation and Regional Effects

- The new ground-motion model is capable of predicting 5%-damped horizontal spectral acceleration between $0.01s \leq T \leq 4.0s$ as well as PGA and PGV.

- The model-developing dataset of the new GMPE is bounded for Joyner-Boore distance, magnitude and site condition ranges of $R_{JB} \leq 200km$, $4.0 \leq M_w \leq 7.6$ and $150m/s \leq V_{S30} \leq 1200m/s$, respectively. However, the functional form of the GMPE provides to extend the magnitude limit up to M_w 8.0.

- The proposed GMPE accounts for anelastic attenuation and magnitude-dependent (heteroscedastic) standard deviation.

- The examinations emphasize that the hypocentral depth distribution of shallow active crustal events in Iran and Turkey, the differences in near-surface velocity profiles, Q-factors, the variations in kappa as a function of M_w, R_{JB} and V_{S30} result in dissimilar trends in the spectral estimates of Iran and Turkey.

- The above observations result in yielding larger spectral amplitudes and slower attenuation rates with distance in Iranian earthquakes than those in Turkish events at short- and long-period spectral ordinates.

- These facts also lead to dissimilarities between ground-motion estimates of the new predictive model and those of NGA-West2 and pan-European ground-motion relations. The differences are prominent both small and large magnitudes and far source predictions.

7.1.3. Testing of GMPEs for PSHA and Logic-Tree Framework

- The proposed method (EDR: Euclidean Distance-Based Ranking) based on Euclidean distance concept is capable of selection and ranking of predictive models for establishing ground-motion logic-tree applications in PSHA.

- The EDR method can separately handle the aleatory variability (i.e., standard deviation of the GMPEs) and the model bias between the observed data and median estimations of the candidate GMPEs (i.e., trend).

- The above indexes, MDE (i.e., aleatory variability) and κ (i.e., model bias), or their combination (i.e., actual EDR index) can be used in ranking of GMPEs to construct ground-motion logic-tree frameworks.

- Distinct utilization of MDE and κ indexes would provide meaningful conception for site-specific hazard studies whereas their combination EDR can be regarded as a useful tool for regional hazard studies.

- The practicality of the proposed method with respect to MDE, κ and EDR indexes are discussed through a case study considering a suite of candidate GMPEs and selecting a ground-motion database. The results of the case study depict that the ranking of the candidate GMPEs may alter with respect to separate consideration of EDR components or actual EDR index.

- The case study also indicates that the ground-motion relations with simpler functional forms generally rank at the top of the list.

- The other practical tool which is offered to suitably capture the epistemic uncertainty in seismic hazard analysis by evaluating the performances of alternative logic-tree frameworks is essentially based on seismic hazard sensitivity analyses.

- The new approach is intensely endorsed to be practiced together with other well-structured testing methods in the literature.

- The accompanying set of ground-motion models and corresponding weights are established such that none of the individual GMPEs in a logic tree control the overall hazard at an objective-specific location.

- The conducted practical application of the approach displays that even though the selected GMPEs for establishing logic-tree setups are the best performing ones in the region of interest, some GMPEs tend to dominate the resultant hazard. However, the new tool detects these undesirable cases in an effective manner.

- Thanks to the data-driven testing methods (NSE - Nash and Sutcliffe, 1970; LH - Scherbaum et al., 2004; LLH - Scherbaum et al., 2009; EDR - Kale and Akkar, 2013), trellis charts and logic-tree based sensitivity analyses; the ground-motion logic-tree framework for PSHA applications in EMME region is established.

- The selection of GMPEs and corresponding branch weights are totally based on the statistical methods and reliable approaches in the open literature because no expert judgment or degree of belief is conveyed during the advance of the EMME project. Therefore the consequent logic-tree framework is believed to be objective.

- The preliminary hazard outcomes point out that the seismic hazard results of the SHARE and EMME for the selected locations in the logic-tree based sensitivity analyses are comparable; however, the hazard results obtained from the SHARE logic-tree setup are slightly more conservative.

7.2. Suggestions for Further Work

The EMME database is a comprehensive representation of strong ground-motion data acquisition in the Middle East region. However, when the number of ground-motion data within the entire database and the sub dataset serving for testing of ground-motion relations are compared, more than half of the recordings cannot be used in ground-motion related studies. Turkish and Iranian strong-motion data significantly suffer from this issue. While only 60% (1078 records) of the Turkish ground-motion records are included in the predictive model testing database, the percentage for the Iranian accelerograms is just about 20%. For Iran, 660 recordings are used from a total number of 2988 accelerograms. This issue appears in a more dramatic manner for the high standard sub datasets from which predictive models are developed. In this case, the percentage of the usable data 39% (670 records) and 18% (528 records) for Turkey and Iran, respectively. The main reasons for this issue would be listed as non existence of moment magnitude and double-couple fault plane solutions (particularly for small magnitude events), unreliable site conditions and recordings not obtained from free field stations. In this respect, the researchers should be fully supported for conducting comprehensive long-term research projects on fixing these issues in accordance with the improvements of existing metadata information. These advences result in obtaining more reliable ranking of GMPEs, developing well-constrained predictive

models, identifying the regional effects elaborately and reducing the epistemic uncertainty.

The Iranian strong-motion data archive whose metadata information is compiled under the scope of this thesis should be incorporated into the RESORCE by unifying the data processing with individually selected filter cut-off frequencies. In addition, the Caucasusian and Jordanian accelerograms in EMME database can also be trasferred to the RESORCE. Besides, the metadata information of these databanks should be updated periodically following the advences in the related topics.

The last suggestion is related to the subject of characterizing the epistemic uncertainty which is modeled by logic-tree framework deployed in seismic hazard applications. Although there has been numerous papers published on identifying the logic-tree frameworks, their establishment and application details has not been studied in sufficient depth. The second half of the thesis is devoted to proposing alternative methods on this subject. However, more systematic studies encouraged by the seismological community would be helpful and can provide alternative perspectives to the researchers.

REFERENCES

Abrahamson NA and Bommer JJ (2005). Probability and uncertainty in seismic hazard analysis, *Earthquake Spectra* 21, 603-607.

Abrahamson N and Silva W (2008). Summary of the Abrahamson & Silva NGA ground-motion relations. *Earthquake Spectra* 24, no. 1, 67-97.

Abrahamson N, Silva W, Kamai R (2014). Summary of the ASK14 Ground-Motion Relation for Active Crustal Regions. *Earthquake Spectra* 30, no. 3, 1025-1055.

Abrahamson NA and Youngs RR (1992). A stable algorithm for regression analyses using the random effects model. *Bull Seismol Soc Am* 82, 505-510.

Akıncı A and Eyidoğan H (1996). Frequency-dependent attenuation of S and coda waves in Erzincan region (Turkey). *Phys. Earth. Planet. In.* 97, 109-119.

Akkar S and Bommer JJ (2006). Influence of long-period filter cut-off on elastic spectral displacements. *Earthq. Eng. Struct. Dynam.* 35, no. 9, 1145-1165.

Akkar S and Bommer JJ (2007). Empirical Prediction Equations for Peak Ground Velocity Derived from Strong-Motion Records from Europe and the Middle East. *Bull Seismol Soc Am* 97, no. 2, 511-530.

Akkar S and Bommer JJ (2010). Empirical equations for the prediction of PGA, PGV and spectral accelerations in Europe, the Mediterranean region and the Middle East. *Seismol. Res. Lett.* 81, no. 2, 195-206.

Akkar S, Bossu R, Cauzzi C, Clinton J, D'amico M, Van Eck T, Frobert L, Godey S, Gueguen P, Kästli P, Luzi L, Pacor F, Pequegnat C, Puglia R, Russo E, Sleeman R (2014e). Network of European Research Infrastructures for Earthquake Risk Assessment and Mitigation (NERA)-Networking Accelerometric Networks and Sm Data Users (NA3). *Second European Conference on Earthquake Engineering and Seismology, İstanbul, Turkey*.

Akkar S and Çağnan Z (2010). A local ground-motion predictive model for Turkey and its comparison with other regional and global ground-motion models. *Bull. Seismol. Soc. Am.* 100, no. 6, 2978-2995.

Akkar S, Çağnan Z, Yenier E, Erdoğan Ö, Sandıkkaya MA, Gülkan P (2010). The recently compiled Turkish strong motion database: preliminary investigation for seismological parameters. *Journal of Seismology* 14, 457-479.

Akkar S, Kale Ö, Yenier E, Bommer JJ (2011). The high-frequency limit of usable response spectral ordinates from filtered analogue and digital strong-motion accelerograms. *Earthq. Eng. Struct. Dynam.* 40, 1387-1401.

Akkar S and Kale Ö (2014). Reply to "Comment on 'A New Procedure for Selecting and Ranking Ground-Motion Prediction Equations (GMPEs): The Euclidean Distance-Based Ranking (EDR) Method' by Özkan Kale and Sinan Akkar" by Sum Mak, Robert Alan Clements and Danijel Schorlemmer. *Bull Seismol Soc Am* in press.

Akkar S, Kale Ö, Ansari A, Durgaryan R, Askan Gündoğan A, Hamzehloo H, Harmandar E, Tsereteli N, Waseem M, Yazjeen T, Yılmaz MT (2014a). EMME Strong-Motion Database Serving for Predictive Model Selection to EMME Ground-Motion Logic-Tree Applications, *Second European Conference on Earthquake Engineering and Seismology, İstanbul, Turkey*, Paper No. 3220.

Akkar S, Sandıkkaya MA, Ay BÖ (2014d). Compatible ground-motion prediction equations for damping scaling factors and vertical-to-horizontal spectral amplitude ratios for the broader Europe region. *Bull. Earthquake Eng.* 12, no. 1, 517-547.

Akkar S, Sandıkkaya MA, Bommer JJ (2014b). Empirical ground-motion models for point- and extended-source crustal earthquake scenarios in Europe and the Middle East. *Bull. Earthquake Eng.* 12, 359-387.

Akkar S, Sandıkkaya MA, Senyurt M, Azari Sisi A, Ay BÖ, Traversa P, Douglas J, Cotton F, Luzi L, Hernandez B, Godey S (2014c). Reference database for seismic ground-motion in Europe (RESORCE). *Bull. Earthquake Eng.* 12, 311-339.

Akkar S, Douglas J, Di Alessandro C, Campbell KW, Somerville PG, Cotton F, Silva W, Baker J (2012). Defining a consistent strategy to model ground motion parameters for the GEM-PEER Global GMPEs Project. *15th World Conference on Earthquake Engineering, Lisbon, Portugal*, Paper No. 2743.

Akyol N and Karagöz Ö (2009). Empirical attenuation relationships for western Anatolia, Turkey. *Turkish Journal of Earth Sciences* 18, 351-382.

Al Atik L and Youngs RR (2014). Epistemic Uncertainty for NGA-West2 Models. *Earthquake Spectra*, 30, no. 3, 1301-1318.

Alavijeh HM, Sinaiean F, Farzanegan E (2010). Site geology investigations in accelerometric stations using seismic refraction method, Vol. 4- Lorestan and Hamedan Provinces, Research report, BHRC publication No. R-534 (in Farsi).

Ambraseys NN (1975). Trends in engineering seismology in Europe. *Proceedings of Fifth European Conference on Earthquake Engineering*, 3, 39-52.

Ambraseys NN (1990). Uniform magnitude re-evaluation of European earthquake associated with strong-motion records. *Earthquake Engineering and Structural Dynamics*, 19, 1-20.

Ambraseys NN and Bommer JJ (1990). Uniform magnitude re-evaluation for the strong-motion database of Europe and adjacent regions. *European Earthquake Engineering*, 4, 3-16.

Ambraseys NN and Bommer JJ (1991). Database of European strong-motion records. *European Earthquake Engineering*, 5, 18-37.

Ambraseys NN, Douglas J, Sigbjörnsson R, Berge-Thierry C, Suhadolc P, Costa G, Smit PM (2004b). Dissemination of European Strong-Motion Data, Volume 2. *Proceedings of the 13th World Conference on Earthquake Engineering, Vancouver, British Columbia, Canada*.

Ambraseys NN, Smit P, Douglas J, Margaris B, Sigbjörnsson R, Olafsson S, Suhadolc P, Costa G (2004a). Internet site for European strong-motion data. *Bollettino di Geofisica Teorica ed Applicata*, 45, 113-129.

Ambraseys NN, Douglas J, Sarma SK, Smit PM (2005). Equations for the estimation of strong ground motions from shallow crustal earthquakes using data from Europe and the Middle East: Horizontal peak ground acceleration and spectral acceleration. *Bull. Earthquake Eng.* 3, no. 1, 1-53.

Ambraseys, NN, Simpson KA, Bommer JJ (1996). Prediction of horizontal response spectra in Europe. *Earthq Eng Struct Dynam* 25, no. 4, 371-400.

Ambraseys N, Smit P, Berardi R, Rinaldis D, Cotton F, Berge-Thierry C (2000). Dissemination of European Strong-Motion Data. CD-ROM collection. *European Commission, Directorate General XII, Science, Research and Development, Environment and Climate Programme,* Bruxelles.

Ancheta TD, Robert BD, Stewart PS, Seyhan E, Silva WJ, Chiou BSJ, Wooddell KE, Graves RW, Kottke AR, Boore DM, Kishida T, Donahue JL (2014). NGA-West 2 Database. *Earthquake Spectra* 30, no. 3, 989-1005.

Anderson JG and Hough SE (1984). A model for the shape of the fourier amplitude spectrum of acceleration at high frequencies. *Bull Seismol Soc Am* 74, no. 5, 1969-1993.

Arango MC, Strasser FO, Bommer JJ, Cepeda JM, Boroschek R, Hernandez DA, Tavera H (2012). An evaluation of the applicability of current ground-motion models to the South and Central American subduction zones. *Bull. Seism. Soc. Am* 102, no. 1, 143-168.

Arroyo D and Ordaz M (2011). On the Forecasting of Ground-Motion Parameters for Probabilistic Seismic Hazard Analysis, *Earthquake Spectra* 27, 1-21.

ASCE (2010). Minimum Design Loads for Buildings and Other Structures (7-10). *American Society of Civil Engineers*, ASCE/SEI7-10.

Atkinson GM and Boore DM (2003). Empirical groundmotion relations for subduction zone earthquakes and their application to Cascadia and other regions. *Bull. Seismol. Soc. Am.* 93, 1703-1729.

Atkinson GM and Morrison M (2009). Observations on Regional Variability in Ground-Motion Amplitudes for Small-to-Moderate Earthquakes in North America. *Bull. Seismol. Soc. Am.* 99, no. 4, 2393-2409.

Aydan Ö (2007). Inference of seismic characteristics of possible earthquakes and liquefaction and landslide risks from active faults. *The 6th National Conference on Earthquake Engineering of Turkey*, 1, 563-574.

Aydan Ö, Sedaki M, Yarar R (1996). The seismic characteristics of Turkish earthquakes. *Proceedings of Eleventh World Conference on Earthquake Engineering* Paper no. 1270.

Beauval C, Tasan H, Laurendeau A, Delavaud E, Cotton F, Guéguen Ph, Kühn N (2012a). On the testing of ground-motion prediction equations against small magnitude data. *Bull. Seism. Soc. Am.*102, no. 5, 1994-2007.

Beauval C, Cotton F, Abrahamson N, Theodoulidis N, Delavaud E, Rodriguez L, Scherbaum F, Haendel A (2012b). Regional differences in subduction ground motions. *Proceedings of the 15th World Conference on Earthquake Engineering*, Lisbon, Portugal, 24-28 September 2012.

Bender B (1984). Incorporating acceleration variability into seismic hazard analysis. *Bull. Seism. Soc. Am.* 74, no. 4, 1451-1462.

Beyer K and Bommer JJ (2006). Relationships between median values and between aleatory variabilities for different definitios of the horizontal component of motion. *Bull. Seismol. Soc. Am.* 96, no. 4A, 1512-1522.

Bindi D, Luzi L, Massa M, Pacor F (2010). Horizontal and vertical ground motion prediction equations derived from the Italian Accelerometric Archive (ITACA). *Bull. Earthquake Eng.* 8, no. 5, 1209-1230.

Bindi D, Luzi L, Pacor F, Franceschina G, Castro RR (2006). Ground-Motion Predictions from Empirical Attenuation Relationships versus Recorded Data: The Case of the 1997–1998 Umbria-Marche, Central Italy, Strong-Motion Data Set. *Bull. Seismol. Soc. Am.* 96, no. 3, 984-1002.

Bindi D, Massa M, Luzi L, Ameri G, Pacor F, Puglia R, Augliera P (2014). Pan-European ground-motion prediction equations for the average horizontal component of PGA, PGV, and 5%-damped PSA at spectral periods up to 3.0 s using the RESORCE dataset, *Bull. Earthquake Eng.* 12, 391-430.

Bindi D, Pacor F, Luzi L, Puglia R, Massa M, Ameri G, Paolucci R (2011). Ground motion prediction equations derived from the Italian strong motion database. *Bull. Earthquake Eng.* 9, 1899-1920.

Bindi D, Parolai S, Grosser H, Milkereit C, Durukal E (2007). Empirical ground-motion prediction equations for northwestern Turkey using the aftershocks of the 1999 Kocaeli earthquake. *Geophys. Res. Lett.* 34 (L08305).

Bommer JJ (2012). Challenges of Building Logic Trees for Probabilistic Seismic Hazard Analysis. *Earthquake Spectra* 28, no. 4, 1723-1735.

Bommer JJ, Akkar S, Kale Ö (2011). A model for vertical-to-horizontal response spectral ratios for Europe and the Middle East. *Bull. Seismol. Soc. Am.* 101, no. 4, 1783-1806.

Bommer JJ, Douglas J, Scherbaum F, Cotton F, Bungum H, Fäh D (2010). On the Selection of Ground-Motion Prediction Equations for Seismic Hazard Analysis. *Seism. Res. Lett.* 81, 783-793.

Bommer JJ and Scherbaum F (2005). Capturing and limiting ground-motion uncertainty in seismic hazard assessment. *Directions in Strong Motion Instrumentation, Springer*, 25-40.

Bommer JJ and Scherbaum F (2008). The use and misuse of logic-trees in probabilistic seismic hazard analysis. *Earthquake Spectra* 24, 997-1009.

Bommer JJ, Scherbaum F, Bungum H, Cotton F, Sabetta F, Abrahamson NA (2005). On the use of logic trees for ground-motion prediction equations in seismic-hazard analysis. *Bull. Seismol. Soc. Am.* 95, 377-389.

Bommer JJ, Stafford PJ, Alarcón JE (2009). Empirical Equations for the Prediction of the Significant, Bracketed, and Uniform Duration of Earthquake Ground Motion. *Bull. Seismol. Soc. Am.* 99, no. 6, 3217-3233.

Bommer JJ, Stafford PJ, Akkar S (2010). Current empirical ground-motion prediction equations for Europe and their application to Eurocode 8. *Bull. Earthquake Eng.* 8, 5-26.

Bommer JJ, Stafford PJ, Alarcón JE, Akkar S (2007). The influence of magnitude range on empirical ground-motion prediction. *Bull. Seismol. Soc. Am.* 97, 2152-2170.

Boore DM and Atkinson GM (2007). Boore-Atkinson NGA Ground Motion Relations for the Geometric Mean Horizontal Component of Peak and Spectral Ground Motion Parameters. PEER 2007/01, Pacific Earthquake Engineering Research Center, University of California, Berkeley, California.

Boore DM and Atkinson G (2008). Ground-Motion Prediction Equations for the Average Horizontal Component of PGA, PGV, and 5%-Damped PSA at Spectral Periods between 0.01 s and 10.0 s. *Earthquake Spectra* 24, no. 1, 99-138.

Boore DM, Azari Sisi A, Akkar S (2012). Using pad-stripped acausally filtered strong-motion data. *Bull. Seismol. Soc Am.* 102, 751-760.

Boore DM, Stewart JP, Seyhan E, Atkinson GM (2014). NGA-West 2 Equations for Predicting PGA, PGV, and 5%-Damped PSA for Shallow Crustal Earthquakes. *Earthquake Spectra* 30, no. 3, 1057-1085.

Boore DM, Watson-Lamprey J, Abrahamson NA (2006). Orientation-independent measures of ground motion. *Bull. Seismol. Soc. Am.* 96, no. 4A, 1502-1511.

Bozorgnia Y, Abrahamson NA, Al Atik L, Ancheta TD, Atkinson GM, Baker JW, Baltay A, Boore DM, Campbell KW, Chiou BSJ, et al. (2014). NGA-West2 Research Project, *Earthquake Spectra* 30, no. 3, 973-987.

Bragato PL and Slejko D (2005). Empirical ground-motion attenuation relations for the eastern Alps in the magnitude range 2.5–6.3. *Bull. Seismol. Soc. Am.* 95, no. 1, 252-276.

Building Seismic Safety Council (BSSC) (2009). 2009 NEHRP Recommended Seismic Provisions For New Buildings and Other Structures: Part 1, Provisions, Federal Emergency Management Agency (P-750), Washington, D.C.

Campbell KW and Bozorgnia Y (2006). Next Generation Attenuation (NGA) empirical ground motion models: can they be used in Europe? *Proceedings of the first European conference on earthquake engineering and seismology* Paper No. 458.

217

Campbell KW and Bozorgnia Y (2008). NGA ground motion model for the geometric mean horizontal component of PGA, PGV, PGD and 5% damped linear elastic response spectra for periods ranging from 0.01 to 10 s. *Earthquake Spectra* 24, no. 1, 139-171.

Campbell KW and Bozorgnia Y (2014). NGA-West2 Ground Motion Model for the Average Horizontal Components of PGA, PGV, and 5%-Damped Linear Acceleration Response Spectra. *Earthquake Spectra* 30, no. 3, 1087-1115.

Cauzzi C and Faccioli E (2008). Broadband (0.05 to 20 s) prediction of displacement response spectra based on worldwide digital records. *Journal of Seismology* 12, no. 4, 453-475.

CEN (2004). Eurocode 8: Design of structures for earthquake Resistance - Part 1: General rules, seismic actions, and rules for buildings, EN 1998-1:2004, Comité Européen de Normalisation, Brussels.

Chiou B, Darragh R, Gregor N, Silva W (2008). NGA project strong-motion database. *Earthquake Spectra* 24, no. 1, 23-44.

Chiou BS-J and Youngs RR (2008). An NGA model for the average horizontal component of peak ground motion and response spectra. *Earthquake Spectra* 24, no. 1, 173-215.

Chiou BS-J and Youngs RR (2014). Update of the Chiou and Youngs NGA Model for the Average Horizontal Component of Peak Ground Motion and Response Spectra. *Earthquake Spectra* 30, no. 3, 1117-1153.

Chiou B, Youngs R, Abrahamson N, Addo K (2010). Ground-Motion Attenuation Model for Small-To-Moderate Shallow Crustal Earthquakes in California and Its Implications on Regionalization of Ground-Motion Prediction Models. *Earthquake Spectra* 26, 907-926.

Cotton F, Scherbaum F, Bommer JJ, Bungum H (2006). Criteria for Selecting and Adjusting Ground-Motion Models for Specific Target Regions: Application to Central Europe and Rock Sites. *Journal of Seismology* 10, 137-156.

Delavaud E, Cotton F, Akkar S, Scherbaum F, Danciu L, Beauval C, Drouet S, Douglas J, Basili R, Sandıkkaya MA, Segou M, Faccioli E, Theodoulidis N (2012b). Toward a Ground-Motion Logic Tree for Probabilistic Seismic Hazard Assessment in Europe. *Journal of Seismology* 16, 451-473.

Delavaud E, Scherbaum F, Kuehn N, Allen T (2012a). Testing the Global Applicability of Ground-Motion Prediction Equations for Active Shallow Crustal Regions. *Bull. Seismol. Soc. Am.* 102, no. 2, 707-721.

Delavaud E, Scherbaum F, Kuehn N, Riggelsen C (2009). Information-Theoretic Selection of Ground-Motion Prediction Equations for Seismic Hazard Analysis: An Applicability Study Using Californian Data. *Bull. Seismol. Soc. Am.* 99, no. 6, 3248-3263.

Devore JL (2004). Probability and Statistics for Engineering and the Sciences. *Thomson Learning Inc., MA*.

Douglas J (2003). What is a poor quality strong-motion record? *Bull. Earthquake Eng.* 1, 141-156.

Douglas J (2004). An investigation of analysis of variance as a tool for exploring regional differences in strong ground motions. *Journal of Seismology* 8, 485-496.

Douglas J (2007). On the regional dependence of earthquake response spectra. *ISET Journal of Earthquake Technology* 44, no. 1, 71-99.

Douglas J (2010) Assessing the epistemic uncertainty of ground-motion predictions. *Proceedings of the Ninth US National and 10thCanadian Conference on Earthquake Engineering Toronto, Canada* Paper No 219.

Douglas J (2011). Ground-motion prediction equations 1964-2010. PEER 2011/102.

Douglas J (2012). Consistency of ground-motion predictions from the past four decades: peak ground velocity and displacement, Arias intensity and relative significant duration, *Bull. Earthquake Eng.* 10, 1339-1356.

Douglas J, Akkar S, Ameri G, Bard P-Y, Bindi D, Bommer JJ, Bora SS, Cotton F, Derras B, Hermkes M, Kuehn NM, Luzi L, Massa M, Pacor F, Riggelsen C, Sandıkkaya MA, Scherbaum F, Stafford PJ, Traversa P (2014). Comparisons among the five ground-motion models 1 developed using RESORCE for the prediction of response spectral accelerations due to earthquakes in Europe and the Middle East. *Bull. Earthquake Eng.* 12, no. 1, 341-358.

Douglas J and Boore DM (2011). High-frequency filtering of strong-motion records. *Bull. Earthq. Eng.* 9, 395-409.

Douglas J, Gehl P, Bonilla LF, Gelis C (2010). A K model for mainland France. *Pure Appl. Geophys.* 167, 1303-1315.

Engdahl ER, Jackson JA, Myers SC, Bergman EA, Priestley K (2006). Relocation and assessment of seismicity in the Iran region. *Geophys. J. Int.* 167, 761-778.

Erdik M, Fahjan Y, Ozel O, Alcik H, Mert A, Gul M (2003). Istanbul Earthquake Rapid Response and Early Warning System, *Bull. Earthquake Eng.* 1, 157-163.

Esteva L and Rosenblueth E (1964). Espectros de temblores a distancias moderadas y grandes. *Boletin Sociedad Mexicana de Ingenieria Sesmica* 2, 1-18, In Spanish.

Faccioli E, Villani M, Vanini M, Cauzzi C (2010). Mapping Seismic Hazard for the Needs of Displacement-Based Design: The Case of Italy. *Advances in Performance-Based Earthquake Engineering* 13, no. 1, 3-14.

Farzanegan E, Alavijeh HM, Sinaiean F (2010). Site geology investigations in accelerometric stations using seismic refraction method, Vol.3-Hormozgan and south of Fars provinces, Research report, BHRC publication No. R-533 (in Farsi).

Farzanegan E, Alavijeh HM, Sinaiean F (2010). Site geology investigations in accelerometric stations using seismic refraction method, Vol.5- Fars province, Research report, BHRC publication No. R-535 (in Farsi).

Fukushima Y, Berge-Thierry C, Volant P, Griot-Pommera D-A, Cotton F (2003). Attenuation relation for western Eurasia determined with recent near-fault records from California, Japan and Turkey. *J. Earthquake Eng.* 7, no. 4, 573-598.

Ghasemi H, Zare M, Fukushima Y, Koketsu K (2009). An empirical spectral ground-motion model for Iran. *Journal of Seismology* 13, 499-515.

Ghodrati Amiri G, Mahdavian A, Dana FM (2007). Attenuation relationships for Iran. *J. Earthquake Eng.* 11, no. 4, 469-492.

Ghodrati Amiri G, Khorasani M, Mirza Hessabi M, Razavian Amrei SA (2010). Ground-motion prediction equations of spectral ordinates and Arias intensity for Iran. *J. Earthquake Eng.* 14, no. 1, 1-29.

Giardini D (1999). The Global Seismic Hazard Assessment Program 1992-1999. *Annali Geofis.* 42, no. 6, 957-974.

Gregor N, Abrahamson NA, Atkinson GM, Boore DM, Bozorgnia Y, Campbell KW, Chiou BS-J, Idriss IM, Kamai R, Seyhan E, Silva W, Stewart JP, Youngs R (2014). Comparison of NGA-West2 GMPEs. *Earthquake Spectra*, 30, no. 3, 1179-1197.

Gülkan P and Kalkan E (2002). Attenuation modeling of recent earthquakes in Turkey. *Journal of Seismology* 6, no. 3, 397-409.

Hamzehloo H and Mahood M (2012). Ground-Motion Attenuation Relationship for East Central Iran. *Bull. Seismol. Soc. Am.* 102, no. 6, 2677-2684.

Harmandar E (2009). Spatial variation of strong ground motion, Ph. D. Dissertation, Bogaziçi University, İstanbul, Turkey.

Hassani B, Zafarani H, Farjoodi J, Ansari A (2011). Estimation of site amplification, attenuation and source spectra of S-waves in the East-Central Iran. *Soil Dynam. Earthquake Eng.* 31, 1397-1413.

Hintersberger E, Scherbaum F, Hainzl S (2007). Update of likelihood-based ground-motion model selection for seismic hazard analysis in western central Europe. *Bull. Earthquake Eng.* 5, 1-16.

Horasan G, Kaşlılar-Özcan A, Boztepe-Güney A, Türkelli N (1998). S-wave attenuation in the Marmara region, northwestern Turkey. *Geophys. Res. Lett.* 25, no. 14, 2733-2736.

Horasan G and Boztepe-Güney A (2004). S-wave attenuation in the Sea of Marmara, Turkey. *Phys. Earth. Planet In.* 142, 215-224.

Inan E, Çolakoglu Z, Koç N, Bayülke N, Çoruh E (1996). Earthquake catalogs with acceleration records from 1976 to 1996. Technical Report General Directorate of Disaster Affairs, Earthquake Research Department, Ankara, Turkey.

Jiménez MJ, Giardini D, Grünthal G, and SESAME working group (2001). Unified seismic hazard modelling throughout the Mediterranean region, *Bollettino Di Geofisica Teorica Ed. Applicata* 42, no. 1-2, 3-18.

Joyner WB and Boore DM (1981). Peak horizontal acceleration and velocity from strong-motion records including records from the 1979 Imperial Valley, California, earthquake. *Bull. Seismol. Soc. Am.* 71, 2011-2038.

Kadirioğlu FT, Kartal RF, Kılıç T, Kalafat D, Duman TY, Özalp S, Emre Ö (2014). An improved earthquake catalog (M ≥ 4) and empirical magnitude conversion relations for Turkey and near surrounding (1900-2012) *Bull. Earthquake Eng.* submitted.

Kaklamanos J, Boore DM, Thompson EM, Campbell KW (2010). Implementation of the Next Generation Attenuation (NGA) ground-motion prediction equations in Fortran and R, *U.S. Geol. Surv. Open-File Rept. 2010-1296*, 43 p.

Kaklamanos J and Baise LG (2011). Model Validations and Comparisons of the Next Generation Attenuation of Ground Motions (NGA–West) Project. *Bull. Seismol. Soc. Am.* 101, no. 1, 160-175.

Kaklamanos, J, Baise LG, Boore DM (2011). Estimating unknown input parameters when implementing the NGA ground-motion prediction equations in engineering practice. *Earthquake Spectra* 27, 1219-1235.

Kale Ö and Akkar S (2012). A method to determine the appropriate GMPEs for a selected seismic prone region. *15th World Conference on Earthquake Engineering, Lisbon, Portugal*, Paper No. 2827.

Kale Ö and Akkar S (2013). A new procedure for selecting and ranking ground-motion prediction equations (GMPEs): the Euclidean-Distance Based Ranking (EDR) method. *Bull. Seismol. Soc. Am.* 103, no. 2A, 1069-1084.

Kale Ö and Akkar S (2013). Türkiye için geliştirilen yeni bir yer hareketi tahmin denklemi ve bu denklemin Orta Doğu bölgesinde yapılacak sismik tehlike çalışmaları için uygunluğunun test edilmesi, *2. Türkiye Deprem Mühendisliği ve Sismoloji Konferansı, Hatay, Turkey* Paper No. 172 (In Turkish).

Kale Ö, Akkar S, Ansari A, Hamzehloo H (2014). A ground-motion predictive model for Iran and Turkey for horizontal PGA, PGV and 5%-damped response spectrum: Investigation of possible regional effects. *Bull. Seismol. Soc. Am.*, submitted.

Kalkan E and Gülkan P (2004). Site-dependent spectra derived from ground motion records in Turkey. *Earthquake Spectra* 20, 1111-1138.

Khademi MH (2002). Attenuation of peak and spectral accelerations in the Persian plateau. *Proceedings of Twelfth European Conference on Earthquake Engineering* Paper no 330.

Kulkarni RB, Youngs RR, Coppersmith KJ (1984). Assessment of confidence intervals for results of seismic hazard analysis. *Eighth World Conference on Earthquake Engineering, International Association for Earthquake Engineering, Tokyo, Japan* 1, 263-270.

Lin P-S and Lee C-T (2008). Ground-motion attenuation relationships for subduction zone earthquakes in northeastern Taiwan. *Bull. Seismol. Soc. Am.* 98, 220-240.

Luzi L, Hailemikael S, Bindi D, Pacor F, Mele F, Sabetta F (2008). ITACA (ITalian ACcelerometric Archive): A Web Portal for the Dissemination of Italian Strong-motion Data. *Seismol. Res. Lett.* 79, no. 5, 716-722.

Mahdavian A (2006). Empirical evaluation of attenuation relations of peak ground acceleration in the Zagros and central Iran. *Proceedings of First European Conference on Earthquake Engineering and Seismology (a joint event of the 13th ECEE & 30th General Assembly of the ESC)* Paper no 558.

Mak S, Clements RA, Schorlemmer D (2014). Comment on 'A New Procedure for Selecting and Ranking Ground-Motion Prediction Equations (GMPEs): The Euclidean Distance-Based Ranking (EDR) Method' by Özkan Kale and Sinan Akkar. *Bull. Seismol. Soc. Am.* in press.

Massa M, Morasca P, Moratto L, Marzorati S, Costa G, Spallarossa D (2008). Empirical ground-motion prediction equations for northern Italy using weak- and strong-motion amplitudes, frequency content, and duration parameters. *Bull. Seismol. Soc. Am.* 98, no. 3, 1319-1342.

McGarr A (1984). Scaling of Ground Motion Parameters, State of Stress, and Focal Depth, *J. Geophys. Res.* 89, no. B8, 6969-6979.

Mousavi M, Ansari A, Zafarani H, Azarbakht A (2012). Selection of ground motion prediction models for seismic hazard analysis in the Zagros region, Iran. *J. Earthquake Eng.* 16, 1184-1207.

Nash JE and Sutcliffe JV (1970). River flow forecasting through conceptual models: Part I - A discussion of principles. *J. Hydrol.* 10, 282-290.

Nowroozi AA (2005). Attenuation relations for peak horizontal and vertical accelerations of earthquake ground motion in Iran: A preliminary analysis. *Journal of Seismology and Earthquake Engineering* 7, no. 2, 109-128.

Özbey C, Sari A, Manuel L, Erdik M, Fahjan Y (2004). An empirical attenuation relationship for northwestern Turkey ground motion using a random effects approach. *Soil Dynam. Earthquake Eng.* 24, no. 2, 115-125.

Pagani M, Monelli D, Weatherill G, Danciu L, Crowley H, Silva V, Henshaw P, Butler L, Nastasi M, Panzeri L, Simionato M, Vigano D (2014). OpenQuake Engine: An Open Hazard (and Risk) Software for the Global Earthquake Model, *Seismol. Res. Lett.* 85, no. 3, 692-702.

Petersen MD, Frankel AD, Harmsen SC, Mueller CS, Haller KM, Wheeler RL, Wesson RL, Zeng Y, Boyd OS, Perkins DM, Luco N, Field EH, Wills CJ, Rukstales, KS (2008). Documentation for the 2008 Update of the United States National Seismic Hazard Maps, *U.S. Geological Survey Open-File Report* 2008-1128, USGS, Reston, VA.

Power M, Chiou B, Abrahamson N, Bozorgnia Y, Shantz T, Roblee C (2008). An overview of the NGA project. *Earthquake Spectra* 24, no. 1, 3-21.

Ramazi HR and Schenk V (1994). Preliminary results obtained from strong ground motion analzses of Iranian earthquakes. *Proceedings of the XXIV General Assembly of the ESC*, III, 1762-1770.

Restrepo-Velez LF and Bommer JJ (2003). An Exploration of the Nature of the Scatter in Ground-Motion Prediction Equations and the Implications for Seismic Hazard Assessment. *J. Earthquake Eng.* 7, no. SI1, 171-199.

Sabetta F, Lucantoni A, Bungum H, Bommer JJ (2005). Sensitivity of PSHA results to ground motion prediction relations and logic-tree weights, *Soil Dynam. Earthquake Eng.* 25, 317-329.

Sabetta F and Pugliese A (1996). Estimation of response spectra and simulation of nonstationary earthquake ground motions. *Bull. Seismol. Soc. Am.* 86, no. 2, 337-352.

Sadeghi H, Shooshtari A, Jaladat M (2010). Prediction of horizontal response spectra of strong ground motions in Iran and its regions. *Proceedings of the Ninth U.S. National and 10th Canadian Conference on Earthquake Engineering: Reaching Beyond Borders* Paper no: 861.

Saffari H, Kuwata Y, Takada S, Mahdavian A (2012). Updated PGA, PGV, and Spectral Acceleration Attenuation Relations for Iran. *Earthquake Spectra* 28, 257-276.

Sandıkkaya MA and Akkar S (2013). Reference Database for Seismic Ground-Motion in Europe (Version 2). EERC-METU, Ankara, Turkey.

Sandıkkaya MA, Akkar S, Bard P-Y (2013). A nonlinear site amplification model for the new pan-European ground-motion prediction equations, *Bull. Seismol. Soc. Am*. 103, no. 1, 19-32.

Sandıkkaya MA, Yılmaz MT, Bakır BS, Yılmaz Ö (2010). Site classification of Turkish national strong-motion stations. *Journal of Seismology* 14, 543-563.

Scasserra G, Stewart JP, Bazzurro P, Lanzo G, Mollaioli F (2009). A Comparison of NGA Ground-Motion Prediction Equations to Italian Data. *Bull. Seismol. Soc. Am.* 99, no. 5, 2961-2978.

Scherbaum F, Bommer JJ, Bungum H, Cotton F, Abrahamson NA (2005). Composite ground-motion models and logic-trees: methodology, sensitivities and uncertainties, *Bull. Seismol. Soc. Am.* 95, 1575-1593.

Scherbaum F, Cotton F, Smit P (2004). On the Use of Response Spectral-Reference Data for the Selection and Ranking of Ground-Motion Models for Seismic-Hazard Analysis in Regions of Moderate Seismicity: The Case of Rock Motion. *Bull. Seismol. Soc. Am.* 94, no. 6, 2164-2185.

Scherbaum F, Delavaud E, Riggelsen C (2009). Model selection in seismic hazard analysis: An information-theoretic perspective. *Bull. Seismol. Soc. Am.* 99, no. 6, 3234-3247.

Scherbaum F and Kuehn NM (2011). Logic tree branch weights and probabilities: Summing up to one is not enough. *Earthquake Spectra* 27, 1237-1251.

Schwarz J, Ende C, Habenberger J, Lang DH, Baumbach M, Grosser H, Milereit C, Karakisa S, Zünbül S (2002). Horizontal and vertical response spectra on the basis of strong-motion recordings from the 1999 Turkey earthquakes. *Proceedings of the XXVIII General Assembly of the European Seismological Commission (ESC)*.

Shoja-Taheri J, Naserieh S, Hadi G (2010). A Test of the Applicability of NGA Models to the Strong Ground-Motion Data in the Iranian Plateau. *J. Earthquake Eng.* 14, 278-292.

Sinaiean F, Alavijeh HM, Farzanegan E (2008). Site geology investigations in accelerometric stations using seismic refraction method, Vol. 1- 50 stations, Research report, BHRC publication No. R-511 (in Farsi).

Sinaiean F, Farzanegan E, Alavijeh HM (2010). Site geology investigations in accelerometric stations using seismic refraction method, Vol. 2- Ardebil and east Azarbayjan provinces, Research report, BHRC publication No. R-532 (in Farsi).

Sinaiean F, Farzanegan E, Alavijeh HM (2010). Site geology investigations in accelerometric stations using seismic refraction method, Vol. 7- Semnan, Golestan and Mazandaran provinces, Research report, BHRC publication No. R-537 (in Farsi).

Snoke JA (2003) FOCMEC: Focal Mechanism Determinations, *International Handbook of Earthquake and Engineering Seismology* 81B:1629-1632. Academic Press, UK.

Stafford PJ, Strasser FO, Bommer JJ (2008). An evaluation of the applicability of the NGA models to ground-motion prediction in the Euro-Mediterranean region. *Bull. Earthquake Eng.* 6, 149-177.

Stewart JP, Douglas J, Javanbarg M, Abrahamson NA, Bozorgnia Y, Boore DM, Campbell KW, Delavaud E, Erdik M, Stafford PJ (2014). Selection of groundmotion prediction equations for the global earthquake model. *Earthquake Spectra*, doi:10.1193/013013EQS017M.

Strasser FO, Abrahamson NA, Bommer JJ (2009). Sigma: Issues, Insights, and Challenges. *Seismol. Res. Lett.* 80, no. 1, 40-56.

Theodulidis N, Cultrera G, Tento A, Faeh D, Atakan K, Bard P-Y, Panou A, and the SESAME-Team (2004). Empirical evaluation of the horizontal-to-vertical spectral ratio technique: results from the SESAME project. *13th World Conference on Earthquake Engineering*.

Theodulidis N, Kalogeras I, Papazachos C, Karastathis V, Margaris B, Papaioannou Ch, Skarlatoudis A (2004). HEAD 1.0: A Unified HEllenic Accelerogram Database. *Seismol. Res. Lett.* 75, 36-45.

Traversa P, Akkar S, Ameri G, Cotton F, Douglas J, Frobert L, Godey S, Hernandez B, Luzi L, Sandikkaya MA (2014). REference databaSe fOR seismiC groundmotion in Europe. *Second European Conference on Earthquake Engineering and Seismology, İstanbul, Turkey*.

Tromans IJ and Bommer JJ (2002). The attenuation of strong-motion peaks in Europe. *In: Proceedings of Twelfth European Conference on Earthquake Engineering*, Paper no.394.

Ulusay R, Tuncay E, Sonmez H, Gokceoglu C (2004). An attenuation relationship based on Turkish strong motion data and iso-acceleration map of Turkey. *Eng. Geol.* 74, no. 3-4, 265-291.

Ulutaş E and Özer MF (2010). Empirical attenuation relationship of peak ground acceleration for eastern Marmara region in Turkey. *The Arabian Journal for Science and Engineering* 35, no. 1A, 187-203.

Wells DL and Coppersmith KJ (1994). New empirical relationships among magnitude, rupture length, rupture width, rupture area, and surface displacement. *Bull. Seismol. Soc. Am*. 84, 974-1002.

Yenier E and Atkinson GM (2014). Equivalent Point-Source Modeling of Moderate-to-Large Magnitude Earthquakes and Associated Ground-Motion Saturation Effects. *Bull. Seismol. Soc. Am.* 104, no. 3, 1458-1478.

Yenier E, Sandıkkaya MA, Akkar S (2010). Report on the fundamental features of the extended strong motion databank prepared for the SHARE project. *pp. 44. Deliverable 4.1 of Seventh Framework Programme Project Seismic Hazard Harmonization in Europe (SHARE)*, 34 pages, Ankara.

Youngs RR, Chiou BS-J, Silva WJ, Humphrey JR (1997). Strong ground motion attenuation relationships for subduction zone earthquakes. *Seismol. Res. Lett.* 68, 58-73.

Zafarani H, Hassani B, Ansari A (2012). Estimation of earthquake parameters in the Alborz seismic zone, Iran using generalized inversion method. *Soil Dynam. Earthquake Eng.* 42, 197-218.

Zafarani H and Soghrat M (2012). Simulation of Ground Motion in the Zagros Region of Iran Using the Specific Barrier Model and the Stochastic Method. *Bull. Seismol. Soc. Am.* 102, no. 5, 2031-2045.

Zare M, Amini H, Yazdi P, Sesetyan K, Demircioglu MB, Kalafat D, Erdik M Giardini D, Khan MA, Tsereteli N (2014). Recent developments of the Middle East catalog, *Journal of Seismology* 18, 749-772.

Zare M, Ghafory-Ashtiany M, Bard P-Y (1999). Attenuation law for the strong-motions in Iran. *Proceedings of the Third International Conference on Seismology and Earthquake Engineering, Tehran* 1, 345-354.

Zare M and Sabzali S (2006). Spectral attenuation of strong motions in Iran. *Proceedings of Third International Symposium on the Effects of Surface Geology on Seismic Motion*, Paper no 146, 749-758.

Zhao JX, Zhang J, Asano A, Ohno Y, Oouchi T, Takahashi T, Ogawa H, Irikura K, Thio HK, Somerville PG, Fukushima Y (2006). Attenuation relations of strong ground motion in Japan using site classification based on predominant period. *Bull. Seismol. Soc. Am.* 96, no. 3, 898-913.

APPENDIX A

ENTIRE LIST OF THE REGRESSION COEFFICIENTS OF THE PROPOSED GMPE

This appendix provides the entire list of the regression coefficients of the ground-motion prediction equation given in Chapter 3 of this thesis.

Table A.1 Period-dependent f_{site} coefficients (Sandıkkaya et al., 2013).

Period (s)	sb$_1$	sb$_2$	Period (s)	sb$_1$	sb$_2$
PGA	-0.41997	-0.28846	0.48	-0.94384	-0.38532
PGV	-0.72057	-0.19688	0.5	-0.95097	-0.37956
0.01	-0.41729	-0.28685	0.55	-0.96584	-0.36610
0.02	-0.39998	-0.28241	0.6	-0.97746	-0.35382
0.03	-0.34799	-0.26842	0.65	-0.98670	-0.34252
0.04	-0.27572	-0.24759	0.7	-0.99416	-0.33206
0.05	-0.21231	-0.22385	0.75	-1.00027	-0.32233
0.075	-0.13909	-0.17798	0.8	-1.00532	-0.31322
0.1	-0.26492	-0.28832	0.85	-1.00956	-0.30466
0.11	-0.31346	-0.31798	0.9	-1.01314	-0.29659
0.12	-0.36002	-0.34246	0.95	-1.01619	-0.28896
0.13	-0.40424	-0.36297	1	-1.01881	-0.28172
0.14	-0.44592	-0.38036	1.1	-1.01720	-0.26827
0.15	-0.48496	-0.39525	1.2	-1.00204	-0.25599
0.16	-0.52137	-0.40811	1.3	-0.98810	-0.24469
0.17	-0.55520	-0.41930	1.4	-0.97519	-0.23423
0.18	-0.58656	-0.42911	1.5	-0.96317	-0.22449
0.19	-0.61558	-0.43774	1.6	-0.95193	-0.21538
0.2	-0.64239	-0.44574	1.7	-0.94136	-0.20682
0.22	-0.69002	-0.45499	1.8	-0.93141	-0.19876
0.24	-0.73062	-0.45939	1.9	-0.92199	-0.19112
0.26	-0.76530	-0.45988	2	-0.91305	-0.18388
0.28	-0.79499	-0.45739	2.2	-0.89645	-0.17043
0.3	-0.82052	-0.45287	2.4	-0.88129	-0.15815
0.32	-0.84256	-0.44255	2.6	-0.86735	-0.14685
0.34	-0.86167	-0.43399	2.8	-0.85444	-0.13639
0.36	-0.87832	-0.42592	3	-0.84242	-0.12665
0.38	-0.89288	-0.41829	3.2	-0.83118	-0.11754
0.4	-0.90568	-0.41105	3.4	-0.82062	-0.10899
0.42	-0.91697	-0.40417	3.6	-0.81066	-0.10092
0.44	-0.92698	-0.39760	3.8	-0.80124	-0.09329
0.46	-0.93589	-0.39133	4	-0.79231	-0.08605

232

Table A.2 Period-dependent sigma coefficients (Δ values in parenthesis designate the differences in the regression coefficients between Turkey and Iran).

Period (s)	a_1 (Δa_1)	a_2 (Δa_2)	sd_1 (Δsd_1)	sd_2 (Δsd_2)
PGA	0.57 (0.12)	0.45 (0.05)	1.0521 (-0.0808)	0.7203 (-0.325)
PGV	0.56 (0.14)	0.46 (-0.02)	1.0449 (-0.0597)	0.6452 (-0.3013)
0.01	0.574 (0.116)	0.453 (0.047)	1.0444 (-0.0723)	0.715 (-0.3231)
0.02	0.577 (0.113)	0.455 (0.045)	1.0424 (-0.0701)	0.7137 (-0.318)
0.03	0.581 (0.109)	0.458 (0.042)	1.0459 (-0.0705)	0.7113 (-0.3143)
0.04	0.584 (0.106)	0.46 (0.04)	1.0557 (-0.0597)	0.7155 (-0.3064)
0.05	0.588 (0.122)	0.463 (0.037)	1.0609 (-0.07)	0.7166 (-0.277)
0.075	0.597 (0.143)	0.469 (0.031)	1.0692 (-0.0994)	0.7677 (-0.3045)
0.1	0.606 (0.154)	0.475 (0.025)	1.0429 (-0.0486)	0.7735 (-0.3358)
0.11	0.61 (0.15)	0.478 (0.022)	1.0324 (-0.0299)	0.7871 (-0.3353)
0.12	0.613 (0.147)	0.48 (0.02)	1.0208 (-0.0134)	0.7783 (-0.3139)
0.13	0.617 (0.143)	0.483 (0.007)	1.0216 (0.007)	0.7598 (-0.2962)
0.14	0.621 (0.139)	0.485 (-0.005)	1.0194 (0.0126)	0.7517 (-0.276)
0.15	0.624 (0.136)	0.488 (-0.018)	1.0063 (0.0394)	0.7442 (-0.2839)
0.16	0.628 (0.132)	0.49 (-0.03)	0.998 (0.0701)	0.738 (-0.2872)
0.17	0.631 (0.129)	0.493 (-0.043)	0.9896 (0.0827)	0.7484 (-0.2998)
0.18	0.635 (0.125)	0.495 (-0.045)	0.9854 (0.0952)	0.7472 (-0.3074)
0.19	0.639 (0.121)	0.498 (-0.048)	0.9801 (0.0998)	0.731 (-0.2957)
0.2	0.642 (0.118)	0.5 (-0.05)	0.9781 (0.1081)	0.7213 (-0.305)
0.22	0.649 (0.111)	0.505 (-0.055)	0.9712 (0.1097)	0.712 (-0.2934)
0.24	0.657 (0.103)	0.51 (-0.06)	0.9699 (0.0932)	0.6901 (-0.2827)
0.26	0.664 (0.096)	0.515 (-0.065)	0.9611 (0.088)	0.6732 (-0.2711)
0.28	0.671 (0.089)	0.52 (-0.07)	0.9466 (0.0956)	0.6714 (-0.2806)
0.3	0.678 (0.082)	0.525 (-0.075)	0.9407 (0.0759)	0.6547 (-0.2651)
0.32	0.686 (0.074)	0.53 (-0.08)	0.9515 (0.0568)	0.6515 (-0.2734)
0.34	0.693 (0.067)	0.535 (-0.085)	0.9448 (0.0578)	0.649 (-0.2567)
0.36	0.7 (0.06)	0.54 (-0.09)	0.9344 (0.0643)	0.6545 (-0.2637)
0.38	0.7 (0.06)	0.545 (-0.095)	0.9406 (0.056)	0.6504 (-0.2487)
0.4	0.7 (0.06)	0.55 (-0.1)	0.943 (0.0563)	0.6413 (-0.2308)
0.42	0.695 (0.065)	0.55 (-0.1)	0.9449 (0.0541)	0.6316 (-0.2137)
0.44	0.689 (0.071)	0.55 (-0.1)	0.9444 (0.0506)	0.6357 (-0.2121)
0.46	0.684 (0.076)	0.55 (-0.1)	0.9438 (0.0435)	0.6483 (-0.2137)

Table A.2 Cont'd.

Period (s)	a_1 (Δa_1)	a_2 (Δa_2)	sd_1 (Δsd_1)	sd_2 (Δsd_2)
0.48	0.679 (0.081)	0.55 (-0.1)	0.9441 (0.0316)	0.6528 (-0.1932)
0.5	0.673 (0.087)	0.55 (-0.1)	0.9519 (0.0209)	0.6496 (-0.1724)
0.55	0.66 (0.1)	0.55 (-0.1)	0.995 (-0.0014)	0.6487 (-0.1709)
0.6	0.647 (0.113)	0.55 (-0.1)	1.0137 (0)	0.6535 (-0.2182)
0.65	0.633 (0.127)	0.55 (-0.1)	1.0208 (-0.0038)	0.6655 (-0.2325)
0.7	0.62 (0.14)	0.55 (-0.1)	1.0406 (-0.0085)	0.6683 (-0.2522)
0.75	0.62 (0.14)	0.55 (-0.0875)	1.0489 (-0.0161)	0.6582 (-0.2379)
0.8	0.62 (0.14)	0.55 (-0.075)	1.0375 (-0.0119)	0.6562 (-0.2272)
0.85	0.62 (0.15)	0.55 (-0.0625)	1.0394 (-0.027)	0.647 (-0.235)
0.9	0.62 (0.16)	0.55 (-0.05)	1.0423 (-0.0403)	0.6488 (-0.273)
0.95	0.62 (0.16)	0.55 (-0.0375)	1.0512 (-0.0595)	0.6383 (-0.2706)
1	0.62 (0.16)	0.55 (-0.025)	1.0534 (-0.0793)	0.6342 (-0.2569)
1.1	0.62 (0.16)	0.55 (0)	1.0679 (-0.1023)	0.6204 (-0.2664)
1.2	0.62 (0.16)	0.55 (0.025)	1.0859 (-0.1188)	0.625 (-0.2623)
1.3	0.62 (0.16)	0.55 (0.05)	1.0731 (-0.117)	0.6291 (-0.2512)
1.4	0.62 (0.16)	0.55 (0.05)	1.0873 (-0.1313)	0.6199 (-0.2496)
1.5	0.62 (0.16)	0.55 (0.05)	1.0988 (-0.1337)	0.6173 (-0.2358)
1.6	0.62 (0.16)	0.55 (0.05)	1.1058 (-0.1317)	0.612 (-0.2193)
1.7	0.62 (0.16)	0.55 (0.05)	1.1108 (-0.1408)	0.5923 (-0.205)
1.8	0.62 (0.16)	0.55 (0.05)	1.1301 (-0.1764)	0.5859 (-0.1834)
1.9	0.62 (0.16)	0.55 (0.05)	1.1503 (-0.2051)	0.5787 (-0.1626)
2	0.62 (0.16)	0.55 (0.05)	1.1594 (-0.2183)	0.5724 (-0.1482)
2.2	0.62 (0.16)	0.55 (0.05)	1.16 (-0.2181)	0.5943 (-0.1665)
2.4	0.62 (0.16)	0.55 (0.05)	1.1567 (-0.2186)	0.61 (-0.165)
2.6	0.62 (0.16)	0.55 (0.05)	1.1543 (-0.2273)	0.6053 (-0.1535)
2.8	0.62 (0.16)	0.55 (0.05)	1.1563 (-0.2228)	0.6098 (-0.1372)
3	0.62 (0.16)	0.55 (0.05)	1.1596 (-0.2262)	0.6251 (-0.1356)
3.2	0.62 (0.16)	0.55 (0.05)	1.1615 (-0.2261)	0.6362 (-0.1266)
3.4	0.62 (0.16)	0.55 (0.05)	1.1266 (-0.2638)	0.636 (-0.1887)
3.6	0.62 (0.16)	0.55 (0.05)	1.093 (-0.2538)	0.6231 (-0.183)
3.8	0.62 (0.16)	0.55 (0.05)	1.0749 (-0.2603)	0.6244 (-0.1667)
4	0.62 (0.16)	0.55 (0.05)	1.0373 (-0.2279)	0.5409 (-0.0862)

Table A.3 Period-dependent regression coefficients of the ground-motion model (Δ values in parenthesis designate the differences in the regression coefficients between Turkey and Iran)

Period (s)	b_1 (Δb_1)	b_3 (Δb_3)	b_4 (Δb_4)	b_8 (Δb_8)	b_9 (Δb_9)	b_{10} (Δb_{10})
PGA	1.74221 (-0.21234)	-0.07049 (-0.03826)	-1.18164 (0.1721)	-0.01329 (-0.11697)	-0.09158 (0)	-0.00156 (0.00156)
PGV	5.58266 (0.20834)	-0.13822 (-0.05505)	-0.94043 (0.04886)	-0.17037 (0.17037)	-0.08609 (0)	-0.00052 (0.00052)
0.01	1.75746 (-0.22738)	-0.06981 (-0.03877)	-1.18362 (0.17408)	-0.01349 (-0.11677)	-0.09158 (0)	-0.00156 (0.00156)
0.02	1.78825 (-0.241)	-0.07058 (-0.03674)	-1.18653 (0.17587)	-0.01189 (-0.11837)	-0.09158 (0)	-0.0016 (0.0016)
0.03	1.87916 (-0.25702)	-0.06976 (-0.0337)	-1.19699 (0.16911)	-0.00748 (-0.12278)	-0.09158 (0)	-0.0017 (0.0017)
0.04	2.00393 (-0.2526)	-0.06732 (-0.0285)	-1.21315 (0.16032)	0.00788 (-0.13814)	-0.09158 (0)	-0.00182 (0.00182)
0.05	2.16076 (-0.24029)	-0.06226 (-0.02834)	-1.24101 (0.16138)	0.03907 (-0.16933)	-0.09158 (0)	-0.00197 (0.00197)
0.075	2.52625 (-0.13086)	-0.05082 (-0.03978)	-1.3039 (0.16548)	0.08131 (-0.21157)	-0.09158 (0)	-0.00235 (0.00235)
0.1	2.72364 (-0.02321)	-0.05217 (-0.03843)	-1.32996 (0.15961)	0.1 (-0.23026)	-0.09158 (0)	-0.00267 (0.00267)
0.11	2.79879 (-0.05859)	-0.05423 (-0.03653)	-1.33631 (0.17102)	0.1 (-0.23026)	-0.09158 (0)	-0.00277 (0.00277)
0.12	2.87745 (-0.1335)	-0.05676 (-0.03451)	-1.34267 (0.18621)	0.1 (-0.23026)	-0.09158 (0)	-0.00285 (0.00285)
0.13	2.89671 (-0.16885)	-0.05922 (-0.03456)	-1.33525 (0.19374)	0.095 (-0.22526)	-0.09158 (0)	-0.00291 (0.00291)
0.14	2.91231 (-0.20629)	-0.06162 (-0.03478)	-1.32731 (0.20038)	0.08169 (-0.21195)	-0.09158 (0)	-0.00295 (0.00295)
0.15	2.91835 (-0.23382)	-0.06397 (-0.03475)	-1.31888 (0.20607)	0.06727 (-0.19753)	-0.09158 (0)	-0.00296 (0.00296)
0.16	2.92057 (-0.26156)	-0.06626 (-0.03524)	-1.30999 (0.21079)	0.0546 (-0.18486)	-0.09158 (0)	-0.00295 (0.00295)
0.17	2.9155 (-0.28983)	-0.0685 (-0.03551)	-1.30069 (0.21458)	0.04338 (-0.17364)	-0.09158 (0)	-0.00292 (0.00292)
0.18	2.90336 (-0.31207)	-0.07069 (-0.03578)	-1.29102 (0.21744)	0.03335 (-0.16361)	-0.09158 (0)	-0.00288 (0.00288)
0.19	2.88447 (-0.32851)	-0.07284 (-0.03605)	-1.28102 (0.21942)	0.02435 (-0.15461)	-0.09158 (0)	-0.00282 (0.00282)
0.2	2.85623 (-0.33645)	-0.07494 (-0.03634)	-1.27072 (0.22054)	0.0162 (-0.14646)	-0.09158 (0)	-0.00275 (0.00275)
0.22	2.78548 (-0.34013)	-0.07902 (-0.03692)	-1.24942 (0.22046)	0.00201 (-0.08594)	-0.09158 (0)	-0.00258 (0.00258)
0.24	2.70779 (-0.3387)	-0.08294 (-0.03752)	-1.22742 (0.2176)	-0.00996 (-0.02889)	-0.09158 (0)	-0.0024 (0.0024)

Table A.3 Cont'd.

Period (s)	b_1 (Δb_1)	b_3 (Δb_3)	b_4 (Δb_4)	b_8 (Δb_8)	b_9 (Δb_9)	b_{10} (Δb_{10})
0.26	2.62349 (-0.33138)	-0.08672 (-0.03813)	-1.20502 (0.21242)	-0.02021 (0.02021)	-0.09158 (0)	-0.00226 (0.00226)
0.28	2.53452 (-0.31901)	-0.09036 (-0.03875)	-1.1825 (0.20538)	-0.02913 (0.02913)	-0.09158 (0)	-0.00215 (0.00215)
0.3	2.44252 (-0.30222)	-0.09387 (-0.03939)	-1.16008 (0.19687)	-0.03697 (0.03697)	-0.09158 (0.00185)	-0.00204 (0.00204)
0.32	2.34886 (-0.28152)	-0.09726 (-0.04003)	-1.13796 (0.18725)	-0.04395 (0.04395)	-0.09158 (0.00975)	-0.00194 (0.00194)
0.34	2.25469 (-0.25734)	-0.10054 (-0.04068)	-1.11632 (0.17687)	-0.05021 (0.05021)	-0.09158 (0.02148)	-0.00185 (0.00185)
0.36	2.16096 (-0.23009)	-0.10372 (-0.04132)	-1.09527 (0.16596)	-0.05588 (0.05588)	-0.09158 (0.04408)	-0.00177 (0.00177)
0.38	2.06843 (-0.20013)	-0.10679 (-0.04198)	-1.07492 (0.15478)	-0.06106 (0.06106)	-0.09158 (0.06881)	-0.00168 (0.00168)
0.4	1.97772 (-0.16785)	-0.10977 (-0.04263)	-1.05535 (0.1435)	-0.06582 (0.06582)	-0.09158 (0.09158)	-0.00161 (0.00161)
0.42	1.88929 (-0.13363)	-0.11266 (-0.04328)	-1.03659 (0.13226)	-0.07021 (0.07021)	-0.09158 (0.09158)	-0.00153 (0.00153)
0.44	1.8035 (-0.09787)	-0.11547 (-0.04393)	-1.01869 (0.12119)	-0.0743 (0.0743)	-0.0807 (0.0807)	-0.00146 (0.00146)
0.46	1.72061 (-0.06098)	-0.11819 (-0.04458)	-1.00165 (0.11037)	-0.07813 (0.07813)	-0.05565 (0.05565)	-0.0014 (0.0014)
0.48	1.64078 (-0.02333)	-0.12084 (-0.04522)	-0.98547 (0.09987)	-0.08172 (0.08172)	-0.03289 (0.03289)	-0.00133 (0.00133)
0.5	1.5641 (0.01469)	-0.12342 (-0.04586)	-0.97014 (0.08974)	-0.08511 (0.08511)	-0.01297 (0.01297)	-0.00127 (0.00127)
0.55	1.38635 (0.10888)	-0.12955 (-0.04745)	-0.93538 (0.06616)	-0.09286 (0.09286)	0 (0)	-0.00113 (0.00113)
0.6	1.22784 (0.19792)	-0.1353 (-0.049)	-0.90533 (0.04522)	-0.0998 (0.0998)	0 (0)	-0.00099 (0.00099)
0.65	1.08684 (0.27818)	-0.1407 (-0.05051)	-0.87944 (0.02683)	-0.10613 (0.10613)	0 (0)	-0.00087 (0.00087)
0.7	0.96118 (0.34767)	-0.14577 (-0.052)	-0.85717 (0.01081)	-0.11201 (0.11201)	0 (0)	-0.00076 (0.00076)
0.75	0.84856 (0.40612)	-0.15056 (-0.05345)	-0.83799 (-0.00312)	-0.11756 (0.11756)	0 (0)	-0.00066 (0.00066)
0.8	0.74687 (0.45455)	-0.15509 (-0.05485)	-0.82143 (-0.01521)	-0.12285 (0.12285)	0 (0)	-0.00056 (0.00056)
0.85	0.6543 (0.49481)	-0.15938 (-0.05621)	-0.80711 (-0.02571)	-0.12796 (0.12796)	0 (0)	-0.00047 (0.00047)
0.9	0.56939 (0.5291)	-0.16345 (-0.05754)	-0.79468 (-0.03485)	-0.13293 (0.13293)	0 (0)	-0.00038 (0.00038)
0.95	0.49101 (0.55941)	-0.16731 (-0.05883)	-0.78385 (-0.04282)	-0.13782 (0.13782)	0 (0)	-0.0003 (0.0003)

Table A.3 Cont'd.

Period (s)	b_1 (Δb_1)	b_3 (Δb_3)	b_4 (Δb_4)	b_8 (Δb_8)	b_9 (Δb_9)	b_{10} (Δb_{10})
1	0.41833 (0.58724)	-0.17099 (-0.06008)	-0.77438 (-0.04979)	-0.14267 (0.14267)	0 (0)	-0.00022 (0.00022)
1.1	0.28765 (0.63819)	-0.17784 (-0.06247)	-0.75874 (-0.06129)	-0.14621 (0.14621)	0 (0)	-0.00008 (0.00008)
1.2	0.17365 (0.68187)	-0.18409 (-0.06473)	-0.74652 (-0.07024)	-0.14621 (0.14621)	0 (0)	0 (0)
1.3	0.07306 (0.71463)	-0.18983 (-0.06684)	-0.73683 (-0.07731)	-0.14621 (0.14621)	0 (0)	0 (0)
1.4	-0.01759 (0.73649)	-0.19511 (-0.06884)	-0.72905 (-0.08295)	-0.14621 (0.14621)	0 (0)	0 (0)
1.5	-0.10161 (0.75311)	-0.19999 (-0.07073)	-0.72272 (-0.08751)	-0.14621 (0.14621)	0 (0)	0 (0)
1.6	-0.18105 (0.77054)	-0.20452 (-0.07251)	-0.71752 (-0.09124)	-0.14621 (0.14621)	0 (0)	0 (0)
1.7	-0.25586 (0.78844)	-0.20873 (-0.0742)	-0.71319 (-0.09432)	-0.14621 (0.14621)	0 (0)	0 (0)
1.8	-0.32454 (0.80172)	-0.21266 (-0.07579)	-0.70957 (-0.09687)	-0.14621 (0.14621)	0 (0)	0 (0)
1.9	-0.38743 (0.81363)	-0.21633 (-0.0773)	-0.7065 (-0.09902)	-0.14621 (0.14621)	0 (0)	0 (0)
2	-0.45413 (0.83361)	-0.21978 (-0.07873)	-0.70389 (-0.10083)	-0.14621 (0.14621)	0 (0)	0 (0)
2.2	-0.58191 (0.87641)	-0.22606 (-0.08139)	-0.6997 (-0.10372)	-0.14621 (0.14621)	0 (0)	0 (0)
2.4	-0.68595 (0.89547)	-0.23166 (-0.08378)	-0.69654 (-0.10586)	-0.14621 (0.14621)	0 (0)	0 (0)
2.6	-0.78166 (0.90619)	-0.23667 (-0.08597)	-0.6941 (-0.10749)	-0.14621 (0.14621)	0 (0)	0 (0)
2.8	-0.87027 (0.90982)	-0.24119 (-0.08796)	-0.69218 (-0.10875)	-0.14621 (0.14621)	0 (0)	0 (0)
3	-0.95276 (0.90733)	-0.2453 (-0.08977)	-0.69065 (-0.10974)	-0.14621 (0.14621)	0 (0)	0 (0)
3.2	-1.02993 (0.89952)	-0.24903 (-0.09145)	-0.6894 (-0.11054)	-0.14621 (0.14621)	0 (0)	0 (0)
3.4	-1.10242 (0.88703)	-0.25246 (-0.09299)	-0.68837 (-0.11119)	-0.14621 (0.14621)	0 (0)	0 (0)
3.6	-1.17077 (0.87039)	-0.2556 (-0.09442)	-0.68752 (-0.11172)	-0.14621 (0.14621)	0 (0)	0 (0)
3.8	-1.23542 (0.85006)	-0.2585 (-0.09574)	-0.68681 (-0.11215)	-0.14621 (0.14621)	0 (0)	0 (0)
4	-1.29675 (0.82641)	-0.26119 (-0.09696)	-0.6862 (-0.11252)	-0.14621 (0.14621)	0 (0)	0 (0)

APPENDIX B

CLARIFICATION OF SELECTING SMALL-SIGMA PREDICTIVE MODEL BY EDR METHOD

Adapted from Akkar S and Kale Ö (2014). Reply to "Comment on 'A New Procedure for Selecting and Ranking Ground-Motion Prediction Equations (GMPEs): The Euclidean Distance-Based Ranking (EDR) Method' by Özkan Kale and Sinan Akkar" by Sum Mak, Robert Alan Clements and Danijel Schorlemmer. Bulletin of the Seismological Society of America, in press.

The MDE component of EDR method (Kale and Akkar, 2013) considers the discrete occurrence probabilities of absolute differences between the logarithms of observed data (*a*) and a range of ground-motion estimates (y_j, $j = 1,…,N$) computed from a ground-motion prediction equation (GMPE). The logarithms of ground-motion estimates (y_j) as well as the differences between the logarithms of observed data and ground-motion estimates ($d_j = a - y_j$) are assumed to be normally distributed. This concept is illustrated in Figure B.1.a. Figure B.1.b shows the assumed normal distribution of discrete differences given in Figure B.1.a. The parameter *D* is used as the random variable for representing the logarithmic differences. The mean and standard deviation of this distribution are designated as μ_D and σ_D, respectively. σ_D is equal to the total standard deviation of the considered GMPE (σ_{GMPE}) as given in Equation (4.3.b) in Chapter 4. Note that when the computed difference is zero, the observed data point and the ground-motion estimate are equal to each other. The ground-motion estimates are

computed by considering a predetermined range of σ_D. Since σ_D and σ_{GMPE} are equal to each other, the sigma range mimics the randomness in ground motions and the way it is handled by GMPEs. The use of $\pm 3\sigma_D$ about μ_D is proposed to account for randomness in ground motions and the effect of σ_{GMPE} on ground-motion estimates. The corresponding upper and lower bound d_j values are designated as d_{max} in this procedure. Therefore, d_1 and d_N in Figures B.1.a and B.1.b are the upper and lower bound d_{max} values of the MDE illustration.

The logarithmic differences of observed and estimated ground motions are analogous to residual analysis. For a set of discrete differences (i.e., $d_j, j = 1,..,N$), the occurrence probability of any difference within an infinitesimal bandwidth, dd, is

$$Pr\left(-\frac{dd}{2} < D - d_j < \frac{dd}{2}\right)$$

(B.1)

The shaded area in Figure B.1.b shows the probability in Equation (B.1). However, the Euclidean distance based approach is preferred in this method as it yields non-negative differences between the observed data and ground-motion estimates, which make it more suitable for an index definition. Thus, the above probability expression is modified as

$$Pr\left(-\frac{dd}{2} < |D| - |d_j| < \frac{dd}{2}\right)$$

(B.2)

The explicit form of Equation (B.2) is given in Equation (B.3).

$$
\begin{aligned}
Pr&\left(|d_j| - \frac{dd}{2} < |D| < |d_j| + \frac{dd}{2}\right) \\
&= Pr\left(|D| < |d_j| + \frac{dd}{2}\right) - Pr\left(|D| < |d_j| - \frac{dd}{2}\right) \\
&= Pr\left(-|d_j| - \frac{dd}{2} < D < |d_j| + \frac{dd}{2}\right) - Pr\left(-|d_j| + \frac{dd}{2} < D < |d_j| - \frac{dd}{2}\right)
\end{aligned}
$$

(B.3)
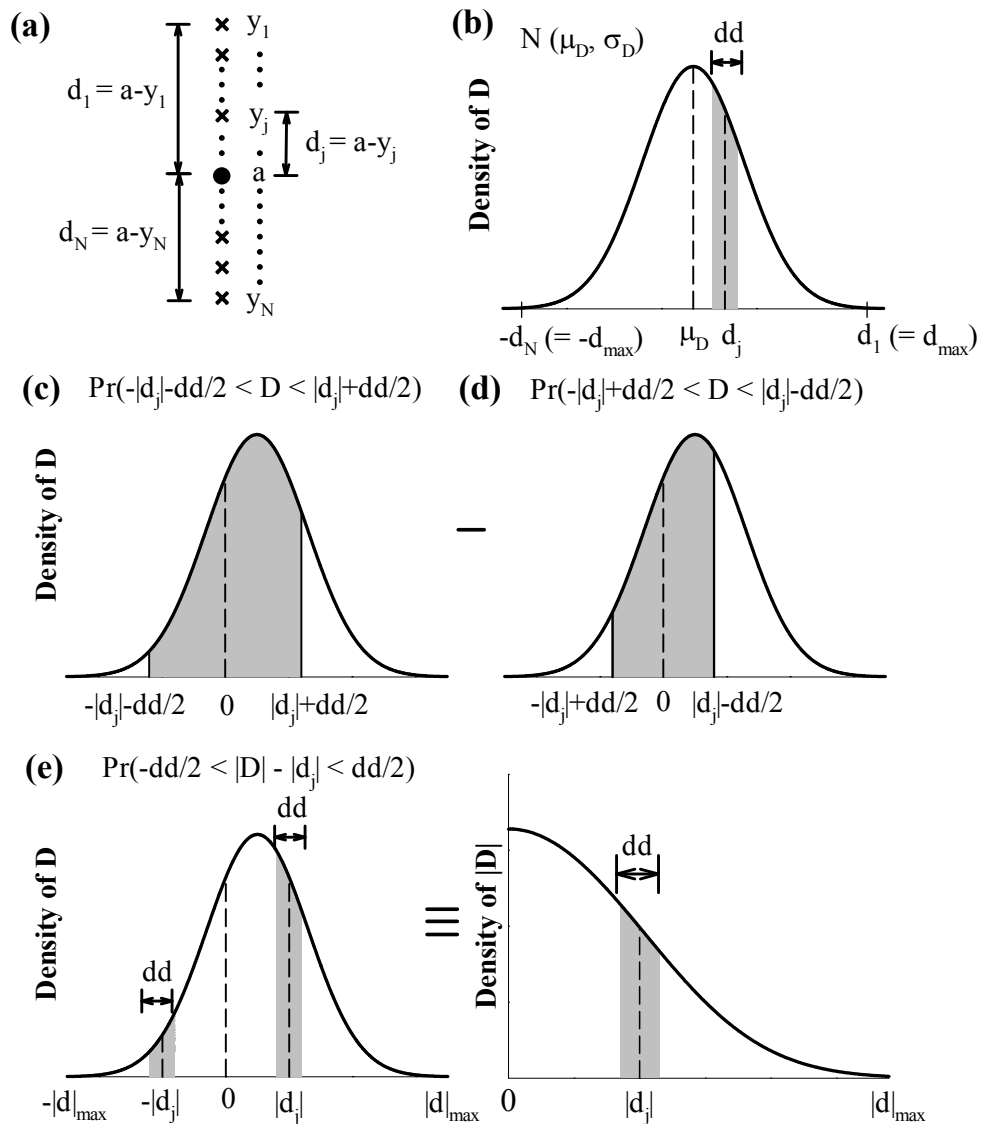
Figure B.1 Conceptual illustration of MDE for a single data point in a given ground-motion database.

The graphical illustrations of first and second terms in Equation (B.3) are given in Figures 4.3.a and 4.3.b in Chapter 4. Their difference is the occurrence probability of $|d_j|$ within the interval dd as given in Equation (B.2). This occurrence probability in terms of D and $|D|$ are given in Figures 4.3.c and 4.3.d in Chapter 4, respectively. For completeness, Figures B.1.c and B.1.d show the graphical illustration of each term in Equation (B.3). Figure B.1.e displays the difference between these terms

that essentially yields the intervals considered while computing the occurrence probability of $|d_j|$ within a bandwidth dd in MDE.

The occurrence probabilities of $|d_j|$ are the integral component of MDE index and their contribution underlines the likelihood of the differences between the observed data point and ground-motion estimates of the considered GMPE. It is believed that consideration of $|d_j|$ together with their occurrence probabilities, which results in a weighted average is a viable index for the evaluation of GMPEs for a given ground-motion dataset.

MDE score is low for the predictive model with smaller standard deviation when the median estimates of candidate GMPEs are very close to each other. This case is discussed in Chapter 4 via Figure 4.6 for two fictitious GMPEs designated as Model 1 and Model 2. Both GMPEs have the same median but the standard deviation of Model 2 is larger with respect to the other GMPE. Figure 4.6 in Chapter 4 is given in a different format in Figure B.2 in this section. The normal distributions that account for the occurrence probability of logarithmic differences, d_j, for these models have the same μ_D because both GMPEs give the same median estimate for the observed data point. The MDE score of Model 2 will be larger than that of Model 1 for this case because the occurrence probabilities of large $|d_j|$ values will be higher for Model 2. This fact is also illustrated in Figure B.2. As indicated, the lower MDE score for small-sigma GMPE is conditional on the similarity of median ground-motion estimates of candidate predictive models.

GMPEs constitute a set of functions in terms of main seismological estimator parameters to describe the ground-motion amplitudes of the complicated earthquake process. Their modeling limitations to estimate future ground motions should be considered carefully in their evaluation. Given a ground-motion database, a predictive model that yields larger occurrence probabilities to capture the outliers in the database does not warranty its better performance. To this end, the cases in which standard deviation of predictive model coincides with that of the

database would be meaningful only in the statistical sense. It fails to represent the current practice. More specifically, testing and ranking of GMPEs is a multidimensional problem. The MDE component of the proposed procedure measures the performance of candidate GMPEs in terms of modeling the uncertainty in ground-motion estimates. This fact is shown by the case study described in the following paragraphs.
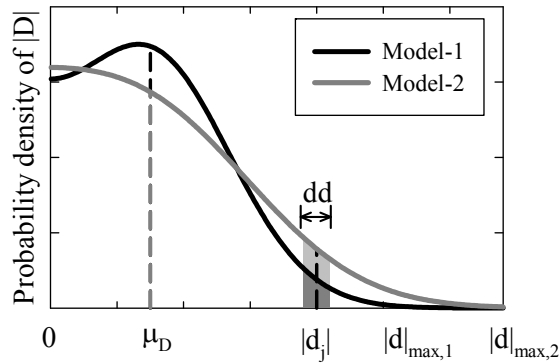
Figure B.2 Probability density functions of absolute differences for two GMPEs that have the same median ground-motion estimates. The sigma of Model 2 is larger than that of Model 1. The occurrence probability of $|d_j|$ for Model 2 is the sum of light and dark gray areas. The occurrence probability of $|d_j|$ for Model 1 is the dark gray area.

Three strong-motion databases are simulated by constraining the magnitude, site class and faulting mechanism. The simulated datasets are generated by introducing different levels of uncertainty to the median rock PGA estimates of Akkar et al. (2014) for strike-slip earthquakes of M_w 7. The datasets are simulated for random source-to-site distances that take values less than 100 km. The databases are opted to represent the realistic trends of strong-motion data in the current GMPE studies. They are constrained to magnitude, site class and fault type because the aim is to develop simple models from each one of these datasets to estimate the distance-dependent variation of PGAs and their associated uncertainties (σ_{GMPE}). It is believed that constrained, but as realistic as possible, datasets together with simple functional forms showing the overall features of each dataset simplify our

243

discussions on the topic of interest. Equation (B.4) shows the generic functional form used in the models. The standard deviations of these databases and the models developed from them are not the same at any distance bin. This observation is frequently experienced by the GMPE developers.

$$ln(\,PGA\,) = b_1 + b_2\,ln\,\sqrt{R^2 + 8^2} + \varepsilon\sigma_{GMPE} \qquad\qquad (B.4)$$

Figure B.3 shows the distance-dependent variations of each database and median $\pm$ σ_{GMPE} estimates of corresponding ground-motion equations. Note that Model 2 has the largest σ_{GMPE} as the corresponding database shows more dispersive features (Figure B.3.b). The median PGA estimates of Model 1 and Model 2 almost overlap each other (Figure B.3.d) as the corresponding databases picture similar median trends with different dispersion characteristics. Model 3 yields the lowest median PGA estimates as the overall data pattern shows smaller PGA amplitudes with respect to other two databases.
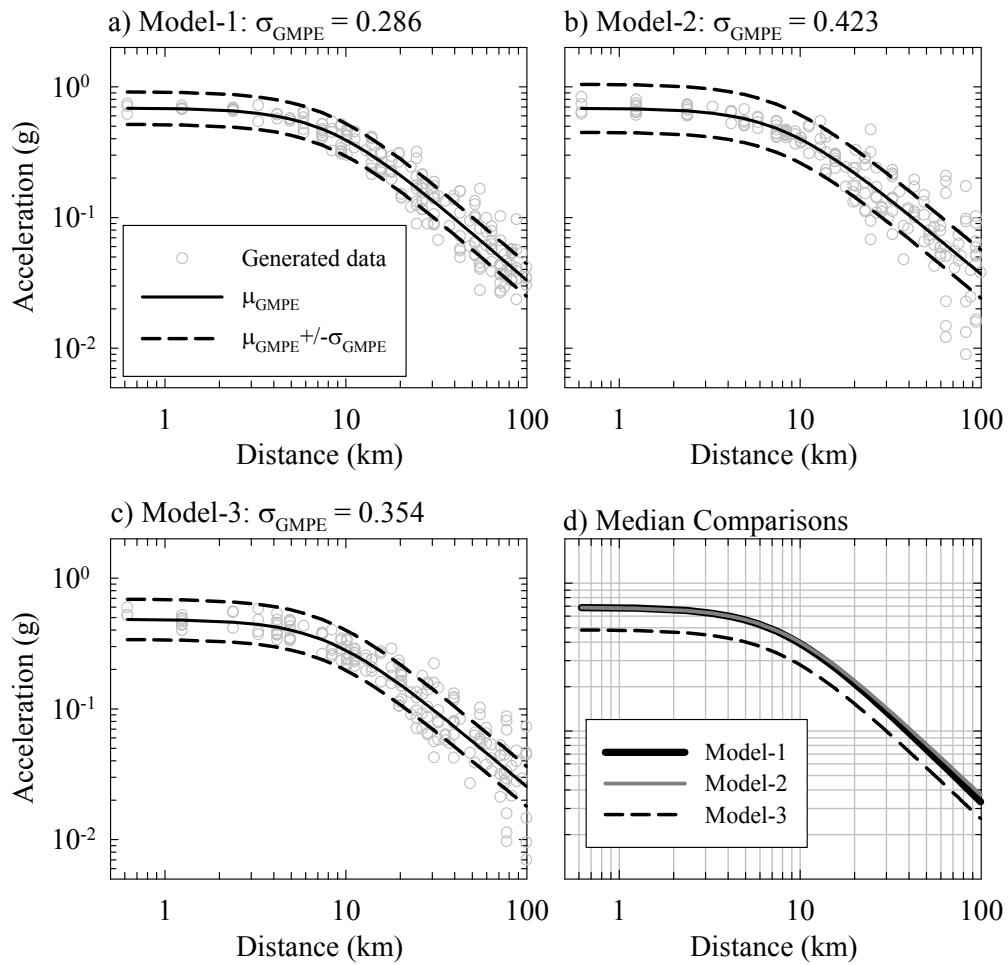
Figure B.3 GMPEs developed from simulated datasets and their median comparisons.

An independent database is simulated for testing and ranking of the three GMPEs given in Figure B.3. The independent dataset is also constrained to the rock PGA estimates of Akkar et al. (2014) GMPE for M_w 7 and strike-slip fault mechanism. The randomness and overall PGA trends in this new database is a compromise of uncertainty levels in the previously simulated three datasets. Table B.1 shows the corresponding MDE results whereas Figure B.4 shows the details of MDE calculations for an arbitrary data point from the independent database. The MDE scores are computed for $\pm 3\sigma_D$ as suggested in Chapter 4. Note that σ_D corresponds to the standard deviation of each predictive model as stated previously. The listed MDE scores in Table B.1 suggest the better performance of Model 3 for the test-

bed database. The MDE score of Model 3 is followed by those of Model 1 and Model 2. The latter two models are similar in median PGA estimations (Figure B.3.d) with $\sigma_{GMPE1} < \sigma_{GMPE2}$. The standard deviation of Model 3 takes a value between σ_{GMPE1} and σ_{GMPE2} such that $\sigma_{GMPE2} > \sigma_{GMPE3} > \sigma_{GMPE1}$. As depicted from the upper panel in Figure B.4 the occurrence probabilities of $|d_j|$ at the tail portion of $|D|$ for Model 2 are significantly larger than those of Model 1 albeit their almost overlapping median PGA estimates. Notwithstanding, although the standard deviation of Model 3 is larger than the standard deviation of Model 1, the occurrence probabilities of $|d_j|$ for the latter GMPE are considerably higher for large $|d_j|$ values. The computed occurrence probabilities for each GMPE, when multiplied by the corresponding $|d_j|$ values, yield larger weighted averages for Model 2 that eventually leads to a higher MDE score for this GMPE. The lower panel in Figure B.4 illustrates the products of occurrence probabilities of $|d_j|$ with the corresponding $|d_j|$ for the same arbitrary data point. Eventually, for the given case study, the uncertainty in the ground-motion trends of the test-bed database is better represented by Model 3 whose standard deviation is between the other two candidate GMPEs. Therefore, the MDE index is not inclined to select the predictive model with the smallest σ_{GMPE}. Such a case would only occur when the median trends of two or more GMPEs overlap each other. The MDE index combines the absolute differences between the logarithms of observed data and ground-motion estimates together with their occurrence probabilities to describe how well a GMPE can represent the ground-motion uncertainty in a given database.

Table B.4 MDE scores of the GMPEs and their ranking for the test-bed database.

GMPE	MDE	Rank
Model-1	0.543	2
Model-2	0.612	3
Model-3	0.454	1
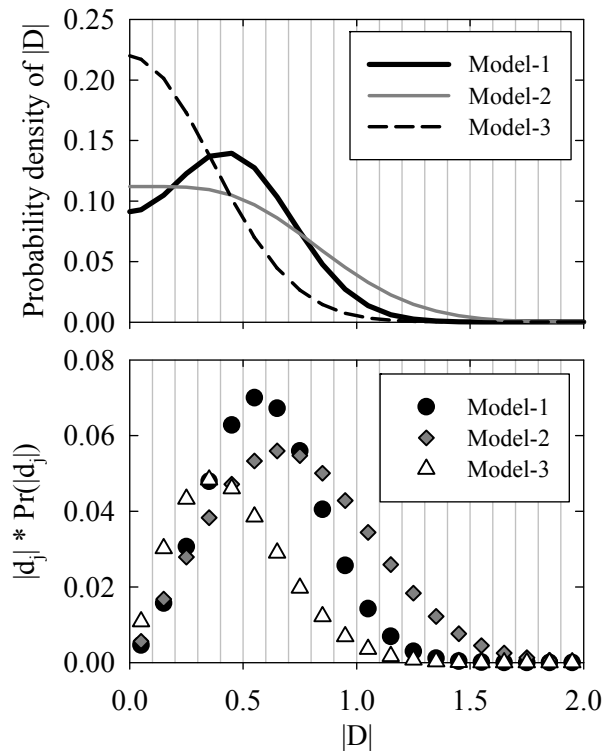
Figure B.4 Top panel: Probability density functions of |D| for each GMPE for an arbitrary point in the test-bed dataset. Bottom panel: The products of occurrence probabilities, |d_j|, with corresponding d_j for each GMPE.

PERIOD DEPENDENT RESULTS OF THE DATA-DRIVEN TESTING METHODS AND TRELLIS CHARTS OF SELECTED GMPEs
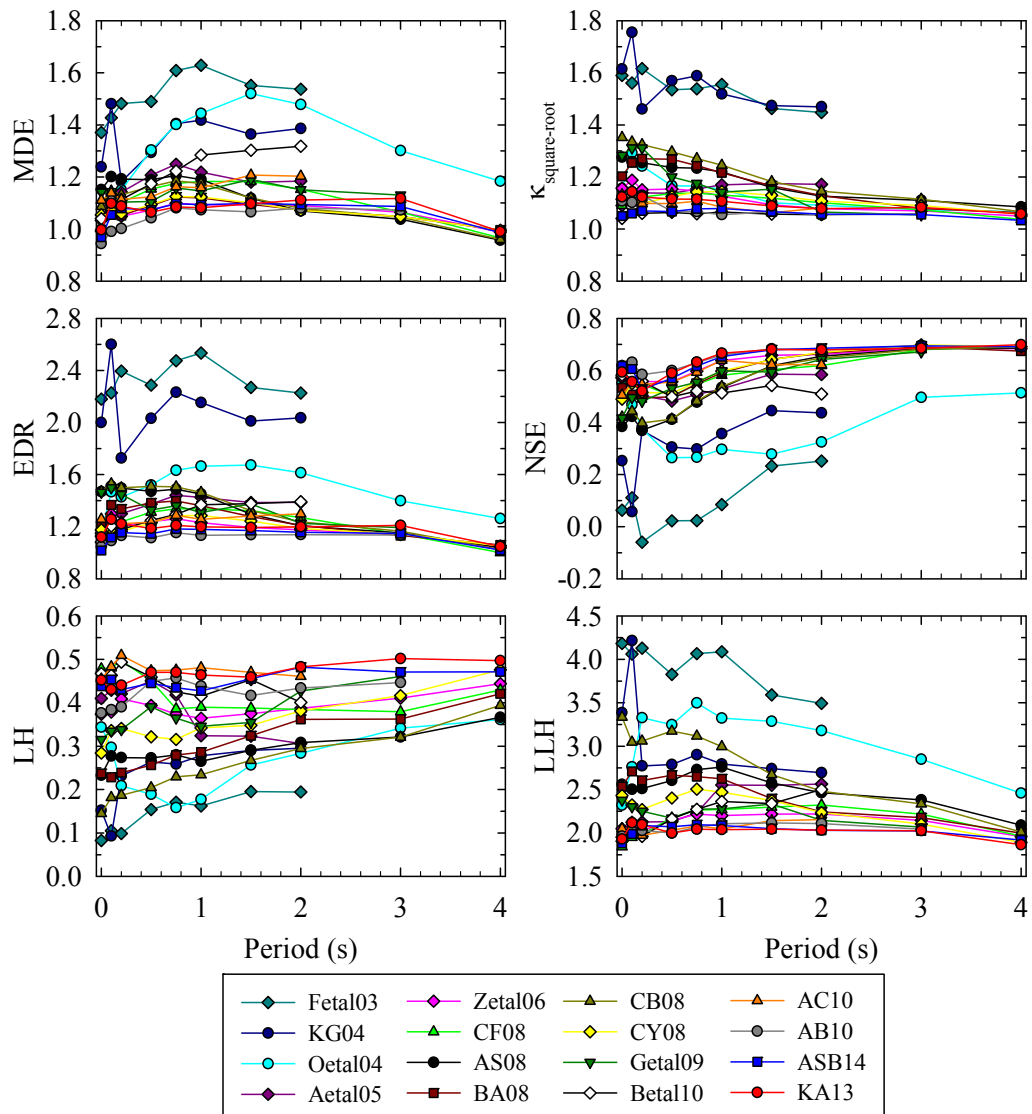
Figure C.1 Consideration of the entire EMME database.

Table C.1 Consideration of the entire EMME database.

Rank	GMPE	MDE
1	AB10	1.035
2	ASB14	1.070
3	Zetal06	1.073
4	KA13	1.078
5	BA08	1.080
6	CY08	1.088
7	CF08	1.129
8	CB08	1.136
9	Getal09	1.142
10	AC10	1.152
11	AS08	1.165
12	Aetal05	1.166
13	Betal10	1.196
14	Oetal04	1.303
15	KG04	1.346
16	Fetal03	1.512

Rank	GMPE	Kappa
1	Betal10	1.061
2	ASB14	1.066
3	AB10	1.081
4	AC10	1.098
5	KA13	1.112
6	CF08	1.119
7	CY08	1.120
8	Zetal06	1.137
9	Aetal05	1.143
10	Oetal04	1.171
11	Getal09	1.205
12	BA08	1.219
13	AS08	1.220
14	CB08	1.269
15	Fetal03	1.538
16	KG04	1.556

Rank	GMPE	EDR
1	AB10	1.118
2	ASB14	1.141
3	KA13	1.198
4	CY08	1.219
5	Zetal06	1.219
6	CF08	1.264
7	AC10	1.264
8	Betal10	1.268
9	BA08	1.316
10	Aetal05	1.335
11	Getal09	1.376
12	AS08	1.423
13	CB08	1.442
14	Oetal04	1.518
15	KG04	2.099
16	Fetal03	2.324

Rank	GMPE	NSE
1	AB10	0.635
2	ASB14	0.619
3	KA13	0.615
4	Zetal06	0.600
5	AC10	0.579
6	CF08	0.578
7	CY08	0.566
8	BA08	0.560
9	Aetal05	0.542
10	Getal09	0.539
11	Betal10	0.539
12	CB08	0.495
13	AS08	0.484
14	Oetal04	0.353
15	KG04	0.315
16	Fetal03	0.091

Rank	GMPE	LH
1	AC10	0.476
2	KA13	0.459
3	Betal10	0.447
4	ASB14	0.446
5	CF08	0.432
6	AB10	0.418
7	Aetal05	0.385
8	Zetal06	0.382
9	Getal09	0.359
10	CY08	0.333
11	BA08	0.277
12	AS08	0.275
13	Oetal04	0.239
14	KG04	0.233
15	CB08	0.218
16	Fetal03	0.145

Rank	GMPE	LLH
1	ASB14	2.036
2	KA13	2.037
3	AB10	2.051
4	AC10	2.067
5	CF08	2.137
6	Zetal06	2.150
7	Betal10	2.189
8	Getal09	2.266
9	Aetal05	2.274
10	CY08	2.375
11	BA08	2.553
12	AS08	2.589
13	CB08	2.985
14	KG04	3.037
15	Oetal04	3.118
16	Fetal03	3.930
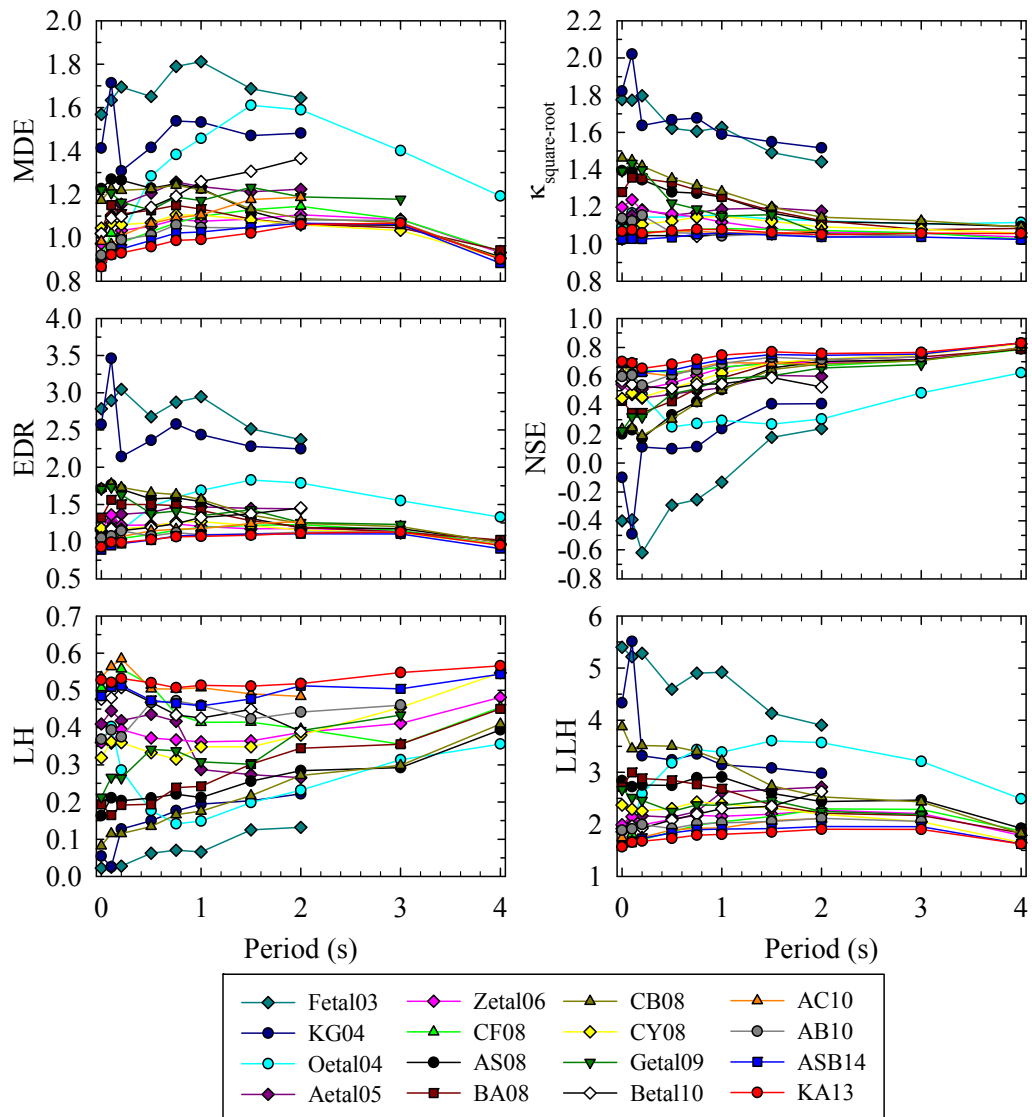
Figure C.2 Consideration of the Turkish sub-database.

Table C.2 Consideration of the Turkish sub-database.

Rank	GMPE	MDE
1	KA13	0.967
2	ASB14	0.986
3	AB10	1.014
4	CF08	1.047
5	Zetal06	1.064
6	AC10	1.074
7	CY08	1.074
8	BA08	1.106
9	Aetal05	1.177
10	Betal10	1.184
11	Getal09	1.188
12	CB08	1.191
13	AS08	1.206
14	Oetal04	1.271
15	KG04	1.484
16	Fetal03	1.685

Rank	GMPE	Kappa
1	ASB14	1.039
2	Betal10	1.050
3	AC10	1.063
4	KA13	1.068
5	CF08	1.080
6	AB10	1.084
7	CY08	1.121
8	Oetal04	1.139
9	Zetal06	1.148
10	Aetal05	1.168
11	Getal09	1.249
12	BA08	1.271
13	AS08	1.277
14	CB08	1.327
15	Fetal03	1.642
16	KG04	1.685

Rank	GMPE	EDR
1	ASB14	1.025
2	KA13	1.033
3	AB10	1.098
4	CF08	1.131
5	AC10	1.141
6	CY08	1.205
7	Zetal06	1.220
8	Betal10	1.244
9	Aetal05	1.375
10	BA08	1.407
11	Oetal04	1.448
12	Getal09	1.485
13	AS08	1.546
14	CB08	1.584
15	KG04	2.510
16	Fetal03	2.764

Rank	GMPE	NSE
1	KA13	0.715
2	ASB14	0.693
3	AC10	0.658
4	CF08	0.654
5	AB10	0.642
6	Zetal06	0.592
7	CY08	0.563
8	Betal10	0.546
9	Aetal05	0.532
10	BA08	0.507
11	Getal09	0.462
12	AS08	0.403
13	CB08	0.402
14	Oetal04	0.385
15	KG04	0.099
16	Fetal03	-0.209

Rank	GMPE	LH
1	AC10	0.522
2	KA13	0.519
3	ASB14	0.487
4	CF08	0.469
5	Betal10	0.454
6	AB10	0.425
7	Zetal06	0.371
8	Aetal05	0.369
9	CY08	0.345
10	Getal09	0.303
11	Oetal04	0.244
12	BA08	0.234
13	AS08	0.220
14	CB08	0.159
15	KG04	0.144
16	Fetal03	0.066

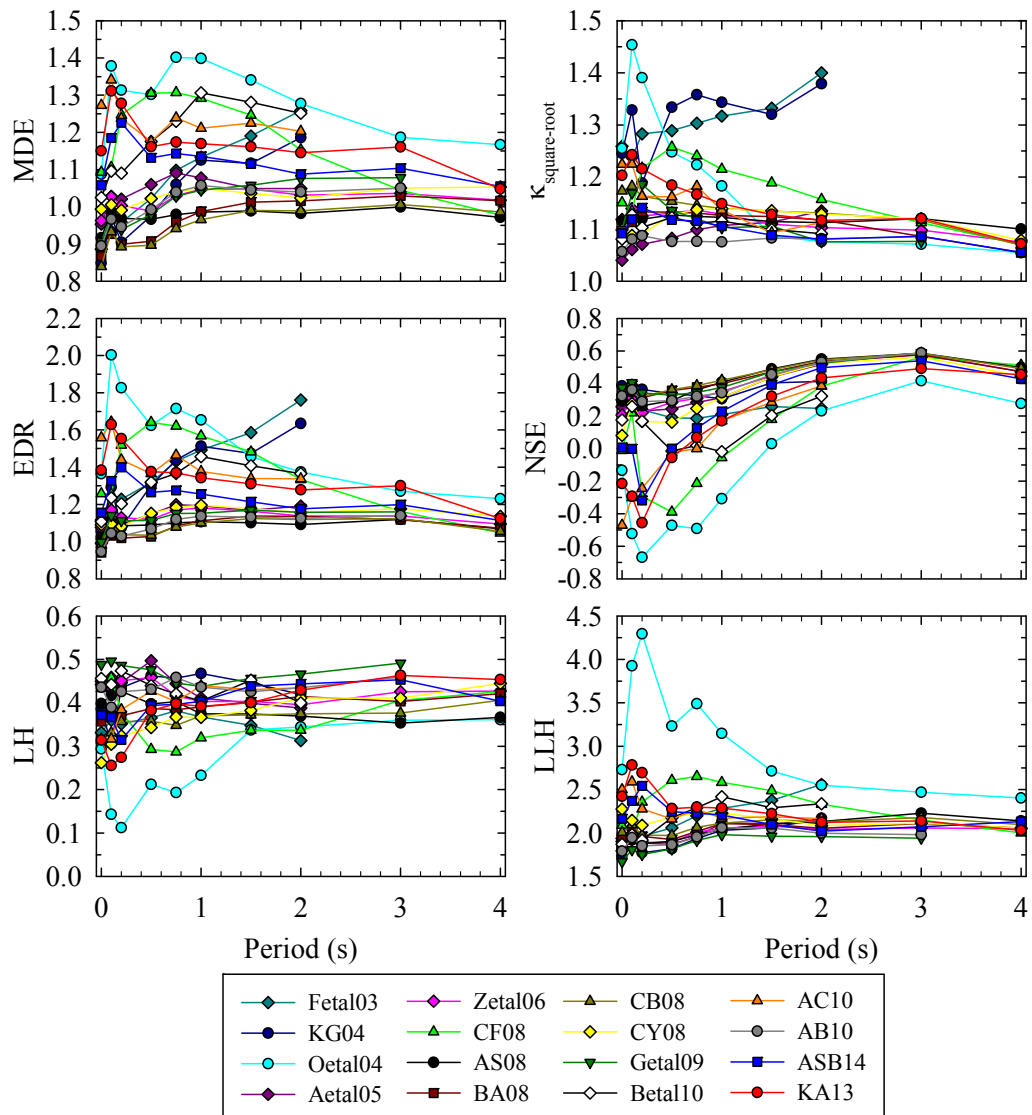| Rank	GMPE	LLH
1	KA13	1.748
2	ASB14	1.813
3	AC10	1.888
4	CF08	1.934
5	AB10	1.990
6	Zetal06	2.127
7	Betal10	2.163
8	Aetal05	2.315
9	CY08	2.319
10	Getal09	2.416
11	BA08	2.684
12	AS08	2.737
13	Oetal04	2.959
14	CB08	3.279
15	KG04	3.619
16	Fetal03	4.795

Figure C.3 Consideration of the Iranian sub-database.

Table C.3 Consideration of the Iranian sub-database.

Rank	GMPE	MDE
1	CB08	0.931
2	BA08	0.947
3	AS08	0.972
4	AB10	0.998
5	Getal09	1.001
6	Zetal06	1.017
7	CY08	1.020
8	KG04	1.024
9	Aetal05	1.041
10	Fetal03	1.060
11	ASB14	1.135
12	Betal10	1.182
13	KA13	1.194
14	CF08	1.219
15	AC10	1.238
16	Oetal04	1.312

Rank	GMPE	Kappa
1	AB10	1.077
2	Aetal05	1.088
3	Betal10	1.106
4	ASB14	1.108
5	CY08	1.118
6	AS08	1.120
7	BA08	1.120
8	Zetal06	1.124
9	Getal09	1.124
10	CB08	1.153
11	AC10	1.162
12	KA13	1.176
13	CF08	1.195
14	Oetal04	1.239
15	Fetal03	1.303
16	KG04	1.312

Rank	GMPE	EDR
1	BA08	1.061
2	CB08	1.072
3	AB10	1.075
4	AS08	1.089
5	Getal09	1.124
6	Aetal05	1.134
7	CY08	1.141
8	Zetal06	1.143
9	ASB14	1.258
10	Betal10	1.308
11	KG04	1.348
12	Fetal03	1.386
13	KA13	1.405
14	AC10	1.441
15	CF08	1.460
16	Oetal04	1.627

Rank	GMPE	NSE
1	CB08	0.405
2	Getal09	0.395
3	BA08	0.395
4	AS08	0.376
5	AB10	0.365
6	KG04	0.359
7	Zetal06	0.332
8	Aetal05	0.327
9	CY08	0.277
10	Fetal03	0.252
11	Betal10	0.139
12	ASB14	0.116
13	KA13	-0.003
14	CF08	-0.023
15	AC10	-0.025
16	Oetal04	-0.292

Rank	GMPE	LH
1	Getal09	0.469
2	Betal10	0.436
3	Aetal05	0.433
4	AB10	0.430
5	Zetal06	0.428
6	KG04	0.422
7	AS08	0.395
8	AC10	0.394
9	ASB14	0.391
10	BA08	0.384
11	KA13	0.356
12	CF08	0.355
13	CB08	0.353
14	Fetal03	0.352
15	CY08	0.345
16	Oetal04	0.234

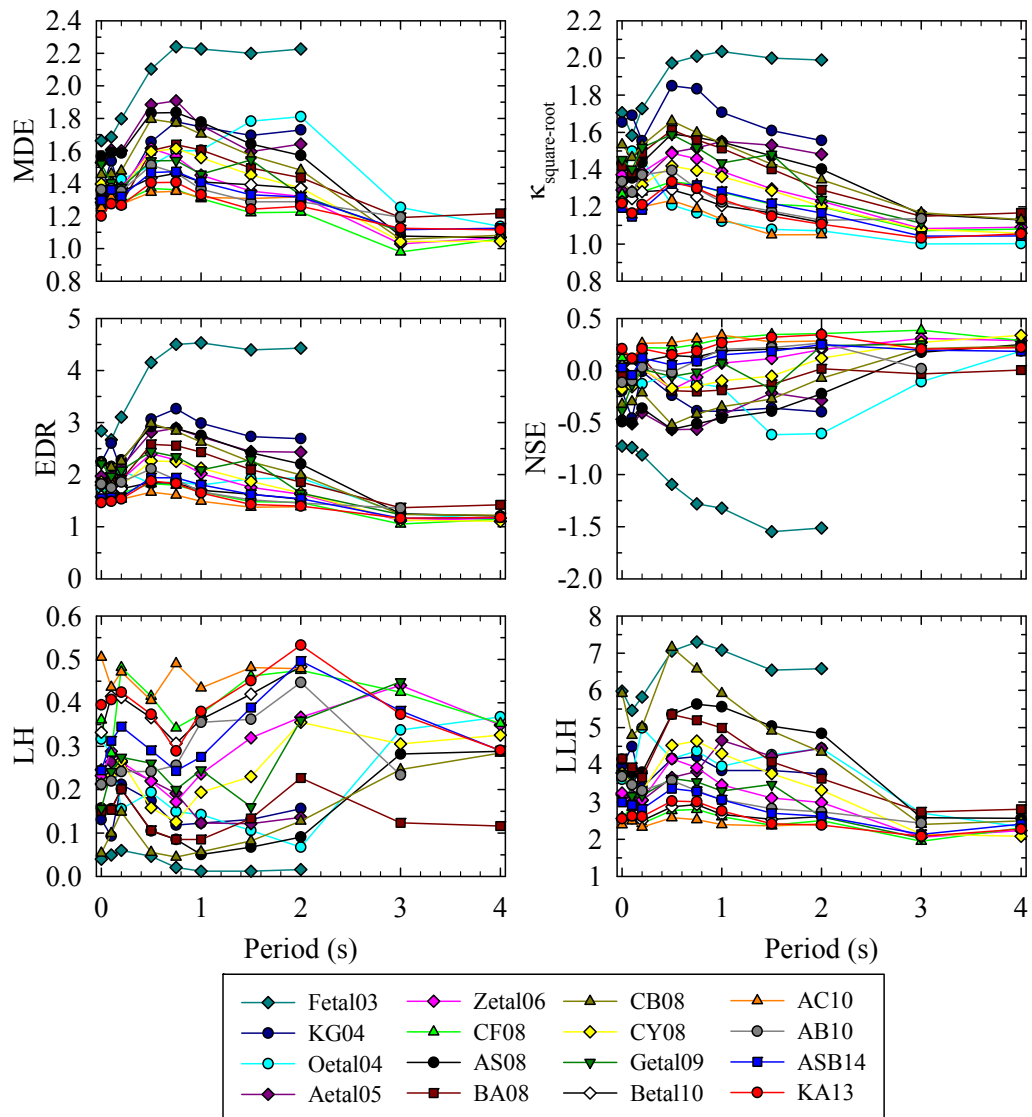| Rank	GMPE	LLH
1	Getal09	1.858
2	AB10	1.940
3	KG04	1.946
4	Aetal05	1.971
5	AS08	1.973
6	Zetal06	1.980
7	BA08	2.017
8	CB08	2.064
9	Betal10	2.161
10	Fetal03	2.161
11	CY08	2.174
12	ASB14	2.235
13	AC10	2.291
14	KA13	2.389
15	CF08	2.390
16	Oetal04	3.260

Figure C.4 Consideration of the Caucasian sub-database.

Table C.4 Consideration of the Caucasian sub-database.

Rank	GMPE	MDE
1	KA13	1.298
2	CF08	1.307
3	AC10	1.310
4	ASB14	1.372
5	AB10	1.375
6	Betal10	1.380
7	Zetal06	1.420
8	BA08	1.462
9	Getal09	1.464
10	CY08	1.469
11	Oetal04	1.544
12	CB08	1.590
13	KG04	1.605
14	AS08	1.676
15	Aetal05	1.691
16	Fetal03	2.018

Rank	GMPE	Kappa
1	AC10	1.152
2	KA13	1.216
3	Betal10	1.223
4	ASB14	1.228
5	Oetal04	1.246
6	CF08	1.270
7	AB10	1.276
8	CY08	1.325
9	Zetal06	1.374
10	Aetal05	1.433
11	Getal09	1.455
12	BA08	1.459
13	AS08	1.477
14	CB08	1.513
15	KG04	1.682
16	Fetal03	1.878

Rank	GMPE	EDR
1	AC10	1.509
2	KA13	1.583
3	CF08	1.662
4	Betal10	1.688
5	ASB14	1.689
6	AB10	1.759
7	Oetal04	1.897
8	CY08	1.951
9	Zetal06	1.958
10	Getal09	2.135
11	BA08	2.141
12	CB08	2.414
13	Aetal05	2.432
14	AS08	2.483
15	KG04	2.707
16	Fetal03	3.828

Rank	GMPE	NSE
1	AC10	0.250
2	KA13	0.225
3	CF08	0.211
4	Betal10	0.131
5	ASB14	0.103
6	AB10	0.072
7	Zetal06	0.011
8	Getal09	-0.057
9	CY08	-0.084
10	BA08	-0.086
11	Oetal04	-0.213
12	KG04	-0.305
13	CB08	-0.309
14	Aetal05	-0.432
15	AS08	-0.439
16	Fetal03	-1.129

Rank	GMPE	LH
1	AC10	0.463
2	KA13	0.407
3	CF08	0.399
4	Betal10	0.387
5	ASB14	0.324
6	AB10	0.292
7	Zetal06	0.262
8	Getal09	0.237
9	CY08	0.222
10	Aetal05	0.194
11	Oetal04	0.176
12	BA08	0.143
13	KG04	0.142
14	AS08	0.114
15	CB08	0.083
16	Fetal03	0.032

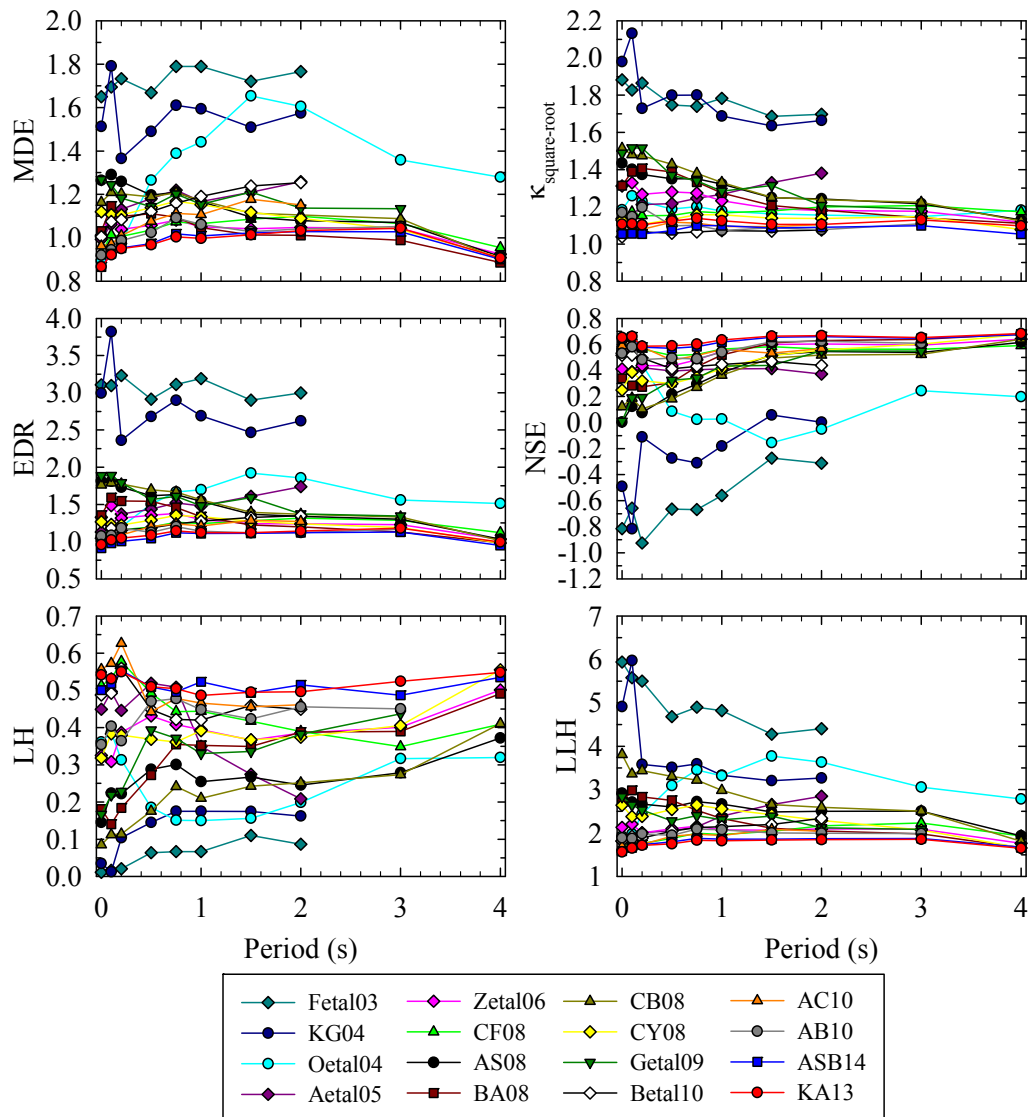| Rank	GMPE	LLH
1	AC10	2.434
2	CF08	2.615
3	Betal10	2.655
4	KA13	2.671
5	ASB14	2.969
6	AB10	3.244
7	Getal09	3.333
8	Zetal06	3.365
9	Aetal05	3.780
10	CY08	3.888
11	KG04	3.960
12	Oetal04	4.190
13	BA08	4.375
14	AS08	4.770
15	CB08	5.580
16	Fetal03	6.480

Figure C.5 Consideration of the normal faulting sub-database.

Table C.5 Consideration of the normal faulting sub-database.

Rank	GMPE	MDE		Rank	GMPE	Kappa		Rank	GMPE	EDR
1	KA13	0.969		1	ASB14	1.049		1	Betal10	1.067
2	ASB14	0.975		2	KA13	1.080		2	ASB14	1.076
3	AB10	1.012		3	AB10	1.130		3	AC10	1.094
4	CF08	1.039		4	AC10	1.172		4	KA13	1.114
5	Zetal06	1.056		5	CF08	1.212		5	AB10	1.119
6	BA08	1.069		6	Betal10	1.218		6	CY08	1.133
7	AC10	1.071		7	CY08	1.275		7	CF08	1.166
8	CY08	1.125		8	Zetal06	1.329		8	Oetal04	1.194
9	Betal10	1.141		9	BA08	1.405		9	Aetal05	1.242
10	Aetal05	1.153		10	Aetal05	1.437		10	Zetal06	1.258
11	CB08	1.170		11	Oetal04	1.510		11	BA08	1.311
12	Getal09	1.193		12	AS08	1.606		12	AS08	1.340
13	AS08	1.195		13	CB08	1.626		13	Getal09	1.379
14	Oetal04	1.270		14	Getal09	1.648		14	CB08	1.387
15	KG04	1.556		15	KG04	2.817		15	Fetal03	1.779
16	Fetal03	1.727		16	Fetal03	3.070		16	KG04	1.804

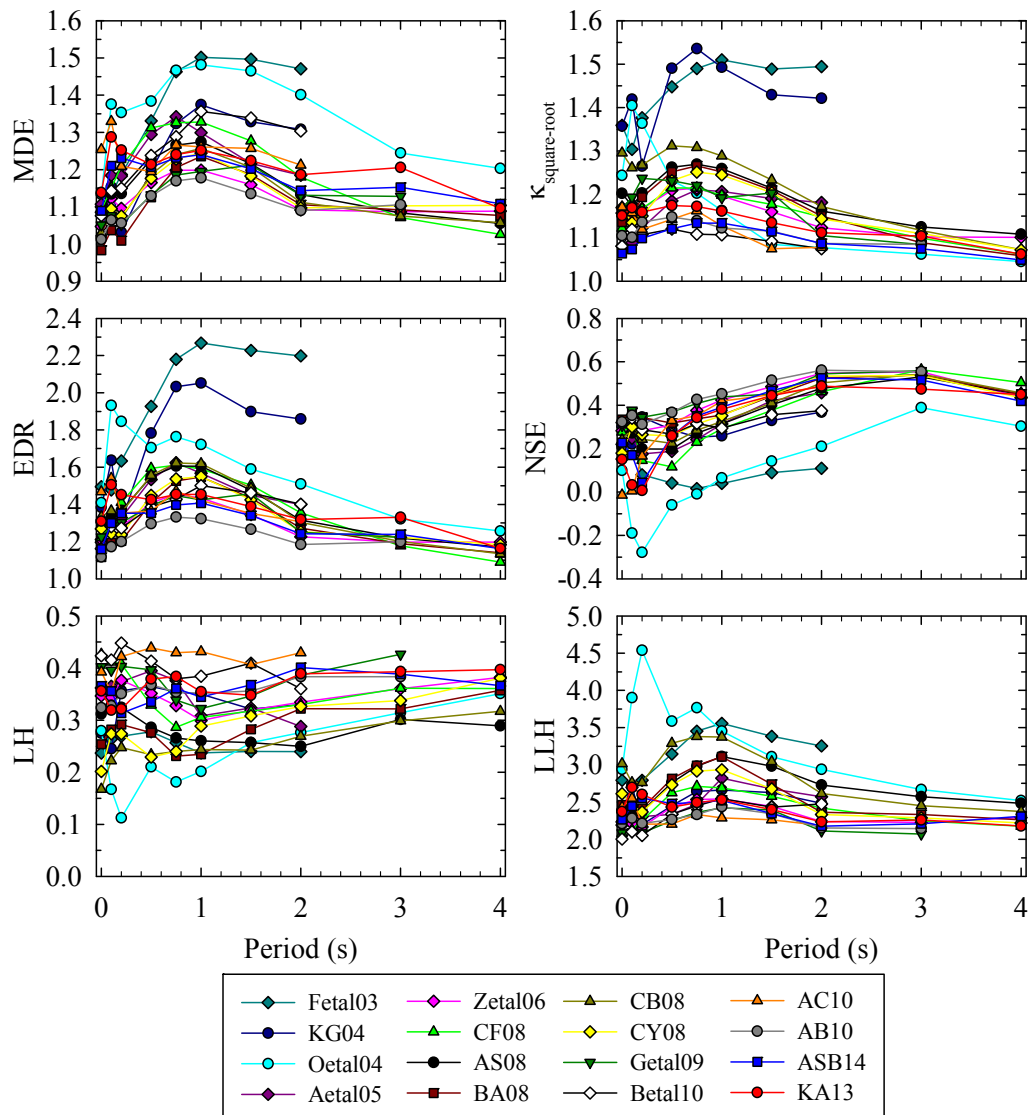| Rank	GMPE	NSE		Rank	GMPE	LH		Rank	GMPE	LLH
1	KA13	0.632		1	KA13	0.514		1	KA13	1.753
2	ASB14	0.621		2	ASB14	0.514		2	ASB14	1.780
3	CF08	0.562		3	AC10	0.508		3	AC10	1.885
4	AC10	0.561		4	CF08	0.476		4	CF08	1.907
5	AB10	0.546		5	Betal10	0.468		5	AB10	1.981
6	Zetal06	0.488		6	AB10	0.425		6	Betal10	2.060
7	Betal10	0.466		7	Aetal05	0.407		7	Zetal06	2.103
8	Aetal05	0.439		8	Zetal06	0.376		8	Aetal05	2.224
9	BA08	0.425		9	CY08	0.368		9	Getal09	2.437
10	CY08	0.386		10	Getal09	0.303		10	CY08	2.481
11	Getal09	0.310		11	BA08	0.278		11	BA08	2.536
12	CB08	0.281		12	AS08	0.243		12	AS08	2.658
13	AS08	0.271		13	Oetal04	0.238		13	Oetal04	2.951
14	Oetal04	0.188		14	CB08	0.179		14	CB08	3.171
15	KG04	-0.265		15	KG04	0.123		15	KG04	3.922
16	Fetal03	-0.610		16	Fetal03	0.055		16	Fetal03	5.012

Figure C.6 Consideration of the reverse faulting sub-database.

Table C.6 Consideration of the reverse faulting sub-database.

Rank	GMPE	MDE
1	AB10	1.104
2	BA08	1.111
3	Getal09	1.129
4	Zetal06	1.135
5	CB08	1.148
6	CY08	1.148
7	AS08	1.184
8	ASB14	1.194
9	KG04	1.217
10	KA13	1.224
11	Aetal05	1.226
12	CF08	1.234
13	Betal10	1.237
14	AC10	1.248
15	Fetal03	1.335
16	Oetal04	1.383

Rank	GMPE	Kappa
1	AB10	1.236
2	ASB14	1.319
3	Zetal06	1.335
4	BA08	1.338
5	Getal09	1.348
6	Betal10	1.362
7	CY08	1.370
8	AC10	1.409
9	KA13	1.413
10	Aetal05	1.423
11	AS08	1.444
12	CF08	1.448
13	CB08	1.455
14	Oetal04	1.685
15	KG04	1.744
16	Fetal03	1.926

Rank	GMPE	EDR
1	Betal10	1.101
2	ASB14	1.103
3	AB10	1.119
4	AC10	1.129
5	KA13	1.154
6	Aetal05	1.158
7	CF08	1.171
8	Zetal06	1.176
9	CY08	1.191
10	Getal09	1.194
11	BA08	1.201
12	AS08	1.218
13	Oetal04	1.221
14	CB08	1.267
15	KG04	1.426
16	Fetal03	1.434

Rank	GMPE	NSE
1	AB10	0.414
2	Getal09	0.405
3	BA08	0.377
4	Zetal06	0.377
5	CY08	0.331
6	Betal10	0.319
7	CB08	0.315
8	ASB14	0.304
9	KG04	0.295
10	AS08	0.293
11	Aetal05	0.283
12	CF08	0.276
13	AC10	0.274
14	KA13	0.263
15	Fetal03	0.095
16	Oetal04	-0.003

Rank	GMPE	LH
1	AC10	0.413
2	Betal10	0.404
3	Getal09	0.374
4	KA13	0.356
5	ASB14	0.356
6	AB10	0.352
7	CF08	0.352
8	Aetal05	0.349
9	Zetal06	0.337
10	KG04	0.325
11	AS08	0.285
12	BA08	0.272
13	CY08	0.268
14	Fetal03	0.253
15	CB08	0.233
16	Oetal04	0.211

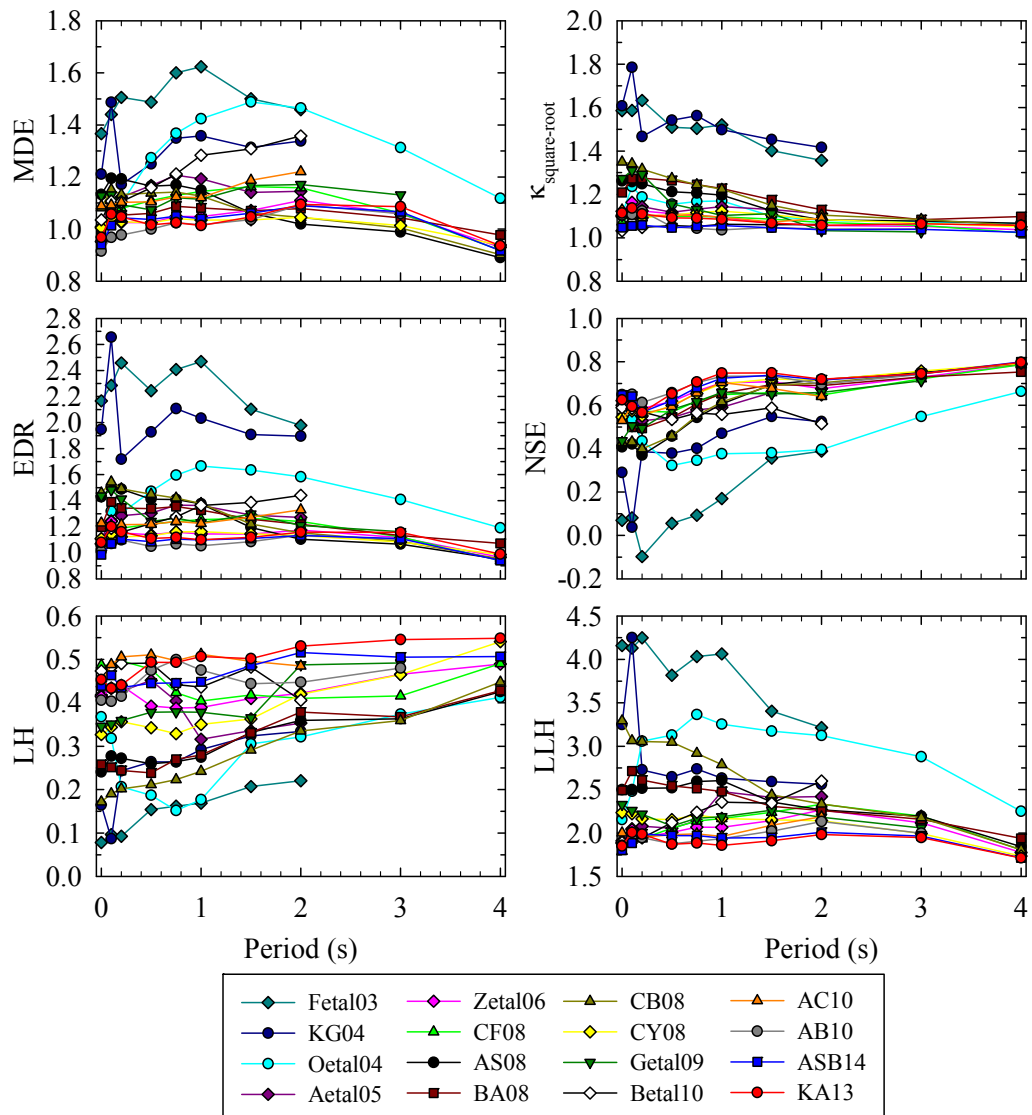| Rank	GMPE	LLH
1	Getal09	2.225
2	AB10	2.278
3	Betal10	2.299
4	AC10	2.306
5	Zetal06	2.349
6	ASB14	2.409
7	CF08	2.435
8	Aetal05	2.461
9	KA13	2.469
10	KG04	2.520
11	CY08	2.628
12	BA08	2.670
13	AS08	2.707
14	CB08	3.030
15	Fetal03	3.134
16	Oetal04	3.529

Figure C.7 Consideration of the strike-slip faulting sub-database.

Table C.7 Consideration of the strike-slip sub-database.

Rank	GMPE	MDE
1	AB10	1.004
2	CY08	1.032
3	KA13	1.034
4	ASB14	1.035
5	Zetal06	1.043
6	BA08	1.064
7	CF08	1.104
8	CB08	1.110
9	Getal09	1.125
10	AC10	1.130
11	Aetal05	1.136
12	AS08	1.136
13	Betal10	1.196
14	Oetal04	1.267
15	KG04	1.310
16	Fetal03	1.498

Rank	GMPE	Kappa
1	ASB14	1.050
2	Betal10	1.055
3	AB10	1.069
4	CF08	1.092
5	KA13	1.094
6	AC10	1.100
7	CY08	1.103
8	Zetal06	1.105
9	Aetal05	1.126
10	Oetal04	1.150
11	Getal09	1.176
12	AS08	1.199
13	BA08	1.225
14	CB08	1.250
15	Fetal03	1.512
16	KG04	1.541

Rank	GMPE	EDR
1	AB10	1.072
2	ASB14	1.086
3	KA13	1.131
4	CY08	1.138
5	Zetal06	1.152
6	CF08	1.206
7	AC10	1.243
8	Betal10	1.263
9	Aetal05	1.279
10	BA08	1.304
11	Getal09	1.322
12	AS08	1.365
13	CB08	1.390
14	Oetal04	1.454
15	KG04	2.024
16	Fetal03	2.264

Rank	GMPE	NSE
1	AB10	0.680
2	KA13	0.670
3	ASB14	0.667
4	Zetal06	0.645
5	CY08	0.632
6	CF08	0.621
7	AC10	0.619
8	Aetal05	0.591
9	BA08	0.590
10	Getal09	0.575
11	Betal10	0.563
12	CB08	0.535
13	AS08	0.527
14	Oetal04	0.423
15	KG04	0.379
16	Fetal03	0.139

Rank	GMPE	LH
1	AC10	0.492
2	KA13	0.482
3	Betal10	0.463
4	ASB14	0.460
5	CF08	0.450
6	AB10	0.446
7	Zetal06	0.411
8	Aetal05	0.392
9	Getal09	0.381
10	CY08	0.354
11	AS08	0.285
12	BA08	0.281
13	Oetal04	0.254
14	KG04	0.247
15	CB08	0.233
16	Fetal03	0.147

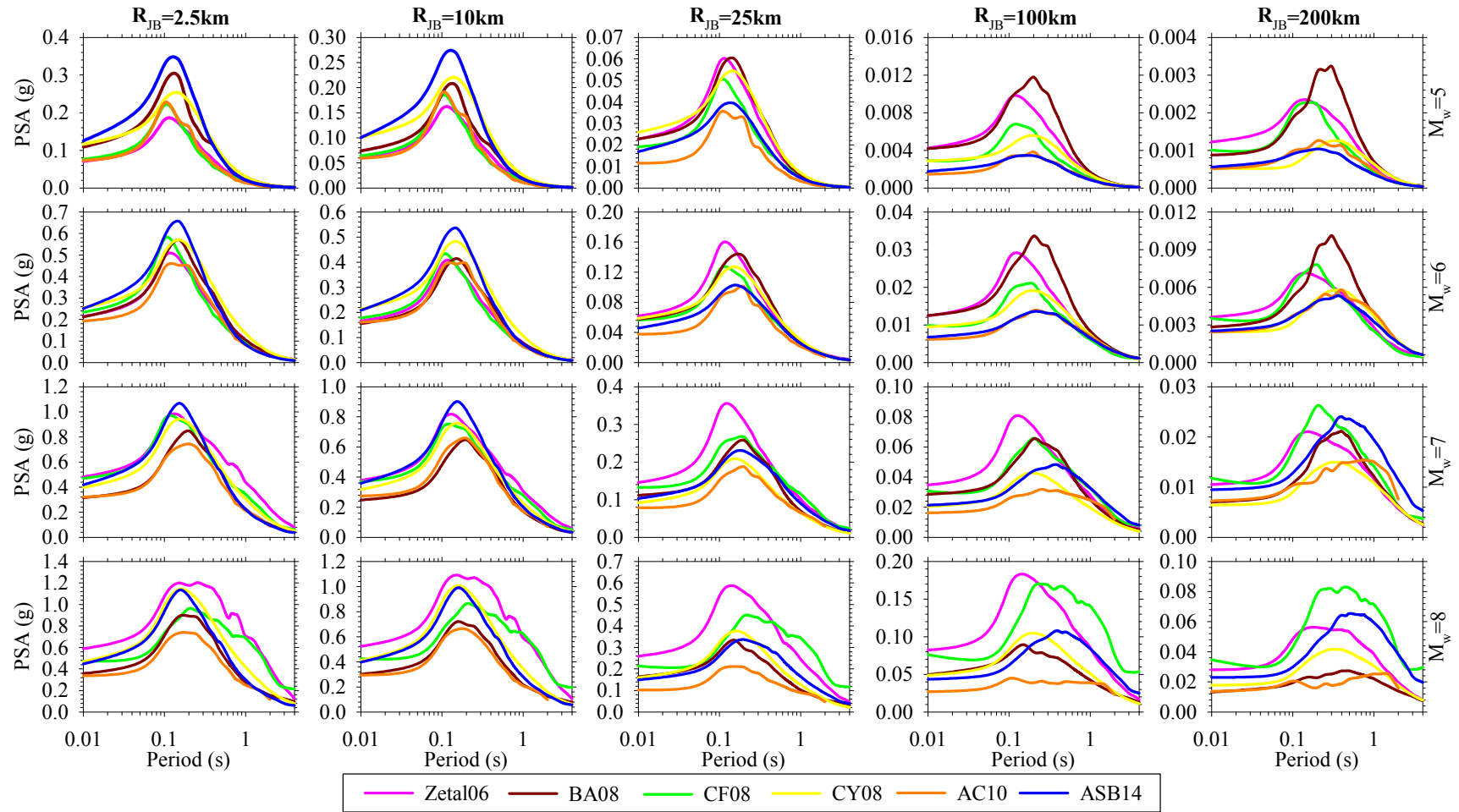| Rank	GMPE	LLH
1	KA13	1.918
2	ASB14	1.939
3	AB10	1.952
4	AC10	2.015
5	Zetal06	2.057
6	CF08	2.071
7	CY08	2.180
8	Betal10	2.187
9	Aetal05	2.189
10	Getal09	2.211
11	AS08	2.481
12	BA08	2.490
13	CB08	2.867
14	KG04	2.924
15	Oetal04	2.967
16	Fetal03	3.884

Figure C.8 Trellis chart for PSA response spectra of the GMPEs (normal events, median estimates and V_{S30}=760m/s).
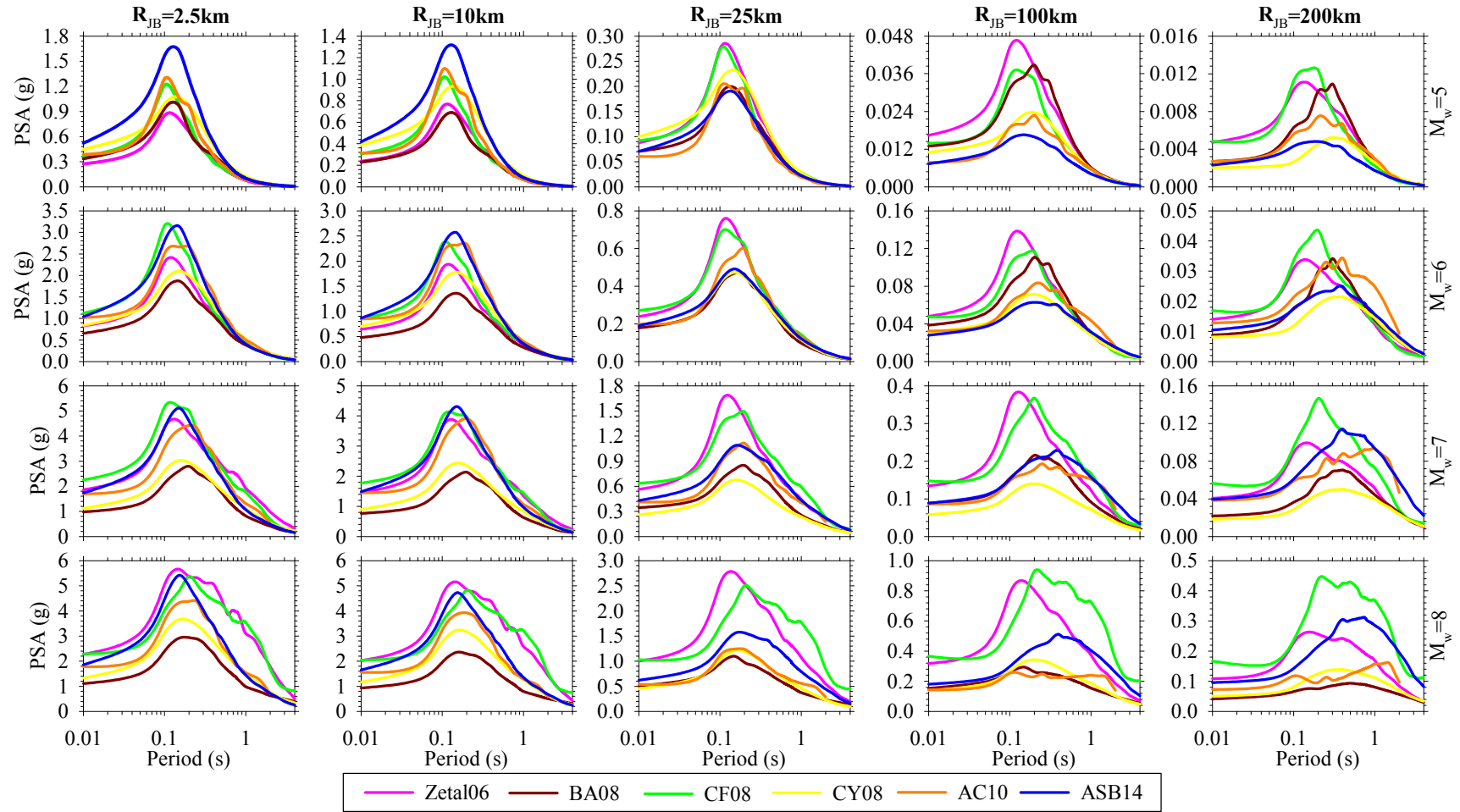
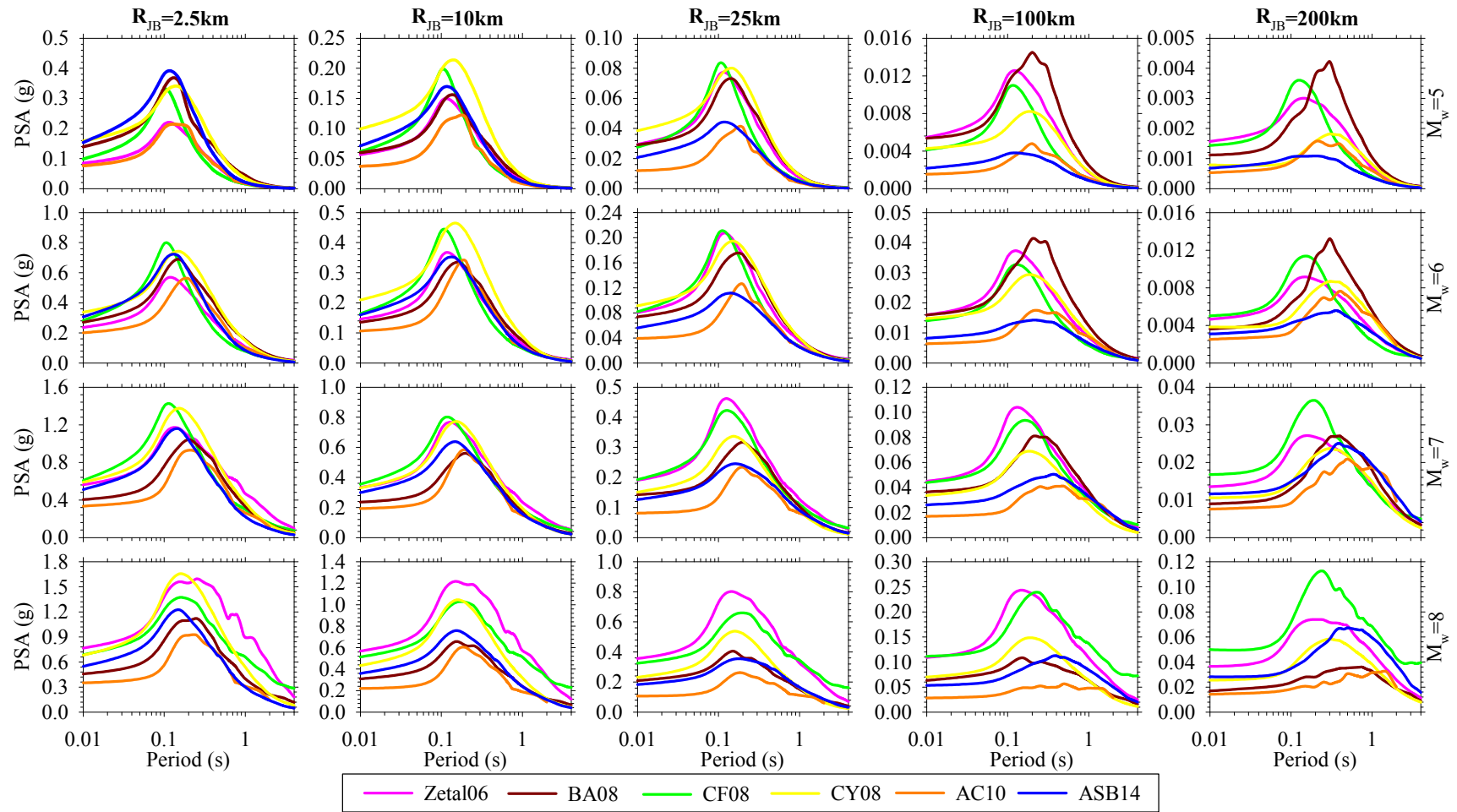Figure C.9 Trellis chart for PSA response spectra of the GMPEs (normal events, median+2sigma estimates and V_{S30}=760m/s).

Figure C.10 Trellis chart for PSA response spectra of the GMPEs (reverse events, median estimates and V_{S30}=760m/s).

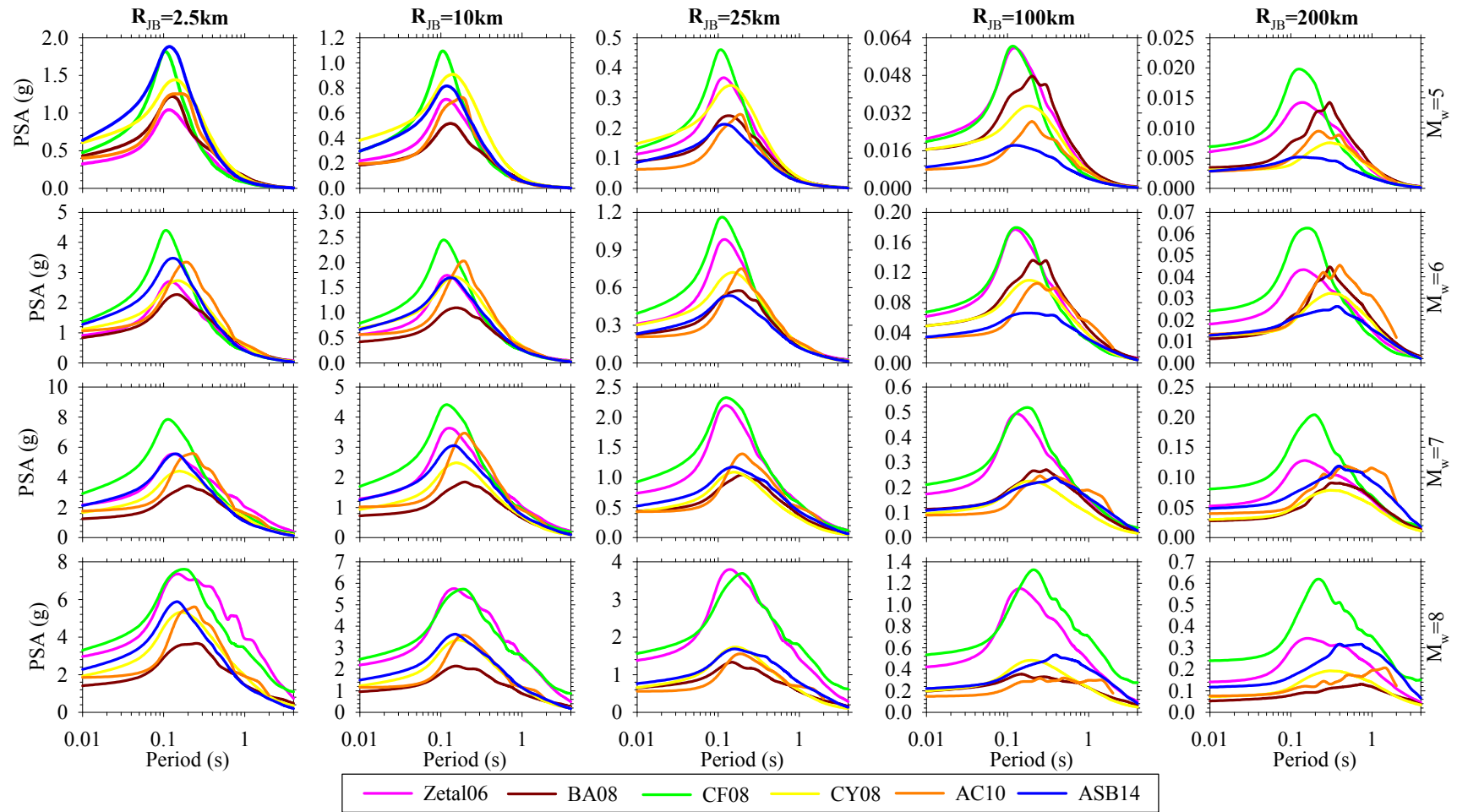Figure C.11 Trellis chart for PSA response spectra of the GMPEs (reverse events, median+2sigma estimates and V_{S30}=760m/s).

APPENDIX D

**RESULTS OF LOGIC-TREE BASED SENSITIVITY ANALYSES
AND CONCLUDING HAZARD MAPS OF SELECTED REGIONS**

This appendix provides the normalized spectral acceleration scatter plots of Aegean, NAF and Mersin regions for each alternative logic trees given in Chapter 6 (Figures D.1 to D.9). The comparative hazard maps of Aegean, NAF and Mersin regions are also given in this appendix (Figures D.10 to D.18).
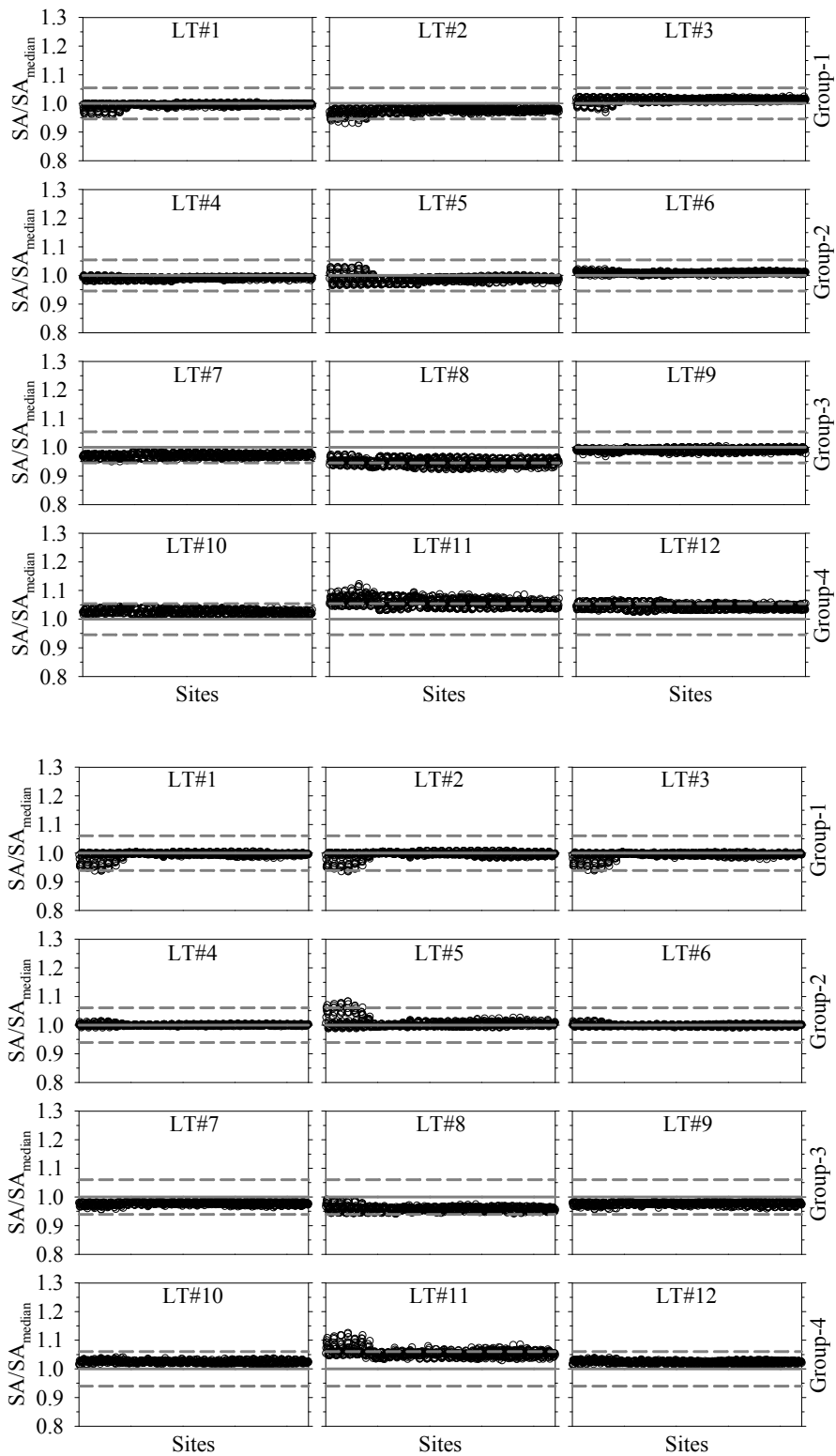
Figure D.1 Results of logic-tree based sensitivity analysis of Aegean region for
return period of 475yrs and PGA (top group), T=0.2s (bottom group).
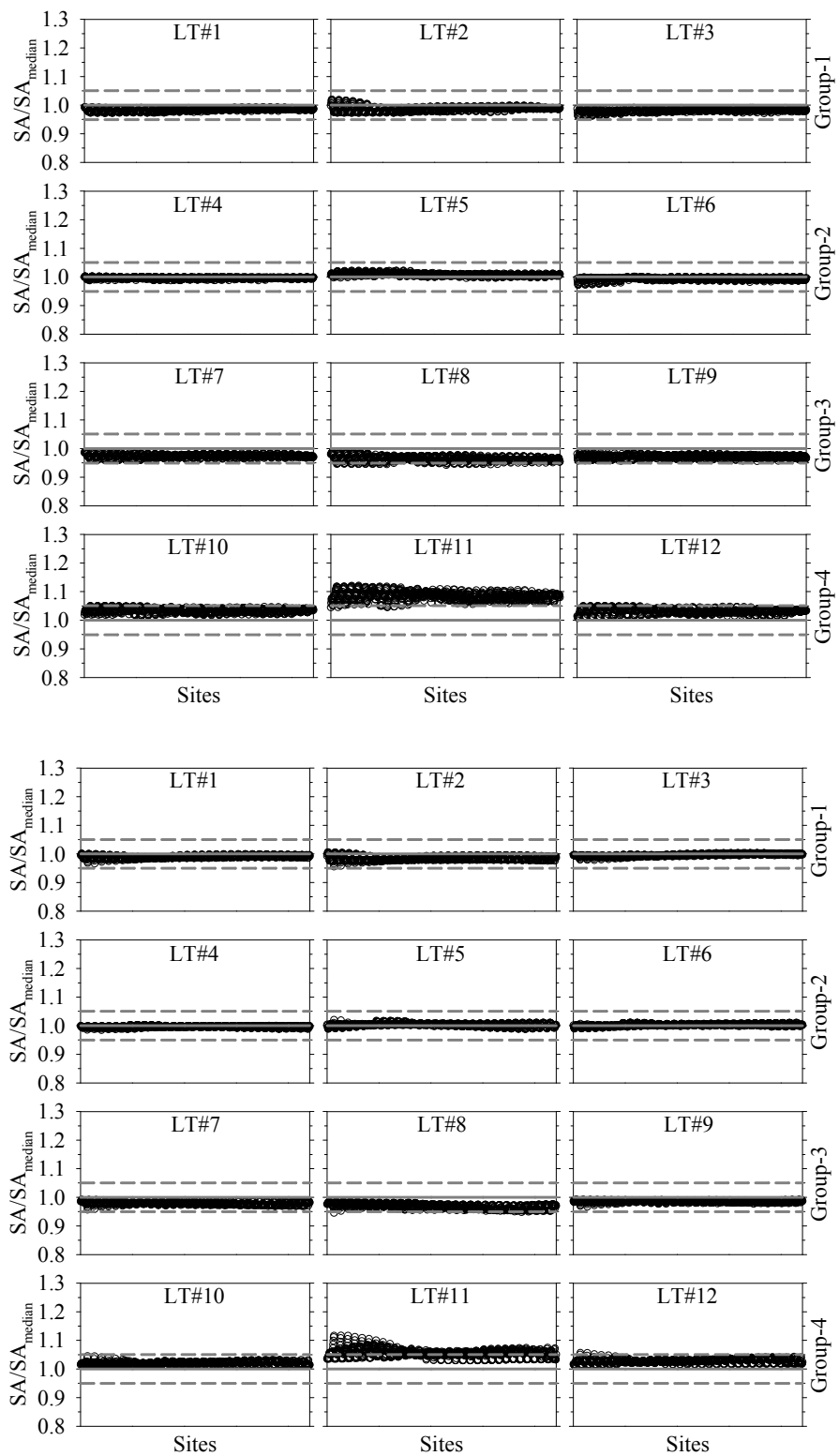
Figure D.2 Results of logic-tree based sensitivity analysis of Aegean region for
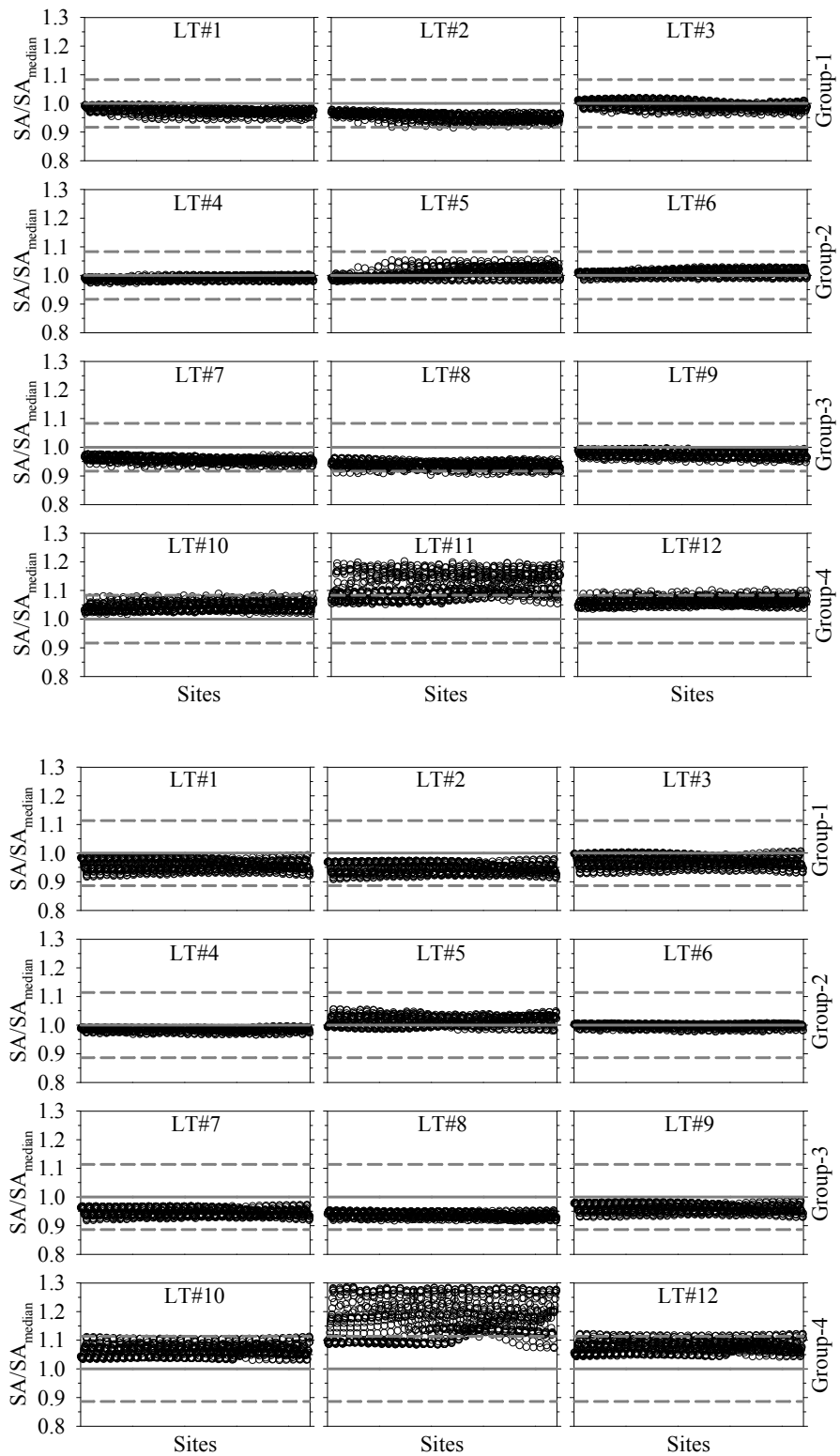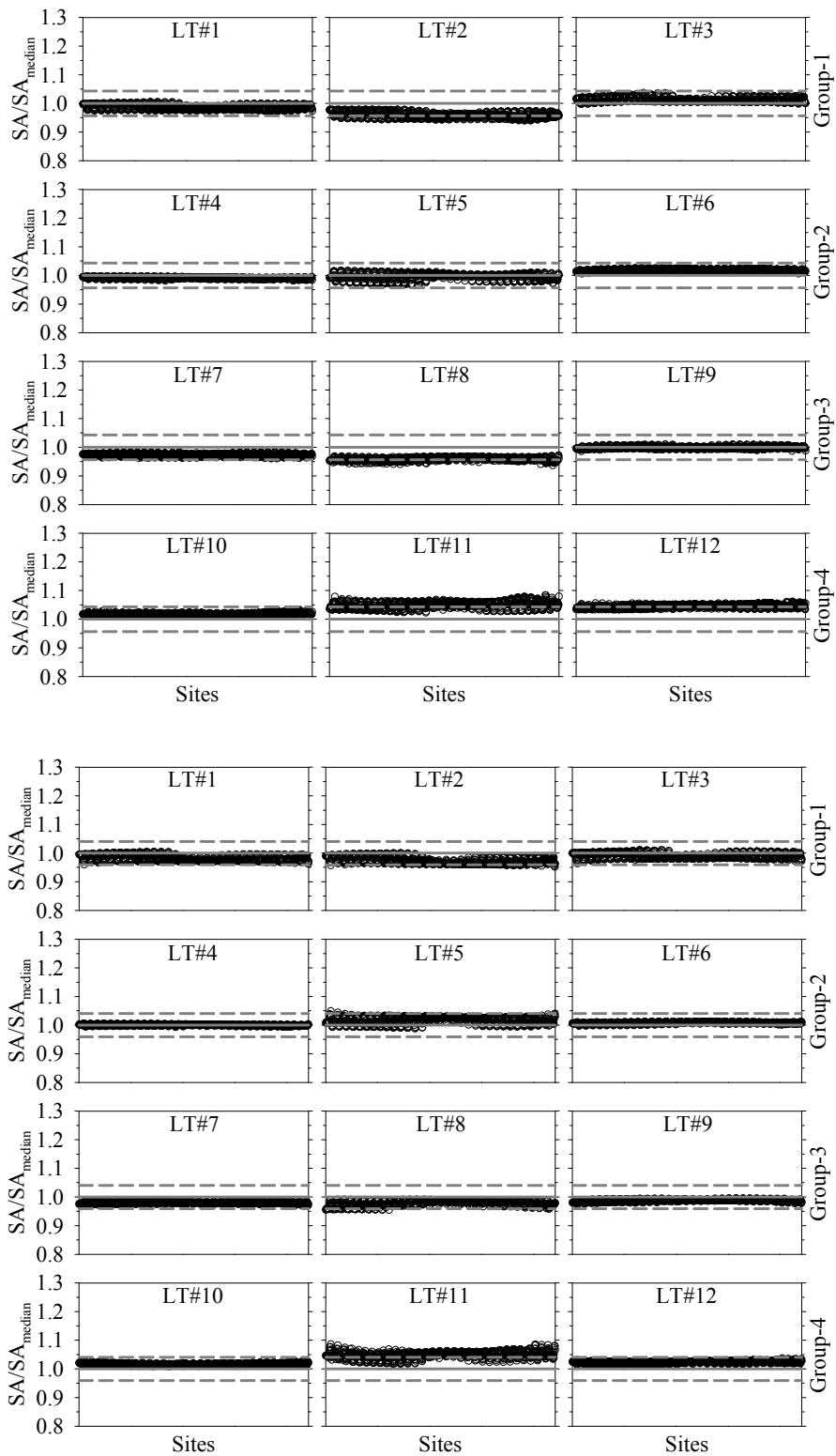return period of 475yrs and T=1.0s (top group), T=2.0s (bottom group).
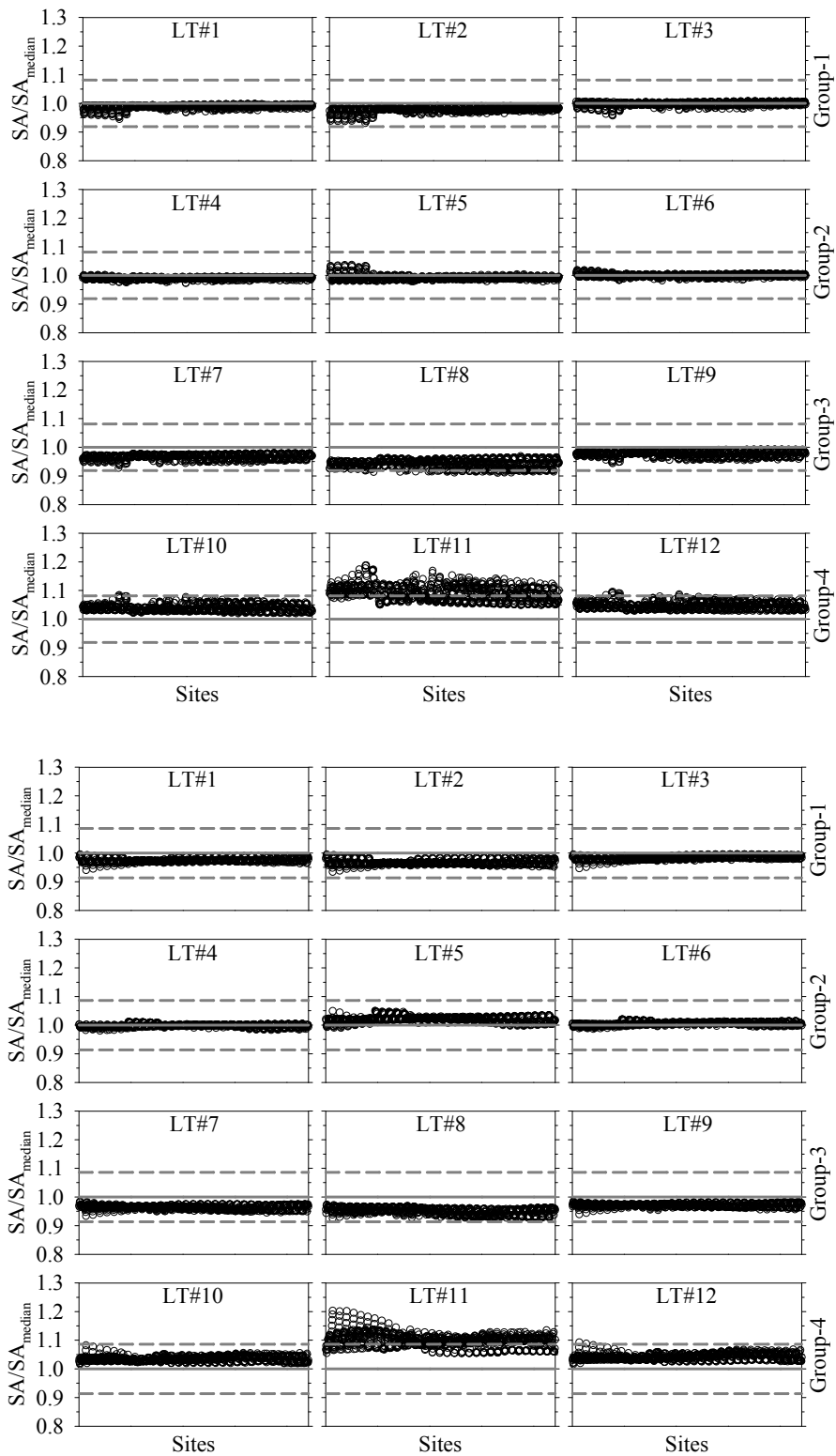
Figure D.3 Results of logic-tree based sensitivity analysis of Aegean region for
return period of 2475yrs and PGA (top group), T=2.0s (bottom group).
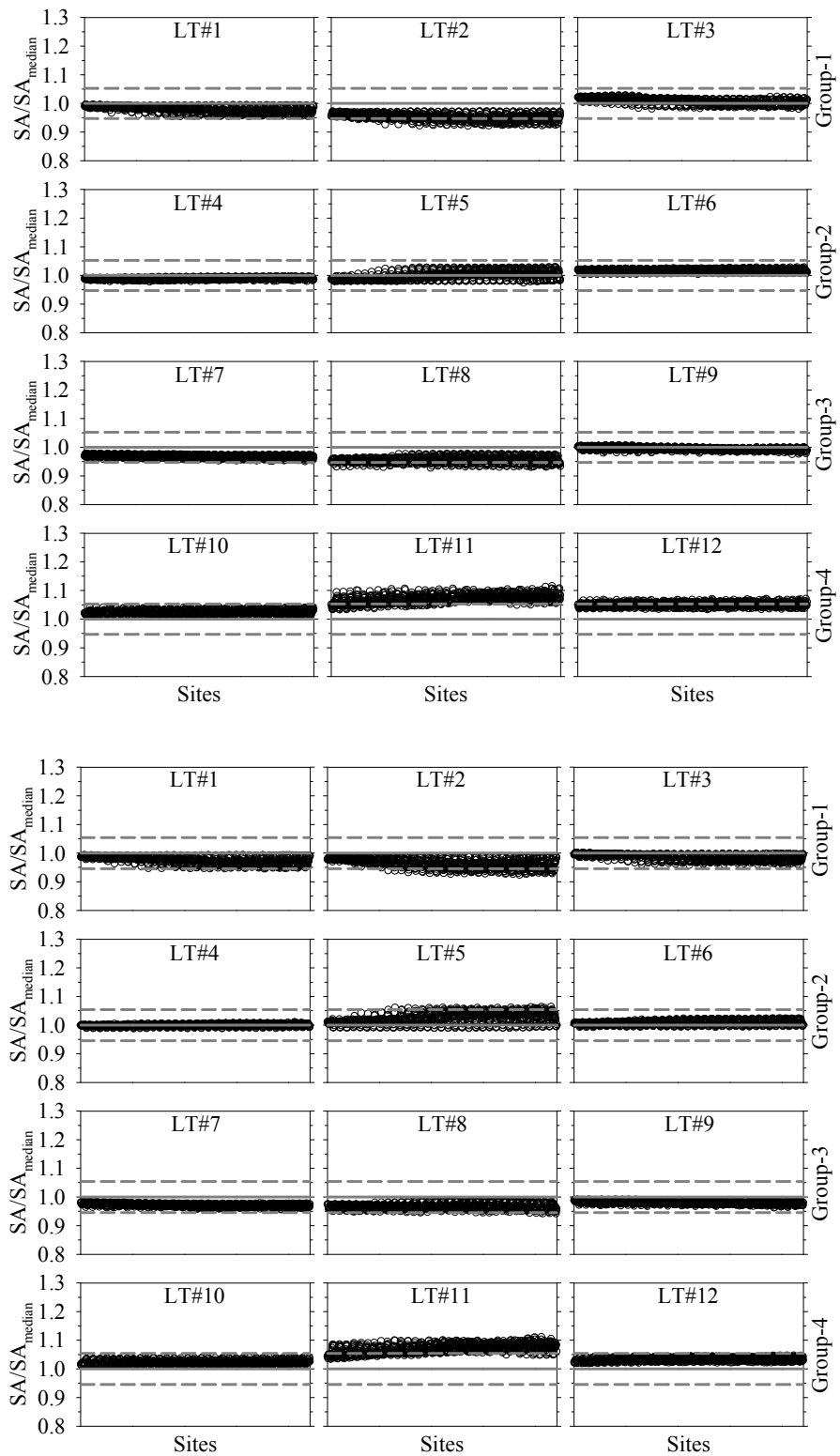
Figure D.4 Results of logic-tree based sensitivity analysis of NAF region for return period of 475yrs and PGA (top group), T=0.2s (bottom group).
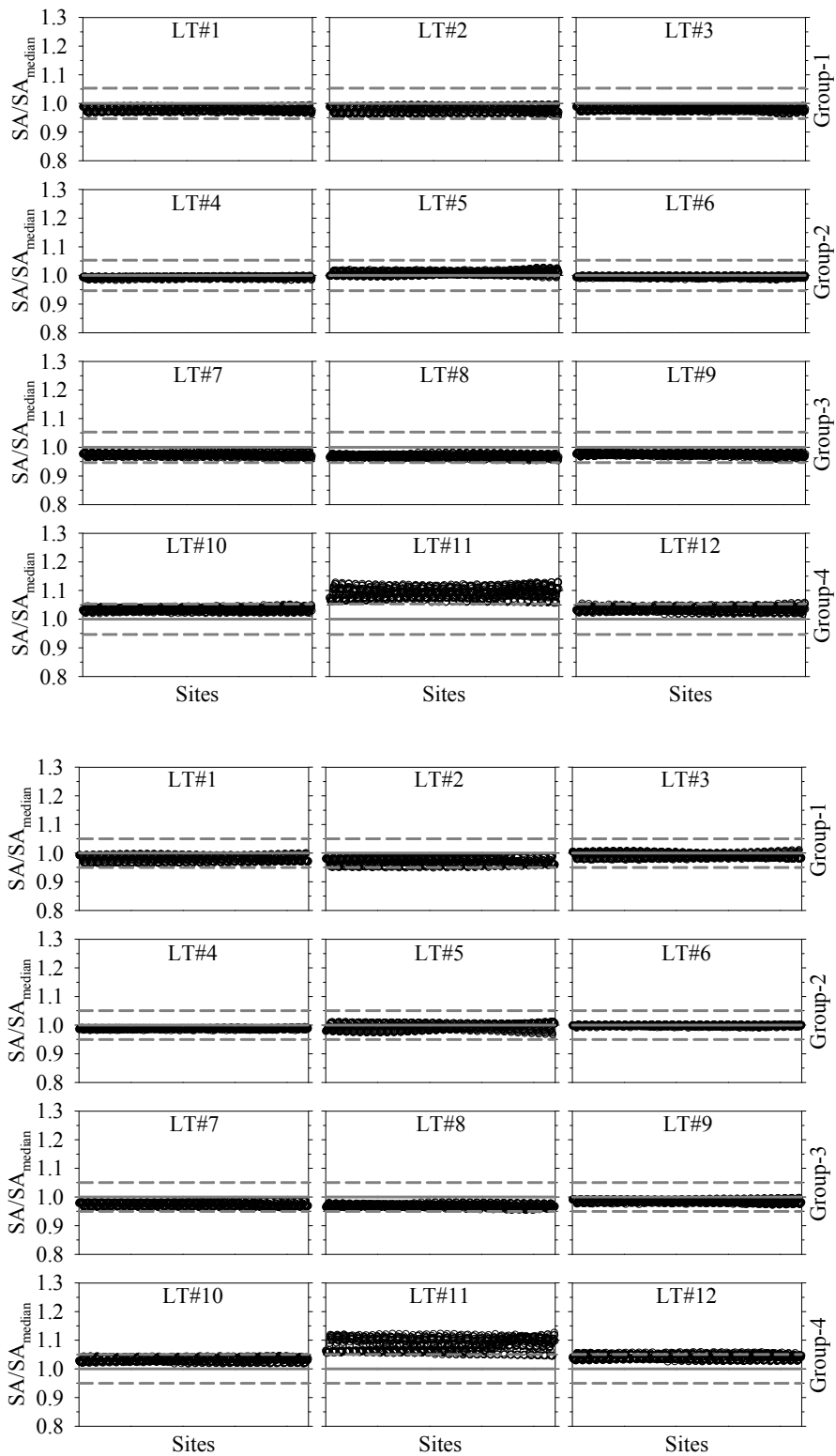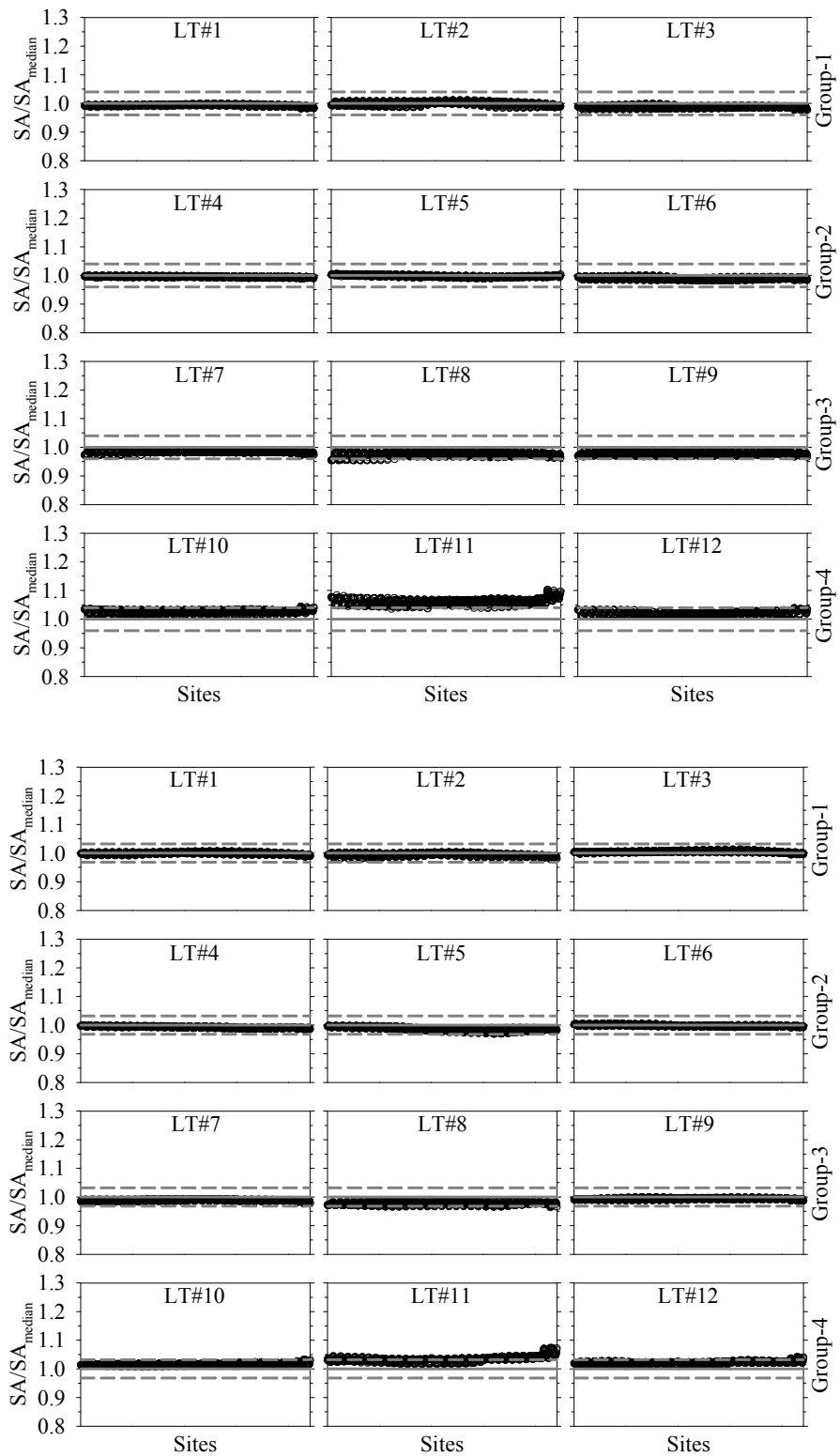
Figure D.5 Results of logic-tree based sensitivity analysis of NAF region for return
period of 475yrs and T=1.0s (top group), T=2.0s (bottom group).

Figure D.6 Results of logic-tree based sensitivity analysis of NAF region for return period of 2475yrs and PGA (top group), T=2.0s (bottom group).
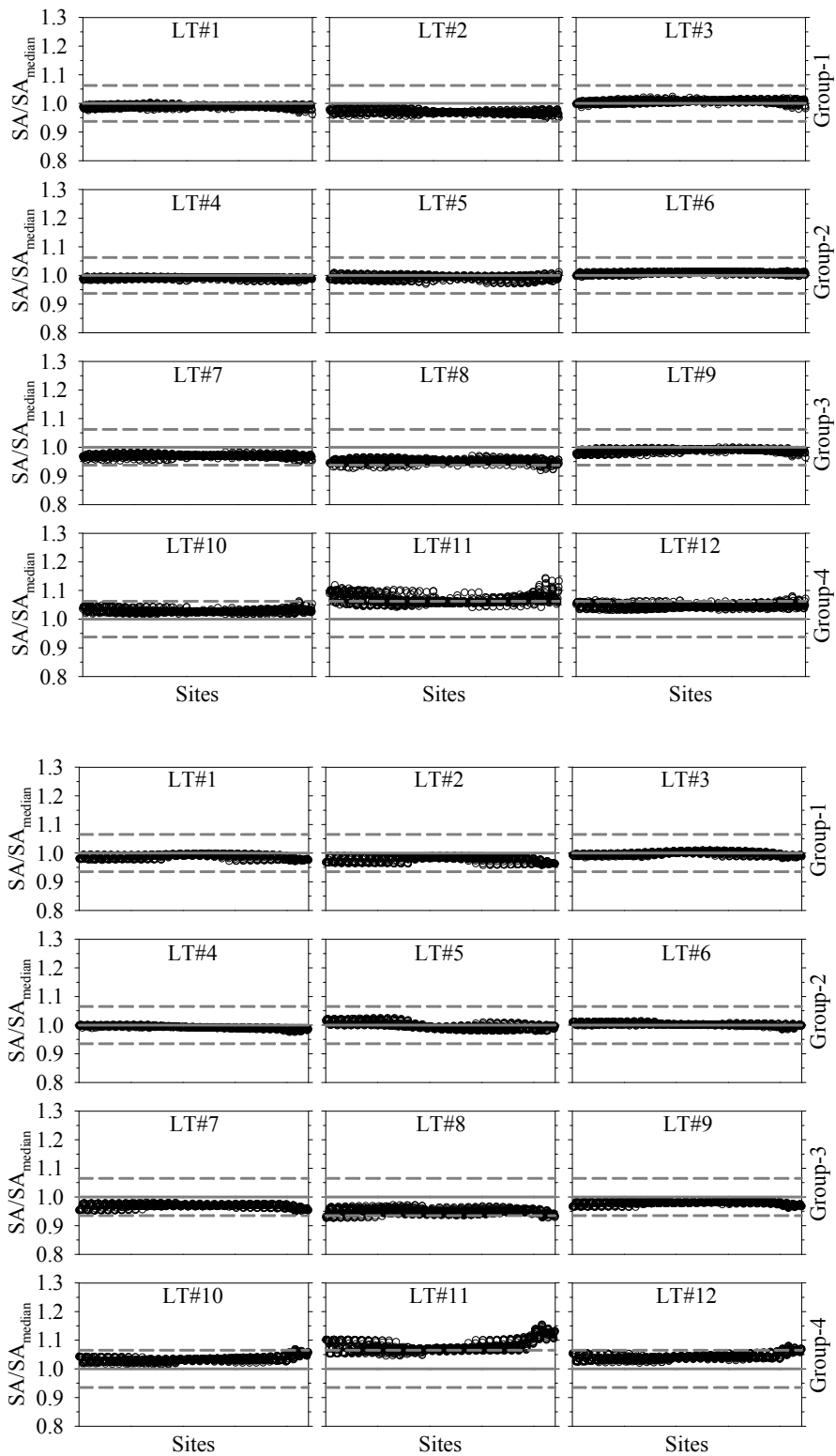
Figure D.7 Results of logic-tree based sensitivity analysis of Mersin region for

return period of 475yrs and PGA (top group), T=0.2s (bottom group).

Figure D.8 Results of logic-tree based sensitivity analysis of Mersin region for return period of 475yrs and T=1.0s (top group), T=2.0s (bottom group).

Figure D.9 Results of logic-tree based sensitivity analysis of Mersin region for return period of 2475yrs and PGA (top group), T=2.0s (bottom group).
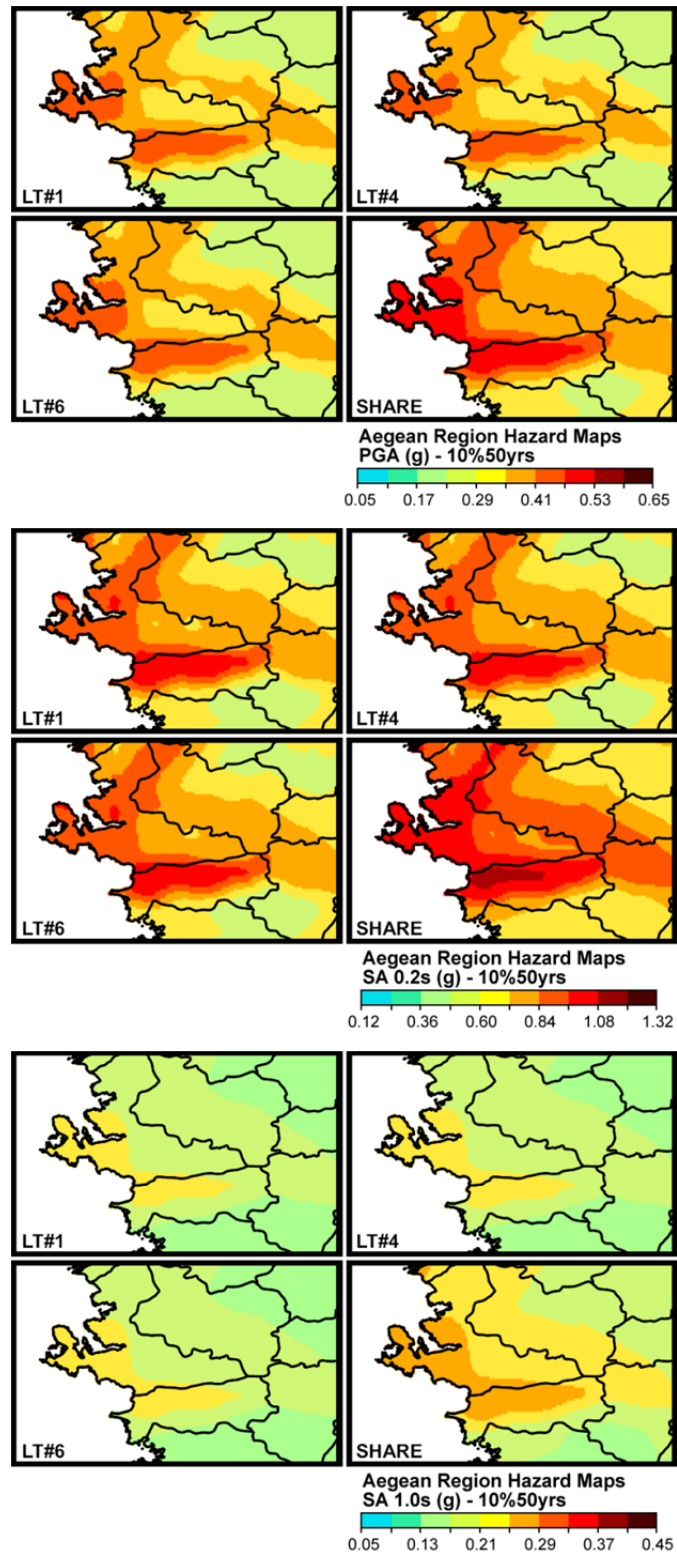
Figure D.10 Comparison of PGA (top), T=0.2s (middle) and T=1.0s (bottom) Aegean region hazard maps computed from LT#1, LT#4 and LT#6 for 475yrs return period. The lower right panels in each group give the SHARE hazard map.
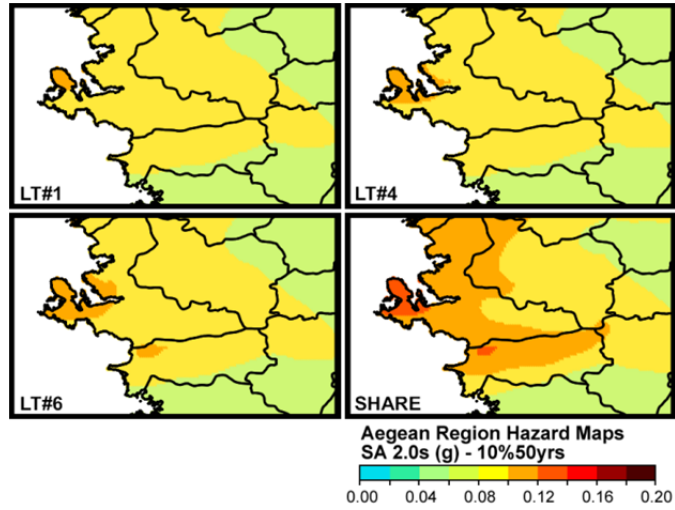
Figure D.11 Comparison of T=2.0s Aegean region hazard maps computed from
LT#1, LT#4 and LT#6 for 475yrs return period. The lower right panels in each
group give the SHARE hazard map.
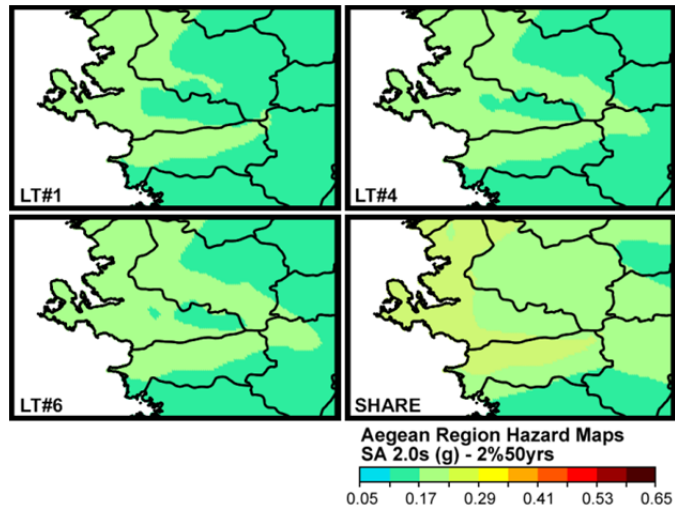

Figure D.12 Comparison of T=2.0s Aegean region hazard maps computed from
LT#1, LT#4 and LT#6 for 2475yrs return period. The lower right panels in each
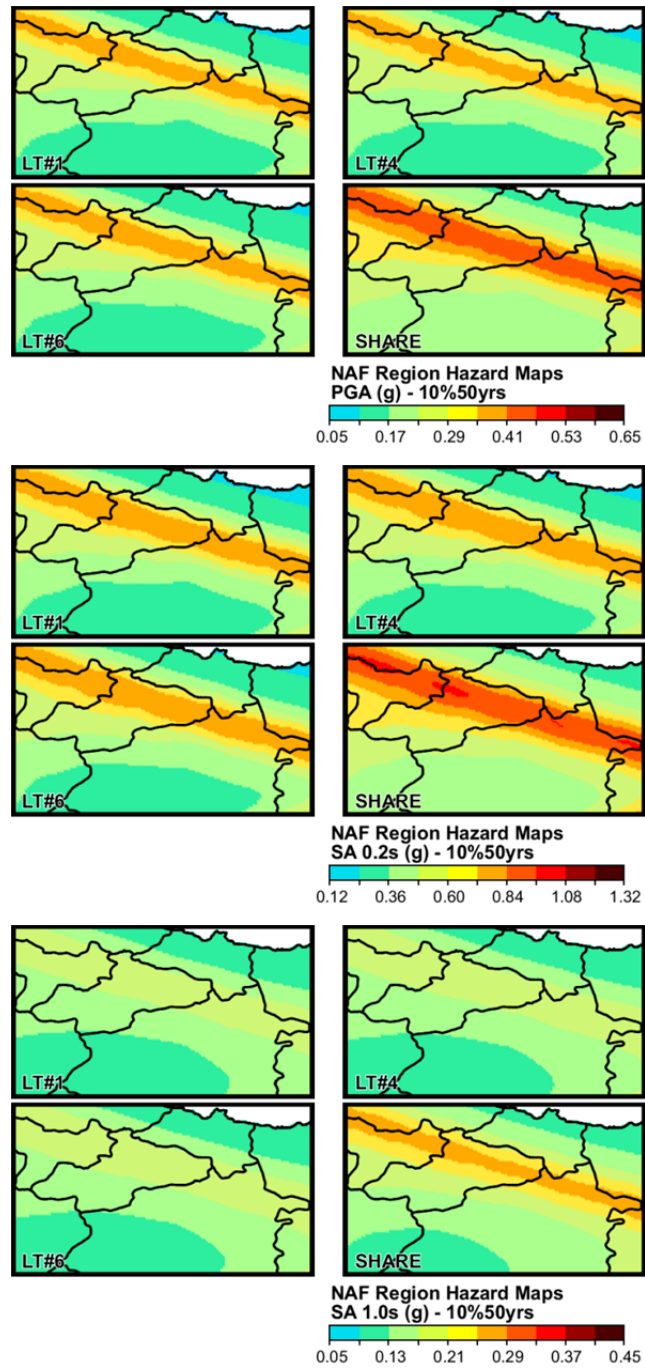group give the SHARE hazard map.

278

Figure D.13 Comparison of PGA (top), T=0.2s (middle) and T=1.0s (bottom) NAF region hazard maps computed from LT#1, LT#4 and LT#6 for 475yrs return period. The lower right panels in each group give the SHARE hazard map.

Figure D.14 Comparison of T=2.0s NAF region hazard maps computed from LT#1, LT#4 and LT#6 for 475yrs return period. The lower right panels in each group give the SHARE hazard map.
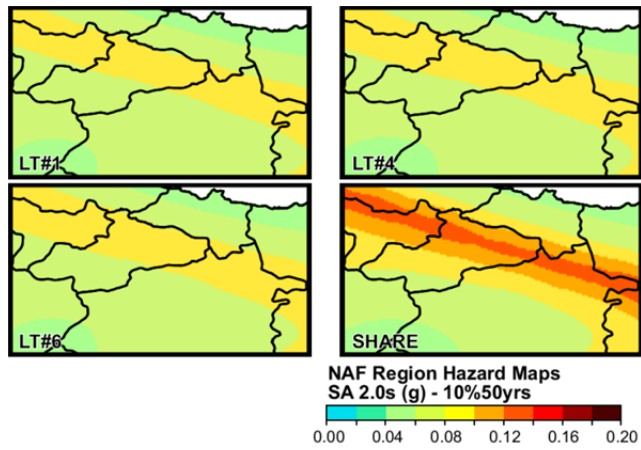

Figure D.15 Comparison of T=2.0s NAF region hazard maps computed from LT#1, LT#4 and LT#6 for 2475yrs return period. The lower right panels in each group give the SHARE hazard map.

Figure D.16 Comparison of PGA (top), T=0.2s (middle) and T=1.0s (bottom) Mersin region hazard maps computed from LT#1, LT#4 and LT#6 for 475yrs return period. The lower right panels in each group give the SHARE hazard map.

Figure D.17 Comparison of T=2.0s Mersin region hazard maps computed from LT#1, LT#4 and LT#6 for 475yrs return period. The lower right panels in each group give the SHARE hazard map.
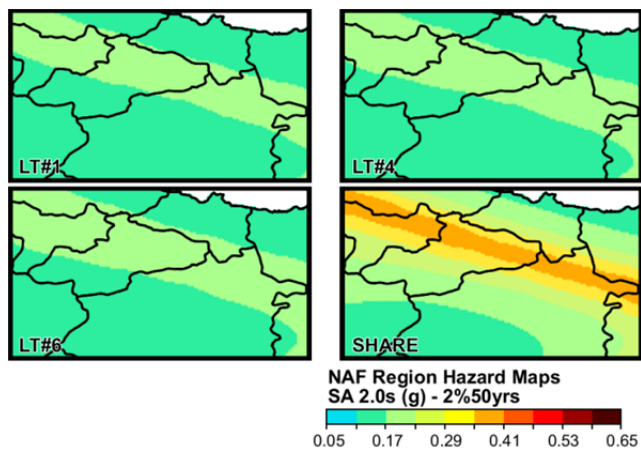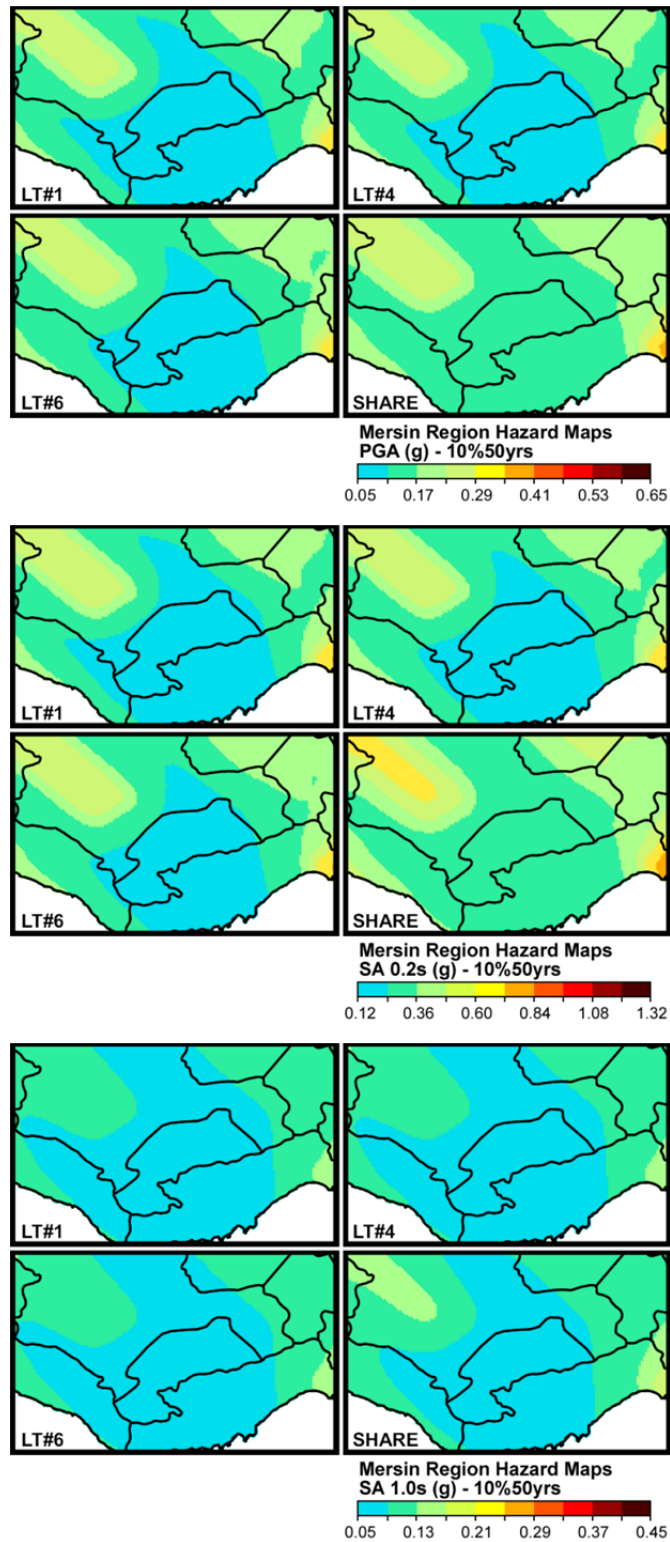

Figure D.18 Comparison of T=2.0s Mersin region hazard maps computed from LT#1, LT#4 and LT#6 for 2475yrs return period. The lower right panels in each group give the SHARE hazard map.
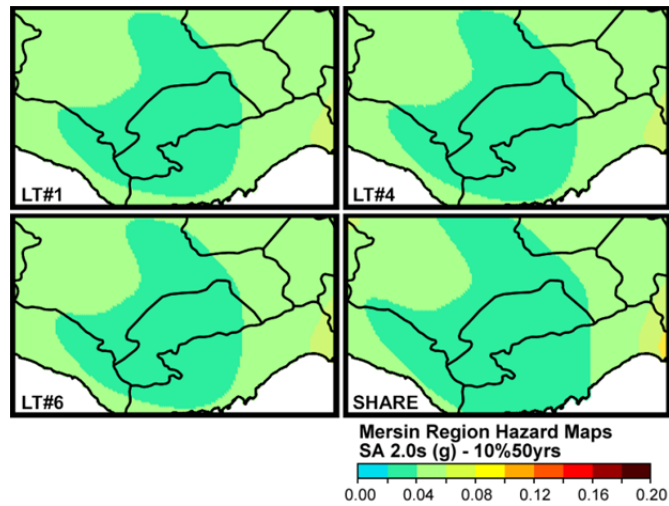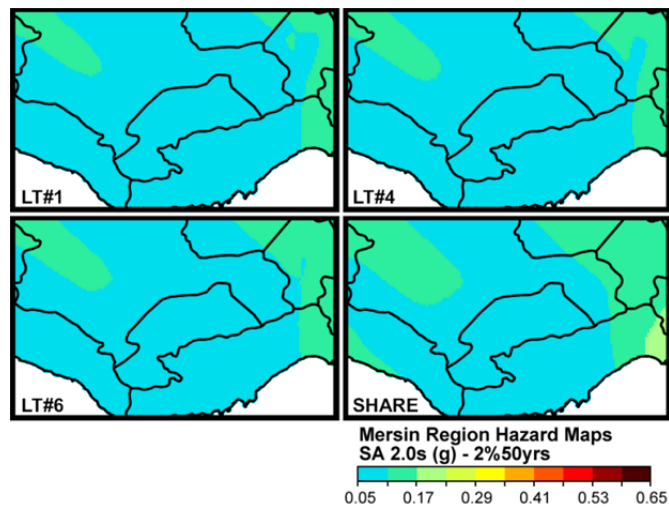
EXTENDING AKKAR AND ÇAĞNAN (2010) GMPE FOR SPECTRAL PERIODS LONGER THAN 2.0s

Akkar and Çağnan (2010) GMPE is going to be implemented in the EMME GMPEs logic-tree for regions of shallow active crustal earthquakes. This model (abbreviated as AC10 hereafter) estimates ground-motion intensities (spectral accelerations, SA) for periods (T) smaller than 2.0s. The other GMPEs that are going to be considered in the EMME GMPEs logic-tree are Akkar et al. (2014) - ASB14, Chiou and Youngs (2008) - CY08, and Zhao et al. (2006) - Zetal06 that can estimate SA for periods, at least, up to 4.0s, which is the target spectral period limit in EMME. The spectral period differences between AC10 and the rest of the GMPEs may cause a discontinuity (jump) in the uniform hazard spectrum (UHS) computed for the active shallow crustal EMME regions. Thus, the spectral ordinate estimations of AC10 are extended between $2.0 < T \leq 4.0$ to warrant a smooth variation of UHS in shallow active crustal regions covered by EMME. This short document describes the steps followed to achieve above objective. The first four steps describe extension of median SA estimations of AC10 for $T > 2.0s$. The last step documents the suggested period-dependent standard deviation (sigma) of AC10 for $T > 2.0s$

Step #1. Compute SA($T \geq 2.0s$) / SA($T = 2.0s$) ratios (abbreviated as ratios hereafter) for different magnitude (M_w) and distance (R_{JB} or R_{RUP}) scenarios for a generic rock site ($V_{S30} = 760$ m/s) by using ASB14, CY08 and Zetal06. (Note that consideration of other site classes do not change the results as their effects on ground-motion amplitudes

will be diminished while taking the ratios. Moreover EMME PSHA is only for generic rock sites). The earthquake scenarios consider a perfect strike-slip fault (dip angle is $90°$). The depth-to-top-of-rupture (Z_{TOR}) that accounts for the ground-motion amplitude differences between buried and surface ruptures are used while converting the predetermined R_{JB} distances to R_{RUP}. CY08 and Zetal06 use the latter distance metric. Z_{TOR} expression provided by Chiou and Youngs (2008) is used for distance conversion. Thus, the source-to-site distance values are consistent for each GMPE used in this exercise. Figure E.1 presents the variations of ratios for each M_w-R_{JB} scenario and for each GMPE. The distance effect is minimal in the variation of ratios.

Step #2.   Then the variation of ratios by ignoring the distance effects is studied. The average ratios for each GMPE ($\overline{\text{Ratio}}_{\text{GMPE}_i}$, i = 1, 2, 3) that disregard distance effects are given in Figure E.2 for different magnitudes. Figure E.2 also shows the ratios computed by averaging 3 $\overline{\text{Ratio}}_{\text{GMPE}_i}$ ($\overline{\text{Ratio}}_{\text{allGMPEs}}$) at each magnitude level.   In a way, $\overline{\text{Ratio}}_{\text{GMPE}_i}$ disregards the ratio differences originating from each GMPE. The ratio trends of each GMPE (i.e., $\overline{\text{Ratio}}_{\text{GMPE}_i}$) and $\overline{\text{Ratio}}_{\text{allGMPEs}}$ are similar to each other.

Step #3. $\overline{\text{Ratio}}_{\text{allGMPEs}}$ curves given in Figure E.2 are used to extend AC10 estimations for $T \geq 2.0s$. These are given in Figures E.3 - E.11 in terms of spectral displacement (SD; better illustrates the differences at longer periods). These figures also display the extended AC10 spectral ordinates computed from the consideration of both magnitude and distance influences (already discussed in Step #1) that are separately provided by ABS14, CY08 and Zetal06. The spectral ordinate differences between the average SD curves (via $\overline{\text{Ratio}}_{\text{allGMPEs}}$) and those computed from the latter set are negligible in many cases.

Step #4. Under these observations, the magnitude-dependent (but GMPE independent) $\overline{Ratio}_{allGMPEs}$ curves for extending the spectral ordinates of AC10 beyond T = 2.0s are proposed. These are listed in Table E.2. Equation (E.1) that yields very close $\overline{Ratio}_{allGMPEs}$ values to those presented in Table E.2 is also provided. The coefficients of Equation (E.1) are given in Table E.1. As indicated both sources of information can equally be applicable while extending AC10 for periods longer than 2s.

Step #5. Figure E.12 shows the period-dependent sigma of all GMPEs used in EMME GMPEs logic-tree. CY08 models sigma in terms of magnitude, soil behavior and event-based differences (mainshock vs. aftershock). The rest of the GMPEs only consider period dependency in sigma. AC10 sigma is plotted for periods up to 2.0s in Figure E.12. The overall trends indicate similar sigma patterns between AC10 and ASB14 for T ≤ 2.0s. This is speculatively expected because AC10 uses the Turkish dataset of the pan-European dataset utilized by ASB14. Thus, the sigma ratios between AC10 and ASB14 are used for T ≤ 2.0s to estimate AC10 sigmas beyond T = 2.0s. The AC10 to ASB14 sigma ratios (Table E.3) for T ≤ 2.0s are fairly constant and fluctuate about 1.14. However, direct use of 1.14 while extending AC10 sigmas beyond T = 2.0s causes an unexpected jump at the cutoff period (T = 2.0s). Thus, we slightly changed this average modification factor to obtain a smoother sigma variation for AC10 for T > 2.0s. In essence, the value of 1.11 is proposed to use as the modifying factor to estimate AC10 sigmas beyond T = 2.0s. The use of 1.11, instead of 1.14, does not make a huge impact on the estimated AC10 sigmas but results in a smooth transition while extending AC10 sigma for T > 2.0s. The proposed sigma values of AC10 for T > 2.0s are given in Table E.4.

$$\overline{\text{Ratio}}_{\text{allGMPEs}} = \left(a_1 + a_2 \cdot M_w + a_3 \cdot M_w^2 \right) \cdot T^{\left(b_1 + b_2 \cdot M_w + b_3 \cdot M_w^2 \right)}$$ (E.1)

Table E.1 Magnitude and period dependent coefficients of Equation (E.1).

a_1	a_2	a_3	b_1	b_2	b_3
15.17063	-3.38508	0.22543	-5.78063	1.12156	-0.06989

Table E.2 Magnitude-dependent $\overline{\text{Ratio}}_{\text{allGMPEs}}$ values up to 4.0s.

Period	$M_w 4.0$	$M_w 4.5$	$M_w 5.0$	$M_w 5.5$	$M_w 6.0$	$M_w 6.5$	$M_w 7.0$	$M_w 7.5$	$M_w 8.0$
2.1	0.898	0.907	0.916	0.925	0.932	0.939	0.943	0.946	0.946
2.2	0.802	0.819	0.836	0.853	0.868	0.880	0.888	0.894	0.894
2.3	0.722	0.745	0.769	0.793	0.813	0.830	0.842	0.849	0.850
2.4	0.645	0.675	0.705	0.735	0.761	0.782	0.797	0.806	0.807
2.5	0.580	0.614	0.649	0.683	0.713	0.737	0.754	0.764	0.765
2.6	0.533	0.568	0.604	0.639	0.671	0.697	0.715	0.726	0.727
2.7	0.490	0.525	0.562	0.599	0.633	0.660	0.679	0.691	0.691
2.8	0.448	0.485	0.523	0.561	0.596	0.623	0.643	0.656	0.657
2.9	0.410	0.447	0.485	0.524	0.559	0.588	0.608	0.621	0.621
3.0	0.374	0.410	0.449	0.488	0.524	0.553	0.574	0.587	0.587
3.1	0.353	0.389	0.428	0.466	0.502	0.531	0.552	0.565	0.565
3.2	0.335	0.370	0.408	0.446	0.482	0.511	0.532	0.544	0.544
3.3	0.311	0.346	0.384	0.424	0.460	0.490	0.512	0.525	0.524
3.4	0.288	0.324	0.362	0.402	0.440	0.470	0.492	0.505	0.505
3.5	0.267	0.302	0.341	0.382	0.420	0.452	0.475	0.488	0.488
3.6	0.246	0.282	0.321	0.363	0.402	0.434	0.458	0.472	0.472
3.7	0.230	0.266	0.305	0.347	0.386	0.419	0.443	0.457	0.457
3.8	0.214	0.250	0.289	0.331	0.371	0.404	0.428	0.443	0.442
3.9	0.199	0.234	0.273	0.316	0.356	0.390	0.414	0.429	0.428
4.0	0.183	0.218	0.258	0.301	0.342	0.376	0.401	0.416	0.415

Table E.3 AC10 to ASB14 sigma ratios for T ≤ 2.0s.

Period	$\sigma_{AC10} / \sigma_{ASB14}$
PGA	1.17
0.05	1.11
0.1	1.11
0.15	1.13
0.2	1.16
0.25	1.18
0.3	1.16
0.35	1.15
0.4	1.14
0.45	1.14
0.5	1.13
0.6	1.13
0.65	1.13
0.7	1.13
0.75	1.14
0.8	1.15
0.9	1.16
1	1.16
1.25	1.15
1.5	1.14
1.75	1.13
2	1.11

Table E.4 Proposed sigma values of AC10 for T > 2.0s.

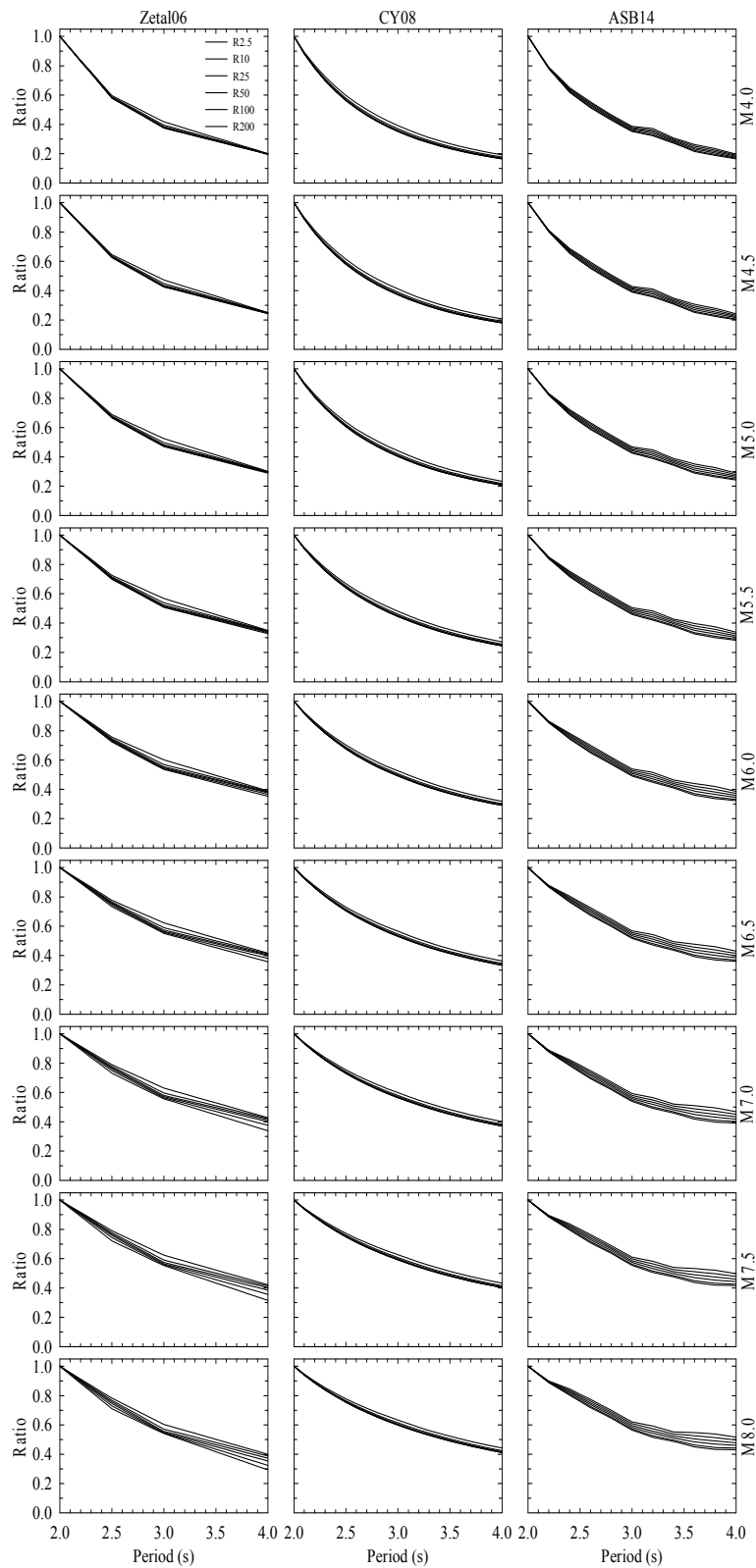| Period	σ_{AC10}
2.1	0.9035
2.2	0.9022
2.3	0.9048
2.4	0.9074
2.5	0.9071
2.6	0.9067
2.7	0.9077
2.8	0.9087
2.9	0.9029
3.0	0.8972
3.1	0.8929
3.2	0.8887
3.3	0.8758
3.4	0.8628
3.5	0.8616
3.6	0.8604
3.7	0.8530
3.8	0.8457
3.9	0.8196
4.0	0.7935

Figure E.1 SA(T ≥ 2.0s) / SA(T = 2.0s) variations for each M_w-R_{JB} scenario and for each GMPE.
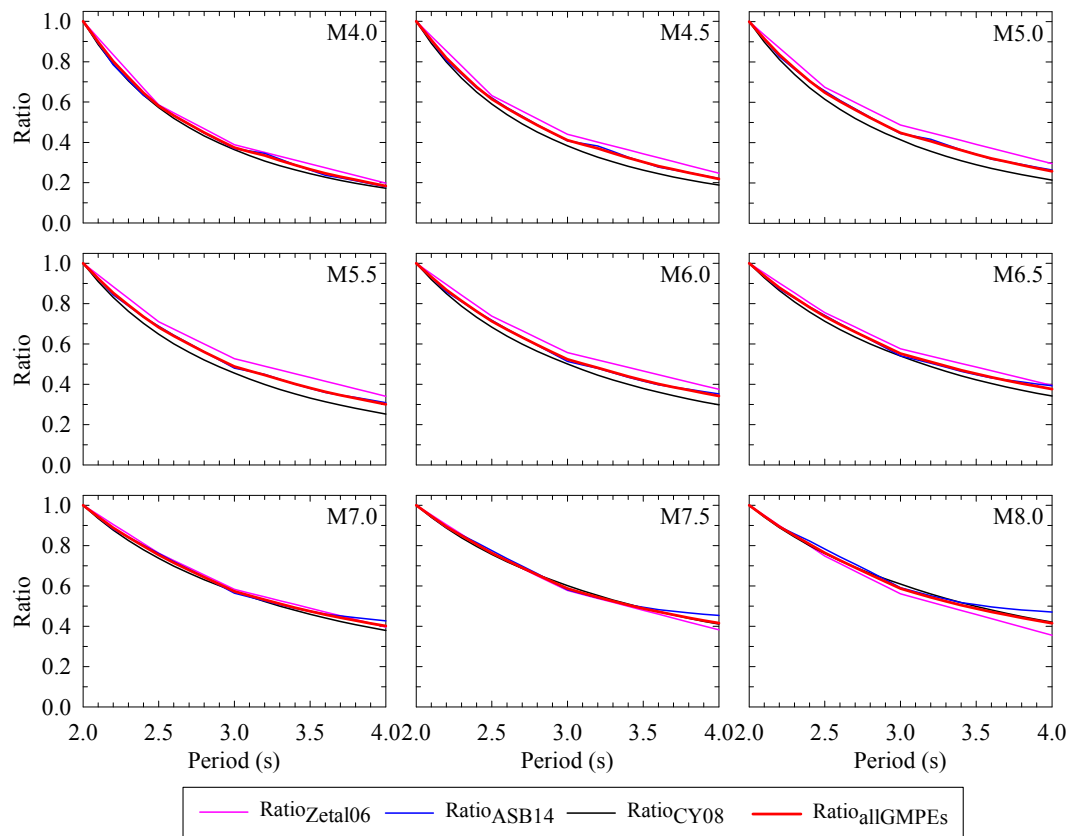
Figure E.2 Average SA(T ≥ 2.0s) / SA(T = 2.0s) ratios for each GMPE ($\overline{\text{Ratio}}_{\text{GMPE}_i}$)

and ratios computed by averaging 3 $\overline{\text{Ratio}}_{\text{GMPE}_i}$ ($\overline{\text{Ratio}}_{\text{allGMPEs}}$) at each magnitude
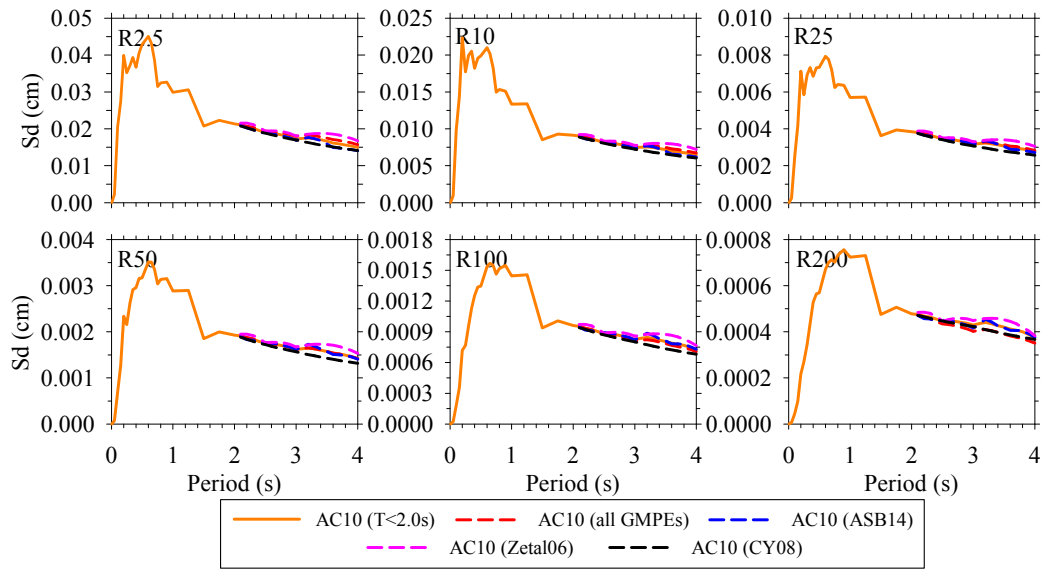
level.

Figure E.3 Extended AC10 spectral ordinates obtained from $\overline{Ratio}_{allGMPEs}$ (red curve) and those computed from ABS13, CY08 and Zetal06 by considering the magnitude and distance influences at the same time. Plots show AC10 variation for M_w 4.0.
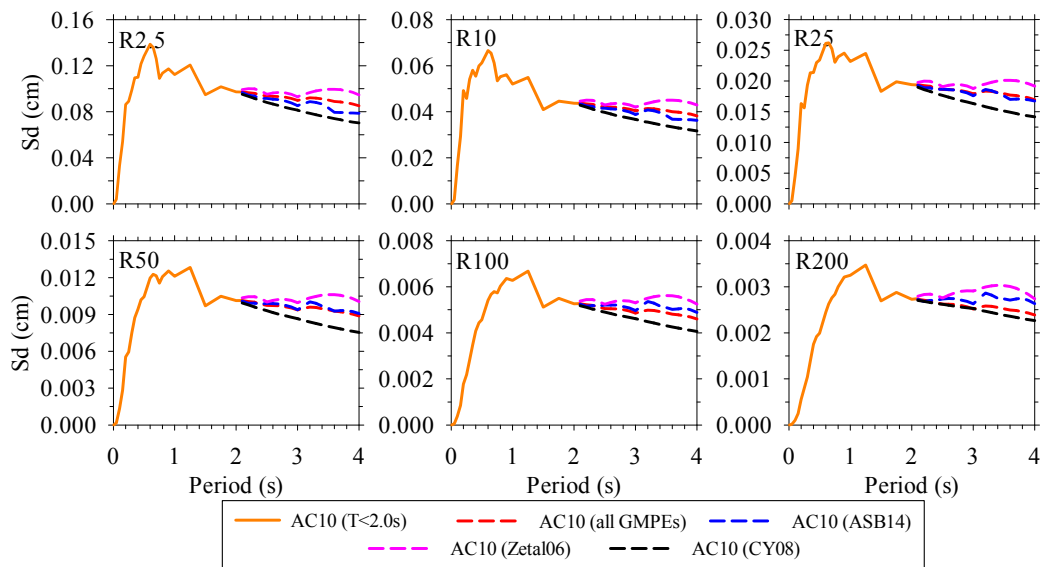

Figure E.4 Extended AC10 spectral ordinates obtained from $\overline{Ratio}_{allGMPEs}$ (red curve) and those computed from ABS14, CY08 and Zetal06 by considering the magnitude and distance influences at the same time. Plots show AC10 variation for M_w 4.5.
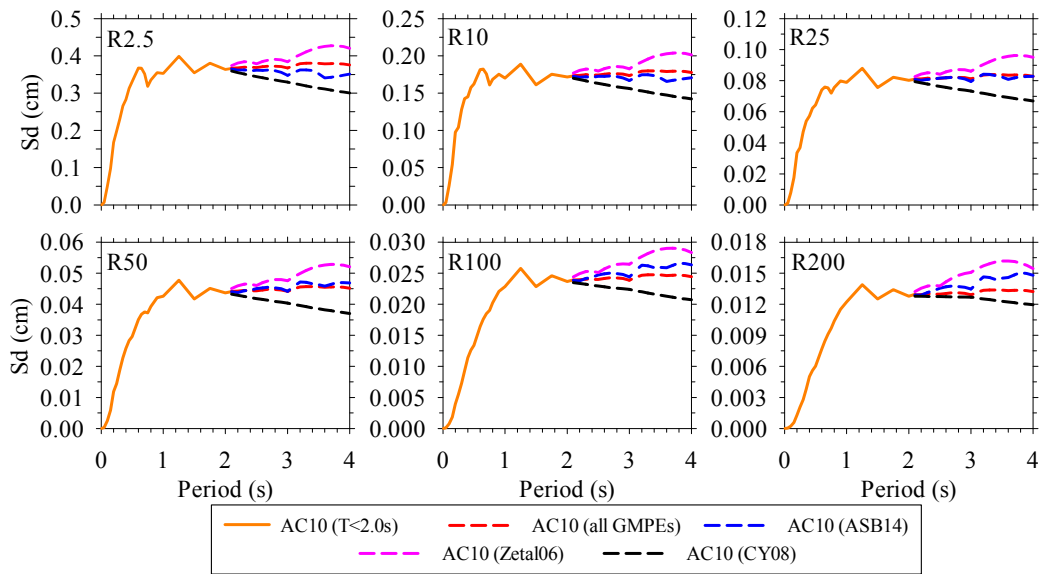
290

Figure E.5 Extended AC10 spectral ordinates obtained from $\overline{\text{Ratio}}_{\text{allGMPEs}}$ (red curve) and those computed from ABS14, CY08 and Zetal06 by considering the magnitude and distance influences at the same time. Plots show AC10 variation for M_w 5.0.

Figure E.6 Extended AC10 spectral ordinates obtained from $\overline{\text{Ratio}}_{\text{allGMPEs}}$ (red curve) and those computed from ABS14, CY08 and Zetal06 by considering the magnitude and distance influences at the same time. Plots show AC10 variation for M_w 5.5.
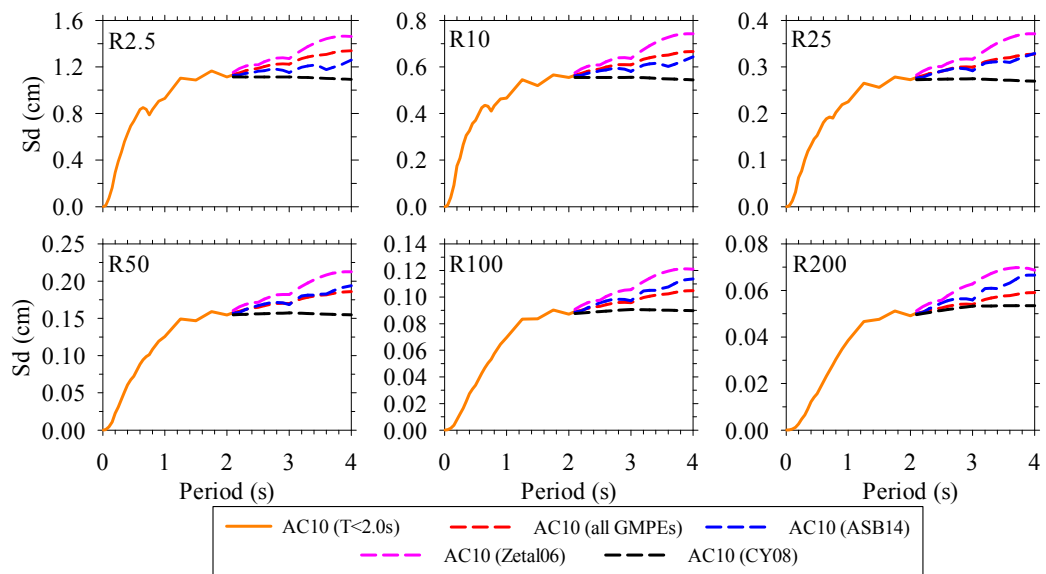
Figure E.7 Extended AC10 spectral ordinates obtained from $\overline{\text{Ratio}}_{\text{allGMPEs}}$ (red curve) and those computed from ABS14, CY08 and Zetal06 by considering the magnitude and distance influences at the same time. Plots show AC10 variation for M_w 6.0.
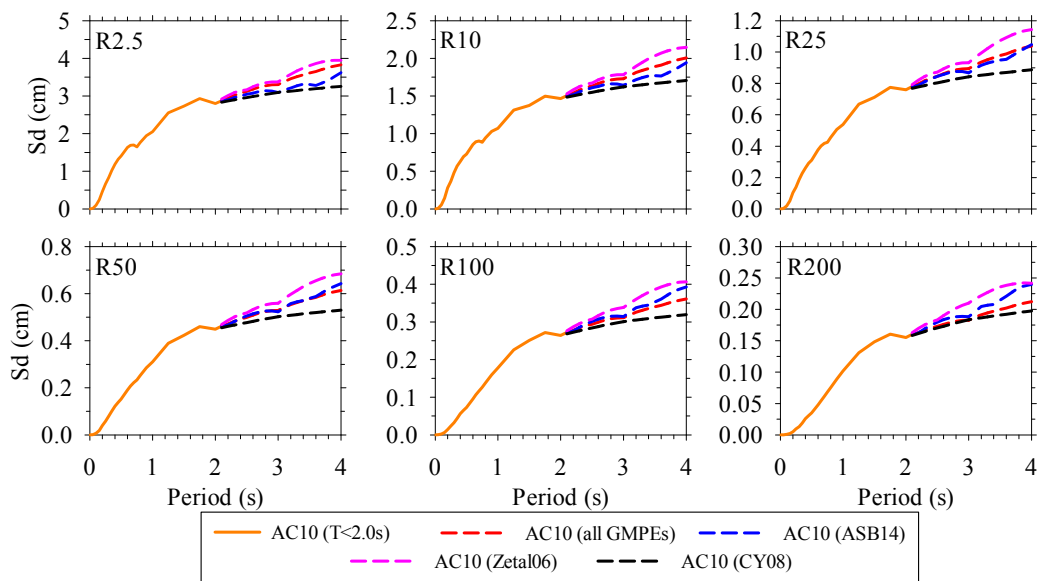

Figure E.8 Extended AC10 spectral ordinates obtained from $\overline{\text{Ratio}}_{\text{allGMPEs}}$ (red curve) and those computed from ABS14, CY08 and Zetal06 by considering the magnitude and distance influences at the same time. Plots show AC10 variation for M_w 6.5.

Figure E.9 Extended AC10 spectral ordinates obtained from $\overline{\text{Ratio}}_{\text{allGMPEs}}$ (red curve) and those computed from ABS14, CY08 and Zetal06 by considering the magnitude and distance influences at the same time. Plots show AC10 variation for M_w 7.0.
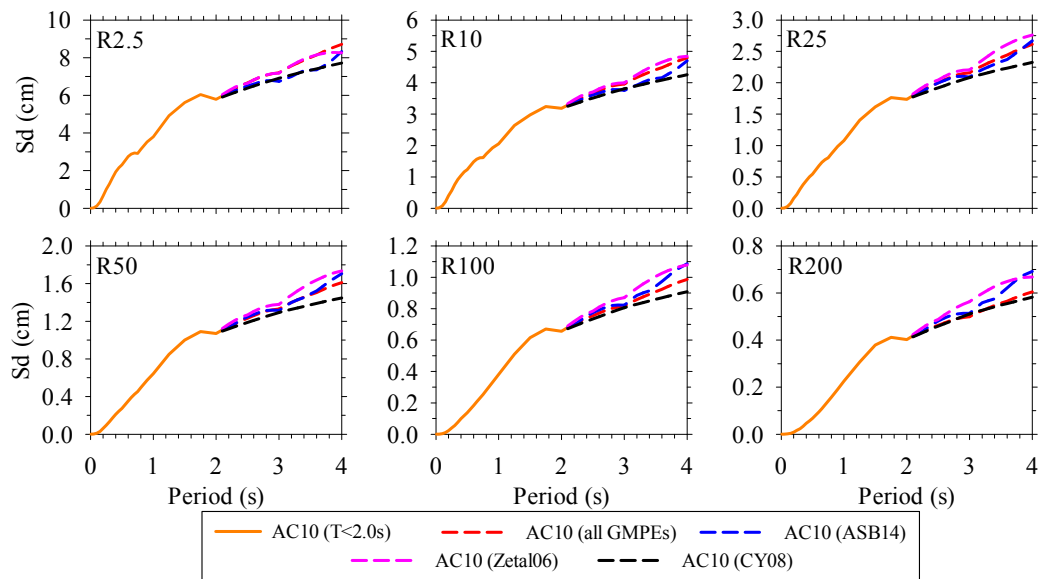

Figure E.10 Extended AC10 spectral ordinates obtained from $\overline{\text{Ratio}}_{\text{allGMPEs}}$ (red curve) and those computed from ABS14, CY08 and Zetal06 by considering the magnitude and distance influences at the same time. Plots show AC10 variation for M_w 7.5.
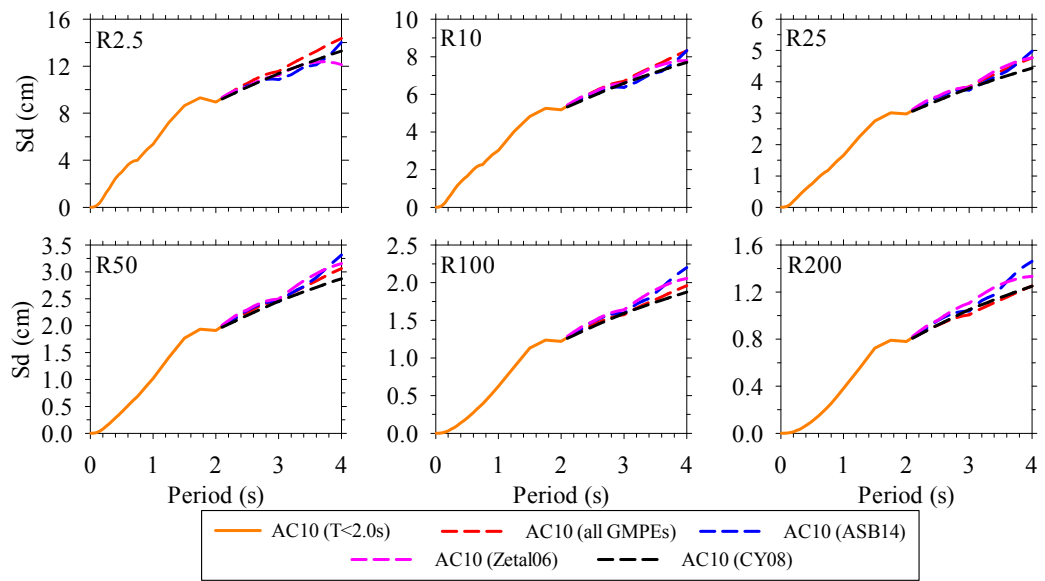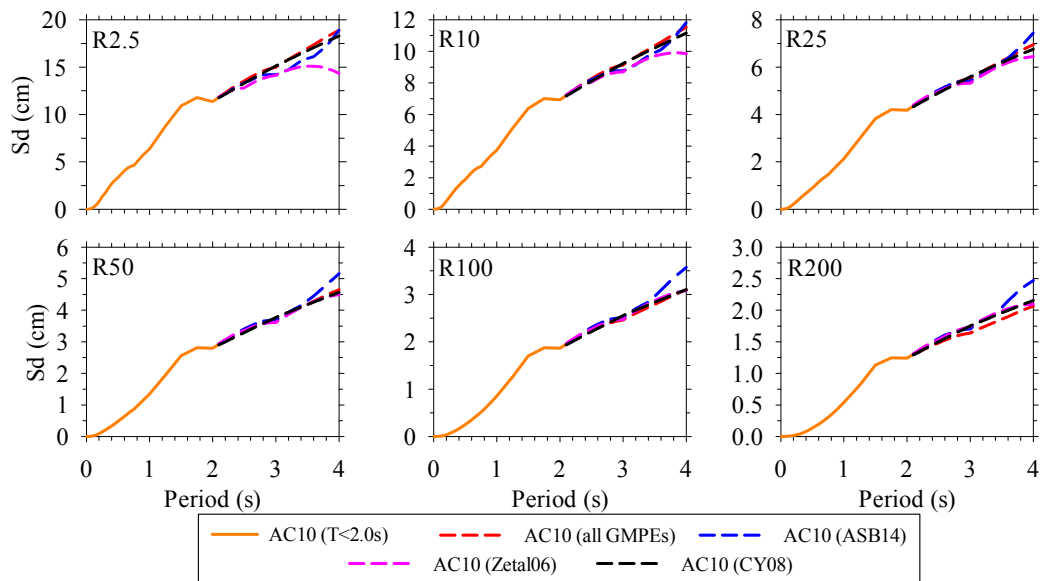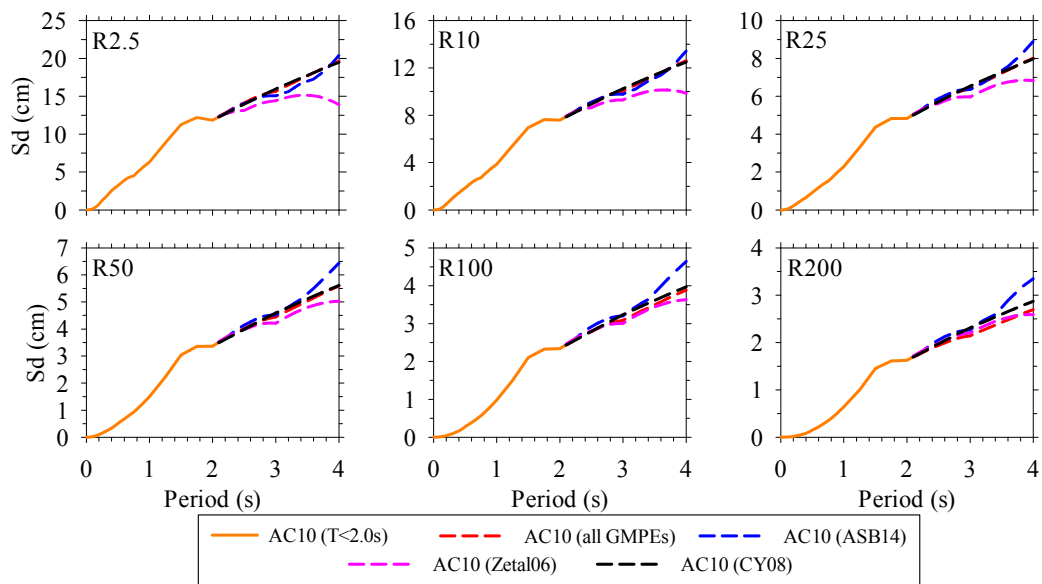
Figure E.11 Extended AC10 spectral ordinates obtained from $\overline{\text{Ratio}}_{\text{allGMPEs}}$ (red curve) and those computed from ABS14, CY08 and Zetal06 by considering the magnitude and distance influences at the same time. Plots show AC10 variation for M_w 8.0.
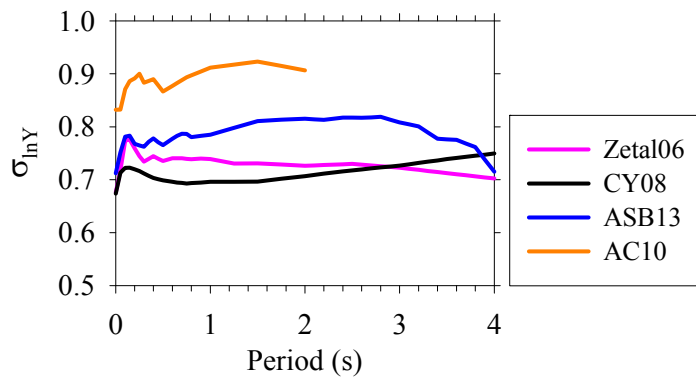

Figure E.12 Period-dependent sigmas of all GMPEs.

CURRICULUM VITAE

ÖZKAN KALE

Mailing Adress:
Middle East Technical University
Department of Civil Engineering
Earthquake Engineering Research Center
K6 Building, Room No: 110
06800, Ankara, Turkey
Phone: +90 535 3144837
E-mail: ozkankale@gmail.com
Web page: http://www.metu.edu.tr/~okale/

PERSONAL INFORMATION

Date of birth   : 02 September, 1981
Marital status   : Married
Military service   : Done

EDUCATION

Ph. D., Civil Engineering, 2010-present (expected September 2014)
Middle East Technical University
Research Advisor: Prof. Dr. Sinan Akkar
Research Co-Advisor: Dr. Laurentiu Danciu
Proposed Thesis Title: Practical Tools for Ranking and Selection of Ground-Motion Prediction Equations (GMPEs) for Probabilistic Seismic Hazard Assessment and Development of a Regional GMPE

M. Sc., Civil Engineering, 2006-2009
Middle East Technical University
Research Advisor: Prof. Dr. Sinan Akkar
Thesis Title: An Empirical Relationship Based on High-Pass Filtering to Estimate Usable Period Range for Nonlinear SDOF Response

B. Sc., Civil Engineering, 2000-2005
Dokuz Eylül University

Research Assistant
2010-present, Department of Civil Engineering, Middle East Technical University

Invited Researcher
2012 (January 30 to February 6), Swiss Seismological Service, ETH Zurich

Project Assistant
2006-2009, Department of Civil Engineering, Middle East Technical University

HONORS

- Ranked second among all of the Dokuz Eylül University Civil Engineering students in year 2005.

THESIS

- Kale, Ö., (2014). Practical Tools for Ranking and Selection of Ground-Motion Prediction Equations (GMPEs) for Probabilistic Seismic Hazard Assessment and Development of a Regional GMPE, Ph.D. Thesis, Department of Civil Engineering, Middle East Technical University, Ankara.
- Kale, Ö., (2009). An Empirical Relationship Based on High-Pass Filtering to Estimate Usable Period Range for Nonlinear SDOF Response, M.Sc. Thesis, Department of Civil Engineering, Middle East Technical University, Ankara.

PEER-REVIEWED JOURNAL PAPERS COVERED BY SCI

- Kale, Ö., Akkar, S., Ansari, A. and Hamzehloo, H. (2014). A ground-motion predictive model for Iran and Turkey for horizontal PGA, PGV and 5%-damped response spectrum: Investigation of possible regional effects, Bulletin of the Seismological Society of America, submitted.
- Akansel, V.H., Ameri, G., Askan, A., Caner, A., Erdil, B., Kale, Ö. and Okuyucu, D. (2014). The 23 October 2011 M_w 7.0 Van (Eastern Turkey) Earthquake: Characteristics of Recorded Strong Ground Motions and Post Earthquake Condition Assessment of Infrastructure and Cultural Heritage, Earthquake Spectra, 30, 2, 657-682.
- Okuyucu, D., Kale, Ö., Erdil, B., Caner, A., Askan, A. and Akansel, V.H. (2014). Evaluation of Successful Seismic Bridge Design Practice in Turkey, Journal of Performance of Constructed Facilities ASCE, 28, 4-12.
- Kale, Ö. and Akkar, S. (2013). A New Procedure for Selecting and Ranking Ground-Motion Prediction Equations (GMPEs): Euclidean Distance-Based Ranking (EDR) Method, Bulletin of the Seismological Society of America, 103, 2A, 1069-1084.

PEER-REVIEWED JOURNAL PAPERS COVERED BY SCI (Cont'd.)

- Bommer, J.J., Akkar, S. and Kale, Ö. (2011). A Model for Vertical-to-Horizontal Response Spectral Ratios for Europe and the Middle East, Bulletin of the Seismological Society of America, 101, 4, 1783-1806.
- Akkar, S., Kale, Ö., Yenier, E. and Bommer J.J. (2011). The High-Frequency Limit of Usable Response Spectral Ordinates from Filtered Analogue and Digital Strong-Motion Accelerograms, Earthquake Engineering and Structural Dynamics, 40, 1387-1401.

CHAPTERS IN SCIENTIFIC BOOKS

- Akkar, S., Gülkan, P. and Kale, Ö. (2010). Uncertainty in Nonlinear SDOF Response Due to Long-Period Noise of Accelerograms, Advances in Performance-Based Earthquake Engineering, vol.13, part 1, 69-78.

CONFERENCE PROCEEDINGS

- Akkar, S. and Kale, Ö. (2014). Developments in Ground Motion Predictive Models and Accelerometric Data Archiving in the Broader European Region, Second European Conference on Earthquake Engineering and Seismology, İstanbul, Turkey, EAEE Theme Lecture No. 35.
- Kale, Ö. and Akkar, S. (2013). Türkiye için Geliştirilen Yeni Bir Yer Hareketi Tahmin Denklemi ve Bu Denklemin Orta Doğu Bölgesinde Yapılacak Sismik Tehlike Çalışmaları için Uygunluğunun Test Edilmesi, 2. Türkiye Deprem Mühendisliği ve Sismoloji Konferansı, MKU, Hatay, Paper No. 172.
- Kale, Ö. and Akkar, S. (2012). A Method to Determine the Appropriate GMPEs for a Selected Seismic Prone Region, 15th World Conference on Earthquake Engineering, Lisbon, Portugal, Paper No. 2827.
- Kale, Ö. and Akkar, S. (2011). Yerel ve Global Yer Hareketi Tahmin Denklemlerinin Türkiye için Uygulanabilecek Sismik Tehlike Analizlerinde Kullanılabilirliklerinin Test Edilmesi, 1. Türkiye Deprem Mühendisliği ve Sismoloji Konferansı, METU, Ankara, Paper No. 111.
- Kale, Ö., Akkar, S. and Erberik, M.A., (2008). Influence of Low-Cut Filter Frequency on Nonlinear Oscillator Displacements Computed from Non-Degrading to Degrading Hysteretic Models, 14th World Conference on Earthquake Engineering, Beijing, China, Paper No. 02-0091.

TECHNICAL PRESENTATIONS

- Akkar, S., Kale, Ö., Ansari, A., Durgaryan, R., Askan Gündoğan, A., Hamzehloo, H., Harmandar, E., Tsereteli, N., Waseem, M., Yazjeen, T. and Yılmaz, M.T. (2014). EMME Strong-Motion Database Serving For Predictive Model Selection to EMME Ground-Motion Logic-Tree Applications, Second European Conference on Earthquake Engineering and Seismology, İstanbul, Turkey, Abstract No. 3220.
- Kale, Ö. ve Akkar, S. (2014). Investigation of Regional Differences Between Turkey and Iran on the Use of Strong-Motion Data Trends, Second European Conference on Earthquake Engineering and Seismology, İstanbul, Turkey, Abstract No. 1658.
- Kale, Ö. and Akkar, S. (2013). A New Ground-Motion Prediction Equation for Turkey and the Testing of Its Applicability to Middle East Region, SSA 2013 Annual Meeting, Salt Lake City, Utah, USA.
- Hamzehloo, H., Ansari, A. and Kale, Ö. (2012). Recent Developments on Iranian SM Database Under the EMME, 33rd General Assembly of the European Seismological Commission, Moscow, Russia.
- Kale, Ö., Akkar, S. and Danciu, L. (2012). Testing of Ground-Motion Prediction Equations for the Earthquake Model of the Middle East Region (EMME) Project and Its Consequential Effects on PSHA, 7th Gulf Seismic Forum, Jeddah, Saudi Arabia.
- Kale, Ö. and Bindi, D. (2010). Utility Software for Data Processing, Iternational Training Course on Seismology, Seismic Data Analysis, Hazard Assessment and Risk Mitigation, Ankara, Turkey.

OTHER TECHNICAL REPORTS

- Kale, Ö., Akkar, S., Yakut, A. and Çeken, U. (2014). Yer Hareketi Tahmin Denklemleri (YHTD) ve Epistemik Model Belirsizliği içinYHTD Mantık Ağacı Uygulaması, Progress Report, UDAP-Ç-13-06 Project.
- 9 Kasım 2011 Van Earthquake Report (2012). 9 Kasım 2011 Mw 5.6 Van-Edremit Depremi Sismik Ve Yapısal Hasara İlişkin Gözlemler, METU-EERC/İMO 2012-01, Ankara, Turkey.
- 23 Ekim 2011 Van Earthquake Report (2011). 23 Ekim 2011 Mw 7.2 Van Depremi Sismik ve Yapısal Hasara İlişkin Saha Gözlemleri, METU/EERC 2011-04, Ankara, Turkey.
- Sucuoğlu, H. and Kale, Ö. (2011). Abstracts Book, 1. Türkiye Deprem Mühendisliği ve Sismoloji Konferansı, METU, Ankara.

SOFTWARE

- Utility Software for Data Processing, USDP (2008). Department of Civil Engineering, Middle East Technical University, Ankara, Turkey, available on Internet at http://www2.ce.metu.edu.tr/~sakkar/usdp.html.

JOURNAL PAPERS IN PROGRESS

- Kale, Ö. and Akkar, S. (2014). An Auxiliary Tool to Build Ground-Motion Logic-Tree Framework for Probabilistic Seismic Hazard Assessment.
- Kale, Ö., Akkar, S., Yakut, A. and Çeken, U. (2014). Strong-Motion Data-Driven Selection of Ground-Motion Prediction Equations and Establishment of Logic-Tree Framework for Seismic Hazard Assessment in Turkey.
- Şeşetyan, K., Demircioğlu, M.B. and Kale, Ö. (2014). A Probabilistic seismic hazard assessment for Turkey: Model combinations and outputs

REVIEWING ACTIVITIES

- Bulletin of the Seismological Society of America
- Natural Hazards

TEACHING EXPERIENCE

CE490 - Introduction to Earthquake Resistant Design
2014, Teaching Assistant, Middle East Technical University

SAP2000 Training Course
2009-2013, Instructor, Turkish Chamber of Civil Engineers
2012, Instructor, KOLTEK Consulting Co.

CE388 - Fundamentals of Steel Design
2012-2014, Teaching Assistant, Middle East Technical University

CE7014 - Engineering Seismology
2010&2011, Teaching Assistant, Middle East Technical University

CE586 - Earthquake Engineering
2008&2009, Teaching Assistant, Middle East Technical University

RESEARCH PROJECTS INVOLVED

213M245 (Determination of the Design Spectrum Corner Periods and Soil Amplification Factors from Probabilistic Seismic Hazard Analysis Conducted to the Selected Regions in Turkey funded by the Scientific Research and Technical Council of Turkey)
2014-2015, Project Assisstant
All studies in the scope of the project

UDAP-Ç-13-06 (Updating the Seismic Hazard Maps of Turkey funded by AFAD and DASK)
2013-2014, Project Assisstant
Ground-Motion Prediction Equations (GMPEs)

EMME (Earthquake Model of the Middle East Region Project funded by Global Earthquake Model)
2009-2013, Project Assisstant
Ground-Motion Modeling

SHARE (Seismic Hazard Harmonization in Europe Project funded by Global Earthquake Model)
2009-2013, Project Assisstant
Earthquake Catalog Compilation and Ground-Motion Data Processing

105G016 (Turkish National Strong Motion Project funded by the Scientific Research and Technical Council of Turkey)
2005-2009, Project Assisstant
Earthquake Catalog Compilation

PROFESSIONAL PROJECTS INVOLVED

- Researcher in "Probabilistic Seismic Hazard Assessment Based Design Spectrum of Erzincan Dereköy Dam", 2013.
- Researcher in "Probabilistic Seismic Hazard Assessment of Afyon Artifical Ponds", 2013.
- Researcher in "Site-Specific Seismic Hazard Analysis to Obtain Earthquake Design Loads for Seismic Design of Building and Non-Building Structures in Bandırma II - Enerjisa Combined Cycle Power Plant", 2012.

COMPUTER SKILLS

- Windows, Ubuntu
- Microsoft Office Applications (Word, Excel, PowerPoint)
- AutoCAD, Macromedia Applications (Dreamviewer, Fireworks)
- Intel Visual Fortran, Matlab
- SAP 2000, EZ-FRISK, Openquake
- Quantum GIS

ASSOCIATION MEMBERSHIPS

- Turkish Chamber of Civil Engineers
- Earthquake Engineering Association of Turkey
- Seismological Society of America

OTHER ACTIVITIES

- Member of Turkish Chamber of Civil Engineers Vocational Training Courses Committee (2012-2013).
- Vice Chairman of METU Tennis Society (2008-2012).
- Conference secretary at "1. Türkiye Deprem Mühendisliği ve Sismoloji Konferansı" organized by Earthquake Engineering Association of Turkey in Middle East Technical University, Ankara, 2011.